



# University of HUDDERSFIELD

## University of Huddersfield Repository

Liu, Fulong

Online Identification of Vehicle Dynamic Systems for Condition Monitoring

### Original Citation

Liu, Fulong (2020) Online Identification of Vehicle Dynamic Systems for Condition Monitoring. Doctoral thesis, University of Huddersfield.

This version is available at <http://eprints.hud.ac.uk/id/eprint/35357/>

The University Repository is a digital collection of the research output of the University, available on Open Access. Copyright and Moral Rights for the items on this site are retained by the individual author and/or other copyright owners. Users may access full items free of charge; copies of full text items generally can be reproduced, displayed or performed and given to third parties in any format or medium for personal research or study, educational or not-for-profit purposes without prior permission or charge, provided:

- The authors, title and full bibliographic details is credited in any copy;
- A hyperlink and/or URL is included for the original metadata page; and
- The content is not changed in any way.

For more information, including our policy and submission procedure, please contact the Repository Team at: [E.mailbox@hud.ac.uk](mailto:E.mailbox@hud.ac.uk).

<http://eprints.hud.ac.uk/>

# **Online Identification of Vehicle Dynamic Systems for Condition Monitoring**

**Fulong Liu**

A thesis submitted to the University of Huddersfield in partial fulfilment of the requirements for the degree of Doctor of Philosophy

School of Computing and Engineering

The University of Huddersfield

January 2020



---

---

## COPYRIGHT STATEMENT

---

---

- i. The author of this thesis (including any appendices and/or schedules to this thesis) owns any copyright in it (the “Copyright”) and s/he has given The University of Huddersfield the right to use such copyright for any administrative, promotional, educational and/or teaching purposes.
- ii. Copies of this thesis, either in full or in extracts, may be made only in accordance with the regulations of the University Library. Details of these regulations may be obtained from the Librarian. This page must form part of any such copies made.
- iii. The ownership of any patents, designs, trademarks and any and all other intellectual property rights except for the Copyright (the “Intellectual Property Rights”) and any reproductions of copyright works, for example graphs and tables (“Reproductions”), which may be described in this thesis, may not be owned by the author and may be owned by third parties. Such Intellectual Property Rights and Reproductions cannot and must not be made available for use without the prior written permission of the owner(s) of the relevant Intellectual Property Rights and/or Reproductions.

---

---

## DECLARATION

---

---

No portion of the work referred to in this thesis has been submitted in support of an application for another degree or qualification of this or any other university or other institutes of learning.

*(Fulong Liu)*

---

---

## ABSTRACT

---

---

This PhD project focuses on developing online monitoring approaches for suspension systems based on vibration analysis, aiming at guaranteeing the safe and efficient operations of vehicles including the railway and autonomous vehicles.

Based on Operational Modal Analysis (OMA), which has been proven more effective in the field of structural health monitoring, a novel OMA algorithm, entitled the Correlation Signal Subset-based Stochastic Subspace Identification (CoSS-SSI), is proposed in this thesis to identify the inherent vibration modes of a car body and railway bogie frame to assess the health of the vehicle suspension system. The proposed novel OMA method is developed in the knowledge that the basic framework of SSI makes it applicable to nonlinear systems with nonstationary responses in the presence of high noise levels.

For the CoSS-SSI method, the measured raw signals are divided into short segments; then the correlation function of each data segment is calculated, which performs the first noise reduction. After that, the obtained correlation function for the segments are divided into subsets according to their minimum amplitudes, and then each subset is averaged to further reduce the noise. Different correlation signal subsets can reduce nonlinear effects such as high damping, on OMA. Lastly, each subset of the averaged correlation signals is utilised to accurately identify the modal parameters based on SSI.

A 3-DOF vibration system was developed in an initial simulation study developed to evaluate the performance of CoSS-SSI, which showed that CoSS-SSI was superior to other conventional OMA methods like Cov-SSI in extracting useful modal information on system behaviour. In addition, a quarter vertical vehicle model was constructed to investigate the effects of periodic pulses and harmonics on OMA. It was found that periodic pulses have no impacts on OMA, but harmonics can cause significant adverse effect. Then, cepstrum editing was introduced to eliminate the harmonic effect on OMA, and its performance was first verified by simulated data and later by experimental data obtained from full-scale rig tests.

Experimental studies were carried out to verify the feasibility of applying the proposed method for the online monitoring of suspension systems. In the first set of experiments, accelerometers were installed at the four corners of a car body and it was shown that with

CoSS-SSI these comprised a robust and cost-efficient system for monitoring the suspension system. These results were confirmed by using CoSS-SSI to identify the modal parameters of a road vehicle suspension using the measured vibrations of a real car running normally on a traditional country road near Huddersfield, UK. These experiments confirmed that CoSS-SSI had the capability to extract the inherent vibration modes of the vehicle suspension system.

Importantly, a 1/5<sup>th</sup> scale roller rig and then an Y25 bogie were employed to verify the potential of CoSS-SSI for railway vehicle suspension monitoring. The outcomes from roller rig experiments showed that the novel CoSS-SSI proposed here is also feasible for the successful online monitoring of railway vehicle suspension systems.

---

---

## ACKNOWLEDGMENT

---

---

This PhD project is sponsored by the Fee-waiver Scholarship scheme from the University of Huddersfield (UoH) and a scholarship from China Scholarship Council (CSC). I would like to give my grateful acknowledgements to the UoH and CSC for their financial support to make this research smooth.

I want to express my thanks to my main supervisor, Professor Andrew D. Ball, for the continued encouragement and endless support through this research.

I am sincerely grateful to my co-supervisor, Professor Fengshou Gu, a principal research fellow at the UoH, for his invaluable guidance in the research, and sincere and warm-hearted help in my life.

I would like to thank my colleagues and friends in the Centre for Efficiency and Performance Engineering (CEPE), School of Computing and Engineering at the UoH. I was fortunate to have nice peers in my research group.

Special thanks extended to my fiancée, Xueyang Fang, for her understanding, support and encouragement during the PhD study.

Finally, I would like to thank my parents, brother and other relatives for their long-term understanding and support of my study.

---

---

---

## TABLE OF CONTENTS

---

---

COPYRIGHT STATEMENT.....	a
DECLARATION.....	b
ABSTRACT .....	c
ACKNOWLEDGMENT .....	e
TABLE OF CONTENTS .....	i
LIST OF FIGURES .....	vii
LIST OF TABLES .....	xi
LIST OF ABBREVIATIONS .....	xii
LIST OF PUBLICATIONS.....	xiii
CHAPTER 1 INTRODUCTION .....	1
1.1 Research background.....	2
1.2 Research motivation .....	3
1.3 Research aim and objectives.....	4
1.4 Structure of thesis .....	4
CHAPTER 2 LITERATURE REVIEW .....	7
2.1 Background of condition monitoring.....	8
2.1.1 Condition monitoring techniques .....	8
2.1.2 Vibration signal processing techniques .....	9
2.1.2.1 Time-domain analysis .....	10
2.1.2.2 Frequency-domain analysis.....	10
2.1.2.3 Time-frequency domain analysis .....	11
2.2 Condition monitoring techniques for vehicle suspension systems .....	12
2.2.1 Road vehicle suspension monitoring.....	12
2.2.1.1 Model-based methods .....	12

2.2.1.2	Data-based methods .....	14
2.2.2	Railway vehicle suspension monitoring.....	15
2.2.2.1	In-depot methods .....	16
2.2.2.2	Wayside methods .....	17
2.2.2.3	On-board methods.....	17
2.3	OMA for condition monitoring .....	22
2.3.1	Frequency-domain methods .....	24
2.3.2	Time-domain methods.....	25
2.3.3	Other methods .....	26
2.3.4	OMA applications .....	26
2.4	Findings .....	28
CHAPTER 3 FRAMEWORKS OF STOCHASTIC SUBSPACE IDENTIFICATION .		29
3.1	Introduction .....	30
3.2	Vibration system dynamic models .....	30
3.2.1	State-space model.....	31
3.2.2	Stochastic state-space model.....	33
3.3	Stochastic Subspace Identification (SSI).....	36
3.3.1	Notations of Stochastic Subspace Identification.....	36
3.3.2	Covariance-Driven Stochastic Subspace Identification (Cov-SSI).....	38
3.3.3	Modal parameter extraction .....	41
3.3.4	Stabilisation Diagram (SD) .....	43
3.4	Findings .....	44
CHAPTER 4 CORRELATION SIGNAL SUBSET-BASED STOCHASTIC SUBSPACE IDENTIFICATION.....		45
4.1	Introduction .....	46
4.2	Correlation Signal Subset-based SSI (CoSS-SSI).....	46

4.2.1	Theoretical background of CoSS-SSI.....	46
4.2.2	Procedure for CoSS-SSI.....	48
4.3	Effectiveness verification of CoSS-SSI.....	52
4.3.1	3-DOF model description.....	52
4.3.2	Modal identification results and analysis .....	55
4.4	Findings .....	63
<b>CHAPTER 5 OPERATIONAL MODAL ANALYSIS IN THE PRESENCE OF HARMONICS .....</b>		<b>65</b>
5.1	Introduction.....	66
5.2	Cepstrum editing (CE).....	67
5.3	Feasibility of cepstrum editing for removing harmonics.....	69
5.3.1	Quarter vehicle model description.....	69
5.3.2	Excitation model.....	70
5.3.3	Simulation results .....	71
5.3.3.1	Modal parameters extracted from raw signals .....	71
5.3.3.2	Modal parameters extracted from filtered signals.....	77
5.4	Findings .....	80
<b>CHAPTER 6 CONDITION MONITORING OF ROAD VEHICLE SUSPENSION SYSTEMS USING CoSS-SSI.....</b>		<b>81</b>
6.1	Introduction.....	82
6.2	Simplified suspension system.....	82
6.2.1	Overview of road vehicle suspension.....	82
6.2.2	Introduction of the simplified suspension system .....	84
6.2.3	3-DOF model and theoretical modal parameters.....	85
6.2.3.1	Measurement of inertia parameters .....	85
6.2.3.2	3-DOF model and theoretical modal parameter calculation .....	86

---

6.2.4	Experimental results and analysis .....	88
6.2.4.1	Experiment set-up .....	88
6.2.4.2	Characteristics of simplified suspension system responses .....	89
6.2.4.3	Modal parameters of a simplified suspension system.....	90
6.3	Vehicle suspension system field test .....	92
6.3.1	7-DOF full vehicle model and theoretical modal parameters .....	93
6.3.1.1	Kinematic equations of a vertical vehicle model.....	93
6.3.1.2	Theoretical modal properties of suspension systems.....	96
6.3.2	Vehicle field test and result analysis .....	98
6.3.2.1	Experiment set-up .....	98
6.3.2.2	Characteristics of vehicle responses .....	99
6.3.2.3	Vehicle suspension under normal condition .....	101
6.3.2.4	Vehicle suspension under abnormal condition .....	106
6.4	Findings .....	109
CHAPTER 7 CONDITION MONITORING OF RAILWAY VEHICLE SUSPENSION SYSTEMS BASED ON A 1/5 <sup>TH</sup> SCALE BOGIE, USING CoSS-SSI...		111
7.1	Introduction .....	112
7.2	7-DOF model of 1/5 <sup>th</sup> scale roller rig .....	112
7.2.1	Roller rig introduction.....	112
7.2.2	Model parameter estimation.....	113
7.2.2.1	Primary suspension stiffness estimation .....	113
7.2.2.2	Mass and moments of inertia of bogie frame.....	116
7.2.3	Theoretical modal parameters of the 1/5 <sup>th</sup> scale bogie.....	117
7.2.3.1	Theoretical modal parameters of the 1/5 <sup>th</sup> scale bogie.....	117
7.2.3.2	Flexural modes of the bogie frame .....	118
7.3	Experimental investigation.....	118

7.3.1	Experiment set-up.....	118
7.3.2	Characteristics of roller rig responses .....	119
7.3.3	1/5 <sup>th</sup> scale bogie with normal suspension .....	120
7.3.4	1/5 <sup>th</sup> scale bogie with abnormal suspension .....	126
7.3.4.1	Fault case 1: Aging of the rubber (harder mount).....	127
7.3.4.2	Fault case 2: Fatigue of the rubber (Softer mount) .....	128
7.4	Findings .....	130
CHAPTER 8 CONDITION MONITORING OF THE SUSPENSION SYSTEM OF AN Y25 BOGIE USING CoSS-SSI.....		131
8.1	Introduction.....	132
8.2	SIMPACK model of tested bogie .....	133
8.2.1	SIMPACK introduction.....	133
8.2.2	Y25 bogie SIMPACK model.....	134
8.2.3	Theoretical modal analysis .....	135
8.3	Experimental investigation .....	136
8.3.1	Experiment set-up.....	136
8.3.2	Loading profile and response analysis .....	139
8.3.2.1	Loading profile of the load cell .....	139
8.3.2.2	Characteristics of the Y25 bogie responses.....	140
8.3.3	OMA via CoSS-SSI combined with cepstrum editing .....	143
8.3.3.1	Cepstrum editing before OMA.....	143
8.3.3.2	CoSS-SSI identification results .....	144
8.4	Findings .....	148
CHAPTER 9 CONCLUSIONS AND FUTURE WORK .....		149
9.1	Thesis objectives and achievements .....	150
9.2	Conclusions.....	152

Table of Contents

---

9.3	Novelty and contributions to knowledge.....	153
9.4	Future work.....	154
	REFERENCES.....	155

---

---

## LIST OF FIGURES

---

---

Figure 1-1 Schematic structure of the thesis .....	6
Figure 2-1 General classification of condition monitoring methods.....	12
Figure 2-2 Block diagram for the Kalman filter [70] .....	18
Figure 2-3 Framework and processes of popular OMA methods .....	24
Figure 3-1 Flowchart of Cov-SSI.....	42
Figure 4-1 Schematic for dividing raw data from $l$ channels into $K$ segments each containing $N$ data points.....	49
Figure 4-2 Flow chart of CoSS-SSI.....	51
Figure 4-3 3-DOF linear vibration system .....	52
Figure 4-4 Time-domain response of the linear 3-DOF vibration system .....	54
Figure 4-5 Amplitude mean values of time-domain responses for every two seconds.....	54
Figure 4-6 PSD of the linear 3-DOF vibration system responses .....	54
Figure 4-7 SDs identified by Cov-SSI.....	56
Figure 4-8 SDs identified by ACS-Cov-SSI.....	56
Figure 4-9 SDs identified by CoSS-SSI .....	58
Figure 4-10 Stable rates of the SDs identified by: (a) Cov-SSI; (b) ACS-Cov-SSI.....	59
Figure 4-11 Stable rates of the SD identified by CoSS-SSI.....	59
Figure 4-12 MAC for mode shapes identified by Cov-SSI.....	61
Figure 4-13 MAC for mode shapes identified by ACS-Cov-SSI.....	61
Figure 4-14 MAC for mode shapes identified by CoSS-SSI .....	62
Figure 5-1 Cepstrum editing procedure to filter harmonic effects for OMA .....	68
Figure 5-2 Short-pass lifter.....	69
Figure 5-3 Quarter vehicle model.....	70
Figure 5-4 Frequency response function of the quarter vehicle model .....	70
Figure 5-5 Car body responses under random excitation only .....	72
Figure 5-6 SD identified by CoSS-SSI for quarter vehicle model excited by white noise random input only.....	72
Figure 5-7 Car body responses under pulse train and random excitations.....	73

Figure 5-8 SD identified by CoSS-SSI for quarter vehicle model excited by pulse train and random inputs..... 74

Figure 5-9 Car body responses under one harmonic, pulse train and random excitations.. 75

Figure 5-10 SD identified by CoSS-SSI for quarter vehicle model excited by one harmonic, pulse train and random inputs ..... 75

Figure 5-11 Car body responses under two harmonics, pulse train and random excitations ..... 76

Figure 5-12 SD identified by CoSS-SSI for quarter vehicle model excited by two harmonics, pulse train and random inputs ..... 77

Figure 5-13 Cepstrum, window function and edited cepstrum ..... 78

Figure 5-14 Carbody responses raw signal and filtered signal ..... 78

Figure 5-15 SD identified by CoSS-SSI for quarter vehicle model excited by one harmonic, pulse train and random inputs using filtered signal..... 79

Figure 5-16 SD identified by CoSS-SSI for quarter vehicle model excited by two harmonics, pulse train and random inputs using filtered signal..... 80

Figure 6-1 Photograph of McPherson suspension system [54]..... 83

Figure 6-2 Categories of popular road vehicle suspension systems [54], [172] ..... 83

Figure 6-3 Photograph of simplified suspension system test rig ..... 84

Figure 6-4 Dimensions of the steel plate (car body) ..... 84

Figure 6-5 Schematic of the simplified suspension system ..... 85

Figure 6-6 Spring stiffness test..... 86

Figure 6-7 Theoretical modal parameters of the simplified suspension system ..... 87

Figure 6-8 Photograph of excitation hammer ..... 88

Figure 6-9 Photograph of the four (CA-YD-185) accelerometers used..... 88

Figure 6-10 Photograph of the four-channel data acquisition system..... 89

Figure 6-11 Responses of simplified suspension system in time-domain ..... 90

Figure 6-12 PSD of the simplified suspension system responses ..... 90

Figure 6-13 SD identified by CoSS-SSI for the simplified suspension system ..... 91

Figure 6-14 Stable modes selected by the ratio of stable points ..... 91

Figure 6-15 Modal parameters of simplified suspension system identified by CoSS-SSI . 91

Figure 6-16 Photograph of employed car for field test ..... 92

Figure 6-17 Schematic of the 7-DOF vehicle model [153]..... 93

Figure 6-18 FRF of 7-DOF full vehicle model.....	97
Figure 6-19 Theoretical modal parameters of the vehicle with healthy suspension systems .....	97
Figure 6-20 Theoretical modal parameters of the vehicle with abnormal suspension systems (Stiffness of FL suspension decreased by 50%).....	98
Figure 6-21 Schematic and photographs of the measurement system.....	99
Figure 6-22 Vehicle response in time-domain as measured by accelerometers at the four corners .....	100
Figure 6-23 PSD of vehicle response at each of the vehicle's four corners.....	100
Figure 6-24 SD identified by ACS-Cov-SSI and the rate of stable points .....	102
Figure 6-25 Modal parameters identified by ACS-Cov-SSI and MAC values .....	102
Figure 6-26 SDs identified by CoSS-SSI and corresponding rates of stable points.....	104
Figure 6-27 Modal parameters identified by CoSS-SSI and corresponding MAC values when the suspension under normal condition .....	105
Figure 6-28 SDs identified by CoSS-SSI for fault suspension and corresponding rates of stable points .....	108
Figure 6-29 Modal parameters identified by CoSS-SSI and corresponding MAC values when the suspension under abnormal condition .....	109
Figure 7-1 1/5 <sup>th</sup> scale roller rig and schematic of the side view .....	113
Figure 7-2 Schematic and photographs of employed stud mounts.....	114
Figure 7-3 INSTRON 3369 Universal Testing System.....	114
Figure 7-4 Force-displacement curves of mounts .....	115
Figure 7-5 Detail of mount installation ( $\theta = \pi/3$ ).....	116
Figure 7-6 3D model of the bogie frame .....	116
Figure 7-7 Theoretical rigid modes of the bogie frame.....	117
Figure 7-8 First four flexural modes of the bogie frame .....	118
Figure 7-9 Raw signals of roller rig responses and corresponding PSD (FL: Front-Left; FR: Front-Right; RL: Rear-Left; RR: Rear-Right).....	120
Figure 7-10 (a) SD identified by Cov-SSI and (b) Rate of stable points.....	121
Figure 7-11 (a) Modes of bogie frame identified by Cov-SSI and (b)MAC values compared with theoretical mode shapes.....	122
Figure 7-12 (a) SD identified by ACS-Cov-SSI and (b) Rate of stable points .....	122

Figure 7-13 (a) Modes of bogie frame identified by ACS-Cov-SSI and (b) MAC values compared with theoretical mode shapes..... 122

Figure 7-14 (a) SDs identified by CoSS-SSI, and (b) Corresponding rate of stable points ..... 124

Figure 7-15 Modes of bogie frame identified by CoSS-SSI and corresponding MAC values compared with theoretical mode shapes..... 125

Figure 7-16 Modes of bogie frame with the harder suspension at FL corner identified by CoSS-SSI and corresponding MAC values compared with theoretical mode shapes ..... 128

Figure 7-17 Modes of bogie frame with the softer suspension at RL corner identified by CoSS-SSI and corresponding MAC values compared with theoretical mode shapes ..... 129

Figure 8-1 Photograph of the full-scale roller rig in the IRR laboratory at UoH..... 133

Figure 8-2 SIMPACK model of Y25 bogie ..... 134

Figure 8-3 Rigid modes of bogie frame related to primary suspension ..... 136

Figure 8-4 Accelerometer installation positions on the Y25 bogie..... 137

Figure 8-5 Schematic of the full-scale test rig and accelerometer positions..... 138

Figure 8-6 Photograph of (a) YE6232B DAQs (b) CA-YD-185 accelerometers (c) YMC 121A20 accelerometers ..... 139

Figure 8-7 Load profile and corresponding load force during the test..... 140

Figure 8-8 Example of a time-domain signal of bogie response..... 141

Figure 8-9 Example of a frequency-domain signal of bogie response..... 142

Figure 8-10 (a) Example of cepstrum; (b) Example of raw and filtered signals in the time-domain..... 143

Figure 8-11 Example of raw and filtered signals in the frequency-domain..... 144

Figure 8-12 SDs identified by CoSS-SSI using raw signal..... 145

Figure 8-13 SDs identified by CoSS-SSI using filtered signal ..... 146

Figure 8-14 Rate of stable points over maximum calculated orders..... 146

Figure 8-15 Rigid modes of Y25 bogie frame identified by CoSS-SSI..... 147

---

---

## LIST OF TABLES

---

---

Table 4-1 Theoretical modal parameters of the 3-DOF linear vibration system.....	52
Table 4-2 Modal results identified by Cov-SSI with errors .....	60
Table 4-3 Modal results identified by ACS-Cov-SSI with errors .....	60
Table 4-4 Modal results identified by CoSS-SSI with errors.....	60
Table 6-1 Specifications of the accelerometer .....	88
Table 6-2 Modal parameters identification errors of the simplified suspension system.....	92
Table 6-3 Parameters of 7-DOF full vehicle model [54].....	94
Table 7-1 Specifications of the roller rig [176] .....	117
Table 8-1 Main properties of the suspension system .....	135
Table 8-2 Mass properties of the mass components.....	135
Table 8-3 Specifications of accelerometers YMC 121A20.....	139

---

---

## LIST OF ABBREVIATIONS

---

---

OMA	Operational Modal Analysis
EMA	Experimental Modal Analysis
CM	Condition Monitoring
FDD	Frequency-Domain Decomposition
SSI	Stochastic Subspace Identification
SHM	Structural Health Monitoring
Cov-SSI	Covariance driven SSI
CoSS-SSI	Correlation Signal Subset based SSI
TSA	Time Synchronous Average
STFT	Short-time Fourier Transform
WT	Wavelet Transform
FDI	Fault Detection and Isolation
PCA	Principle Component Analysis
PP	Peak Picking
LSCF	Least-squares Complex Frequency Domain
NExT	Natural Excitation Technique
LSCE	Least-squares Complex Exponential method
ERA	Eigensystem Realization Algorithm
ARMA	Auto-regressive Moving Average time series model
SD	Stabilization Diagram
MAC	Modal Assurance Criterion
RMS	Root Mean Square
DOF	Degree of Freedom
SNR	Signal to Noise Ratio
CE	Cepstrum Editing

---

---

## LIST OF PUBLICATIONS

---

---

- [1]. **Fulong Liu**, Hao Zhang, Xiaocong He, Yunshi Zhao, Fengshou Gu, and Andrew D. Ball. "Correlation signal based stochastic subspace identification for an online identification of railway vehicle suspension systems." *Vehicle System Dynamics* (2019): 1-21.
- [2]. **Fulong Liu**, Jigang Wu, Fengshou Gu, and Andrew D. Ball. "An introduction of a robust OMA method: CoSS-SSI and its performance evaluation through the simulation and a case study." *Shock and Vibration* (2019): 1-14.
- [3]. Yongbo Li, **Fulong Liu**, Shu Wang, Xihui Liang, and Jiancheng Yin. "Multi-scale symbolic lempel-ziv: an effective feature extraction approach for fault diagnosis of railway vehicle suspension systems." *IEEE Transactions on Industrial Informatics*. (accepted)
- [4]. **Fulong Liu**, Jiongqi Wang, Miaoshuo Li, Fengshou Gu, and Andrew D. Ball. "Operational modal analysis of Y25 bogie via stochastic subspace identification for the condition monitoring of primary suspension systems." In Proceedings of the 13th International Conference on Damage Assessment of Structures, pp. 166-181. Springer, Singapore, 2020.
- [5]. **Fulong Liu**, Jiongqi Wang, Miaoshuo Li, Fengshou Gu, and Andrew D. Ball. "Operational modal analysis in the presence of pulse train and harmonics based on SSI." In Proceedings of the 32nd Condition Monitoring and Diagnostic Engineering Management (COMADEM2019). (In publication)
- [6]. **Fulong Liu**, Fengshou Gu, Andrew D. Ball, Yunshi Zhao, and Bo Peng. "The validation of an ACS-SSI based online condition monitoring for railway vehicle suspension systems using a SIMPACK model." In 2017 23rd International Conference on Automation and Computing (ICAC), pp. 1-6. IEEE, 2017.
- [7]. **Fulong Liu**, Fengshou Gu, Yunshi Zhao, and Andrew Ball. "A validation study of ACS-SSI for online condition monitoring of vehicle suspension systems." *Vibroengineering Procedia* 10 (2016): 369-375.
- [8]. Miaoshuo Li, Xianghong Wang, **Fulong Liu**, Xiaoli Tang, Fengshou Gu, and Andrew D. Ball. "Remote monitoring of wind turbine blades based on high-speed

photogrammetry." Condition Monitoring and Diagnostic Engineering Management (COMADEM2018): 321.

- [9]. Otuyemi, Funso, Haiyang Li, **Fulong Liu**, Jiongqi Wang, Fengshou Gu, and Andrew D. Ball. "Modulation signal bispectrum analysis of motor current signals for condition monitoring of electromechanical systems." In Proceedings of the 13th International Conference on Damage Assessment of Structures, pp. 566-581. Springer, Singapore, 2020.
- [10]. Qin, G., Fengshou Gu, Yuandong Xu, **Fulong Liu**, and Andrew Ball. "Bogie speed estimation and signal source separation via rail vibration analysis." Condition Monitoring and Diagnostic Engineering Management (COMADEM 2017): 200.

---

---

## CHAPTER 1 INTRODUCTION

---

---

*A vehicle's suspension system is vital to its performance, and therefore it is important to have a condition monitoring (CM) mechanism to continually assess its condition.*

*CM has become increasingly important to modern vehicles to ensure safe and efficient operation. In the past few years, online CM has drawn special attention as it can continuously evaluate the status of the monitored system, which is of particular significance with critical systems such as the suspension of a vehicle.*

*This chapter begins by describing the background and motivation of this research. Then the research aim and objectives are presented. Finally, it briefly outlines the contents of this thesis. This chapter also serves to introduce this PhD project which intends to develop an online monitoring method for vehicle suspension systems based on identification of relevant parameters within the vehicle system dynamics through operational modal analysis (OMA).*

## 1.1 Research background

It is well known that the suspension system plays a vital role in ensuring the comfort and safety of those within and around a vehicle. The conventional vehicle suspension system is composed of springs and shock absorbers, which provides the connection between the wheels and the body of the vehicle for the purpose of reducing the vibration or shocks caused by road or track irregularities, maximising vehicle safety, driving performance and passenger comfort. The suspension system is essential for vehicle safety because it has the ability to resist the roll of the vehicle and allow the vehicle to follow the road/track. It is also critical for steering control which is related to the maneuverability of a vehicle. Because of the importance of the suspension system to a vehicle, it has attracted increased attention in recent years, especially with the rapid and significant increase of the speed of railway vehicles, and the rapid development of autonomous vehicle for transport by road.

Condition Monitoring (CM) is a powerful and efficient approach to improve the reliability of the critical components in a machine, reduce maintenance costs and prevent accidents [1]. For instance, numerous techniques have been developed to monitor or diagnose the condition of gears and bearings which are the most common components in machinery [2]. Because the suspension system is an essential part of a vehicle, numerous CM techniques to monitor its status have been proposed and explored.

Generally, available vehicle suspension system monitoring techniques can be classified into model-based and data-based methods [3]. However, these are rarely applied in an operating vehicle on account of their limitations. Specifically, the main limitation of model-based approaches is that a model of the monitored system of great accuracy is required, but a sufficiently accurate model is difficult or even impossible under some circumstances, and so the application of model-based methods is restricted. For data-based techniques, the major challenge is developing a database which includes baselines for all the many different fault cases and various degrees of those faults. Besides, computation cost is another big issue for data-based methods.

CM techniques for railway vehicle suspension systems can be grouped differently according to the position of the sensors used: in-depot, wayside and on-board. As the name implies, the in-depot method is for use in the depot which, of course, will usually interrupt the

vehicle's usage. The wayside method is to detect suspension system faults via transducers installed beside the track or on sleepers, so detection is possible only when the vehicle passes the sensor sites. The on-board method measures the vehicle's responses to diagnose the condition of the vehicle suspension which is achieved by installing transducers at appropriate positions on the vehicle. Both in-depot and wayside methods are unsuitable for vehicle suspension online monitoring. In contrast, the on-board method has the potential to achieve online monitoring if the drawbacks of model-based and data-based methods can be overcome.

Operational Modal Analysis (OMA) has become a hot topic in recent years because of its successful application to monitoring the status of civil engineering structures such as high-rise buildings and long-span bridges [4]. Numerous OMA approaches have been developed and perfected by many researchers to meet different application scenarios. For instance, Frequency-Domain Decomposition (FDD) and Stochastic Subspace Identification (SSI) methods are the most popular frequency-domain and time-domain OMA approaches, respectively. As the application of OMA has been proved successful for structural health monitoring (SHM) in buildings, increased attention has been focused on utilising OMA in mechanical areas for structure optimisation, CM or fault diagnosis [5]–[7]. The results presented in the published papers, see Chapter 2, Literature Review, show that the application of OMA for CM of mechanical systems is a fruitful area for research, and has the potential to achieve online monitoring of vehicle suspension systems.

## **1.2 Research motivation**

With the significant increase of achievable vehicle speeds with high-speed railways [8] and rapid development of self-driving techniques and autonomous vehicles, a CM technique which can achieve online monitoring of the vehicle's suspension system is highly desirable to ensure enhanced vehicle safety. Based on a comparative literature review (see Chapter 2), it has been found that employing OMA to analyse vehicle dynamic systems has the possibility to achieve online monitoring of vehicle suspension systems.

However, the Literature Review identifies the following gaps that have to be filled before using OMA for vehicle suspension system monitoring:

- 1) Most OMA methods have been developed under the assumption of a linear system with white noise excitation, which means the system response should be stationary. However, the excitation from road/track is not white noise. Therefore, the vehicle response will, almost certainly, be nonstationary.
- 2) Most present OMA methods are unable to cope adequately with nonlinear systems. However, vehicle suspension systems are high nonlinear.
- 3) Measurement noise is exceptionally high in field experiments.

### 1.3 Research aim and objectives

This PhD research aims to develop an effective and robust on-board measurement system and a novel OMA approach which allows online monitoring of the vehicle suspension system.

To achieve this research aim, the main objectives are identified and prioritized as follows:

**Objective 1:** To perform a comprehensive literature review of CM techniques which highlights their applications to vehicle suspension monitoring;

**Objective 2:** To review existing OMA techniques and their applications to identify their advantages and disadvantages;

**Objective 3:** To present a novel OMA method to enable the use of OMA in vehicle dynamic identification based on a framework of SSI;

**Objective 4:** To review OMA in the presence of harmonics and evaluate the performance of cepstrum editing for removing harmonic effects;

**Objective 5:** To assess the performance of the novel SSI method which was presented in this thesis for road vehicle suspension online monitoring;

**Objective 6:** To evaluate the performance of the novel SSI method which was presented in this thesis for railway vehicle suspension online monitoring;

### 1.4 Structure of thesis

This thesis is organised into nine chapters to present the work done to achieve the research aim and objectives. The structure of this thesis is presented in Figure 1-1, and the contents of each chapter are briefly listed below:

*Chapter 1* – The first chapter presents the research background, motivation and aim.

**Chapter 2** – This chapter presents a comprehensive literature review of CM and OMA, with emphasis on CM of the vehicle suspension system. The knowledge gaps blocking the use of OMA for analysis of the vehicle dynamics and suspension CM have been extracted from the review.

**Chapter 3** – The framework of SSI is presented in this chapter, which serves as the foundation of the novel OMA method proposed in the following chapter.

**Chapter 4** – A novel OMA method, denoted as Correlation Signal Subset based SSI (CoSS-SSI), is proposed as a means of extracting modal parameters of a nonlinear system with nonstationary responses. The performance of CoSS-SSI was evaluated by a 3-DOF vibration model and compared with conventional OMA approaches.

**Chapter 5** – This chapter begins with a brief overview of OMA in the presence of harmonics as this scenario will occur in the subsequent experimental study. Cepstrum editing (CE) was selected as the tool to remove the effects of harmonic excitations on the OMA. A quarter vehicle model was utilised to evaluate the performance of CE. In the meantime, the influence of periodic pulse excitations on OMA was investigated using the quarter vehicle model.

**Chapter 6** – This chapter begins the experimental verification of the capability of CoSS-SSI to identify the dynamic parameters of the vehicle suspension system for CM. Initially, a simplified suspension system was developed and employed in the experiment. Then, tests were conducted on a road vehicle on a traditional countryside road in the UK.

**Chapter 7** – This chapter presents and assesses the potential of utilising CoSS-SSI for railway vehicle suspension online monitoring via experiments on a 1/5<sup>th</sup> scale roller rig.

**Chapter 8** – This chapter further verifies the performance of the proposed novel method for railway vehicle suspension monitoring via an Y25 bogie tested on a full-scale roller rig. Additionally, the performance of CE for removing harmonic effects on OMA was assessed in the same experiment.

**Chapter 9** – The conclusions, achievements of the research and suggestions for future work are presented in the last chapter.

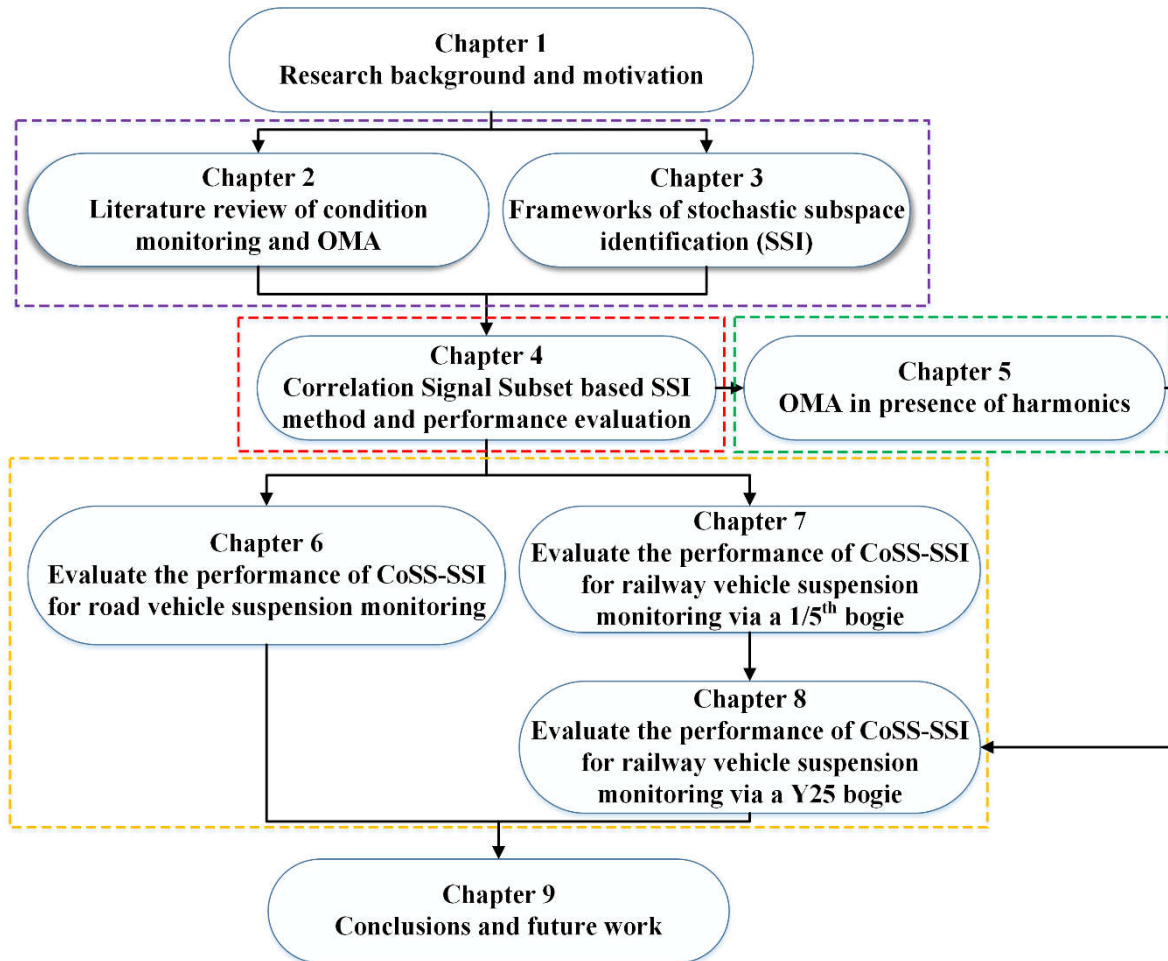


Figure 1-1 Schematic structure of the thesis

---

---

## CHAPTER 2 LITERATURE REVIEW

---

---

*As machines have become more complex and expensive, condition monitoring (CM) has attracted increasing interest. In particular, online CM systems are highly desirable for vehicle suspension systems, especially for railway vehicles which already travel at hundreds of km/hr, with the expectation of these speeds increasing significantly.*

*This chapter begins by reviewing published material concerning CM techniques, after which the focus shifts to CM of vehicle suspension systems. The primary purpose is to identify gaps in existed methods that stop them being used for online monitoring of vehicle suspension systems. An overview of Operational Modal Analysis (OMA) follows to demonstrate the potential use OMA for vehicle suspension monitoring. Finally, the findings of knowledge gaps identified are presented.*

## **2.1 Background of condition monitoring**

Condition Monitoring (CM) has attracted considerable attention in recent decades because of the rapid development of modern industry [9]. Modern industrial equipment is becoming larger, running at higher speed, of increasing complexity and increasingly expensive. It is inevitable that such sophisticated equipment, built at minimum cost, will experience a wide variety of faults and failures. However, any failure will lead to a decrease in machine performance and may result in economic losses, even catastrophic accidents [10]. CM allows for such costly faults and failures to be detected in their early stages and hence corresponding actions to be taken to prevent losses and accidents.

CM is the procedure of measuring the continuous response data of a machine via proper sensors, and then analyzing and interpreting the collected data to diagnose its status; whether healthy or faulty [9], [11]. After which, the appropriate maintenance decision will be recommended, depending on the diagnostic analysis.

The significance of CM for modern machinery is obvious, and the following advantages should be highlighted: first and foremost, CM can prevent catastrophic accidents; secondly, CM can decrease economic losses caused by unforeseen faults or failures; thirdly, timely maintenance is helpful in prolonging the machine's operation life and achieving substantial economic benefits.

Because of the significance of CM, there are a considerable number of techniques that have been developed for monitoring the health of machinery. In the following sub-section, the most common CM techniques will be reviewed, and vibration-based methods will be highlighted.

### **2.1.1 Condition monitoring techniques**

The conceptual basis of CM can be traced back to the earliest development of machinery, and the methods for CM are continually evolving [9], [12]. Generally, CM techniques involve an arrangement of transducers, data acquisition and analysis systems, plus diagnostic methods for the objective of maintaining the equipment in a planned way [13].

Nowadays, a great many of CM techniques have been developed to fit a wide variety of application scenarios. It is well known that vibration analysis is the most commonly used

methods for CM [1], [2], [14], other popular techniques include airborne acoustic analysis, current signal analysis, and lubricant analysis. Airborne acoustic analysis was employed in [15], [16] to monitor the condition of diesel engines. In [2], [17], [18], acoustic emission technology was reviewed and explored for use with the CM of rotating machinery. Current signal analysis is widely used in the detection and localization of faults in induction motors [19], [20]. It has been proven that lubricant analysis [21] and infrared thermography [22] are also effective CM approaches. However, amongst these techniques, vibration analysis continues to be the dominant technology applied for CM [14] because of the merits of the vibration response, which is relatively easy to measure, non-destructive, and sensitive to a wide range of faults [10]. In consequence, vibration analysis has become a comprehensive and low-cost but robust method, which holds great promise for future development.

The accelerometer is the most popular transducer for vibration measurement in practice because of its high reliability, broad frequency response, high dynamic range and insensitivity to temperature [13], [14]. In addition, the widespread application of accelerometers is supported by its decreased manufacturing cost resulting from the rapid development of electronics [14].

Because of the extensive use of accelerometers, a large number of signal processing techniques have been developed to analyse vibration responses, which will be introduced briefly in the next subsection.

### **2.1.2 Vibration signal processing techniques**

It is common knowledge that signal measurements invariably suffer interference from various noise sources, which results in the submersion of information useful for CM. Therefore, a high quality signal processing technique is critical to extract the diagnostic information from the data for reliable and accurate CM. To date, many valuable signal processing techniques have been used to explore and develop effective monitoring systems suitable for different applications. Generally, these techniques can be categorised into four: time domain, frequency domain, time-frequency domain and others such as blind source separation [13]. These will be introduced separately below.

### **2.1.2.1 Time-domain analysis**

The time-domain analysis directly analyses the time series of the collected signals. There are several popular time-domain analysis methods which are simple but powerful, such as correlation analysis and Time Synchronous Averaging (TSA).

The most straightforward approach, however, is to calculate statistical parameters. Numerous statistical parameters are used as indicators of the status of the monitored machine. The frequently used statistical parameters can be divided into two groups: the first group is dimensional parameters, including minimum/maximum value, mean value, variance, standard deviation and root mean square, etc.; the second group is non-dimensional parameters such as shape, crest, impulse and peak factors, kurtosis, etc. [10].

Correlation is another widely used time-domain method, including auto-correlation and cross-correlation. The auto-correlation function is frequently employed to reduce random noises and extract periodic features [23]. The cross-correlation function is the result of comparing the similarity between two signals [23]. It is worth highlighting that the cross-correlation function will contain the periodic component if both signals contain the same regular component over a specific time, and such a feature is invariably meaningful for fault diagnosis.

For random noise reduction, TSA is frequently employed in the CM of rotating equipment, especially machinery with random impulse loads [24], [25]. TSA re-samples the time domain signals to the angle domain, which can remove background noise, and other unrelated impulses in the responses.

In addition, many adaptive filters have been designed to extract fault signals from loud background noise [26], [27]. The adaptive filter can be successfully applied under the assumption that the fault signal contains particular frequency components compared with the noise.

### **2.1.2.2 Frequency-domain analysis**

Frequency-domain analysis is on the basis of the Fourier transform, which provides the possibility to observe the signal from a new aspect. Typical frequency-domain analysis methods include spectrum analysis, cepstrum analysis and envelope analysis. Of these three, spectrum analysis is the oldest and most common approach for CM [10]. The spectrum

presents the distribution of the signal in the frequency domain, and the fault features will become visible when the noise is filtered out.

In recent decades, cepstrum analysis has become popular due to its capability of identifying complex periodic components. For instance, it is possible to discern on a cepstrum, a fault on a bearing or gear via the gearbox responses. However, multiple clusters of modulation sidebands on the spectrum can result in difficulties in fault location [28].

Another popular frequency domain analysis method is envelope analysis, which is also called demodulation analysis. It can extract the low-frequency signals modulated by a high-frequency carrier signal [29].

### **2.1.2.3 Time-frequency domain analysis**

In reality, nonstationary responses are common because of the intrinsic dynamic characteristics of the machinery itself, or from external excitations [30]. Nonstationarity indicates that the statistical parameters and main frequency components of a signal are time-varying. Various time-frequency analysis methods have been developed to suppress the challenge of nonstationary signal analysis for CM [30].

The traditional time-frequency analysis techniques include Short-time Fourier Transform (STFT) and Wavelet Transform (WT). STFT reveals the time-varying features of a signal by slicing it into short segments with appropriate overlapping by a window function and then analysing each part via the Fourier transform [31]. The window length is a critical parameter because it is related to the resolutions of both time and frequency domains.

WT employs not sinusoidal functions but wavelets to decompose a signal. Moreover, a scale variable is added to the time variable in the inner product transform. The scale variable makes the WT a powerful technique for time-frequency localization, and therefore it is suitable for transient signal analysis [30].

The Wigner-Ville Distribution (WVD) is widely used for signal time-frequency analysis. Nonetheless, the WVD is not suitable for multi-component signals on account of cross interference. Unfortunately, most real signals are not a single component, and many improved WVD methods have had to be developed, for example, the adaptive optimal kernel method, Cohen class distribution and reassignment method, etc. [30]. Reference [30] is a decent review of time-frequency analysis methods which can be applied to machinery CM.

Apart from the referred signal processing method, some other effective and useful methods can be employed for CM, these include spectral kurtosis and bispectrum. However, these methods are high order spectrum analysis techniques which can provide better noise suppression ability at the cost of calculation efficiency.

The techniques referred in this section are general approaches, for CM of vehicle suspensions, numerous methods have been developed, and they will be presented in the following section.

## 2.2 Condition monitoring techniques for vehicle suspension systems

The purpose of this PhD project is to develop an online CM method which is suitable for monitoring the suspension systems for both road and railway vehicles. Therefore, CM of suspension systems for both road and railway vehicles will be reviewed in this section.

### 2.2.1 Road vehicle suspension monitoring

Numerous methods have been investigated by various researchers for the effective monitoring of road vehicle suspensions. Generally, these methods can be categorised as model-based or data-based. More detail about the classification of these CM methods is given in Figure 2-1.

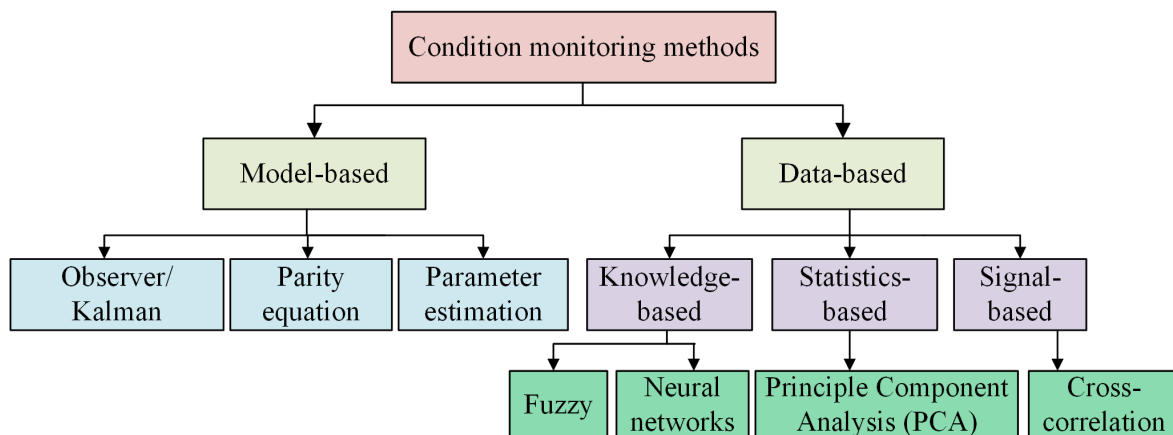


Figure 2-1 General classification of condition monitoring methods

#### 2.2.1.1 Model-based methods

An analytical model is required for model-based methods, the residual between the real system and the analytical model, can be used for fault diagnosis. Model-based fault detection is one of the most common techniques for CM of road vehicle suspension. For instance, a

model-based fault detection method using the so-called quarter-car model was presented in [32]. The results indicated that estimating the characteristic curve of shock absorber has the inherent capability of diagnosing suspension faults. In addition, the resonance frequency has the potential to detect loss of tyre pressure. Similarly, parameter estimation was employed in [33] to diagnose faults in an active suspension. The local linear model tree algorithm was applied in [33] to address the nonlinear dynamics in a real suspension system. The practicability of this method has been confirmed in an experimental study on a test rig [34]. Moreover, the same research team has claimed to have realised the monitoring of an active suspension system using the model-based method proposed by them [35].

In [36], intelligent neural networks using a gradient descent training algorithm were used for the identification of an active suspension system based on a half-car model with the aid of accelerometers placed on the car body. However, only half of the actuator faults were detected, and the defects of springs and dampers were not detected.

In [37], a model-based fault detection and isolation method, using redundant analytical relationships, was employed to monitor the passive suspension system of a 4-wheeled vehicle using a bond graph model. The simulation study in [37] illustrated the possibility to identify and monitor faults in dampers and springs in a passive suspension system.

Two model-based fault detection proposals for semi-active dampers were presented in [38]. The first one estimated damper parameters by the least-squares method, and the second predicted loss of force on the basis of an unknown input observer. The effectiveness of the proposed method was evaluated and compared via simulations using a quarter vehicle model. Comparative results showed that the parameter estimation method could produce a more reliable diagnosis. However, a Linear-Parameter-Varying (LPV) control was proposed in [39], and its ability to diagnose oil leakage from a magnetorheological damper was demonstrated by a simulation study. Recently, the LPV system was adopted in [40] to diagnose faults in an Electro-Rheological damper and its performance demonstrated through simulation and validation tests. The results showed that a damper fault could be estimated efficiently using the proposed scheme.

Semi-active damper fault diagnosis was investigated experimentally in [41]. Two fault detection and isolation methods; one frequency-based and the other model-based, were proposed for the diagnosis of damper faults. Both methods required the quarter vehicle

model; it was found that the requirements of model accuracy for the frequency-based approach were lower but that the experimental results showed that the model-based approach was more robust, though computational cost was higher.

A novel model-based method combining commonly available computational and intelligence techniques was recently proposed for the monitoring of active suspension systems [42]. And in [43], several filters in different finite-frequency domains were designed to solve the fault detect scheme of active suspension systems. The general process of model-based fault detection was presented in [44], and it was illustrated by applying to diagnose degradation of a vehicle suspension system.

Based on the reviewed literature, it can be seen that the common challenge of model-based approaches is developing an accurate model for the diagnosed system.

#### **2.2.1.2 Data-based methods**

The second category of CM techniques is data-based methods, which does not need to develop an analytical model for the diagnosed system but does need a large quantity of data. A detailed classification of data-based methods is shown in Figure 2-1. As an example of statistical-based methods, the Bayesian statistical framework was adopted in [45] to identify potential unsafe suspensions, the effectiveness was evaluated by simulated data. In [46] the Gaussian-Monte Carlo method was used to investigate the mechanism of crack propagation in an automobile suspension coil spring, and then to predict the likely life cycle of that coil spring.

In [47], a method based on the continuous wavelet transform (CWT) was proposed to detect faults in the suspension of a road vehicle. This method was assessed by an ADAMS full vehicle model and laboratory experiments. It was demonstrated that the CWT-based approach has the capability to analyse frequency-time dependent signals for detection of faults in vehicle suspensions.

In [48], the transmissibility of a suspension was monitored to detect a fault present in a magneto-rheological damper. However, the effectiveness of this method was only assessed by simulations. The same research team compared the effectiveness of a force sensor with accelerometer-based transmissibility measurements for fault detection of vehicle suspension systems, and demonstrated that the latter was superior to the former [49].

A similar study was presented in [50] based on transmissibility measurement. In this paper both linear and nonlinear dampers were considered, and the simulation results obtained indicated that the proposed method is a promising way to identify suspension damper faults.

A pure data-driven fault diagnosis method for road vehicle suspension system was proposed in [51]. Four accelerometers at the four corners measured the responses of a car body and were used to diagnose the condition of the suspension system by using possibilistic C-means clustering (PCM) and Fisher discriminant analysis (FDA). The proposed method was assessed by benchmark simulation. The same approach was further evaluated via fuzzy positivistic C-means clustering in [52].

Recently, a SHM method denoted the Dual-Tree Complex Wavelet enhanced Convolutional Long Short-Term Memory (DTCWT-CLSTM) neural network, was proposed in [53] and applied to road vehicle suspension monitoring. The method was evaluated by an experimental study which showed it was effective in refining valuable information for fault detection from the measured vibration signals, and was particularly suitable for vehicle suspension faults. OMA was employed in [54] and [55] for automobile suspension monitoring. This will be discussed further in Section 2.3.

Based on the reviewed literature, it can be seen that the main drawback of data-based methods for CM is the high computational cost and obtaining the appropriate baseline for the various faults.

In short, Section 2.2.1 present an overview of researches related to fault detection of road vehicle suspensions, and the next section will review fault detection schemes proposed for railway vehicle suspension systems.

### **2.2.2 Railway vehicle suspension monitoring**

Railways are one of the most crucial transportation systems for passengers and wares. In order to ensure safety, a large number of techniques have been developed to monitor the status of critical systems within the railway vehicles, especially for high-speed railways, including suspension systems. These techniques can be clustered into three categories according to the location of sensors: in-depot, wayside and on-board. A survey of associated researches is presented below.

### 2.2.2.1 In-depot methods

Although the disadvantages of in-depot methods are well-known, especially having to withdraw the unit from service and send it to a maintenance depot, they are the most common techniques in practice on account of reliability and cost-efficiency. Usually, a maintenance depot will consist of a storage yard, a car cleaning area, an inspection and light maintenance shed, a large maintenance shop and a separate locomotive shop [56].

One of the primary purposes of in-depot detection is to ensure the proper operation of safety suspension systems to prevent disastrous accidents such as derailling, which is directly related to the condition of wheels. Thus, the wheels of a railway vehicle are regularly inspected in-depot [57]. Common diagnostic methods used by workers is to touch the rail wheel's surface or listen to the sound produced when a hammer strikes the wheel. However, the reliability of this method depends on the experience of the worker and it can take some considerable time. Thus, appropriate equipment is in high demand to inspect hundreds of wheels in a day in a depot. The most common equipment for wheel inspection includes ultrasonic, infrared and magnetic-based systems, and many thousands of investigations have been carried out which verify their capabilities.

The ultrasonic inspection technique was explored in [58] for the detection of wheel sub-surface cracks, and the research team designed a multi-probe holder with 14 shear waves to detect tangential-oriented defects and radial defects in different areas of the wheel disk. Similarly, ultrasonic waves were employed in [59]–[61] for adequate assessment of wheel-rail contact anomalies and sub-surface cracks.

The basis of an infrared camera to detect cracks is that the thermal conductivities of steel and air are different. In [62], infrared cameras were employed for crack detection by recording the expansion of the surface of a wheel as it was heated. Magnetic monitoring is a popular non-destructive test and has the potential to monitor the tread surface of wheelset [63].

As mentioned earlier, in-depot detection is the most popular method for railway vehicle fault detection because of its reliability. This reliability can be improved further by combining established techniques with more modern methods.

### **2.2.2.2 Wayside methods**

To overcome the main drawback of in-depot methods and to improve railway vehicle monitoring and enhance vehicle safety and reliability, numerous wayside CM methods have been developed.

The common wayside methods applied in the railway industry for CM have been summarised in [64]–[66], like stress-based and optical fibre-based approaches. Of the suspension systems, wheels have attracted most attention because wheel faults will damage the rails, sleepers and, in an extreme scenario, will result in derailment. A typical wheel fault is called out-of-round, such as slid flats, spalling and shelling [67]. The out-of-round wheel will result in impact loads on the rail, which will damage the track and increase the risk of derailment. Therefore, numerous schemes have been developed to monitor and detect out-of-round wheels, these are mainly strain-based, accelerometer-based and mechanical profile monitors [65], [68]. Moreover, cameras and lasers are frequently employed to monitor the wheel profile [64].

In [66], the statics and dynamics of ballasted railway tracks were reviewed, and a sensor configuration scheme proposed for guidance when choosing wayside monitoring. More wayside monitoring methods for wheel fault detection can be found in [57].

Wayside methods can monitor other critical components, such as axle bearings, sliding wheels and brake systems. It is clear that wayside methods provide a suitable means to monitor the condition of specific aspects of vehicles, but the elastic components of suspension systems cannot be monitored via wayside methods. Thus, wayside methods cannot meet the requirement of online monitoring which is necessary for high-speed railway vehicles. Therefore, numerous researches of on-board methods have been carried out to achieve online monitoring, and an overview of these methods will be presented in the next subsection.

### **2.2.2.3 On-board methods**

As mentioned earlier, many studies into on-board methods for use with monitoring of the suspension system have been conducted, and these can be divided into model-based and data-based.

### (a) Model-based methods

As shown in Figure 2-1, the model-based methods for fault diagnosis can be categorised as observer/Kalman filter-based methods, parameter estimation based methods and parity equation-based methods. Specifically, for rail vehicle suspension monitoring, the first two categories are most common and have been studied widely.

#### i) Observer/Kalman filter-based methods

Kalman filter-based fault detection and isolation (FDI) methods are the most common model-based techniques for railway vehicle suspension monitoring [69]. The Kalman filter was proposed in 1960 by Kalman, to address the general problem of estimating the state of a system with a subset of measured state data [70]. A block diagram of the Kalman filter is presented in Figure 2-2. As can be seen from the figure, a mathematical model is used to predict the system state and the corresponding measurement. A gain matrix is constructed based on the statistical covariance of the system process noise and sensor measurement noise for the correction of model predictions. The Kalman filter can be employed to estimate parameters by extending the estimated state to include unknown parameters [70].

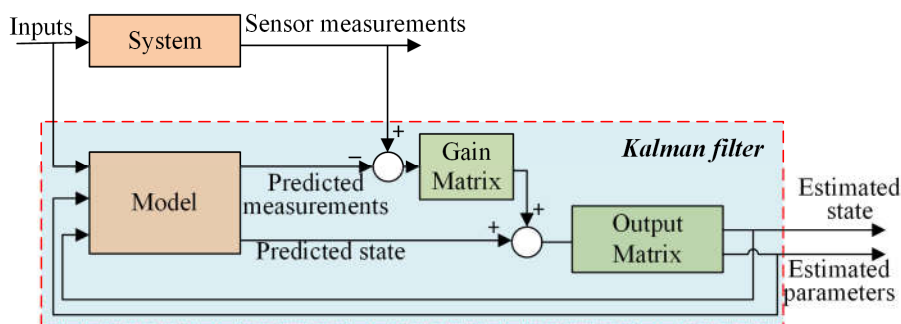


Figure 2-2 Block diagram for the Kalman filter [70]

Since the Kalman filter was first proposed, hundreds of enhanced versions have been developed and applied for different purposes. A Kalman filter-based innovation method was proposed in [71] to detect the lateral suspension faults in railway vehicles and it was demonstrated that the proposed method had the potential for online detection because it was computationally efficient. An interacting multiple-model algorithm was presented in [72], [73] to detect lateral suspension faults by applying the Kalman filter to each sub-model. This method was verified through a simulation study and it was found that it could identify the failure of the lateral damper. Multiple model Kalman filters were used in [74] to detect and isolate faults in a secondary vertical damper, secondary lateral damper and the anti-yaw damper all operating at the same time.

A robust fault detection observer was designed based on generalised Kalman-Yakubovich-Popov (GKYP) lemma to diagnose lateral damper failure [75]. The same research team adopted the Kalman filter to generate residuals for detecting a suspension system fault in a railway vehicle [76]–[78]. A distributed fault detection method was proposed by the same team in [79] for a light rail vehicle suspension system based on state estimation via the Kalman filter. However, all of the methods offered in [76]–[79] were verified by simulation not by experiment.

An observer-based fault detection was proposed in [80] for light rail vehicle suspension systems considering their nonlinearity, and the nonlinear characteristics of dampers in rail vehicle suspension systems were captured by a hybrid extended Kalman filter for fault detection and isolation [81]. In [82], a method denoted as a total measurable fault information residual was used to detect faults in high-speed rail vehicle suspension systems. This paper included a comparison study with classical observer residual-based methods and demonstrated the superiority of the total measurable fault residual method.

Recently, a cubature Kalman filter has been proposed as a solution for the CM of rail vehicle suspension systems [83]. The simulation results show that the cubature Kalman filter has the capability to identify secondary vertical damper faults accurately.

#### *ii) Parameter estimation based methods*

Parameter estimation means estimating the stiffness or damping values of railway vehicle suspension systems, and then the fault diagnosis can be performed by comparing the estimated values with the actual/theoretical values. As mentioned earlier, the Kalman filter can be used to estimate parameters, though there are many other methods suitable for parameter estimation, such as least-squares methods and subspace methods, etc.

An extended Kalman filter-based approach was employed to estimate the wheelsets conicity, the anti-yaw damping and the lateral damping [84]. Similarly, two types of extended Kalman filter and two types of unscented Kalman filter were employed for parameter estimation of rail vehicle secondary suspensions which considered uncertainties due to the track [85].

A Rao-Blackwellized particle filter-based method was presented in [86] for estimation of railway vehicle suspension parameters. The results indicated this is a promising method and it is worth noting the method was verified by real test data. An efficient recursive least

square-based method was proposed in [87] for CM of rail vehicle suspension systems, and this method was also verified by field test data.

A sliding mode-based parameter identification algorithm was proposed in [88] for fault detection of railway vehicle suspension systems. This method can identify the constant as well as time-varying parameters in a finite time. However, the method was validated only by simulated data.

An accurate model is desirable for the referred model-based approaches. However, developing an exact model is a big challenge in reality, and this restricts the application of model-based methods. Two decent overviews for model-based fault-detection of railway vehicle suspension systems can be found in [3], [69].

### **(b) Data-based methods**

As is well known, data-based approaches are widely used in CM, especially with the rapid development of computerised technology. Many of data-based methods are used for railway vehicle suspension monitoring. As shown in Figure 2-1, data-based methods can be classified into statistics-based, knowledge-based (neural networks) and signal-based.

#### *i) Statistics-based methods*

The approach presented in [89] is an excellent example of the statistics-based technique. The statistical parameters were treated in a multidimensional way to decrease their sensitivity to the track excitations. A further study by the same author is presented in [90] and shows that their statistics-based method is enable to detect different kinds of faults in railway vehicle suspension systems.

Wei et al., have explored various statistics-based methods for railway vehicle suspension monitoring [91]–[96]. In particular, Principle Component Analysis (PCA) and Canonical Variate Analysis-based methods were investigated in [91], [94], while Dempster-Shafer (D-S) evidence theory-based methods and Fisher Discriminant Analysis (FDA) were examined in [92], [93], [96]. From these investigations, the consensus was that PCA can identify early fault in suspensions, while the D-S evidence theory-based approach is more robust than the FDA based approach. Furthermore, the same research team compared data-based and model-based methods in [95] and by simulation found that the D-S evidence-based approach outperformed the FDA model based approach.

*ii) Knowledge-based methods*

Big data has become a hot topic in recent years, and many researchers are focusing on big data-based methods for railway vehicle suspension monitoring. In [97], a k-nearest fault classification method was proposed for rail vehicle suspensions based on collected mass data, and this method has been proven to be more reliable than using an artificial neural network.

Later, a new deep neural network was proposed in [98] for high-speed train suspension faults. Compared with classical intelligent diagnostic methods, the superiority of the latest deep neural network has been demonstrated but only by simulation. This deep neural network was further studied in [99]. The results shown that the average diagnosis rate of deep neural network could reach 98.3% with the quickest speed of converging to a critical value.

A similar fault diagnosis method for high-speed railway vehicles was presented in [100], which employed a long-short-term memory (LSTM) recurrent neural network as its basis. The effectiveness of this method was verified by fault data which was generated by a model developed in the multi-body simulation software SIMPACK. The results indicated that the LSTM recurrent neural network could extract the spatial and temporal correlation of fault features from collected signals with no need to preprocess the data or obtain the prior knowledge [100]. The accuracy of this method can be as high as 96.6%.

The convolutional recurrent neural network (CRNN) was explored in [101] as a means of high-speed railway vehicle suspension monitoring. The CRNN not only gave higher accuracy than conventional methods such as the LSTM recurrent neural network referred earlier but also had higher computational efficiency [101].

Fault diagnosis for high-speed train suspension systems was proposed in [102], using a single-layer neural network voting method to fuse multiple channels of data for diagnosing fault. This method was shown to achieve high accuracy for fault datasets generated by a SIMPACK model. The same authors have proposed another novel fault diagnosis method using the residual-squeeze net (RSNet) [103]. The RSNet combines the advantages of one-dimensional convolutional neural networks, residual structure and data fusion. Therefore, the RSNet method has high accuracy, up to 100%, and is robust under various running speeds [103].

*iii) Signal-based methods*

Signal-based methods are the oldest techniques for CM, and still dominate in real applications. A typical application of the signal-based method for railway vehicle suspension monitoring is correlation signal analysis. In 2008, a technique denoted as the “model-less technique” was presented in [104] for the fault detection of railway vehicle suspensions using cross-correlation of two signals collected from each of two bogies. The model-less technique has shown sensitivity and ability to diagnose different fault conditions. As the name of the method indicates, the major superiority of this method is that there is no need to deal with modelling the complex dynamics and nonlinearities of suspension systems. The model-less technique as applied to CM of rail vehicle suspension systems was extended by the same author in [105].

Recently, cross-correlation analysis was adopted by Li et al., to detect faults in heavy goods wagons, focused mainly on bogie bolster spring faults [106]. Only two tri-axial accelerometers were applied on the car body of each wagon to reduce cost while maintaining accuracy of fault diagnosis. However, the detectability of bolster spring faults obtained with this method was validated only through simulation studies. Further research on this topic by the same authors was reported in [107].

Cross-correlation analysis was again used in [108] to detect primary damper faults in railway vehicle suspension systems. The cross-correlation coefficient was obtained as the diagnostic parameter and it is worth noting that the feasibility of this method was verified by field test data.

Section 2.2.2 has reviewed the most common methods for fault detection and CM of railway vehicle suspension systems. The methods have been classified into different groups according to their algorithms.

### **2.3 OMA for condition monitoring**

Operational Modal Analysis (OMA) methods have developed dramatically in recent decades and could be used for railway vehicle suspension monitoring. In particular, OMA is promising as a means to achieve online monitoring, which is highly desirable for railway vehicle suspension systems. Therefore, as part of this PhD project, a novel method based on OMA is explored for use for vehicle suspension online monitoring. First, the conventional OMA methods are reviewed in this section.

OMA, also called output-only modal analysis, is used for dynamic system modal parameter identification. In other word, OMA methods only need responses to extract the modal parameters when the system is under ambient excitation. OMA is considered superior to conventional modal analysis techniques: Experimental Modal Analysis (EMA). Compared with EMA, the main advantages of OMA are [109]:

- 1) OMA is cheaper and more convenient than EMA since there is no need for artificial excitation;
- 2) OMA can obtain the dynamic characteristics of the whole tested system rather than just a part;
- 3) OMA can obtain a system's dynamic features under real operational conditions but not experimental conditions;
- 4) OMA is able to identify close modes;
- 5) OMA has the capability for online CM.

Because of these advantages, numerous OMA methods have been developed, and these are usually divided into frequency-domain and time-domain methods. The time-domain techniques can be further classified as two-stage and one-stage. The framework and processes of the most popular OMA methods are presented in Figure 2-3. The relevant studies and applications are reviewed below.

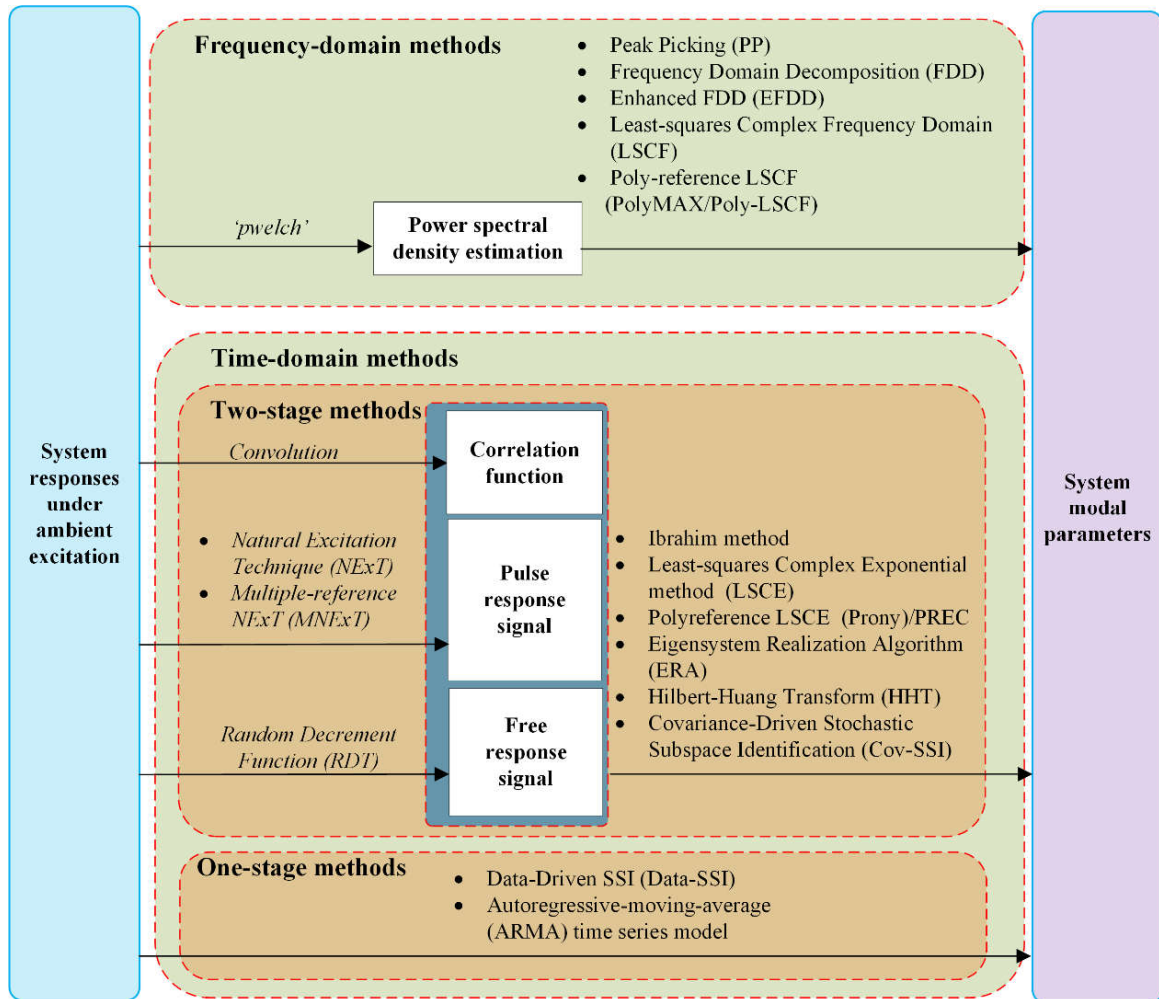


Figure 2-3 Framework and processes of popular OMA methods

### 2.3.1 Frequency-domain methods

For the frequency-domain methods, Peak-Picking (PP) is the simplest technique to estimate the modal parameters. PP is named after the key step of the method: picking the peaks from a spectrum plot as the identified eigenfrequencies [110]. The major issue with the PP method is the accuracy of the identified results, especially for a system with close modes.

Frequency Domain Decomposition (FDD) has been proposed based on the PP method [111]. The FDD technique overcomes the disadvantages of PP by decomposing the spectral density matrix into a set of Single-Degree of Freedom (SDOF) systems via Singular Value Decomposition (SVD). The FDD was widely used, and many enhanced methods were proposed based on FDD, such as Enhanced FDD (EFDD) [112], and Frequency-spatial Domain Decomposition (FSDD) [113].

In 2001, the Least Squares Complex Exponential (LSCE) method, a frequency domain method, was presented to cope with high system orders and high modal overlap, and to make the selection of the model order and relevant physical system poles easier [114]. Moreover, a Poly-reference LSCE method was proposed later to provide considerably improved pole stabilization [115]. Poly-reference LSCE is widely used in commercial modal test systems: LMS Test.Lab [115].

In 2004, an updated Poly-reference LSCF, called PolyMAX is employed by LMS system because this method has the capability to identify the closely space modes and high damping modes compared with other conventional approaches [115]. Such capability is on the basis of the clear Stabilization Diagram (SD) which contains frequency, damping and participation information. The SD identified by PolyMAX is clearer than the ones identified by other approaches. In order to increase the noise suppression ability, a PolyMAX Plus method was proposed by the same research team in 2012 [181]. The main development of PolyMAX Plus method is adding some maximum likelihood estimation features to properly handle the effects of uncertainty and estimate the confidence bounds, which can improve the identification results in case of very noisy data [181].

### **2.3.2 Time-domain methods**

As shown in Figure 2-3, time-domain methods can be divided into two groups: two-stage and one-stage methods. The first stage for the two-stage methods is usually to obtain the correlation, pulse response or free-response functions, and then the obtained functions are used to extract modal information in the second stage.

A good example of the two-stage approach is the Ibrahim Time Domain (ITD) method. The ITD method was first proposed in 1977 based on the Random Decrement Technique (RDT) for modal identification of structures [116], where RDT was employed in the first stage to obtain a free-response signal for the system under random excitation.

In 1985, Juang et al. proposed the Eigensystem Realization Algorithm (ERA) [117], [118] which also uses the free-response signal as obtained in the first stage. In 1995, the Natural Excitation Technique (NExT) was presented as a means of modal testing the permitted structures to be investigated in their actual environments. NExT, as ERA, also uses pulse response function obtained in the first stage [119]. The Covariance-Driven SSI (Cov-SSI)

was proposed in 1999 [120]. This is a robust OMA method employing the correlation function of system response as input.

For the one-stage methods, Data-Driven SSI (DD-SSI) [120] and Autoregressive Moving Average (ARMA) [121] methods are the two most popular approaches, using the collected raw data for modal identification.

### **2.3.3 Other methods**

Besides the classical time-domain and frequency-domain OMA methods reviewed, there have been many related techniques developed in recent years. For instance, a Bayesian approach was proposed, and appears to be becoming popular, for OMA [122], [123]. The uncertainty of system identification is addressed by the Bayesian approach, as the Bayesian approach take modal identification as an inference problem where probability is used as a measure for the relative plausibility of outcomes given both a model of the system and measured data [122].

In addition, transmissibility measurements for OMA are drawing increasing attention because of its ability to successfully extract modal parameters in the presence of harmonics [124]–[128]. While the poles of transmissibility measurements did not match with the poles of the measuring system, it was shown that modal parameters could be extracted by measuring the system's transmissibility when the system was under subject to different excitations [124].

Recently, an output-only damage identification method was presented in [129], [130], which was also developed on the fundamentals of OMA theory. This method combined with PCA theory can be a baseline-free approach. Its performance has been proved by numerical and experimental studies to detect and locate a damage site.

Several reviews of approaches for OMA can be found in [4], [110], [131], [132].

### **2.3.4 OMA applications**

As mentioned earlier, OMA has been widely used for CM in different areas and has been used to estimate the health status of historic buildings [133]–[135]. OMA is popular in the field of civil engineering for monitoring the health of structures, because it is hard to artificially excite buildings, whereas state-of-the-art OMA can accurately extract modal

parameters. For example, SSI was employed in [120] for SHM of a steel mast excited by wind and a bridge subject to normal traffic usage. The condition of an in-service three-span highway bridge was successfully assessed by SSI combined with a wireless sensor networks [136]. Also the dynamic behaviour of the Tamar Suspension Bridge have been investigated by SSI which took into account operational and environmental influences [137]. Generally, a real-time monitoring system is required for the monitoring of important buildings or bridges, with many of the monitoring systems based on OMA [138].

Secondly, OMA is widely used with wind turbines as a powerful means of CM [139]–[143]. In fact, the NExT was initially developed to identify the modal parameters of a parked wind turbine [119]. Moreover, there are many improved OMA algorithms to make them suitable for wind turbines operating under real conditions, these include the automated OMA methods presented in [141].

Last but not least, OMA is a powerful technique for the CM of mechanical systems, and numerous methods have been investigated [6], [117], [144]–[147]. For example, the Poly-reference LSCE and SSI were employed to identify the modal characterisation of the rear suspension of a family car during road tests as early as 1999 [144]. Recently, an improved SSI method was successfully applied to identify the dynamic characteristics of a car suspension system with the aim of using it for CM [54].

Besides, some researches compared the performance between different OMA approaches by implementing to identify the same structure using the same response. In [182], SSI, PolyMAX, ERA and FDD were employed to monitor a confederation bridge using the same datasets. The identification results from these four methods were compared with the modes calculated by the finite element model of the bridge. The identified results show a good correlation with the modal properties calculated by finite element model. Among the four methods, SSI is more consistent in the estimation of frequency, damping and mode shape. Furthermore, it is worth to highlight that SSI outperforms PolyMAX method in mode shape estimation. However, it is noticeable that all four method exhibit higher variance in damping estimation especially for ERA and FDD. Another comparative study can be found in [183] which presents similar conclusions.

It can be seen from this short review, OMA is a powerful and robust approach for SHM or CM of a system under ambient excitation or operating scenario. Note that SSI is an

outstanding algorithm on account of its robustness and accuracy, especially for vehicle suspension system monitoring which is mainly diagnosed according to the change of mode shape.

## **2.4 Findings**

This chapter has presented an overview of literature related to this PhD project. Based on the review, the following conclusions can be drawn:

- 1) CM is meaningful and significant for critical subsystems or components in a mechanical system;
- 2) Vibration-based CM methods are achievable, reliable and cost-efficient;
- 3) The vehicle suspension system has drawn considerable attention because it is critical to the safety and comfort of a vehicle, especially autonomous and high-speed railway vehicles;
- 4) An online CM is desirable for vehicle suspension systems, and the demand is growing with the rapidly increasing speed of railway vehicles and dramatically development of self-driving techniques;
- 5) OMA is a promising technique to achieve online CM;
- 6) SSI is one of the most robust OMA methods and has the potential to attain the goal of online monitoring of vehicle suspension systems.

Based on these findings, this thesis will try to develop an onboard, vibration-based vehicle suspension online CM technique based on SSI.

---

## CHAPTER 3 FRAMEWORKS OF STOCHASTIC SUBSPACE IDENTIFICATION

---

*A number of OMA approaches have been developed in recent years, and from the literature review presented in Chapter 2, it follows that Stochastic Subspace Identification (SSI) is one of the most robust output-only modal identification methods.*

*This chapter gives an overview of the theoretical basis of SSI, with the main focus on Covariance-driven SSI (Cov-SSI). In particular, this chapter describes the theoretical background of the state space model, SSI implementation, modal extraction and possible limitations.*

*This chapter lays the foundation for improving SSI performance for the online monitoring of vehicle suspension systems which will be demonstrated in the next chapter.*

### 3.1 Introduction

The literature review, Chapter 2, has shown that OMA is a practical approach to CM. It is worth mentioning that all basic OMA techniques are established on the fundamental assumptions that the identified system is linear, stationary and observable. Generally, a linear system implies that the response of the system under a specific combination of inputs is equal will always give the same combination of corresponding outputs; the stationarity of a system means its dynamic performances does not change over time, and the observability requires all interested dynamic characteristics can be measured by a proper sensor layout [148], [149].

The excitation is always assumed to be a stationary zero-mean Gaussian white noise. This is a fundamental premise in the field of OMA, and suggests the input is broadband excitation, and therefore all modes of the system can be equally excited [148].

Based on these assumptions, a number of OMA methods have been developed which were reviewed in Section 2.3. Among these referred to, SSI is an excellent OMA method, because of its strong mathematical basis. The first milestone in the development of the SSI method was in 1996 with the publication of *Subspace Identification for Linear Systems: Theory – Implementation – Application* by Van Overschee and Moore [150]. The second milestone in the development of SSI was in 1999 when reference-based SSI was proposed by Peeters and De Roeck [120]. After that, SSI was widely applied in a number of different areas, and many improved SSI methods were proposed for various applications.

It has been demonstrated in [54], [55], [144], [146] that SSI is a promising approach for vehicle suspension real-time CM, and this chapter will present a framework for SSI which acts as a basis for its development and application in the following chapters.

### 3.2 Vibration system dynamic models

A dynamic system can be expressed in different formats for different purposes. The typical dynamic models of vibration systems include the Frequency Response Function, Impulse Response Function, state-space model, Auto-Regressive Moving Average Vector model (ARMAV) and fraction polynomial models. This chapter introduces a framework for SSI,

which is based on the state-space model, and therefore only the state-space model will be explained here. Details of other dynamic models can be found in [149].

### 3.2.1 State-space model

The dynamic behaviour of a linear vibration system can be represented by a set of differential equations. Generally, the differential equations describe the motions of masses which are connected by springs and dampers within the system. For a vibration system with  $n_2$  Degree of Freedom ( $n_2$ -DOF) and  $m$  inputs, the dynamic behaviour can be described by the following linear, second-order differential equation in matrix form [118], [120], [149]:

$$\mathbf{M}\ddot{\mathbf{q}}(t) + \mathbf{C}_2\dot{\mathbf{q}}(t) + \mathbf{K}\mathbf{q}(t) = \mathbf{F}(t) = \mathbf{B}_2\mathbf{u}(t) \quad (3-1)$$

Where  $\mathbf{M}$ ,  $\mathbf{C}_2$  and  $\mathbf{K} \in \mathbb{R}^{n_2 \times n_2}$  denote the mass, damping, and stiffness matrices, respectively;  $\ddot{\mathbf{q}}(t)$ ,  $\dot{\mathbf{q}}(t)$ , and  $\mathbf{q}(t) \in \mathbb{R}^{n_2 \times 1}$  are the acceleration, velocity, and displacement vectors at a continuous-time  $t$ , respectively;  $\mathbf{F}(t) \in \mathbb{R}^{n_2 \times 1}$  is the excitation force. It can be seen that the excitation force vector  $\mathbf{F}(t)$  can be factorised into two matrices, where  $\mathbf{B}_2 \in \mathbb{R}^{n_2 \times m}$  describes the location of excitation, and  $\mathbf{u}(t) \in \mathbb{R}^{m \times 1}$  represents the  $m$  inputs in time.

The purpose of developing a state-space model is to convert the second-order problem into two first-order problems. The conversion process is as follows:

Firstly, the state vector can be defined as:

$$\mathbf{x}(t) = \begin{Bmatrix} \mathbf{q}(t) \\ \dot{\mathbf{q}}(t) \end{Bmatrix} \quad (3-2)$$

Secondly, two new matrices are introduced and defined as:

$$\mathbf{X} = \begin{bmatrix} \mathbf{C}_2 & \mathbf{M} \\ \mathbf{M} & \mathbf{0} \end{bmatrix}, \mathbf{Z} = \begin{bmatrix} \mathbf{K} & \mathbf{0} \\ \mathbf{0} & -\mathbf{M} \end{bmatrix} \quad (3-3)$$

And the inverse matrix of  $\mathbf{X}$  is:

$$\mathbf{X}^{-1} = \begin{bmatrix} \mathbf{0} & \mathbf{M}^{-1} \\ \mathbf{M}^{-1} & -\mathbf{M}^{-1}\mathbf{C}_2\mathbf{M}^{-1} \end{bmatrix}$$

Based on Equations (3-2) and (3-3), the second-order differential equation, Equation (3-1) can be converted into the first-order format:

$$\mathbf{X}\dot{\mathbf{x}}(t) + \mathbf{Z}\mathbf{x}(t) = \begin{bmatrix} \mathbf{B}_2 \\ \mathbf{0} \end{bmatrix} \mathbf{u}(t) \quad (3-4)$$

Then, the continuous state-space equation can be obtained by pre-multiplication by  $\mathbf{X}^{-1}$  of Equation (3-4):

$$\dot{\mathbf{x}}(t) = \mathbf{A}_c \mathbf{x}(t) + \mathbf{B}_c \mathbf{u}(t) \quad (3-5)$$

Where:

$$\mathbf{A}_c = -\mathbf{X}^{-1}\mathbf{Z} = \begin{bmatrix} \mathbf{0} & \mathbf{I} \\ -\mathbf{M}^{-1}\mathbf{K} & -\mathbf{M}^{-1}\mathbf{C}_2 \end{bmatrix} \quad (3-6)$$

$$\mathbf{B}_c = \mathbf{X}^{-1} \begin{bmatrix} \mathbf{B}_2 \\ \mathbf{0} \end{bmatrix} = \begin{bmatrix} \mathbf{0} \\ \mathbf{M}^{-1}\mathbf{B}_2 \end{bmatrix} \quad (3-7)$$

$\mathbf{A}_c \in \mathbb{R}^{n \times n}$  is the state matrix ( $n = 2n_2$ ) and  $\mathbf{B}_c \in \mathbb{R}^{n \times m}$  is the input matrix.

In practice, however, it is impossible to measure all the different motions of a dynamic system. If  $l$  sensors (accelerometers, velocity or displacement transducers) were employed to measure the dynamic response at different locations, the observation equation could be written as [118]:

$$\mathbf{y}(t) = \mathbf{C}_a \ddot{\mathbf{q}}(t) + \mathbf{C}_v \dot{\mathbf{q}}(t) + \mathbf{C}_d \mathbf{q}(t) \quad (3-8)$$

Where  $\mathbf{y}(t) \in \mathbb{R}^{l \times 1}$  are outputs;  $\mathbf{C}_a$ ,  $\mathbf{C}_v$  and  $\mathbf{C}_d \in \mathbb{R}^{l \times n_2}$  are the output matrices for acceleration, velocity and displacement, respectively, with the following definitions:

$$\mathbf{C}_c = [\mathbf{C}_d - \mathbf{C}_a \mathbf{M}^{-1} \mathbf{K} \quad \mathbf{C}_v - \mathbf{C}_a \mathbf{M}^{-1} \mathbf{C}_2] \quad (3-9)$$

$$\mathbf{D}_c = \mathbf{C}_a \mathbf{M}^{-1} \mathbf{B}_2 \quad (3-10)$$

The observation Equation (3-8) can be transformed into:

$$\mathbf{y}(t) = \mathbf{C}_c \mathbf{x}(t) + \mathbf{D}_c \mathbf{u}(t) \quad (3-11)$$

Where  $\mathbf{C}_c \in \mathbb{R}^{l \times n}$  is the output influence matrix and  $\mathbf{D}_c \in \mathbb{R}^{l \times m}$  is the direct transmission matrix.

Equations (3-5) and (3-11) constitute a continuous-time state-space model. However, the measured signal is invariably sampled at discrete time instants, and therefore the continuous-

time state-space model must be converted into a discrete-time format for convenience of application.

The continuous-time state-space model can be discretized according to the sampling rate ( $f_s$ ) during a test, by evaluating the continuous-time equation at all discrete-time instants,  $t = k\Delta t$ , ( $k \in \mathbb{N}$ ,  $\Delta t = 1/f_s$ ). Under the Zero Order Hold (ZOH) assumption, the discrete state-space model can be written as [149]:

$$\mathbf{x}_{k+1} = \mathbf{A}\mathbf{x}_k + \mathbf{B}\mathbf{u}_k \quad (3-12)$$

$$\mathbf{y}_k = \mathbf{C}\mathbf{x}_k + \mathbf{D}\mathbf{u}_k \quad (3-13)$$

Where  $\mathbf{x}_k = \mathbf{x}_k(k\Delta t)$  is the state vector in discrete-time; the subscript  $k$  is the time index of discrete signal;  $\mathbf{A}$  is the discrete state matrix;  $\mathbf{B}$  is the discrete input matrix;  $\mathbf{C}$  is the discrete output matrix and  $\mathbf{D}$  is the direct transmission matrix. In addition, the ZOH assumption indicates the input is piecewise constant over the sampling period [148], [151].

The relations between discrete-time matrices and the corresponding continuous-time matrices can be expressed as follows [149]:

$$\mathbf{A} = \mathbf{e}^{\mathbf{A}_c \Delta t} \quad (3-14)$$

$$\mathbf{B} = (\mathbf{A} - \mathbf{I})\mathbf{A}_c^{-1}\mathbf{B}_c \quad (3-15)$$

$$\mathbf{C} = \mathbf{C}_c \quad (3-16)$$

$$\mathbf{D} = \mathbf{D}_c \quad (3-17)$$

Where  $\mathbf{I}$  is a unit matrix in size of  $n \times n$ . The details of discretization are outside the scope of this study, but can be found in the literature, such as [118].

### 3.2.2 Stochastic state-space model

As only deterministic inputs are considered, it follows that the state-space model represented by Equations (3-12) and (3-13) is deterministic. However, stochastic components (noise) are inevitable in a field test. In particular, the stochastic components include process noise and model inaccuracies, and measurement noise that is the result of sensor inaccuracies. A combined deterministic-stochastic state-space model can be developed when stochastic components are considered, as follows [149]:

$$\mathbf{x}_{k+1} = \mathbf{A}\mathbf{x}_k + \mathbf{B}\mathbf{u}_k + \boldsymbol{\omega}_k \quad (3-18)$$

$$\mathbf{y}_k = \mathbf{C}\mathbf{x}_k + \mathbf{D}\mathbf{u}_k + \mathbf{v}_k \quad (3-19)$$

Where  $\boldsymbol{\omega}_k \in \mathbb{R}^{n \times 1}$  is the process noise;  $\mathbf{v}_k \in \mathbb{R}^{l \times 1}$  is the measurement noise. These noises are both unmeasurable, and therefore are usually assumed to be zero-mean Gaussian white noise [149]:

$$\mathbf{E}[\boldsymbol{\omega}_k] = 0, \mathbf{E}[\mathbf{v}_k] = 0 \quad (3-20)$$

with covariance matrices [120], [149]:

$$\mathbf{E} \left[ \begin{pmatrix} \boldsymbol{\omega}_p \\ \mathbf{v}_p \end{pmatrix} \begin{pmatrix} \boldsymbol{\omega}_q^T & \mathbf{v}_q^T \end{pmatrix} \right] = \begin{pmatrix} \mathbf{Q} & \mathbf{S} \\ \mathbf{S}^T & \mathbf{R} \end{pmatrix} \delta_{pq} \quad (3-21)$$

Where  $\mathbf{E}$  is the expected value of the operator;  $\delta_{pq}$  is the Kronecker delta (if  $p = q$ ,  $\delta_{pq} = 1$ , otherwise  $\delta_{pq} = 0$ ),  $p$  and  $q$  represent two arbitrary time instants. Moreover, the framework of OMA concerning the input  $\mathbf{u}_k$  is unmeasurable. Hence the input  $\mathbf{u}_k$  is implicitly modelled in the noise terms  $\boldsymbol{\omega}_k$  and  $\mathbf{v}_k$  [148]. As a consequence, a discrete-time stochastic state-space model is obtained:

$$\mathbf{x}_{k+1} = \mathbf{A}\mathbf{x}_k + \boldsymbol{\omega}_k \quad (3-22)$$

$$\mathbf{y}_k = \mathbf{C}\mathbf{x}_k + \mathbf{v}_k \quad (3-23)$$

It is worth mentioning that the white noise zero-mean assumption concerning  $\boldsymbol{\omega}_k$  and  $\mathbf{v}_k$  is significant for the OMA method. If the assumption of white noise input is violated, extra poles (false modes) may appear in the state matrix,  $\mathbf{A}$ , and the spurious modes cannot be distinguished from true ones. Besides the input white noise assumption, the stochastic state-space model is also characterized by other properties [148]. Firstly, the stochastic process has to be stationary with zero mean:

$$\mathbf{E}[\mathbf{x}_k \mathbf{x}_k^T] = \boldsymbol{\Sigma}, \mathbf{E}[\mathbf{x}_k] = \mathbf{0} \quad (3-24)$$

Where  $\boldsymbol{\Sigma}$  is the state covariance matrix. Equation (3-24) indicates  $\boldsymbol{\Sigma}$  is independent of time  $k$ . Moreover, as the stochastic noises  $\boldsymbol{\omega}_k$  and  $\mathbf{v}_k$  are independent of the state  $\mathbf{x}_k$ , the following equations can be obtained:

$$\mathbf{E}[\mathbf{x}_k \boldsymbol{\omega}_k^T] = \mathbf{0}, \mathbf{E}[\mathbf{x}_k \mathbf{v}_k^T] = \mathbf{0} \quad (3-25)$$

Based on the referred properties of the stochastic state-space model, the covariance matrix of the state vector  $\mathbf{x}_k$  can be calculated as follows:

$$\begin{aligned}
 \Sigma &= \mathbf{E}[\mathbf{x}_{k+1}\mathbf{x}_{k+1}^T] \\
 &= \mathbf{E}[(\mathbf{A}\mathbf{x}_k + \boldsymbol{\omega}_k)(\mathbf{A}\mathbf{x}_k + \boldsymbol{\omega}_k)^T] \\
 &= \mathbf{A}\mathbf{E}[\mathbf{x}_k\mathbf{x}_k^T]\mathbf{A}^T + \mathbf{A}\mathbf{E}[\mathbf{x}_k\boldsymbol{\omega}_k^T] \\
 &\quad + \mathbf{E}[\mathbf{x}_k\boldsymbol{\omega}_k^T]\mathbf{A}^T + \mathbf{E}[\boldsymbol{\omega}_k\boldsymbol{\omega}_k^T] \\
 &= \mathbf{A}\Sigma\mathbf{A}^T + \mathbf{Q}
 \end{aligned} \tag{3-26}$$

$\mathbf{G}$ , the covariance matrix of the state vector  $\mathbf{x}_k$  and output  $\mathbf{y}_k$ , can be calculated as:

$$\begin{aligned}
 \mathbf{G} &= \mathbf{E}[\mathbf{x}_{k+1}\mathbf{y}_k^T] \\
 &= \mathbf{E}[(\mathbf{A}\mathbf{x}_k + \boldsymbol{\omega}_k)(\mathbf{C}\mathbf{x}_k + \mathbf{v}_k)^T] \\
 &= \mathbf{A}\mathbf{E}[\mathbf{x}_k\mathbf{x}_k^T]\mathbf{C}^T + \mathbf{A}\mathbf{E}[\mathbf{x}_k\mathbf{v}_k^T] \\
 &\quad + \mathbf{E}[\boldsymbol{\omega}_k\mathbf{x}_k^T]\mathbf{C}^T + \mathbf{E}[\boldsymbol{\omega}_k\mathbf{v}_k^T] \\
 &= \mathbf{A}\Sigma\mathbf{C}^T + \mathbf{S} \quad (\mathbf{G} \in \mathbb{R}^{n \times l})
 \end{aligned} \tag{3-27}$$

The covariance matrix of the output vector  $\mathbf{y}_k$ ,  $\Lambda_0$ , can be calculated as:

$$\begin{aligned}
 \Lambda_0 &= \mathbf{E}[\mathbf{y}_k\mathbf{y}_k^T] \\
 &= \mathbf{E}[(\mathbf{C}\mathbf{x}_k + \mathbf{v}_k)(\mathbf{C}\mathbf{x}_k + \mathbf{v}_k)^T] \\
 &= \mathbf{C}\mathbf{E}[\mathbf{x}_k\mathbf{x}_k^T]\mathbf{C}^T + \mathbf{C}\mathbf{E}[\mathbf{x}_k\mathbf{v}_k^T] \\
 &\quad + \mathbf{E}[\mathbf{v}_k\mathbf{x}_k^T]\mathbf{C}^T + \mathbf{E}[\mathbf{v}_k\mathbf{v}_k^T] \\
 &= \mathbf{C}\Sigma\mathbf{C}^T + \mathbf{R}
 \end{aligned} \tag{3-28}$$

Moreover, the state  $\mathbf{x}_{k+i}$  can be obtained by iterative computing of Equation (3-22):

$$\begin{aligned}
 \mathbf{x}_{k+1} &= \mathbf{A}\mathbf{x}_k + \boldsymbol{\omega}_k \\
 \mathbf{x}_{k+2} &= \mathbf{A}\mathbf{x}_{k+1} + \boldsymbol{\omega}_{k+1} \\
 &= \mathbf{A}(\mathbf{A}\mathbf{x}_k + \boldsymbol{\omega}_k) + \boldsymbol{\omega}_{k+1} \\
 &= \mathbf{A}^2\mathbf{x}_k + \mathbf{A}\boldsymbol{\omega}_k + \boldsymbol{\omega}_{k+1} \\
 &\quad \vdots \\
 \mathbf{x}_{k+i} &= \mathbf{A}^i\mathbf{x}_k + \mathbf{A}^{i-1}\boldsymbol{\omega}_k + \mathbf{A}^{i-2}\boldsymbol{\omega}_{k+1} \\
 &\quad + \cdots + \mathbf{A}\boldsymbol{\omega}_{k+i-2} + \boldsymbol{\omega}_{k+i-1}
 \end{aligned} \tag{3-29}$$

Where the subscript  $i$  is the time lag.

Then, the covariance matrix of  $\mathbf{y}_{k+i}$  and  $\mathbf{y}_k$ ,  $\Lambda_i$ , can be calculated based on Equation (3-29):

$$\begin{aligned}
\Lambda_i &= E[\mathbf{y}_{k+i}\mathbf{y}_k^T] \\
&= E[(\mathbf{C}\mathbf{x}_{k+i} + \mathbf{v}_{k+i})(\mathbf{C}\mathbf{x}_k + \mathbf{v}_k)^T] \\
&= E\{\mathbf{C}\{\mathbf{A}^i\mathbf{x}_k + \mathbf{A}^{i-1}\boldsymbol{\omega}_k + \mathbf{A}^{i-2}\boldsymbol{\omega}_{k+1} \\
&\quad + \cdots + \mathbf{A}\boldsymbol{\omega}_{k+i-2} + \boldsymbol{\omega}_{k+i-1}\} + \mathbf{v}_{k+i}\} \\
&\quad (\mathbf{C}\mathbf{x}_k + \mathbf{v}_k)^T\} \\
&= \mathbf{C}\mathbf{A}^i E[\mathbf{x}_k\mathbf{x}_k^T]\mathbf{C}^T + \mathbf{C}\mathbf{A}^{i-1} E[\boldsymbol{\omega}_k\mathbf{v}_k^T] \\
&= \mathbf{C}\mathbf{A}^i \boldsymbol{\Sigma}\mathbf{C}^T + \mathbf{C}\mathbf{A}^{i-1} \mathbf{S} \\
&= \mathbf{C}\mathbf{A}^{i-1}(\mathbf{A}\boldsymbol{\Sigma}\mathbf{C}^T + \mathbf{S}) \\
&= \mathbf{C}\mathbf{A}^{i-1} \mathbf{G} \quad (\Lambda_i \in \mathbb{R}^{l \times l})
\end{aligned} \tag{3-30}$$

The properties represented by Equations (3-26), (3-27), (3-28) and (3-30) imply that the measured data can estimate the output covariance sequence of a stochastic system. In other words, the state-space matrix of the tested system can be obtained by decomposing the estimated output covariance sequence,  $\Lambda_i$ , according to Equations (3-26), (3-27), (3-28) and (3-30), and then the modal parameters of interest can be extracted from the state-space matrix.

### 3.3 Stochastic Subspace Identification (SSI)

This section introduces a basic SSI method for modal parameter identification.

Numerous OMA schemes have been developed on the basis of state-space theory which was introduced in Section 3.2, such as the ARMA and SSI. Two basic SSI methods were proposed: Covariance-driven SSI (Cov-SSI) and Data-Driven SSI (DD-SSI) [114], [142], and [145]. However, the DD-SSI is more time-consuming than Cov-SSI since DD-SSI has to perform QR decomposition [120], [148], [149]. The purpose of this PhD project is to develop an online monitoring system, so computational efficiency is a significant issue, and Cov-SSI is selected as the framework of the following study. Therefore, this section will introduce the Cov-SSI procedure in detail. The introduction will begin with some notations used for SSI.

#### 3.3.1 Notations of Stochastic Subspace Identification

In a real field test, the tested structure could be enormous, and therefore, a vast number of sensors would be needed to obtain all full mode shapes. However, increasing the number of sensors means increasing the cost of a test. Therefore, the reference outputs of the SSI as recommended in [114] and [145] are employed to cope with such a challenge. Notably, the outputs of a large structure will be determined by dividing the scheduled measuring points

into several groups with overlapping sensors, where the overlapping sensors are the reference outputs. Moreover, the candidates for reference outputs are the sensors mounted at locations which contain all the modes in the measured data [120]. That is to say, the reference outputs should not be located at structural nodes. Another advantage of using reference outputs is retaining phase information when averaging to reduce the noise.

If there are  $l$  sensors arranged to measure the response and  $r$  of them were selected as reference outputs, the response can be written as [120]:

$$\mathbf{y}_k = \begin{pmatrix} \mathbf{y}_k^{ref} \\ \tilde{\mathbf{y}}_k^{ref} \end{pmatrix}, \mathbf{y}_k^{ref} = \mathbf{L}\mathbf{y}_k, \mathbf{L} = [\mathbf{I}_r \quad \mathbf{0}] \quad (3-31)$$

Where  $\mathbf{y}_k^{ref} \in \mathbb{R}^{r \times 1}$  are the reference outputs;  $\tilde{\mathbf{y}}_k^{ref} \in \mathbb{R}^{(l-r) \times 1}$  are the other outputs; the subscript  $k$  is the index of discrete sampling time;  $\mathbf{L} \in \mathbb{R}^{r \times l}$  is the matrix of selected reference outputs;  $\mathbf{I}_r$  is a unit matrix in size of  $r \times r$ . Then, the covariance matrices between all outputs vector  $\mathbf{y}_{k+i}$  and the reference outputs  $\mathbf{y}_k^{ref}$  can be calculated as [120]:

$$\mathbf{\Lambda}_i^{ref} = \mathbf{E} \left[ \mathbf{y}_{k+i} \mathbf{y}_k^{refT} \right] = \mathbf{\Lambda}_i \mathbf{L}^T \in \mathbb{R}^{l \times r} \quad (3-32)$$

As can be seen, Equation (3-32) is similar to (3-30). The covariance matrices between state vectors  $\mathbf{x}_{k+1}$  and reference outputs  $\mathbf{y}_k^{ref}$  can be obtained as Equation (3-33), which is similar to (3-27):

$$\mathbf{G}^{ref} = \mathbf{E} \left[ \mathbf{x}_{k+1} \mathbf{y}_k^{refT} \right] = \mathbf{G} \mathbf{L}^T \in \mathbb{R}^{n \times r} \quad (3-33)$$

The import property expressed in Equation (3-30) can also be written as:

$$\mathbf{\Lambda}_i^{ref} = \mathbf{E} \left[ \mathbf{y}_{k+i} \mathbf{y}_k^{refT} \right] = \mathbf{C} \mathbf{A}^{i-1} \mathbf{G}^{ref} \quad (3-34)$$

A block Hankel matrix, with  $2i$  rows and  $j$  columns and constant along its anti-diagonal, can be constructed using the measured outputs  $\mathbf{y}$ . Where  $j$  is also the time lag. In particular, the first  $i$  blocks have  $r$  rows, the last  $i$  blocks have  $l$  rows, and  $j$  is assumed to be infinite ( $j \rightarrow \infty$ ) for the statistical proof of the method. In addition, the Hankel matrix  $\mathbf{H} \in \mathbb{R}^{(r+l)i \times j}$  can be partitioned into two sub-matrices: “past” reference matrix  $\mathbf{Y}_p^{ref}$  and “future” matrix  $\mathbf{Y}_f$ :

$$\mathbf{H} = \frac{1}{\sqrt{j}} \begin{pmatrix} \mathbf{y}_0^{ref} & \mathbf{y}_1^{ref} & \cdots & \mathbf{y}_{j-1}^{ref} \\ \mathbf{y}_1^{ref} & \mathbf{y}_2^{ref} & \cdots & \mathbf{y}_j^{ref} \\ \vdots & \vdots & \ddots & \vdots \\ \mathbf{y}_{i-1}^{ref} & \mathbf{y}_i^{ref} & \cdots & \mathbf{y}_{i+j-2}^{ref} \\ \mathbf{y}_i & \mathbf{y}_{i+1} & \cdots & \mathbf{y}_{i+j-1} \\ \mathbf{y}_{i+1} & \mathbf{y}_{i+2} & \cdots & \mathbf{y}_{i+j} \\ \vdots & \vdots & \ddots & \vdots \\ \mathbf{y}_{2i-1} & \mathbf{y}_{2i} & \cdots & \mathbf{y}_{2i+j-2} \end{pmatrix} = \begin{pmatrix} \mathbf{Y}_{0|i-1}^{ref} \\ \mathbf{Y}_{i|2i-1} \end{pmatrix} \quad (3-35)$$

$$\mathbf{H} = \begin{pmatrix} \mathbf{Y}_{0|i-1}^{ref} \\ \mathbf{Y}_{i|2i-1} \end{pmatrix} = \begin{pmatrix} \mathbf{Y}_p^{ref} \\ \mathbf{Y}_f \end{pmatrix} \begin{matrix} \uparrow ri \text{ "past"} \\ \downarrow li \text{ "future"} \end{matrix} \in \mathbb{R}^{(r+l)i \times j} \quad (3-36)$$

In reality, the data length ( $N_d$ ) of the sampled signal is not infinite, so we have to ensure  $2i + j - 2 < N_d$  when we select the time lag  $i$  and  $j$ . Usually, we set  $j = N_d - 2 * i - 1$ .

The outputs are scaled by  $1/\sqrt{j}$  to maintain their compatibility with the definition of the correlation function as given in the following calculation. The extended observability matrix is defined as:

$$\mathbf{O}_i = \begin{pmatrix} \mathbf{C} \\ \mathbf{CA} \\ \mathbf{CA}^2 \\ \vdots \\ \mathbf{CA}^{i-1} \end{pmatrix} \in \mathbb{R}^{li \times n} \quad (3-37)$$

The matrix pair  $\{\mathbf{A}, \mathbf{C}\}$  is assumed to be observable, that is to say, all the dynamic modes of a system can be observed from the measured data [120]. Additionally, the reference reversed extended stochastic controllability matrix is defined as:

$$\mathbf{C}_i^{ref} = (\mathbf{A}^{i-1} \mathbf{G}^{ref} \quad \mathbf{A}^{i-2} \mathbf{G}^{ref} \quad \cdots \quad \mathbf{A} \mathbf{G}^{ref} \quad \mathbf{G}^{ref}) \quad (3-38)$$

Where  $\mathbf{C}_i^{ref} \in \mathbb{R}^{n \times ri}$ , and the matrix pair  $\{\mathbf{A}, \mathbf{G}^{ref}\}$  is assumed to be controllable, which implies that all the dynamic modes of the system can be excited by the stochastic input.

In short, this subsection introduced the frequently used notations in the SSI algorithms, more details of these notations can be found in [120], [148] and [149]. In the following section details of Cov-SSI will be outlined.

### 3.3.2 Covariance-Driven Stochastic Subspace Identification (Cov-SSI)

Essentially, the Cov-SSI method solves the stochastic realisation problem, which is concerned with identifying a stochastic state-space model using output data only. This

method derives from classical system realisation theory which knows input and output, and the minimal realisation theory as developed by Ho and Kalman [118], [148], [149].

According to its character, Cov-SSI can be classified as a time-domain, parametric, covariance-driven OMA method. The first step is to calculate the covariance matrices using Equation (3-34). Then, these covariance matrices can be gathered into a block Toeplitz matrix which is constant along its diagonal [120]:

$$\mathbf{T}_{1|i}^{ref} = \begin{pmatrix} \Lambda_i^{ref} & \Lambda_{i-1}^{ref} & \cdots & \Lambda_1^{ref} \\ \Lambda_{i+1}^{ref} & \Lambda_i^{ref} & \cdots & \Lambda_2^{ref} \\ \vdots & \vdots & \ddots & \vdots \\ \Lambda_{2i-1}^{ref} & \Lambda_{2i-2}^{ref} & \cdots & \Lambda_i^{ref} \end{pmatrix} \in \mathbb{R}^{li \times ri} \quad (3-39)$$

It can be seen from Equations (3-35) and (3-36) that the block Toeplitz matrix  $\mathbf{T}_{1|i}^{ref}$  is equal to [120]:

$$\mathbf{T}_{1|i}^{ref} = \mathbf{Y}_f \mathbf{Y}_p^{refT} \quad (3-40)$$

Based on Equations (3-34), (3-37) and (3-38), the Toeplitz matrix  $\mathbf{T}_{1|i}^{ref}$  can be decomposed as [120]:

$$\begin{aligned} \mathbf{T}_{1|i}^{ref} &= \begin{pmatrix} \mathbf{C} \\ \mathbf{CA} \\ \mathbf{CA}^2 \\ \vdots \\ \mathbf{CA}^{i-1} \end{pmatrix} (\mathbf{A}^{i-1} \mathbf{G}^{ref} \quad \cdots \quad \mathbf{A} \mathbf{G}^{ref} \quad \mathbf{G}^{ref}) \\ &= \mathbf{O}_i \mathbf{C}_i^{ref} \end{aligned} \quad (3-41)$$

The observability matrix  $\mathbf{O}_i$  and controllability matrix  $\mathbf{C}_i^{ref}$  can be obtained by conducting Singular Value Decomposition (SVD) of the block Toeplitz matrix  $\mathbf{T}_{1|i}^{ref}$  [120]:

$$\begin{aligned} \mathbf{T}_{1|i}^{ref} &= \mathbf{USV}^T = (\mathbf{U}_1 \quad \mathbf{U}_2) \begin{pmatrix} \mathbf{S}_1 & \mathbf{0} \\ \mathbf{0} & \mathbf{0} \end{pmatrix} \begin{pmatrix} \mathbf{V}_1^T \\ \mathbf{V}_2^T \end{pmatrix} \\ &= \mathbf{U}_1 \mathbf{S}_1 \mathbf{V}_1^T = \left( \mathbf{U}_1 \mathbf{S}_1^{\frac{1}{2}} \right) \left( \mathbf{S}_1^{\frac{1}{2}} \mathbf{V}_1^T \right) = \mathbf{O}_i \mathbf{C}_i^{ref} \end{aligned} \quad (3-42)$$

Where  $\mathbf{U} \in \mathbb{R}^{li \times li}$  and  $\mathbf{V} \in \mathbb{R}^{ri \times ri}$  are orthonormal matrices, which means  $\mathbf{U}^T \mathbf{U} = \mathbf{U} \mathbf{U}^T = \mathbf{I} \in \mathbb{R}^{li \times li}$  and  $\mathbf{V}^T \mathbf{V} = \mathbf{V} \mathbf{V}^T = \mathbf{I} \in \mathbb{R}^{ri \times ri}$ ;  $\mathbf{S} \in \mathbb{R}^{li \times ri}$  is a diagonal matrix which contains

the singular values in descending order. Because  $\mathbf{T}_{1|i}^{ref} \in \mathbb{R}^{li \times ri}$  and its inner dimension is  $n$ , it means the number of block  $i$  has to fulfil the condition that:

$$ri \geq n$$

Moreover, it is apparent from the last equality of Equation (3-42) that:

$$\begin{aligned} \mathbf{O}_i &= \mathbf{U}_1 \mathbf{S}_1^{\frac{1}{2}} \\ \mathbf{C}_i^{ref} &= \mathbf{S}_1^{\frac{1}{2}} \mathbf{V}_1^T \end{aligned} \quad (3-43)$$

Where the zero singular values in  $\mathbf{S}_1$  are omitted, and the corresponding vectors are also eliminated.

With the observability matrix  $\mathbf{O}_i$  and controllability matrix  $\mathbf{C}_i^{ref}$ , the state matrix  $\mathbf{A}$  can be directly identified from a shifted block Toeplitz matrix  $\mathbf{T}_{2|i+1}^{ref}$ :

$$\mathbf{T}_{2|i+1}^{ref} = \begin{pmatrix} \Lambda_{i+1}^{ref} & \Lambda_i^{ref} & \cdots & \Lambda_2^{ref} \\ \Lambda_{i+2}^{ref} & \Lambda_{i+1}^{ref} & \cdots & \Lambda_3^{ref} \\ \vdots & \vdots & \ddots & \vdots \\ \Lambda_{2i}^{ref} & \Lambda_{2i-1}^{ref} & \cdots & \Lambda_{i+1}^{ref} \end{pmatrix} = \mathbf{O}_i \mathbf{A} \mathbf{C}_i^{ref} \quad (3-44)$$

$$\mathbf{A} = \mathbf{O}_i^\dagger \mathbf{T}_{2|i+1}^{ref} \mathbf{C}_i^{ref \dagger} = \mathbf{S}_1^{-\frac{1}{2}} \mathbf{U}_1^T \mathbf{T}_{2|i+1}^{ref} \mathbf{V}_1 \mathbf{S}_1^{-\frac{1}{2}} \quad (3-45)$$

Where  $(\blacksquare)^\dagger$  represents the pseudo-inverse of a matrix.

Moreover, it can be seen from Equations (3-37) and (3-38) that the first  $l$  rows of the observability matrix  $\mathbf{O}_i$  is the output matrix  $\mathbf{C}$ .

At this point, the problem of the stochastic state-space model identification is theoretically solved. Nonetheless, the Cov-SSI has two shortcomings in real applications, which are significant. First, in the real world, the data length is not infinite ( $j \neq \infty$ ), and therefore the covariance values computed by Equation (3-40) are only estimates [120]. Secondly, the system order  $n$  is difficult to determine. In theory, it can be determined by inspecting the number of non-zero singular values of the Toeplitz matrix  $\mathbf{T}_{1|i}^{ref}$  calculated by SVD in Equation (3-42). However, the higher singular values are not exactly zero on account of

measurement and computational noises [120]. As a consequence, the model order is usually over-specified.

Eliminating the spurious numerical poles by constructing a Stabilisation Diagram (SD) will be introduced in detail in Section 3.3.4.

### 3.3.3 Modal parameter extraction

From Section 3.3.2 a stochastic state-space model has been identified which uses output data only, and which belongs to the area of system identification. Modal analysis is also considered as a particular type of system identification which describes the behaviour of a system by means of vibration modes, rather than in terms of mathematical parameters. The parameters used to describe a vibration mode include a resonant frequency, a damping ratio and a mode shape [120].

A system's modal parameters can be extracted analytically from the state matrix  $\mathbf{A}$ :

$$\mathbf{A} = \mathbf{\Psi}\mathbf{\Gamma}\mathbf{\Psi}^{-1} \quad (3-46)$$

Where  $\mathbf{\Gamma} = \text{diag}\{\lambda_i\}$  is a diagonal matrix containing the discrete-time complex eigenvalues,  $\mathbf{\Psi}$  is a matrix containing the corresponding discrete-time eigenvectors as columns.  $\mathbf{\Gamma}$  and  $\mathbf{\Psi}$  can be obtained by performing an eigenvalue decomposition on the state matrix  $\mathbf{A}$ . On the basis of the relations expressed in Equations (3-12) and (3-13), the following equation can be obtained [118]:

$$\mathbf{A} = \exp(\mathbf{A}_c\Delta t) \quad (3-47)$$

Therefore, the continuous-time eigenvalues,  $\lambda_{ci}$ , and corresponding eigenvectors,  $\mathbf{\Psi}_c$ , can be expressed as:

$$\begin{aligned} \lambda_{ci} &= \frac{\ln(\lambda_i)}{\Delta t} \\ \mathbf{\Psi}_c &= \mathbf{\Psi} \end{aligned} \quad (3-48)$$

Where the  $\lambda_i$  is the eigenvalues of discrete state matrix  $\mathbf{A}$ . The continuous-time eigenvalues,  $\lambda_{ci}$ , occur in complex conjugate pairs and can be written as:

$$\lambda_{ci}, \lambda_{ci}^* = a_i \pm jb_i, \quad (j = \sqrt{-1}) \quad (3-49)$$

Where  $a_i$  and  $b_i$  are the real and imaginary parts, respectively. At this point, the system's resonant frequencies and damping ratios can be calculated using the following equations [120]:

$$f_i = \frac{\sqrt{a_i^2 + b_i^2}}{2\pi} \quad (3-50)$$

$$\xi_i = \frac{-a_i}{\sqrt{a_i^2 + b_i^2}} \quad (3-51)$$

In addition, the mode shapes can be calculated as:

$$\Phi = C\Psi \quad (3-52)$$

Where  $C$  is the discrete output matrix. Thus the modal parameters, including natural frequencies, damping ratios and mode shapes, of a system have been identified.

In order to clarify the Cov-SSI process it is summarized in a flow chart, as shown in Figure 3-1.

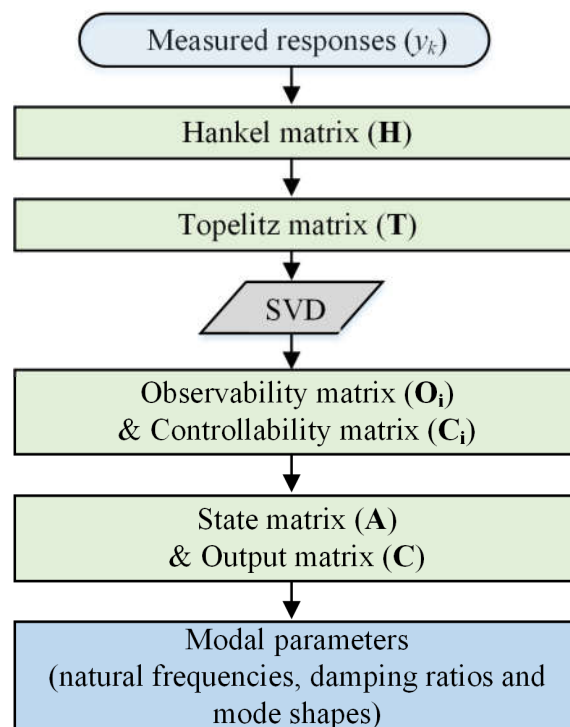


Figure 3-1 Flowchart of Cov-SSI

### 3.3.4 Stabilisation Diagram (SD)

The stabilization diagram (SD) is a powerful tool and frequently employed to filter out spurious modes which can be either due to noise or the mathematical processes used. A SD presents the poles of a system at different model orders [151], that is to say, the Hankel matrix expressed in Equation (3-35) has different block rows by setting continually varying time lag  $i$ . According to Equations (3-39), (3-42) and (3-45), the time lag  $i$  can determine the size of the identified state matrix  $\mathbf{A}$ , so  $i$  is also denoted as the order or the row number of the state matrix.

The stable poles are obtained by comparing the errors in modal parameters obtained from two successive orders. The errors include frequency error ( $\varepsilon_f$ ), damping error ( $\varepsilon_\xi$ ) and mode shape error ( $\varepsilon_{MAC}$ ). Where MAC stands for Modal Assurance Criterion. An error threshold is set for the stable pole which has to satisfy the three error thresholds simultaneously. The errors can be calculated as follows:

$$\frac{f_i - f_{i-1}}{f_i} \times 100\% < \varepsilon_f \quad (3-53)$$

$$\frac{\xi_i - \xi_{i-1}}{\xi_i} \times 100\% < \varepsilon_\xi \quad (3-54)$$

$$MAC(i:i-1) = \frac{|\Phi_i^T \Phi_i|^2}{(\Phi_i^T \Phi_i)(\Phi_{i-1}^T \Phi_{i-1})} \quad (3-55)$$

$$1 - MAC(i:i-1) < \varepsilon_{MAC} \quad (3-56)$$

Where  $f_i$ ,  $\xi_i$  and  $\Phi_i$  are the modal parameters identified when the system order (number of Hankel matrix rows) is  $i$ , which is same as the  $i$  in Eq. (3-34). The spurious modes caused by noise can be filtered out using a SD. However, the SD will not remove the spurious modes resulting from harmonic excitation, this will be discussed in Chapter 5.

Moreover, in this thesis a second threshold is set to identify the relative stable modes based on the SD results. The second threshold is obtained as a percentage by dividing the number of stable points,  $N$ , by the calculated maximum number of orders,  $M$ :

$$\delta = \frac{N}{M} \times 100\% \quad (3-57)$$

$\delta$  is called the rate of stable points, which is an important threshold to identify the system's modes and filter out the false modes. The value of  $\delta$  is determined by the real application

scenario, or the experience. However, it is worth to highlight that a higher value of  $\delta$  indicates a more reliable identification results. According to the previous studies [54], [155], the value of  $\delta$  should be over 0.5 to ensure the reliability of the identified results.

### 3.4 Findings

The primary purpose of this chapter was to review the theoretical background of Cov-SSI and the following advantages of Cov-SSI have been determined:

- 1) Cov-SSI is a reliable and robust approach for OMA since it has been developed on the basis of linear algebra theory;
- 2) Cov-SSI is effective for noise reduction due to the application of SVD during the process;
- 3) Cov-SSI needs lower computation sources with respect to other OMA methods such as DD-SSI and Poly-reference LSCE;
- 4) Cov-SSI is suitable for the identification of close modes.

Based on these advantages, Cov-SSI has been selected as the fundamental algorithm to develop the online monitoring system for vehicle suspension systems. However, Cov-SSI is developed under the assumption that the excitation is white noise and the system is linear, but the white noise assumption is not valid for a real vehicle running on a road/track, and real suspension systems are highly nonlinear. Therefore, Cov-SSI has to be modified and improved for reliable online modal identification of vehicle suspension systems. The enhanced method will be introduced in the next chapter.

---

---

## CHAPTER 4 CORRELATION SIGNAL SUBSET-BASED STOCHASTIC SUBSPACE IDENTIFICATION

---

---

*A novel method, Correlation Signal Subset-based SSI (CoSS-SSI), based on the fundamental SSI method as introduced in Chapter 3 is proposed in this chapter as a basis for the online monitoring of vehicle suspensions.*

*First, the theoretical background of CoSS-SSI is presented, and then the detailed procedure of CoSS-SSI is given. Last but not least, a 3-DOF vibration system is employed to evaluate the performance of the CoSS-SSI.*

*The results indicate that the CoSS-SSI has the capability to identify modal parameters from nonstationary responses contaminated with high noise levels, producing results which are superior to conventional OMA methods.*

## 4.1 Introduction

The aim of this PhD project is to develop an online monitoring system for vehicle suspensions via OMA. Based on a literature review and overview of its mathematical background, Cov-SSI has been selected as the appropriate approach for OMA. However, Cov-SSI, as other output-only methods, must fulfil the two critical assumptions regarding white noise excitation and linear system which are difficult to satisfy in the field tests.

For instance, the excitation from the road/track is never entirely a white noise source for a running vehicle. In addition, vehicle suspension systems are highly nonlinear. As a consequence, the vehicle response is nonstationary, nonlinear and invariably with a low Signal to Noise Ratio (SNR). Hence, direct application of basic Cov-SSI is not appropriate for the OMA of vehicle suspension systems, but an enhanced version of Cov-SSI (Correlation Signal Subset-based SSI, CoSS-SSI) has been developed to reduce the effects of nonlinearity and nonstationary responses. CoSS-SSI will be introduced in detail in Section 4.2, and its effectiveness will be verified in Section 4.3 through numerical studies.

## 4.2 Correlation Signal Subset-based SSI (CoSS-SSI)

This section presents CoSS-SSI in detail: first, the theoretical background, and then the details of the process.

### 4.2.1 Theoretical background of CoSS-SSI

As previously stated, white noise excitation and linear system assumptions are the fundamentals of OMA. However, these two assumptions are difficult to meet in practice. Real road and railway vehicles are complicated dynamic systems and normally run under harsh conditions which result in high noise levels during any measurement process [152]. The vehicle will be subject to time-varying excitations resulting from random local irregularities, humps or potholes on roads or joints on a track. There will also be nonlinearities in the suspension which are inevitable due to the inclusion of nonlinear components such as dampers. As a consequence, the vehicle response is significantly nonstationary, so that the modal parameters will change with responses at different times. As a specific example, the covariance values in the Cov-SSI scheme may vary due to the

response being nonstationary and data length being limited, both of which have an immediate effect and may lead to variation in the results.

Based on these considerations, one can conclude that the nonstationary responses have significance impact on the OMA, which is a common challenge to OMA methods. Numerous studies have been conducted to solve the nonstationary issue. First and foremost, it was proved in principle in [119] that the cross-correlation functions of two stationary processes could be expressed in the same form as a free impulse function [152], [153]. Based on the principle presented in [119], it has been theoretically proven [154] that the nonstationary correlation functions of a structural response evaluated at fixed time instants have the same form of expression form as a structural free response with certain initial conditions [152].

In summary, the theory presented in [154] indicates that the nonstationary problem could be reduced to a stationary problem by evaluating the nonstationary correlation functions at a fixed time instant [152].

A novel method based on Cov-SSI was developed in [7], [155] using the correlation signal rather than original response signal to construct the Hankel matrix to identify the modal parameters of a chassis frame in a heavy-duty dump truck under working conditions. This novel use of Cov-SSI is known as the Average Correlation Signal based Cov-SSI (ACS-Cov-SSI). The average correlation signals are obtained by averaging several correlation signals from several measurements, or one measurement dividing into several segments [7].

It is worth mentioning that the foundation of ACS-Cov-SSI is the correlation function which has the same form as the impulse response function and which contains all the system's modal information. This theoretical fundament is implicit in the Data Correlation-based ERA (DC-ERA), and it has been proven that the DC-ERA is effective for noise reduction [118]. Cov-SSI has the capability to identify close modes and ACS-Cov-SSI was developed to combine the advantages of DC-ERA and Cov-SSI. As referred to earlier, an additional averaging step was added in the ACS-Cov-SSI to enhance the effectiveness of the noise-suppressing. A reference channel is used during the correlation calculation process to retain the phase information for the average action.

The capability of ACS-Cov-SSI has been verified in [7], [155], and the results indicated that ACS-Cov-SSI has excellent ability to suppress high noise levels and strong non-stationarity

in signals collected from the heavy-duty truck when running on an unpaved road. However, the amplitudes of the correlation signals can spread over an extensive dynamic range on account of the strong nonstationary characteristics in the response signals [152], [153]. For ACS-Cov-SSI, the average correlation signals are calculated by simultaneously averaging all correlation signal segments, which means the correlation signals with very low amplitudes could be overwhelmed or neglected [152].

However, low amplitude correlation signals often contain information associated with modes with high damping coefficients [152]. For example, it is well known that vibration modes with high damping are difficult to excite. Hence the low amplitude correlation signals are necessary for modal identification and cannot be neglected. In other words, averaging over a full set of correlation signals in ACS-Cov-SSI could result in inadequate mode identification, losing those which are highly damped [152].

Given nonlinearity is inevitable in vehicle suspension systems, different vibration amplitudes of correlation signal may result from different regimes of a nonlinear system [152]. That is to say, the responses with higher amplitudes may overlap and hide modal parameters which have lower amplitudes. Consequently, the modal parameters identified by ACS-Cov-SSI could appear inconsistent and unrepeatable [152]; the most direct result is that the identified SD is unstable.

From the above analysis a novel method, the Correlation Signal Subset-based Stochastic Subspace Identification (CoSS-SSI) founded on the fundamentals, is proposed to overcome the deficiencies and limitations of the ACS-Cov-SSI. For CoSS-SSI, the correlation signal segments are classified into several subsets according to their magnitudes. Then, each subset of correlation signals is separately averaged, rather than synchronous averaging over all the correlation signal segments. Later, the Cov-SSI is applied to each averaged correlation signal subset to identify the system's modal parameters. The detailed procedure of the CoSS-SSI is presented below.

#### **4.2.2 Procedure for CoSS-SSI**

This subsection will present the detailed procedure of CoSS-SSI. The first step is to obtain several raw signal segments, which is the same procedure as for ACS-Cov-SSI. The raw signal segments can be obtained by repeating the experiment or dividing long segments of

data into several smaller segments, or a combination of both approaches. For example, a dataset of raw signals is recorded from  $l$  channels, which can be divided into  $K$  segments, see Figure 4-1. It can be seen that each segment has the same length ( $N$ ) with  $l$  channels of data.

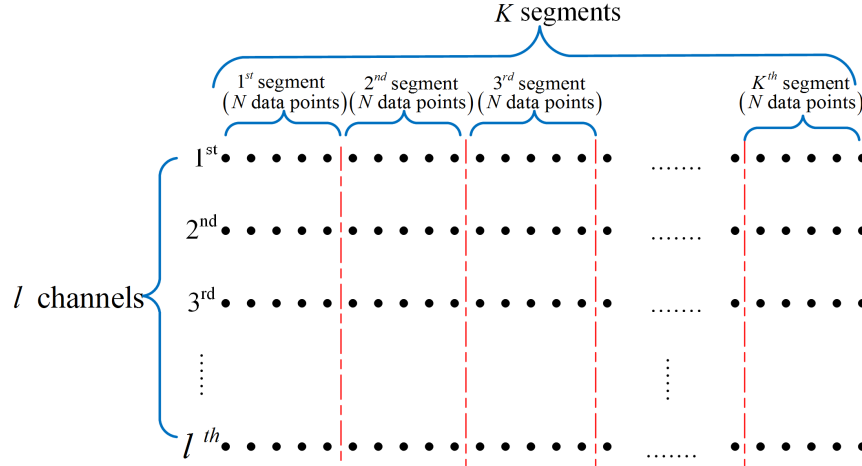


Figure 4-1 Schematic for dividing raw data from  $l$  channels into  $K$  segments each containing  $N$  data points

The second step is to calculate the correlation signals concerning each data segment as follows [7], [152], [153], [155]:

$$r^{ip}(m) = \frac{1}{N} \sum_{n=0}^{N-1-m} y^p(n) y^i(n+m) \quad (4-1)$$

Where  $N$  is the data length of each segment;  $i = 1, 2, 3, \dots, l$  is the channel number;  $m$  is the delay time;  $n$  is the time sequence;  $p$  refers to the  $p^{th}$  channel selected as reference. Generally, the  $p^{th}$  channel should have the highest SNR of all channels. The purpose of choosing a reference channel is to retain the signal phase information for the averaging operation [7], [120], [155]. The FFT algorithm can be applied to improve the correlation signal calculation speed.

With  $l$  channels in total, the number of correlation signals for each segment will be  $l \times l$ , and therefore the total number of correlation signal segments will be  $K \times l^2$ . As mentioned earlier, in order to overcome nonstationary effects, the correlation signals will be classified into several groups with respect to their magnitudes before averaging them.

The Root Mean Square (RMS) value is adopted to represent the signal magnitude in this project. Thus, the third step is to develop an RMS matrix by calculating the RMS values of all correlation signal segments. The size of RMS matrix will be  $K \times l^2$ .

Specific intervals have to be set up to categorise all correlation signals, which is the fourth step. Firstly, the minimum RMS value in each row of the RMS matrix will be selected to form a vector  $\mathbf{R}_m$  of size of  $K \times 1$ . Secondly, the maximum and minimum values of  $\mathbf{R}_m$  will be selected, represented by  $\min(\mathbf{R}_m)$  and  $\max(\mathbf{R}_m)$ . Thirdly, the intervals will be calculated using  $\max(\mathbf{R}_m)$  to minus  $\min(\mathbf{R}_m)$  and then the result will be divided by the subset number  $J$ , where the value of  $J$  is always chosen between 2 and 5 to achieve a balance between the accuracy of identification results and the requirement of calculation speed for online application.

With the obtained specific intervals, the fifth step is to categorise the correlation signal segments into corresponding subsets according to their RMS values as calculated in the third step.

After that, the sixth step is to average the correlation signal segments with respect to each subset, as follows:

$$\overline{r^{ip}(m)} = \frac{1}{K_j} \sum_{k_j=1}^{K_j} r_{k_j}^{ip}(m) \quad (4-2)$$

Where  $K_j$  is the number of correlation signal segments in a single subset.

Then, the seventh step is to use the averaged correlation signals to construct the Hankel matrix, shown as Equation (3-35), and identify the modal parameters for each subset according to the Cov-SSI process introduced in Section 3.3.

According to the process,  $J$  group modal parameters will be identified. However, many of them could be quite close due to some of them being same mode in reality. Therefore, the eighth step, which is also the final step, is integrating the system modes with the modes from all subsets based on the frequency differences and MAC values.

For clarity, the procedure of CoSS-SSI is further summarised in the flow chart shown in Figure 4-2.

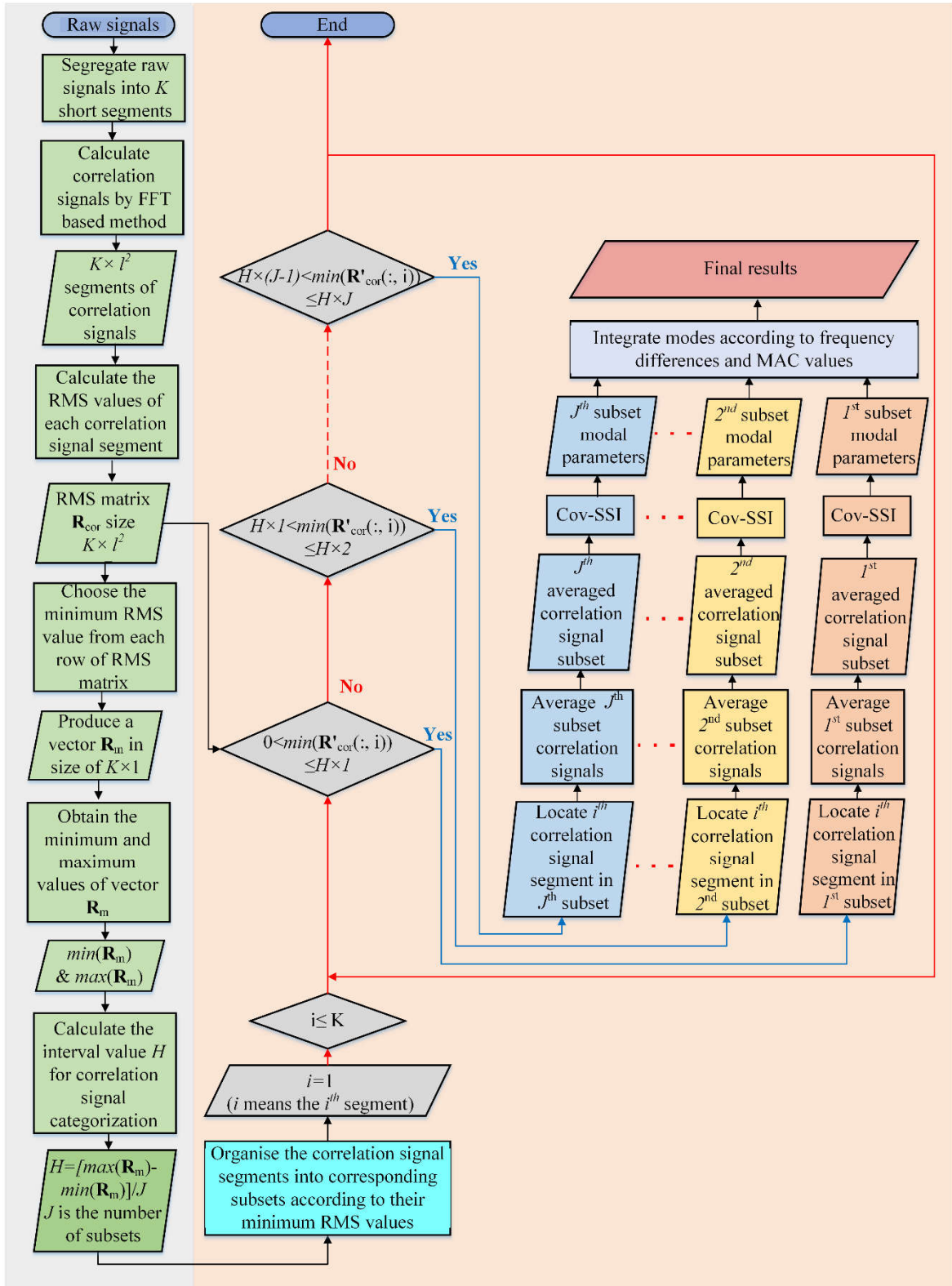


Figure 4-2 Flow chart of CoSS-SSI

### 4.3 Effectiveness verification of CoSS-SSI

The CoSS-SSI was introduced in detail in Section 4.2. In this section, the effectiveness of CoSS-SSI will be verified via a 3-DOF vibration system developed to investigate the superiority of CoSS-SSI when the measured signals have low SNR values and are strongly nonstationary. Its efficiency will be demonstrated by comparing the identified results obtained from Cov-SSI and ACS-Cov-SSI.

#### 4.3.1 3-DOF model description

The linear 3-DOF vibration system is shown in Figure 4-3, which is a mass-spring-damper system. The physical parameters of the system are also given in Figure 4-3. The theoretical modal parameters can be calculated by developing a state-space model according to the theory summarised in Section 3.2.1. The results are tabulated in Table 4-1. It is noted that the third mode has the highest damping ratio.

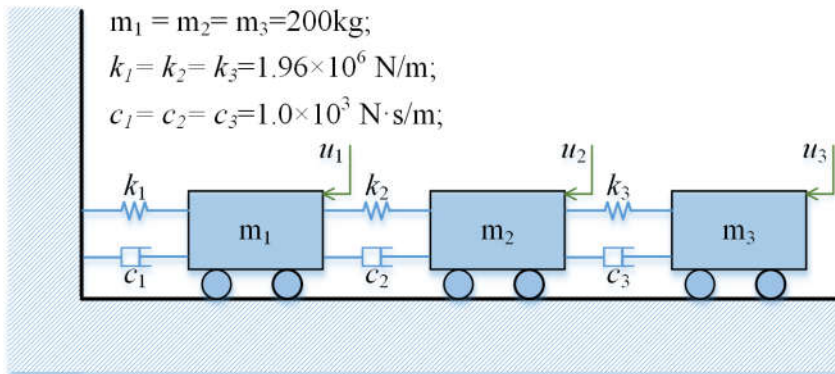


Figure 4-3 3-DOF linear vibration system

Table 4-1 Theoretical modal parameters of the 3-DOF linear vibration system

	Mode 1	Mode 2	Mode 3
Frequency	7.01Hz	19.65Hz	28.39Hz
Damping Ratio	1.12%	3.15%	4.55%

This simulation case is to verify the effectiveness of the proposed novel SSI approach which is an output-only method. Three independent random excitations acting horizontally were separately loaded onto the three masses, and the response of the 3-DOF vibration system was obtained through the *'lsim'* function in MATLAB, and was used as the raw signal for the Cov-SSI, ACS-Cov-SSI and CoSS-SSI methods.

Random excitations band-pass stationary white noise was added to represent multiple random impulsive impacts, mimicking the excitation caused by road bumps or potholes. Some measurement noise is inevitable in reality, so some random noises are added to the obtained noise-free responses,  $\mathbf{y}(k)$ . The final response  $\mathbf{y}_n(k)$  of the 3-DOF vibration system was expressed as:

$$\mathbf{y}_n(k) = \mathbf{y}(k) + \gamma\boldsymbol{\sigma}(k) \quad (4-3)$$

Where  $\boldsymbol{\sigma}(k)$  is a band-pass white noise with  $\sigma(0, 1)$ ; the amplitude factor of  $\boldsymbol{\sigma}(k)$  is defined as follows, which allows for adjusting the SNR of the responses [7], [152], [153], [155]:

$$\gamma = \frac{\sqrt{\sum_{k=1}^N \mathbf{y}(k)^2}}{SNR \sum_{k=1}^N \boldsymbol{\sigma}(k)^2} \quad (4-4)$$

In this simulation case, the sampling rate was set at 500 Hz because the highest resonance frequency in the system was 28.39 Hz. Since ACS-Cov-SSI and CoSS-SSI need several data segments to extract the modal parameters, twenty Monte Carlo simulations were conducted with the data length for each segment 60 s. In order to illustrate the superiority of CoSS-SSI, two SNR scenarios were simulated, high SNR ( $SNR = 10$ ), and low SNR ( $SNR = 0.5$ ).

An example of the acceleration time-domain responses under these two SNR scenarios is presented in Figure 4-4, from which it can be seen that the signal amplitudes are higher when more measurement noise is added to the responses. It is also noticeable that the responses are nonstationary. In order to visually enhance the nonstationary features, the mean values of the time-domain responses were calculated every two seconds, see Figure 4-5. It can be seen that the mean values fluctuated over time. Moreover, it is apparent that the range of amplitude fluctuation for the high measurement noise scenario ( $SNR = 0.5$ ) is wider than low noise which, as would be expected, means the nonstationary character is severer when SNR is smaller.

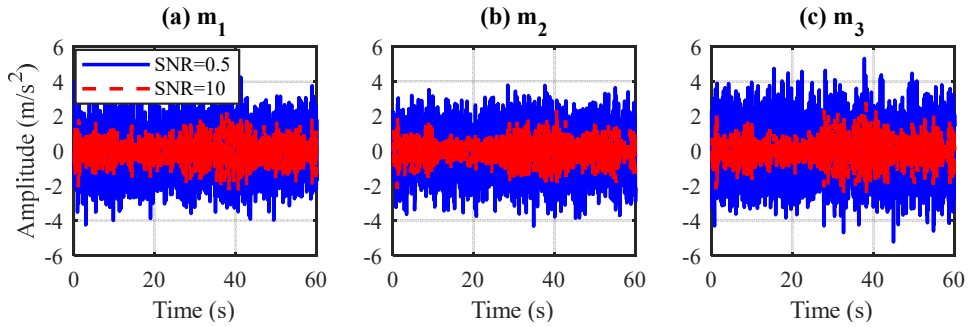


Figure 4-4 Time-domain response of the linear 3-DOF vibration system

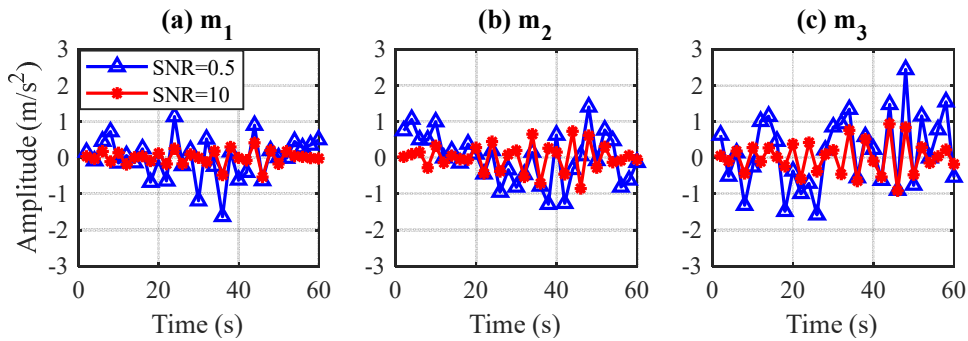


Figure 4-5 Amplitude mean values of time-domain responses for every two seconds

In addition, the corresponding Power Spectrum Density (PSD) of the time-domain responses are presented in Figure 4-6. When the SNR is 10 only two peaks are observable, which correspond to the first and second modes of the 3-DOF system. The third mode is not that much prominent because of its higher damping ratio, 4.55%. It can also be seen from Figure 4-6 that the energy distribution of the system response is affected by measurement noise. Although the main peaks under these two SNR scenarios are almost the same responses for  $m_1$  and  $m_3$ , the second peak (19.65 Hz) and third peak (28.39 Hz) of  $m_2$  are submerged. Therefore, it is reasonable to conclude that the presence of noise will lead to difficulty in modal extraction.

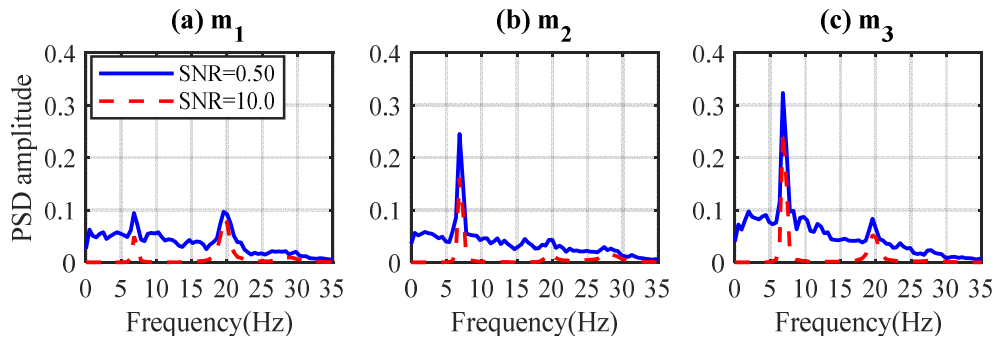


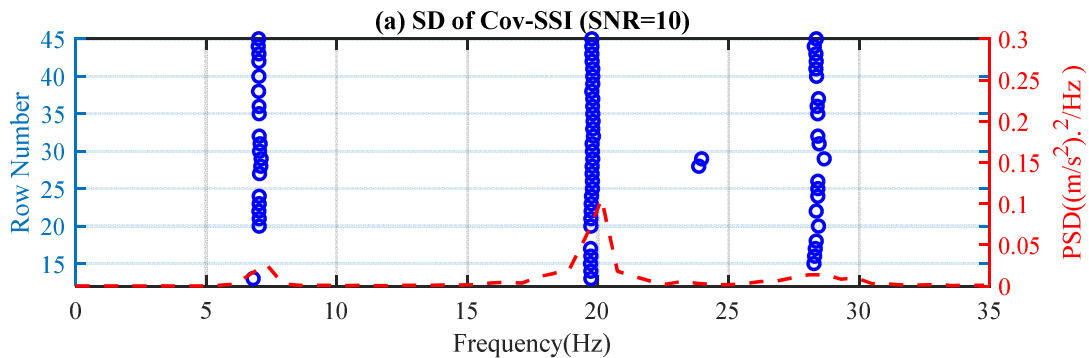
Figure 4-6 PSD of the linear 3-DOF vibration system responses

This subsection introduced a linear 3-DOF vibration system and the characteristics of system responses under two different SNRs. It has been found that noise will lead to severer nonstationary responses and can submerge some modal information, but in the next subsection, the responses collected with the two SNR levels will be used to illustrate the superiority of CoSS-SSI.

### 4.3.2 Modal identification results and analysis

In order to illustrate the superiority of the novel CoSS-SSI method, two other basic methods, Cov-SSI and ACS-Cov-SSI, are used to extract the modal parameters of the linear 3-DOF vibration system from the simulated responses. As mentioned earlier, twenty Monte Carlo simulations were carried out, which yielded twenty segments of response data. The sampling rate was 500 Hz, and the data length for each segment was 60 s. For the Cov-SSI, one data segment is enough for identification, whereas both ACS-Cov-SSI and CoSS-SSI used all twenty data segments. Of course, CoSS-SSI would be identical to ACS-Cov-SSI if the number of subsets  $J$  was reduced to one. In this case, for CoSS-SSI, the subset number  $J$  is set at 3 which can reach a good balance between identification accuracy and computational efficient. Then, according to the procedure introduced previously, the modal parameters of the linear 3-DOF system will be identified.

Firstly, Figures 4-7, 4-8 and 4-9 present the SDs (see Section 3.3.4) for each of the three methods for the linear 3-DOF vibration system is under  $SNR = 10$  and  $SNR = 0.5$ . It is worth to noting that the thresholds of frequency error ( $\varepsilon_f$ ), damping error ( $\varepsilon_\xi$ ), and mode shape error ( $\varepsilon_{MAC}$ ), are set at 0.1, 0.2 and 0.5, respectively. Besides, the row number of the left vertical axis of SD is the time lag of  $i$  in Equation. (3-34), because the row number of the state matrix  $\mathbf{A}$  is determined by the time lag  $i$  according to Equations. (3-44) and (3-45).



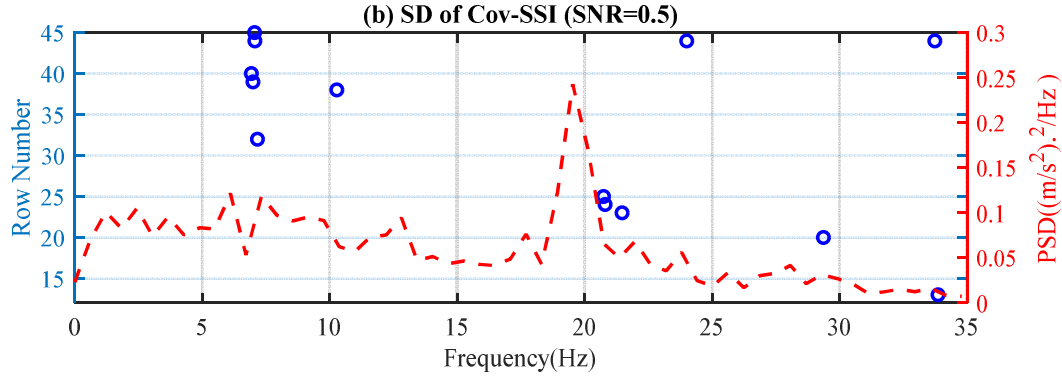


Figure 4-7 SDs identified by Cov-SSI

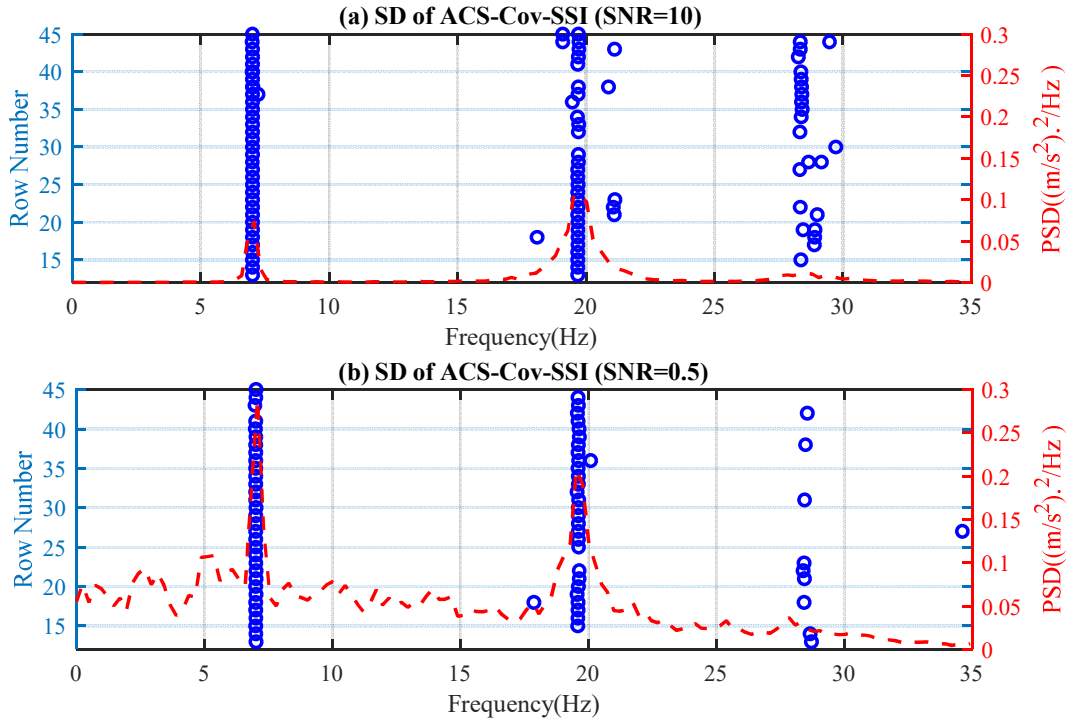
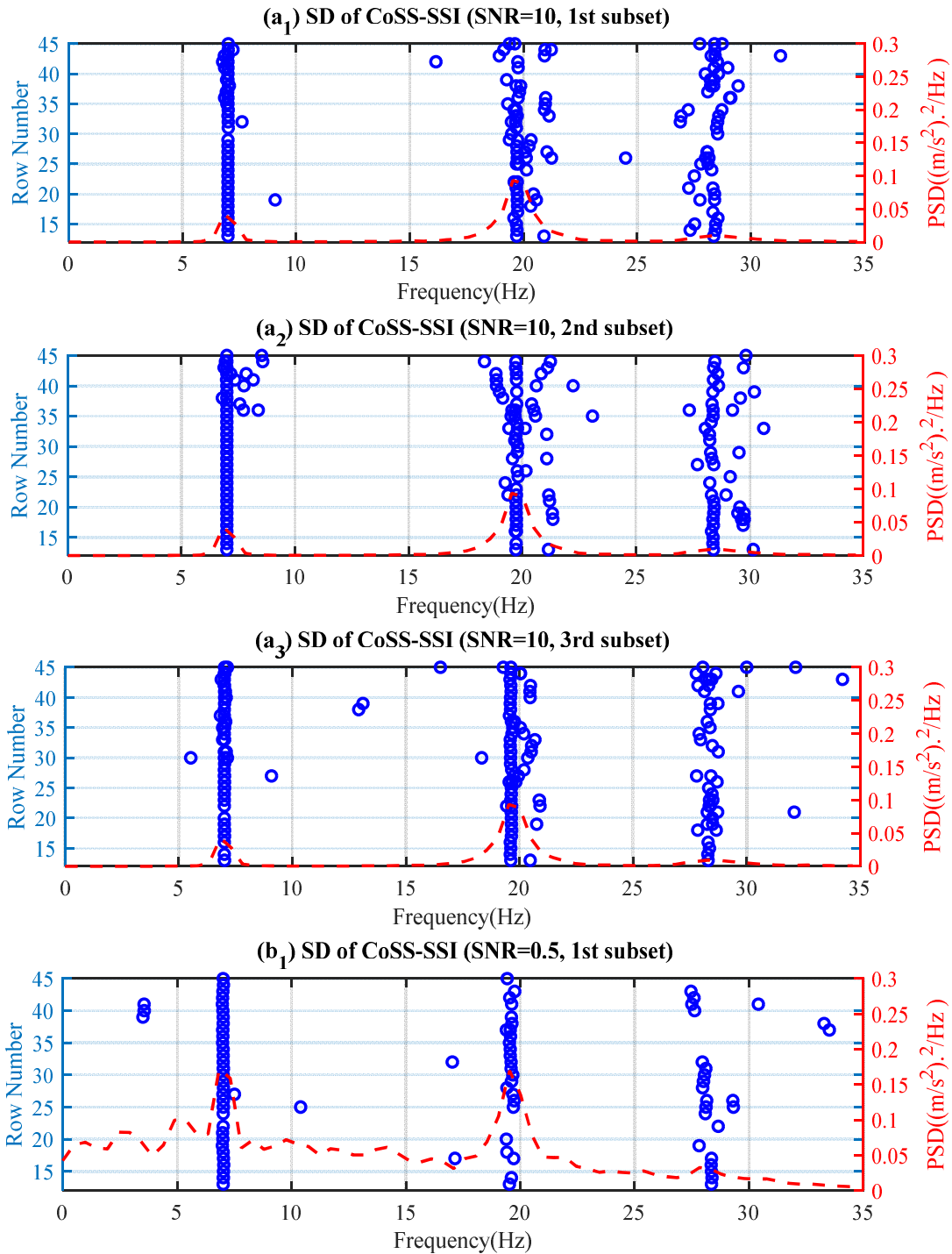


Figure 4-8 SDs identified by ACS-Cov-SSI

It can be seen from Figure 4-7(a) and Figure 4-8(a) that three relatively stable modes were identified by both Cov-SSI and ACS-Cov-SSI when the SNR was 10. It can be seen from Figure 4-7(b) that none of the stable modes were identified by Cov-SSI, and only two relatively stable modes are identified by ACS-Cov-SSI, when the SNR is 0.5, see Figure 4-8(b).

However, as can be seen in Figure 4-9(a<sub>1</sub>, a<sub>2</sub>, a<sub>3</sub>), for which the SNR=10, the SDs identified by CoSS-SSI are messier than for both Cov-SSI and ACS-Cov-SSI. Such a result could be due to correlation signal categorisation before the averaging step, which helped to improve the quality of the signals. Therefore, the threshold  $\varepsilon_f$ ,  $\varepsilon_\xi$  and  $\varepsilon_{MAC}$ , introduced in Section

3.3.4, should be stricter or set to a smaller value. In other words, CoSS-SSI has no advantage if the collected responses are high quality.



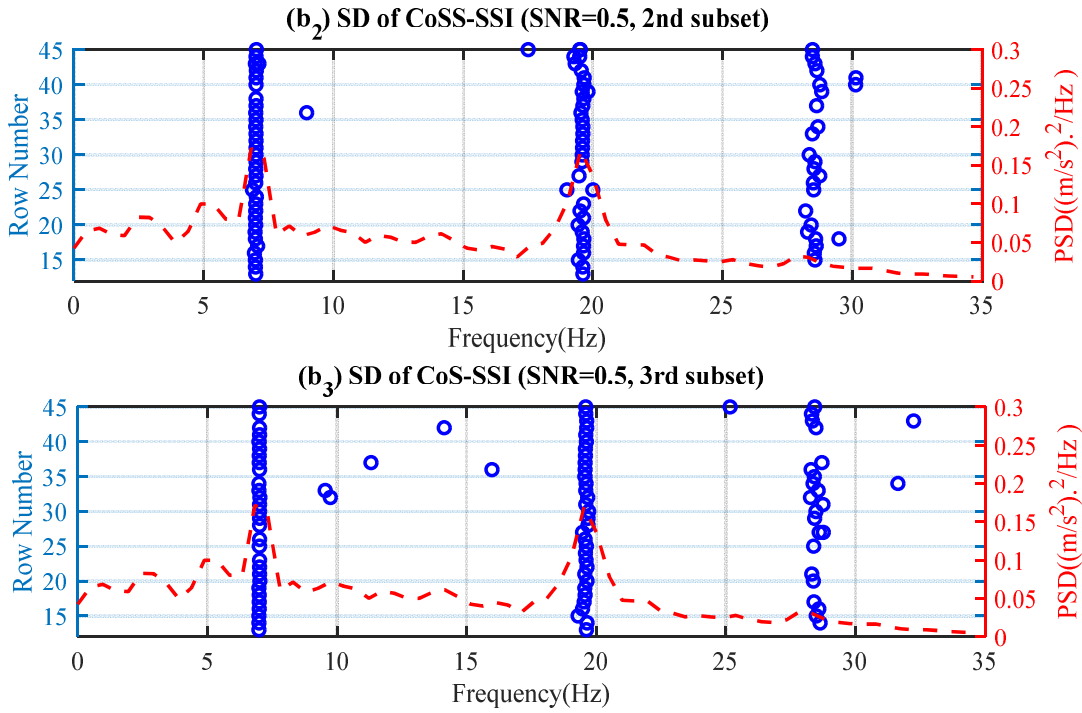


Figure 4-9 SDs identified by CoSS-SSI

Nonetheless, the superiority of CoSS-SSI is demonstrated when the signal quality is poor ( $SNR = 0.5$ ). In contrast to the relatively poor performances of Cov-SSI, and ACS-Cov-SSI, when the SNR is 0.5, all three target modes are successfully identified in the three subsets, as shown in Figures 4-9(b<sub>1</sub>, b<sub>2</sub>, b<sub>3</sub>). The benefits of CoSS-SSI can be seen.

As mentioned in Section 3.3.4, a second threshold ( $\delta$ ) is set according to Equation (3-57) to identify the relatively stable modes. In this simulation the maximum number of calculated orders is set at 45 ( $M = 45$ ). Two examples of calculated stable rates are presented in Figures 4-10 and 4-11. Figure 4-10 shows the stable rates of the SD identified by Cov-SSI and ACS-Cov-SSI when the SNR is 10. Three relative stable modes are selected out for both methods when the second threshold is set at 50%. Figure 4-11 is an example of stable rates of the SD for CoSS-SSI when the SNR is low, 0.5. It can be seen that a stricter second threshold, set at 70%, enabled extraction of the true modes. A more stringent threshold makes the identified results more reliable. In this simulation, the second threshold for Cov-SSI and ACS-Cov-SSI was set at 50%, and for CoSS-SSI was set at 70% for both two SNR scenarios: 10 and 0.5.

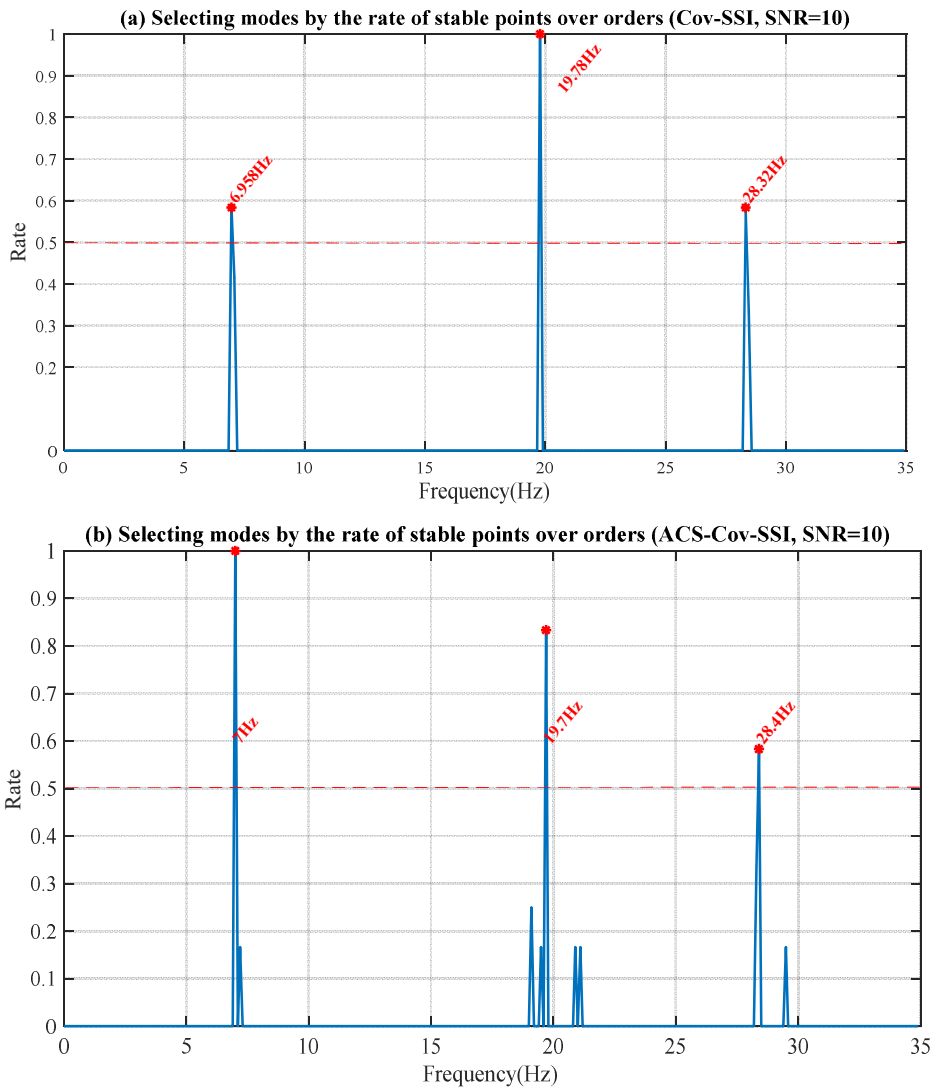


Figure 4-10 Stable rates of the SDs identified by: (a) Cov-SSI; (b) ACS-Cov-SSI

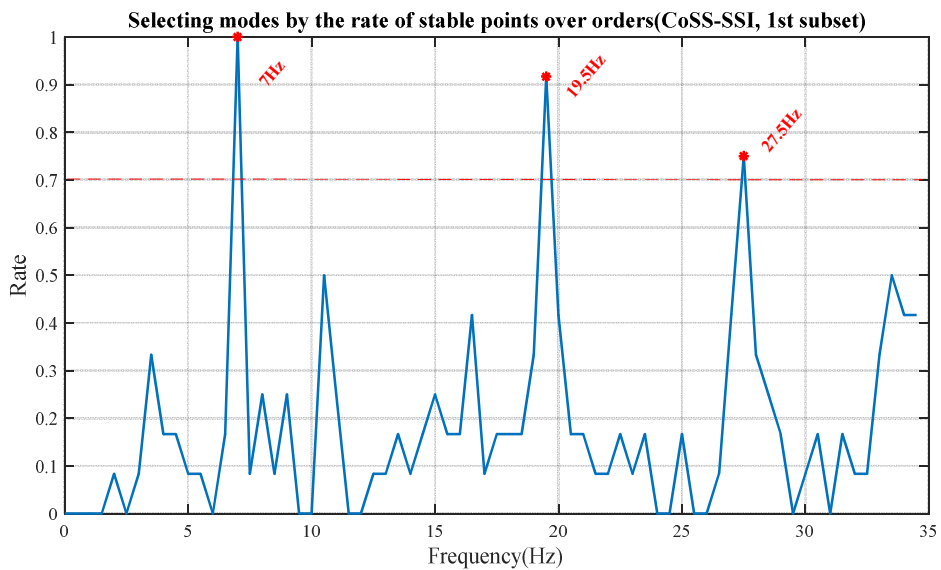


Figure 4-11 Stable rates of the SD identified by CoSS-SSI

Based on the identified SDs and the second threshold, the final identified natural frequencies and damping ratios by Cov-SSI, ACS-Cov-SSI and CoSS-SSI are tabulated in Tables 4-2, 4-3 and 4-4, respectively, which also show the errors between identified results and theoretical values. As can be seen from these three tables, Cov-SSI is unable to extract any mode when the SNR is 0.5, and ACS-Cov-SSI can extract the first two modes but not the third. However, CoSS-SSI successfully identified all three modes in all subsets with acceptable level of errors; even when the second threshold is stricter.

It can be seen that all of the frequency errors are extremely small; most below 1%. However, the error in the damping ratios is comparatively quite large in spite of the signal quality. Nonetheless, such results are reasonable since damping estimation is a challenge common to all modal identification methods, even Experimental Modal Analysis (EMA) methods [153]. The main reason for this challenge is the damping mechanisms are not completely clear. Therefore, the damping ratio performs only a reference role for CM, not a critical one.

Table 4-2 Modal results identified by Cov-SSI with errors

	Mode 1				Mode 2				Mode 3			
	$f_1$	Error	$\xi_1$	Error	$f_2$	Error	$\xi_2$	Error	$f_3$	Error	$\xi_3$	Error
	(Hz)	( $f$ %)	(%)	( $\xi$ %)	(Hz)	( $f$ %)	(%)	( $\xi$ %)	(Hz)	( $f$ %)	(%)	( $\xi$ %)
<b>Theoretical value</b>	7.01	Null	1.12	Null	19.65	Null	3.15	Null	28.39	Null	4.55	Null
<b>SNR=10</b>	7.03	0.37	1.25	11.61	19.67	0.09	3.11	1.27	28.44	0.17	4.30	5.49
<b>SNR=0.5</b>	<i>Null</i>											

Table 4-3 Modal results identified by ACS-Cov-SSI with errors

	Mode 1				Mode 2				Mode 3			
	$f_1$	Error	$\xi_1$	Error	$f_2$	Error	$\xi_2$	Error	$f_3$	Error	$\xi_3$	Error
	(Hz)	( $f$ %)	(%)	( $\xi$ %)	(Hz)	( $f$ %)	(%)	( $\xi$ %)	(Hz)	( $f$ %)	(%)	( $\xi$ %)
<b>Theoretical value</b>	7.01	Null	1.12	Null	19.65	Null	3.15	Null	28.39	Null	4.55	Null
<b>SNR=10</b>	7.01	0.00	1.08	3.57	19.69	0.21	3.29	4.44	28.32	0.26	4.81	5.71
<b>SNR=0.5</b>	7.01	0.00	1.19	6.25	19.68	0.17	3.41	8.25	<i>Null</i>	<i>Null</i>	<i>Null</i>	<i>Null</i>

Table 4-4 Modal results identified by CoSS-SSI with errors

	Mode 1				Mode 2				Mode 3				
	$f_1$	Error	$\xi_1$	Error	$f_2$	Error	$\xi_2$	Error	$f_3$	Error	$\xi_3$	Error	
	(Hz)	( $f$ %)	(%)	( $\xi$ %)	(Hz)	( $f$ %)	(%)	( $\xi$ %)	(Hz)	( $f$ %)	(%)	( $\xi$ %)	
<b>Theoretical value</b>	7.01	Null	1.12	Null	19.65	Null	3.15	Null	28.39	Null	4.55	Null	
<b>SNR=10</b>	<b>S1</b>	7.03	0.22	2.17	93.75	19.33	1.60	4.45	41.27	28.52	0.45	6.53	43.52
	<b>S2</b>	7.01	0.00	1.97	75.89	19.34	1.57	5.91	87.62	28.58	0.66	6.71	47.47
	<b>S3</b>	7.04	0.41	5.17	361.61	19.33	1.6	3.92	24.44	28.51	0.41	5.83	28.13
<b>SNR=0.5</b>	<b>S1</b>	7.02	0.07	3.47	209.82	19.59	0.27	5.14	63.17	28.43	0.14	6.53	43.52
	<b>S2</b>	7.02	0.16	2.58	130.36	19.59	0.27	3.74	18.73	28.51	0.43	3.50	23.08
	<b>S3</b>	7.02	0.16	4.45	297.32	19.59	0.27	3.51	11.43	28.47	0.29	5.53	21.54

Besides the frequency and damping ratio, mode shape is another significant modal parameter. One of the most well-known indicators of mode shape accuracy is the MAC value, which can be calculated by Equation (3-55). The MAC values of the mode shapes identified by the three methods are presented in Figures 4-12, 4-13 and 4-14, where the reference mode shape is the theoretical mode shape. As can be seen from these figures, all of the MAC values for the successfully identified modes are close to unity, which indicates the accuracy and reliability of the proposed method. CoSS-SSI, identifies all mode shapes accurately in all subsets, even under severe measurement noise ( $SNR = 0.5$ ).

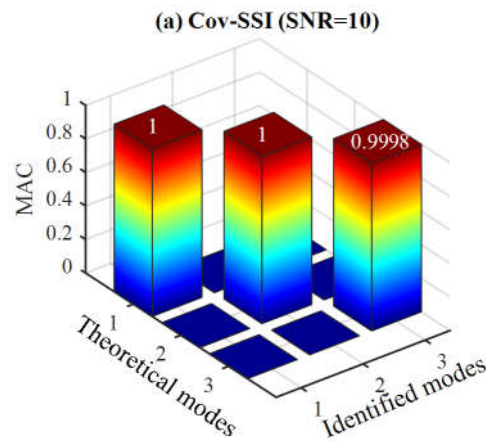


Figure 4-12 MAC for mode shapes identified by Cov-SSI

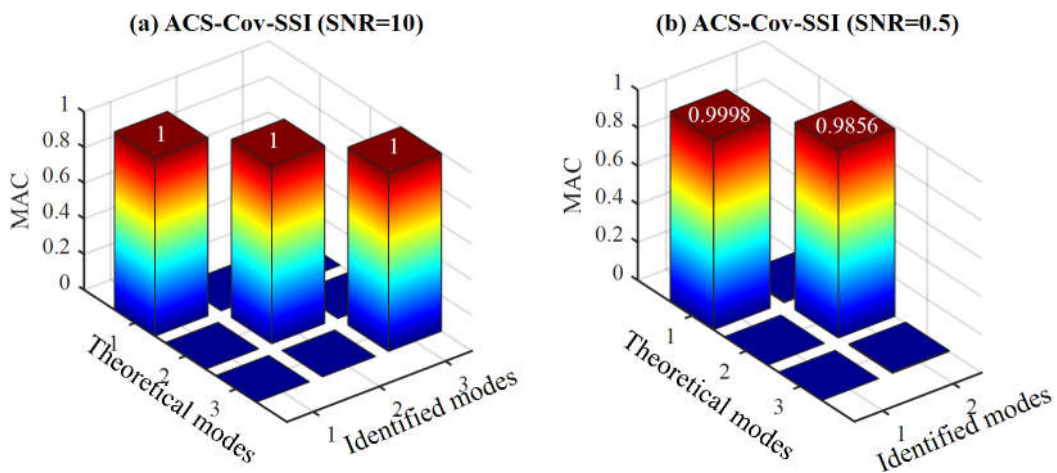


Figure 4-13 MAC for mode shapes identified by ACS-Cov-SSI

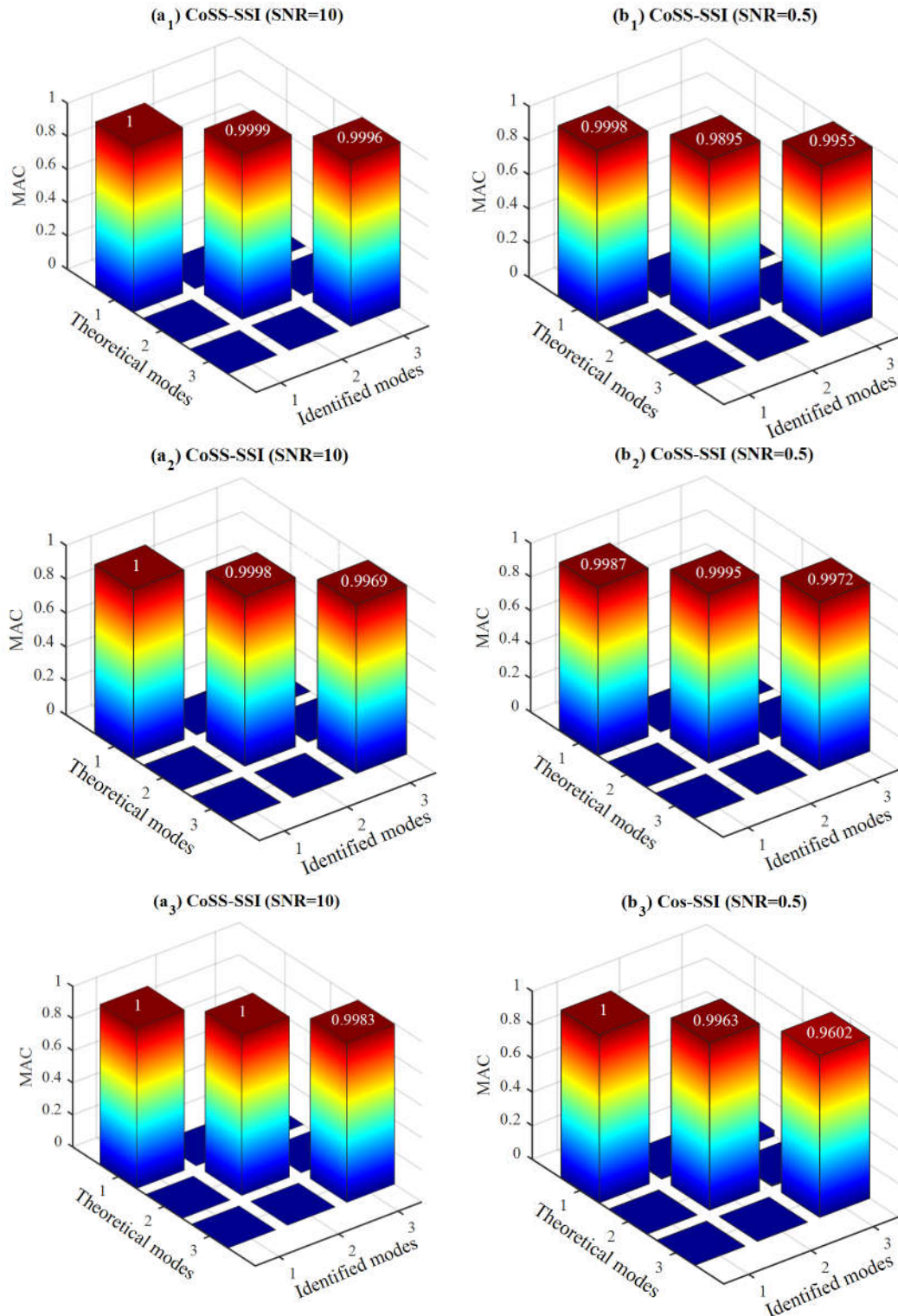


Figure 4-14 MAC for mode shapes identified by CoSS-SSI

Based on the above numerical simulation, the superiority of CoSS-SSI has been clearly demonstrated, especially in nonstationary and high noise scenarios. In reality, field measurements are usually nonstationary and contain high noise levels; as a consequence, CoSS-SSI could be a desirable approach within OMA.

Besides, according to the flowchart of Cov-SSI, Figure 3-1, the modal parameters are extracted from the state matrix  $\mathbf{A}$ . For this 3-DOF system, it is possible to identify the system's matrices of mass( $\mathbf{M}$ ), stiffness( $\mathbf{K}$ ) and damping( $\mathbf{M}$ ) through the identified state matrix( $\mathbf{A}$ ). Then, the physical parameters like system's stiffness and damping can be used as good indexes for CM. However, the dimension of the identified  $\mathbf{A}$  is determined by the row number  $i$  in Equation. (3-34), where the dimension of  $\mathbf{A}$  is  $2i \times 2i$ . It can be seen from the previous identification process that the minimum  $i$  is 12. Therefore, a model reduction method has to be developed to extract system's real state matrix. This is a fruitful area which could be investigated further in the future.

#### 4.4 Findings

A novel OMA method, CoSS-SSI, has been proposed in this chapter and verified by numerical vibration analysis. The following conclusions can be drawn on the basis of the simulation results:

- 1) Conventional OMA methods, such as Cov-SSI and ACS-Cov-SSI, are unable to identify a system's modal parameters when the responses are nonstationary and contain high noise levels;
- 2) CoSS-SSI has the capability to successful extract modal information from nonstationary and low SNR signals;
- 3) CoSS-SSI outperforms traditional OMA methods and could be a promising approach for vehicle suspension online monitoring.

As stated above, real vehicle responses are usually with high noise and nonstationary due to complex road/track excitations and highly nonlinear suspension systems. It has been shown that CoSS-SSI could be utilized for identification of vehicle suspension modal parameters using the car body responses, which is a core part of the online monitoring system for vehicle suspension.

However, the harmonic effects are a common issue occurring during OMA and the next chapter will investigate how to eliminate the effects of harmonic excitations during OMA.



---

---

## CHAPTER 5 OPERATIONAL MODAL ANALYSIS IN THE PRESENCE OF HARMONICS

---

---

*This chapter focuses on the use of Operational Modal Analysis (OMA) in the presence of harmonics. It begins by reviewing the key methods of removing harmonic effects from OMA and selecting cepstrum editing (CE) for eliminating the harmonic effects as it is more efficient and robust for online implementation. The procedure of CE is introduced in detail in Section 5.2, and the effectiveness of CE is verified by investigating the response of a quarter vehicle model under various excitation scenarios.*

*The simulation results show that pulse train excitation has no influence on OMA via CoSS-SSI, but a harmonic load will result in false modes. It is demonstrated that CE can remove such harmonic effects.*

## 5.1 Introduction

As mentioned earlier, most OMA methods are developed under the assumption of white noise excitation. However, harmonic excitations are very common in mechanical systems, especially for those machines which include rotating parts, such as bearings and gears. Conventional OMA approaches are unable to filter out the effects of harmonic excitations and as a result can fail to identify a system's modal parameters accurately [156].

Generally, harmonic excitation can cause failure of OMA in three different ways [157]. First, the harmonic frequency will be identified as one of the structural modes. Second, the harmonic excitation will lead to inaccurate results for damping if the frequency is close to a resonance. Last, harmonic excitations could increase the difficulty of modal identification since the main power of the responses could be around the harmonic frequency, not the natural structural frequencies [157].

Because of the adverse influence of harmonic excitation, a great many extended OMA methods have been developed by numerous researchers to cope with this problem. A review of the related literature can be found in [157], according to which, extended OMA techniques can be categorised into four groups:

- i) Statistics-based methods which employ statistical parameters to filter out the spurious modes resulted from the harmonics. For instance, the Probability Density Function (PDF) is a popular statistical parameter for harmonic mode identification [158], while Kurtosis is also a powerful tool to distinguish false modes which result from harmonics generated by e.g. mechanical systems [159]. However, statistics-based methods are useless if the harmonic frequency is close to one of the system's resonance frequencies or if the system were highly damped.
- ii) Enhanced techniques, which are modified general OMA methods which take harmonic effects into account, such as the modified LSCE [160], modified ERA [161], modified ITD [156] and modified data-driven SSI [162]. Nevertheless, all of these modified OMA methods need to obtain the harmonic frequencies before the identification process, which can be a challenge.
- iii) Transmissibility based OMA (TOMA), a new technique for using OMA usefully in the presence of harmonics, which has developed rapidly in recent years [124]–[128].

However, the resonance frequency range has to be excited persistently for the TOMA methods, which can be difficult to achieve [127], [128].

- iv) Signal pre-process, a technique which is a robust tool for eliminating the harmonic effects before conducting the OMA. In other words, the harmonic influence is removed in advance via particular signal processing techniques. The most popular methods for this purpose include nonparametric Time Synchronous Averaging (TSA) [163] and cepstrum editing (CE) [164], [165]. For TSA, an additional sensor such as a separate encoder is required for the synchronisation, so that CE is the easier and cheaper method.

Moreover, considering computational efficiency, robustness and feasibility, CE outperforms statistics-based methods, modified OMA methods and TOMA methods for OMA in the presence of harmonics. Therefore, in this project, CE will be utilised for removing harmonic sources before applying the proposed novel OMA procedure: CoSS-SSI. The detailed process of CE will be presented in the next section.

## 5.2 Cepstrum editing (CE)

It is over fifty years since the cepstrum was first time proposed as a powerful signal processing tool [165]. References [160] and [161] review the history of the cepstrum which nowadays is widely used [166]. The concept of applying CE to remove harmonics before using a standard OMA procedure was first presented in [167].

The cepstrum is defined as “the inverse Fourier transform of the log power spectrum” [165]–[167]:

$$C_c(\tau) = \mathcal{F}^{-1}\{\ln(X(f))\} = \mathcal{F}^{-1}\{\ln(A(f)) + j\varphi(f)\} \quad (5-1)$$

Where  $X(f)$  is the spectrum obtained by taking the FFT of the raw signal  $x[k]$ , as follows:

$$X(f) = \mathcal{F}\{x[k]\} = A(f)e^{j\varphi(f)} \quad (5-2)$$

The real cepstrum is utilised for CE before the OMA, which is defined by setting the phase  $\varphi(f)$  to zero, and the real cepstrum can be written as:

$$C_r(\tau) = \mathcal{F}^{-1}\{\ln(A(f))\} \quad (5-3)$$

Where  $\tau$  is the quefreny.

The procedure for utilizing CE to filter out harmonic effects is presented in Figure 5-1. The first step is obtaining amplitude ( $A(f)$ ) and phase ( $\varphi$ ) information of the response signal via the FFT. Then the amplitude data, after the logarithmic operation ( $\ln|X(f)|$ ) is used to calculate the real cepstrum ( $C_r(\tau)$ ) by conducting an Inverse Fast Fourier Transform (IFFT), according to Equations (5-1) and (5-3). Afterwards, to obtain the edited cepstrum ( $C_{Er}(\tau)$ ), a short-pass lifter is applied to filter out the influence of harmonics because useful modal information is contained in the start and end portions of the real cepstrum [165]–[167]. Subsequently, a FFT is employed to transfer the edited cepstrum back to the spectrum by combining with the original phase information ( $\varphi$ ), which can provide the complex spectrum. Last but not least, the filtered time-domain signal which can be utilized for the OMA, can be obtained by applying an IFFT to the complex spectrum  $X_E(f)$ , acquired in the previous step.

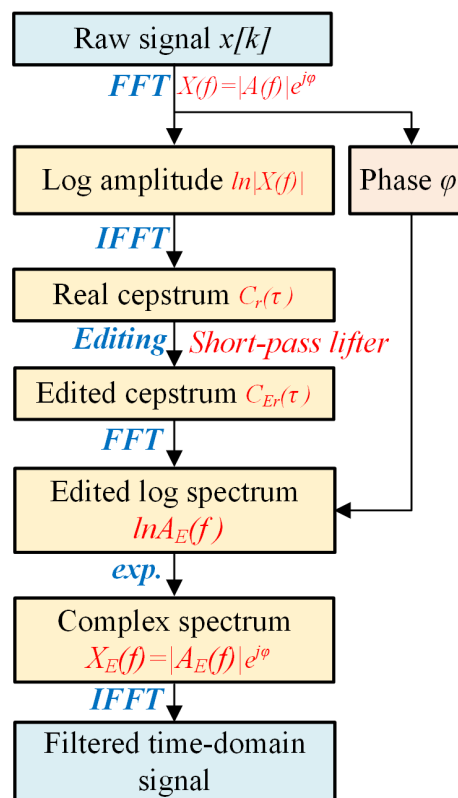


Figure 5-1 Cepstrum editing procedure to filter harmonic effects for OMA

During the CE, extra damping will be introduced into the OMA results if an exponential function is used as the short-pass lifter, in order to overcome this shortcoming, a piecewise

function is defined to play the role of a short-pass lifter. The piecewise function is expressed as Equation (5-4), and the effect of a short-pass lifter is shown in Figure 5-2.

$$f(t) = \begin{cases} 1 & (t < s \text{ or } t > m) \\ 0 & (s < t < m) \end{cases} \quad (5-4)$$

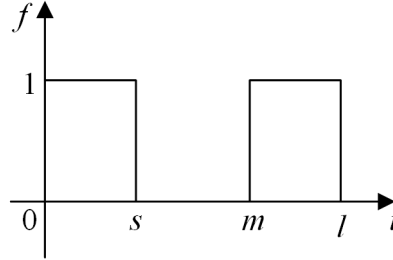


Figure 5-2 Short-pass lifter

Where  $l$  is the data length of the signal, and  $s$  is the data length for the data segment which contains all modal information. Because a cepstrum is a symmetrical signal, the data at the end have to be preserved and the length of the preserved signal at the end should also be  $s$ , so  $s = l - m$ .

In the next section, the effectiveness of CE for removing the harmonic effects before OMA will be verified using a quarter vehicle model.

### 5.3 Feasibility of cepstrum editing for removing harmonics

In this section, a quarter vehicle model will be developed to simulate the responses of a vehicle under various excitation scenarios, and then, the simulated signal will be utilised to evaluate the effectiveness of CE for removing harmonics. Note, CoSS-SSI will be employed as the OMA method.

#### 5.3.1 Quarter vehicle model description

A quarter vehicle model was constructed, as shown in Figure 5-3. The initial purpose of this model is to simulate a railway vehicle bogie being tested on a roller rig, as will be introduced in Chapter 8. The physical parameters of the model are given in Figure 5-3. Based on the given parameters, the system frequency response function can be calculated, and the results are presented in Figure 5-4. It can be seen that the resonance frequencies of this quarter model for bogie frame and wheel are 13.21 Hz and 56.35 Hz, respectively. The corresponding damping ratios for these two modes are 13.10% and 6.33% respectively.

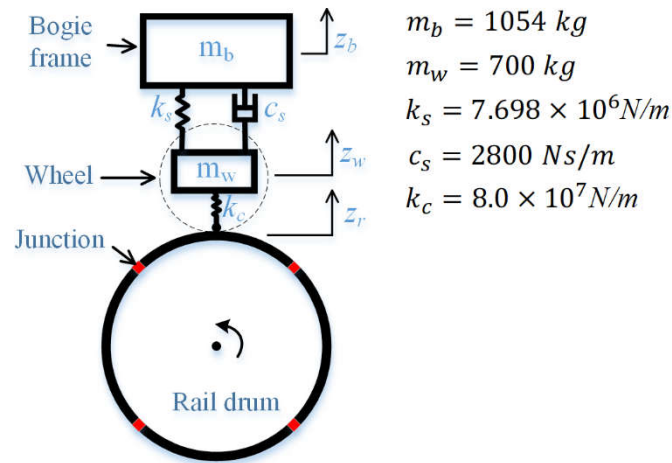


Figure 5-3 Quarter vehicle model

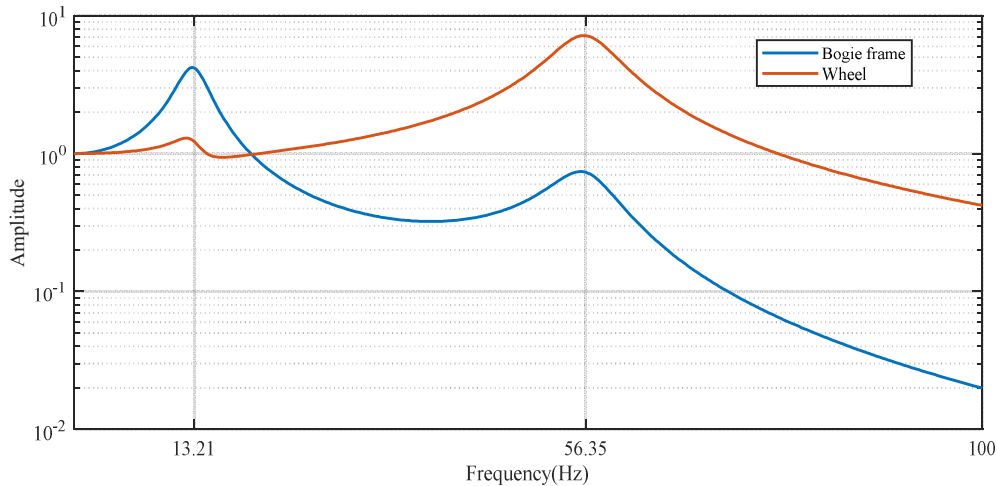


Figure 5-4 Frequency response function of the quarter vehicle model

### 5.3.2 Excitation model

For brevity, a model of inputs is developed to simulate various excitation scenarios, based on the railway vehicle bogie on a roller rig, shown in Figure 5-3. The input model includes three parts: random signal, harmonics and pulse train. Firstly, the random input is due to the roughness of wheel and rail drum surfaces. Harmonic inputs can result from manufacturing and installation errors of rotating parts. Lastly, the pulse train is caused by junctions on the rail drum as shown in Figure 5-3 which are included to emphasise that the rail drum is composed of four rail segments formed into quarters of a circle, which resulted in four junctions on the rail drum and four corresponding pulse train inputs to the system.

Based on the model, the inputs can be written as:

$$y(t) = A_1 y_1(t) + A_2 y_2(t) + A_3 y_3(t) \quad (5-5)$$

Where  $y_1(t)$ ,  $y_2(t)$  and  $y_3(t)$  stand for random, harmonic and pulse train excitations, respectively,  $A_1$ ,  $A_2$  and  $A_3$  are their corresponding amplitudes.

These three excitations can be expressed as:

$$y_1(t) = randn(t) \quad (5-6)$$

$$y_2(t) = \sum_{i=1}^N \sin(2\pi f_i t + \varphi_i) \quad (5-7)$$

$$y_3(t) = \begin{cases} 1 & t = n * 1/f_{ex}, n = 1, 2, 3 \dots \\ 0 & otherwise \end{cases} \quad (5-8)$$

Where  $N$  is the number of harmonics;  $f_i$  and  $\varphi_i$  are the frequency and phase of the  $i^{th}$  harmonic;  $f_{ex}$  is excitation frequency of the pulse train which is equal to four times the rotating frequency.

### 5.3.3 Simulation results

In this section, the effectiveness of CE for removing harmonic effects on OMA results will be verified by loading different excitations. Specifically, in order to investigate the impact of the pulse train and harmonic excitations on the OMA results, the quarter vehicle model was excited first by random input, and then random input in combination with pulse train and harmonic excitation. The modal parameters of the car body responses were identified by using CoSS-SSI.

The sampling rate was 1000 Hz, and the data length of each dataset was 60 s. Each case was simulated ten times to obtain ten datasets.

#### 5.3.3.1 Modal parameters extracted from raw signals

##### (a) Case 1: Random excitation only

In the first test case the quarter vehicle model was excited only by random inputs, when the excitation modal parameters were:

$$A_1 = 0.0001m; A_2 = 0; A_3 = 0;$$

and Equation (5-5) reduced to:

$$y(t) = 0.0001randn(t)$$

An example of the responses of car body under random excitation in the time- and frequency- domains is presented in Figure 5-5. As can be seen from the frequency-domain response that the main power of the signal is around the system's natural resonance frequencies, which are 13.21 Hz and 56.35 Hz.

The SD identified by CoSS-SSI using the ten simulated datasets is shown in Figure 5-6. The correlation signal could be classified in a single subset because the quarter vehicle model is a linear model, and the excitation was pure white noise. Two stable modes, of frequencies 13.19 Hz and 56.42 Hz can be identified based on this SD. The errors between the identified frequencies and theoretical results were 0.15% and 0.12%, respectively. The identified damping ratios were 13.03% and 6.66% respectively for these two modes, with corresponding errors of 0.53% and 5.21%. It can be seen that when the quarter vehicle model was excited only by stationary white noise the modal parameters were identified accurately via CoSS-SSI.

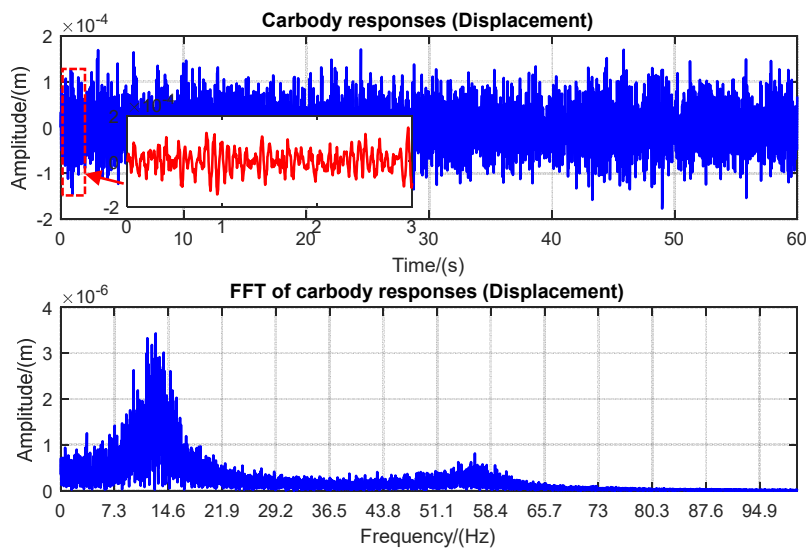


Figure 5-5 Car body responses under random excitation only

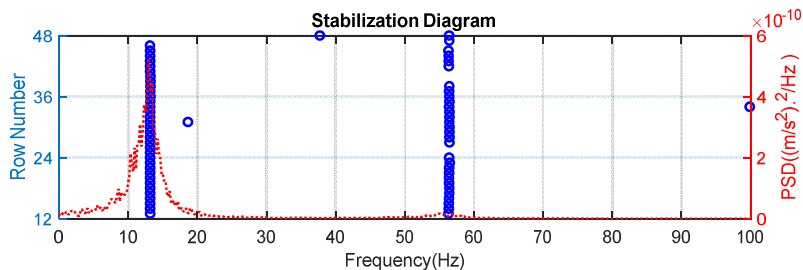


Figure 5-6 SD identified by CoSS-SSI for quarter vehicle model excited by white noise random input only

**(b) Case 2: Pulse train and random excitations**

The second case is with the pulse train excitation added to the random excitation. The additional parameters of the excitation model (Section 5.3.2) are: frequency of the pulse train is as derived from an experimental study on the roller rig ( $f_{ex} = 3.65$  Hz) which will be presented in Chapter 8, and amplitude of the pulse train is  $A_3 = 0.005$  m. The ratio of two signal amplitudes were determined according to the real signal characteristics collected in Chapter 8.

$$A_1 = 0.0001 \text{ m}; A_2 = 0; A_3 = 0.005 \text{ m}; f_{ex} = 3.65 \text{ Hz}$$

Equation (5-5) reduces to:

$$y(t) = 0.0001 \text{randn}(t) + 0.005 y_3(t)$$

$$\text{where } y_3(t) = \begin{cases} 1 & t = n * 1/3.65, n = 1, 2, 3 \dots \\ 0 & \text{otherwise} \end{cases}$$

The responses of the quarter vehicle model under simultaneous pulse train and random excitations are presented in Figure 5-7. As can be seen from the time-domain signal the responses resulting from the pulse train input are clearly apparent. The effect of the pulse train excitation can be seen more clearly in the frequency-domain, where the peaks appear at the integral multiples of the pulse train frequency  $f_{ex} = 3.65$  Hz. It can be seen that the peaks at 14.6 Hz and 54.75 Hz are higher than the adjacent ones as they are close to the natural response frequencies.

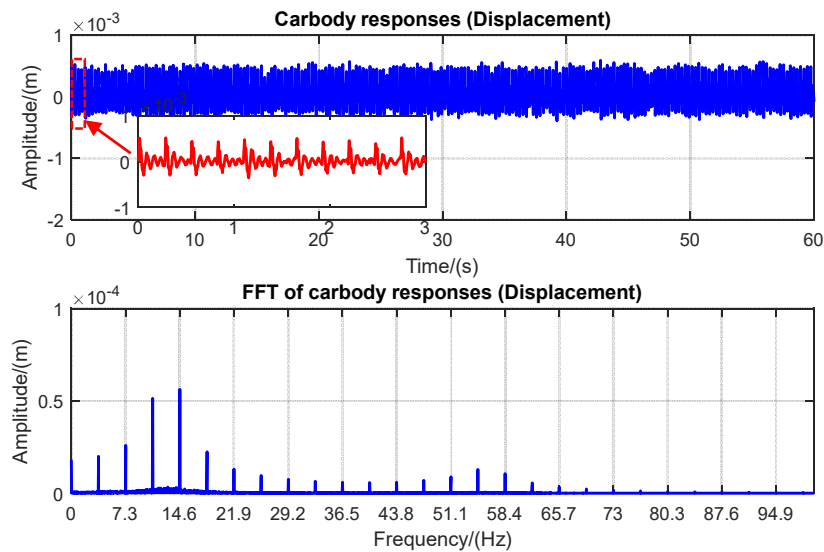


Figure 5-7 Car body responses under pulse train and random excitations

The SD identified by the CoSS-SSI utilising the responses obtained in this case is presented in Figure 5-8. It can be seen the identified stable modes were the same as the SD identified in Case 1 (Figure 5-6). Such results indicate that pulse train excitation has little or no effect on the OMA results. Furthermore, the identified frequencies, in this case, were 13.20 Hz and 56.12 Hz, which were very close to the theoretical resonance frequencies (13.21 Hz and 56.35 Hz). The identified damping ratios for these two modes were 12.11% and 6.40%, respectively, with errors of 7.56% and 1.11%. It can be seen that both frequency and damping ratio were accurately identified.

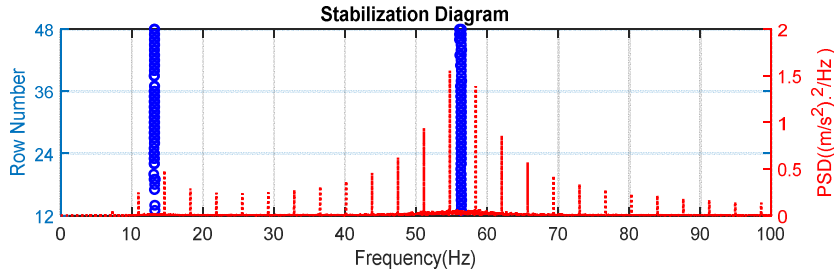


Figure 5-8 SD identified by CoSS-SSI for quarter vehicle model excited by pulse train and random inputs

### (c) Case 3: One harmonic, pulse train and random excitations

In the third case, a harmonic excitation, where  $N = 1$  in Equation (5-7), was added to the excitations of Case 2. As mentioned earlier, harmonic excitation is a common phenomenon in mechanical systems containing a rotating component which invariably means an eccentric load. The harmonic frequency  $f_1$  was set to same as the pulse train frequency  $f_{ex} = 3.65 \text{ Hz}$ , and the harmonic amplitude was set equal to that of the random excitation (0.0001 m).

$$A_1 = 0.0001 \text{ m}; A_2 = 0.0001 \text{ m}; A_3 = 0.005 \text{ m};$$

$$f_{ex} = 3.65 \text{ Hz}; f_1 = 3.65 \text{ Hz}, \varphi_1 = \pi/3;$$

Equation (5-5) reduces to:

$$y(t) = 0.0001 \text{randn}(t) + 0.0001 \sin(2\pi(3.65)t + \pi/3) + 0.005y_3(t)$$

$$\text{where } y_3(t) = \begin{cases} 1 & t = n * 1/3.65, n = 1, 2, 3 \dots \\ 0 & \text{otherwise} \end{cases}$$

Under such excitations, the car body responses are presented in Figure 5-9. The time-domain signal was comparable to the responses obtained in Case 2, and shown in Figure 5-7. This is because the amplitude of the harmonic was small. However, the frequency domain signal

was different from Case 2, specifically, the peak at 3.65Hz was substantially higher than the peak for Case 2, shown in Figure 5-7.

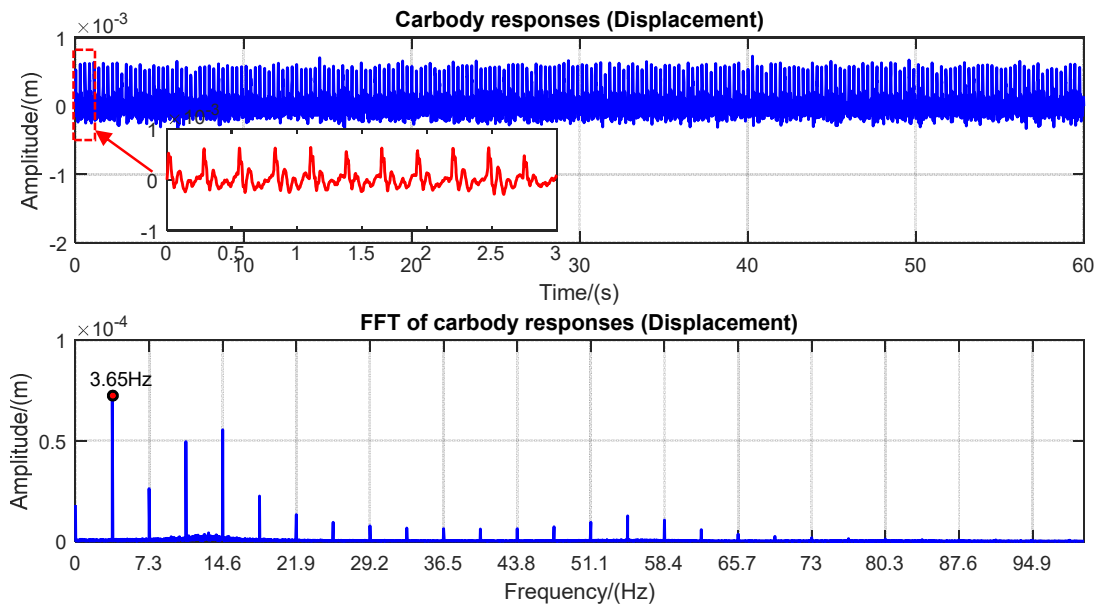


Figure 5-9 Car body responses under one harmonic, pulse train and random excitations

In this case, the identified SD is presented in Figure 5-10. Firstly, it can be seen that three relative stable modes are seen at frequencies of 3.56 Hz, 13.14 Hz and 56.37 Hz. The corresponding damping ratios for these three frequencies were 1.71%, 13.06% and 6.43%, respectively. It is evident that the second and third modes at 13.14 Hz and 56.37 Hz were the true ones, but the mode at 3.56 Hz was false, resulting from the harmonic excitation. Secondly, it can be observed that the mode at 13.14 Hz was unstable until the row number greater than 27, and contained fewer stable modes than the first two cases. Based on these analyses, it can be seen that harmonic excitation has significant effects on the OMA results.

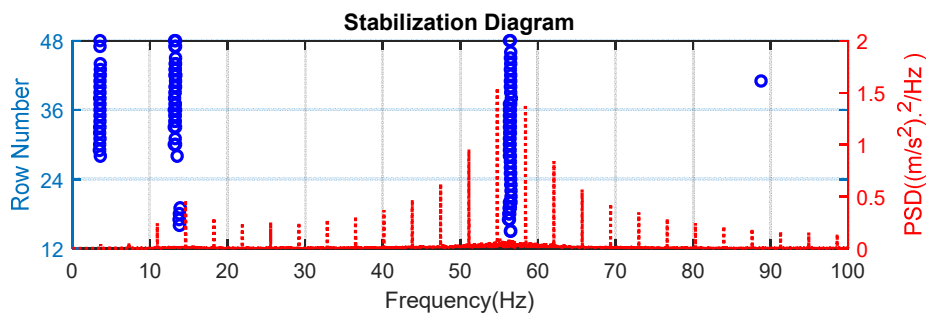


Figure 5-10 SD identified by CoSS-SSI for quarter vehicle model excited by one harmonic, pulse train and random inputs

**(d) Case 4: Two harmonics, pulse train and random excitations**

It has been proved in Case 3 that harmonic excitation has a significant effect on the OMA results. Here we added a second harmonic excitation to the excitations present in Case 3, equivalent to  $N = 2$  in Equation (5-7). The excitation parameters for the second harmonic frequency are: amplitude 0.0001 m, frequency 17.0 Hz, and phase  $\pi/4$ . The frequency and phase were chosen to avoid vibration superposition with the first harmonic.

$$A_1 = 0.0001 \text{ m}; A_2 = 0.0001 \text{ m}; A_3 = 0.005 \text{ m}; f_{ex} = 3.65 \text{ Hz};$$

$$f_1 = 3.65 \text{ Hz}; \varphi_1 = \pi/3; f_2 = 17.0 \text{ Hz}, \varphi_2 = \pi/4$$

Equation (5-5) reduces to

$$y(t) = 0.0001 \text{randn}(t) + 0.0001 \sin(2\pi(3.65)t + \pi/3) \\ + 0.0001 \sin(2\pi(17.0)t + \pi/4) + 0.005y_3(t)$$

$$\text{where } y_3(t) = \begin{cases} 1 & t = n * 1/3.65, n = 1, 2, 3 \dots \\ 0 & \text{otherwise} \end{cases}$$

The car body responses to such excitations is presented in Figure 5-11. It can be seen from the frequency domain signal that a peak appears at 17 Hz which resulted from the second harmonic excitation. Otherwise the features of Figure 5-11 are similar to Figure 5-9.

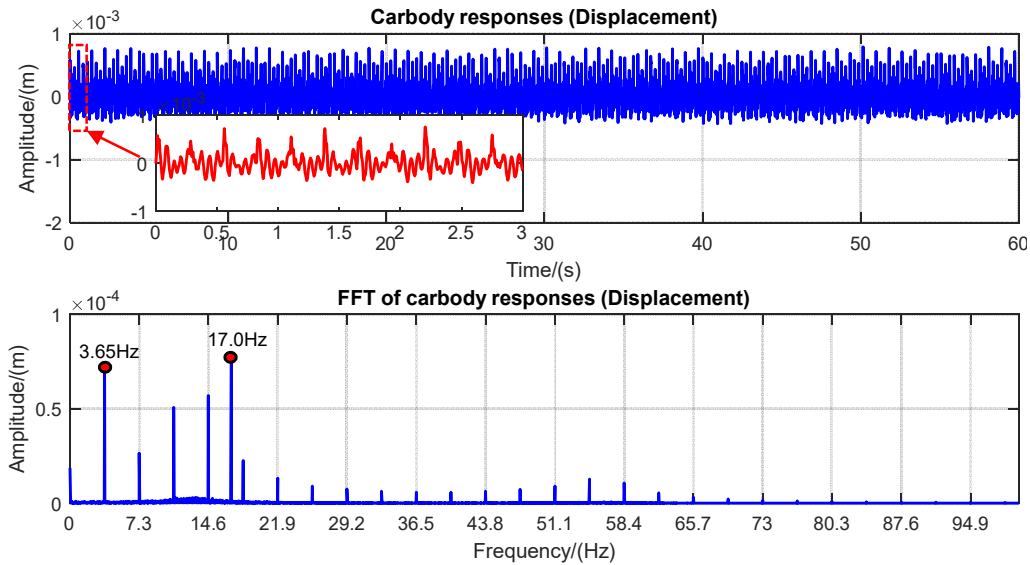


Figure 5-11 Car body responses under two harmonics, pulse train and random excitations

The SD identified by CoSS-SSI in this fourth case is presented in Figure 5-12. There were three relatively stable modes presented in the SD. The first two modes are close to 3.56 Hz and 17.37 Hz, respectively, and it is taken that these were generated by the two harmonics

in the excitations. The identified damping ratios for these two modes were 17.74% and 5.64%. The third mode was close to 56.39Hz, the resonance frequency of the system's second-order mode. However, the first mode of the quarter vehicle system which was around 13.21 Hz is not seen. The failure to identify the system's first natural mode is attributed to the second harmonic frequency being too close to the first resonance frequency.

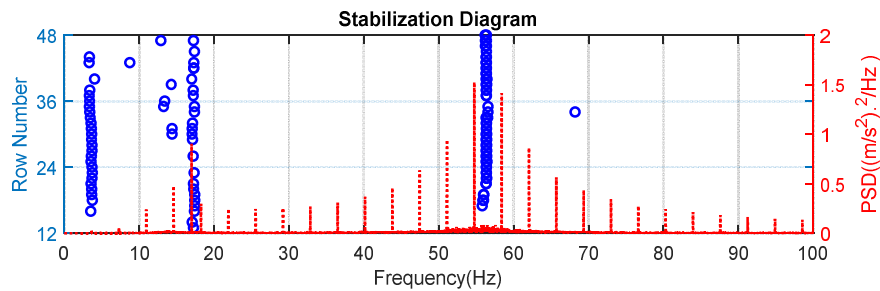


Figure 5-12 SD identified by CoSS-SSI for quarter vehicle model excited by two harmonics, pulse train and random inputs

In summary, OMA in the presence of harmonics will lead to false modes which could be challenging to filter out. Furthermore, the harmonic excitation could lead to true modes being overwhelmed if the harmonic frequency was too close to a system natural frequency. Thus, harmonic effects have to be filtered out before conducting OMA.

### 5.3.3.2 Modal parameters extracted from filtered signals

It has been demonstrated in Section 5.3.3.1 that harmonics can result in false modes, see Cases 3 and 4 above. Therefore, the signals obtained in these two cases will be filtered via CE to filter out the harmonics before conducting modal identification. The modal parameters as extracted from the filtered signal will be presented in the following subsections.

#### (a) Case 1: Excitations contained one harmonic

An example of a real cepstrum applied to the signal obtained in Case 3 of Section 5.3.3.1 (which contained one harmonic frequency in the excitation load) is presented in Figure 5-13. The cepstrum is shown as the blue line, a short-pass lifter is applied to filter out the harmonics which had been introduced. The length of the short-pass lifter  $s$  is set to 0.25 second to filter out all the periodic components and keep the modal information only, as shown in Figure 5-13 as a black line, and the edited cepstrum is the red dash line.

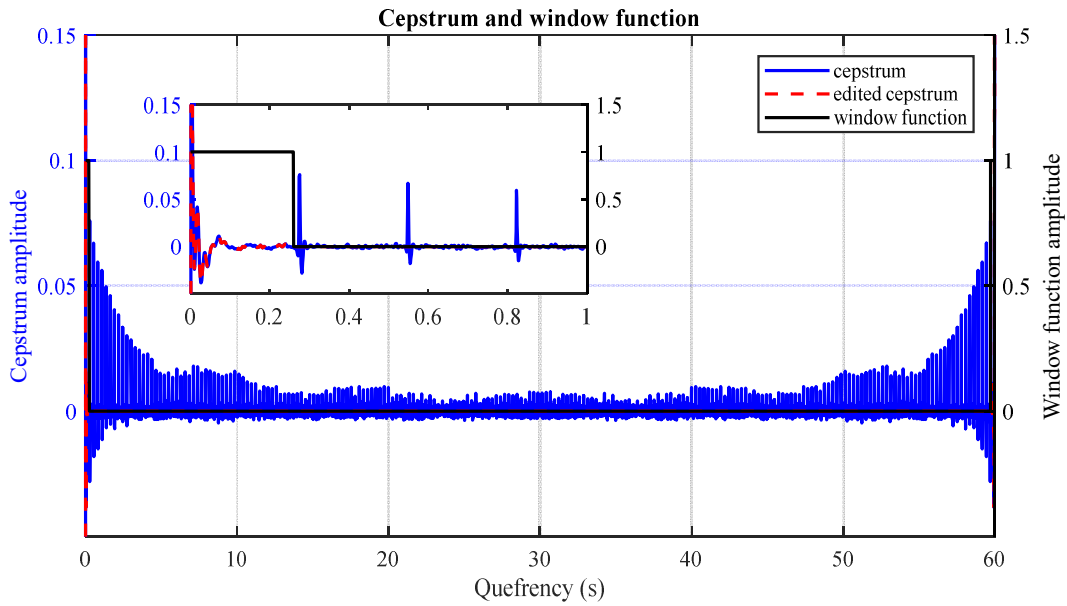


Figure 5-13 Cepstrum, window function and edited cepstrum

According to the CE process, see Section 5.2, an example of the filtered signal in the time- and frequency-domains is presented in Figure 5-14. The raw signal is also presented in Figure 5-14. It can be seen from the time-domain that the amplitude of the signal decreased visibly after the filter process via CE. Moreover, it can be seen from the frequency-domain that the effects of the pulse train and the corresponding harmonic excitations have been filtered out by the CE. We see that the main power contained in the filtered signal is close to system's first natural resonance frequency.

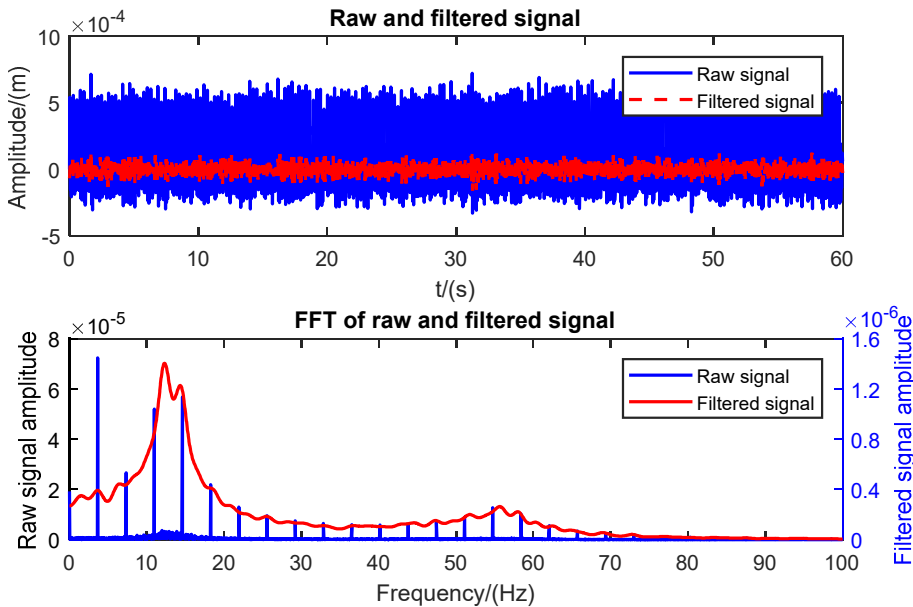


Figure 5-14 Carbody responses raw signal and filtered signal

The filtered signals were used to extract the modal parameters of the quarter vehicle model through CoSS-SSI. The identified SD is shown as in Figure 5-15. Comparing with Figure 5-10, it can be seen that CE improve the SNR for modal identification: that the false mode resulted from the harmonic excitation was successfully filtered out, and the identified stable modes were more stable. In particular, we see the frequency of the first mode is 13.18 Hz and the second one is 56.02 Hz, which are very close to the natural resonant frequencies of 13.21 Hz and 56.35 Hz. The short-pass lifter did not introduce addition damping ratio during the filtering process and the corresponding damping ratios for these two modes are 12.37% and 5.76%, respectively close to the theoretical values of 13.10% and 6.33% calculated for the simulated railway vehicle model. Comparing the identified results with the theoretical values, the frequency errors were 0.23% and 0.59% for the first and second modes respectively; and the damping errors were 5.57% and 9.0%, respectively. These errors are small and quite acceptable. In other words, CE is an effective method for removing harmonic effects from OMA.

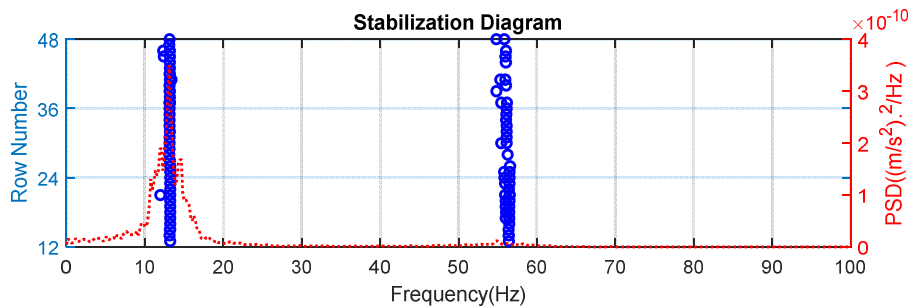


Figure 5-15 SD identified by CoSS-SSI for quarter vehicle model excited by one harmonic, pulse train and random inputs using filtered signal

### (b) Case 2: Excitations contained two harmonics

The effectiveness of CE with OMA to remove the effects of one harmonic has been demonstrated. The next stage was to apply CE to Case 4 of Section 5.3.3.1 with two harmonic excitations. The same CE process as the above was employed, and the identified SD is shown in Figure 5-16. It can be seen that two stable modes of frequencies 13.15 Hz and 56.53 Hz are identified, with damping ratios of 13.01% and 5.65%, respectively. The frequency identification errors are 0.45% and 0.32%, respectively; and the damping ratio identification errors are 0.69% and 10.74%, respectively. The modal parameters were accurately identified using the filtered signal via CE. The effectiveness of CE is evident when comparing Figure 5-16 with Figure 5-12.

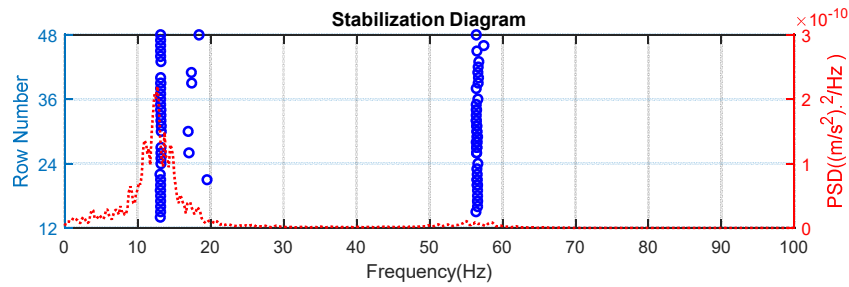


Figure 5-16 SD identified by CoSS-SSI for quarter vehicle model excited by two harmonics, pulse train and random inputs using filtered signal

On the basis of the results obtained in the two last cases of this subsection, it can be concluded that the effectiveness of CE to eliminate harmonic effects has been demonstrated. Therefore, CE will be employed in the following experimental study.

## 5.4 Findings

In this chapter, CE was introduced as a suitable approach to remove harmonic effects contaminating the OMA. Firstly, a quarter vehicle model and an excitation model were developed to verify the influence of a pulse train and harmonic excitations on the OMA identification results. Then, CE was utilised to filter out the harmonic effects. Based on the simulation results, the following conclusions can be drawn:

- 1) The pulse train excitation has no impact on OMA.
- 2) OMA in the presence of harmonics could result in false modes related to the harmonic frequencies.
- 3) OMA in the presence of harmonics could lead to true modes of the system being overwhelmed.
- 4) CE is an effective and achievable approach to remove the harmonic effects contained in OMA results in the presence of harmonic excitation.

Therefore, CE will be employed to filter out the harmonic effects in the following full-scale roll rig experimental study.

---

## CHAPTER 6 CONDITION MONITORING OF ROAD VEHICLE SUSPENSION SYSTEMS USING CoSS-SSI

---

*This chapter focuses on the CM of a vehicle suspension system using OMA, CoSS-SSI, as proposed in Chapter 4. Firstly, a brief overview of a general road vehicle suspension system is presented. Then, a simplified suspension system is developed and employed to evaluate the performance of CoSS-SSI. Last but not least, a field test was conducted on a commercially available car, a Vauxhall Zafira running on a traditional country road near Huddersfield, UK, at an off-peak time. The road vehicle tests included the vehicle suspension subject to normal and abnormal conditions.*

*The experimental results indicated that CoSS-SSI performed excellently in extracting the modal parameters of the road vehicle's suspension systems, and thus offers an attractive possibility for online monitoring.*

## 6.1 Introduction

Considerable research has been conducted to ensure the effective performance of vehicle suspension systems because of their decisive role in determining the comfort and safety of a vehicle [50], [51], [104], [105], [168]–[170]. It has long been understood that CM is an efficient approach for ensuring the continued good performance of vehicle suspension systems. However, while few studies have been conducted to achieve online CM for vehicle suspension systems, it has been demonstrated that OMA is able to provide online CM of, e.g., the structural health of bridges and buildings, and is widely applied [138], [171].

A novel OMA method, CoSS-SSI, was proposed in Chapter 4, for assessing the signal characteristics of vehicle responses. The performance of CoSS-SSI was successful when evaluated by a 3-DOF numerical vibration model. In this chapter, the performance of CoSS-SSI for online CM of a road vehicle's suspension will be verified via two experimental studies. The first on a simplified suspension system, and the second on a real vehicle.

## 6.2 Simplified suspension system

### 6.2.1 Overview of road vehicle suspension

It is well known that suspension systems for road vehicle are an assembly which contains springs, dampers and auxiliary devices to connect the vehicle body and wheels. The spring plays the role of absorbing impacts and provides cushioning in the case of a vehicle hitting a sudden bump. The spring also has the function of resisting movement, such as the rebounds of the wheel [172]. The damper, which is also called a shock absorber, is an energy consuming component and is employed to prevent continuous vibration of the suspension system once it has been set into motion. The location, type and number of springs will vary according to the suspension system with, typically, one damper for each wheel. However, the auxiliary devices are totally different in different types of suspensions. As an example, one of the most popular suspension system, the McPherson suspension, is presented in Figure 6-1.

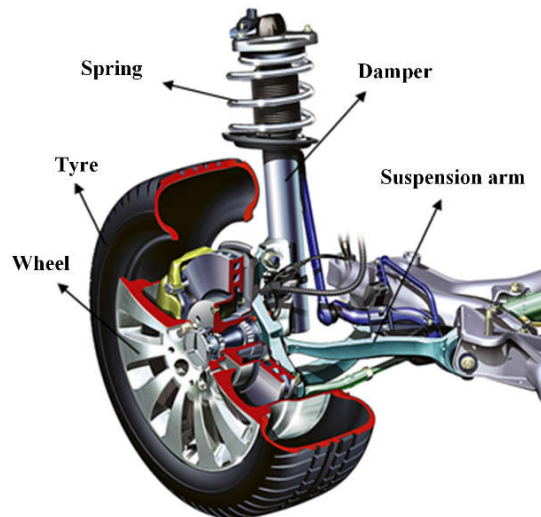


Figure 6-1 Photograph of McPherson suspension system [54]

Vehicle suspension systems can be categorised as dependent, independent and semi-dependent. The categorisations are presented in Figure 6-2, and the MacPherson strut suspension belongs to the independent category. Different types of suspension systems are applied in various vehicles according to their relative advantages, but all suspension systems are designed to safeguard the safety of the occupants, and ensure their comfort. The suspension system will also ensure the vehicle has excellent handling capability. To meet these requirements vehicle suspension systems are complex and nonlinear. Nonetheless, the models developed to investigate a vehicle's dynamic performance invariably describe the suspension system as a combination of a linear spring and a viscous damper, these models are commonly called quarter, half and full vehicle models. The proposed CoSS-SSI, OMA method is also linear.

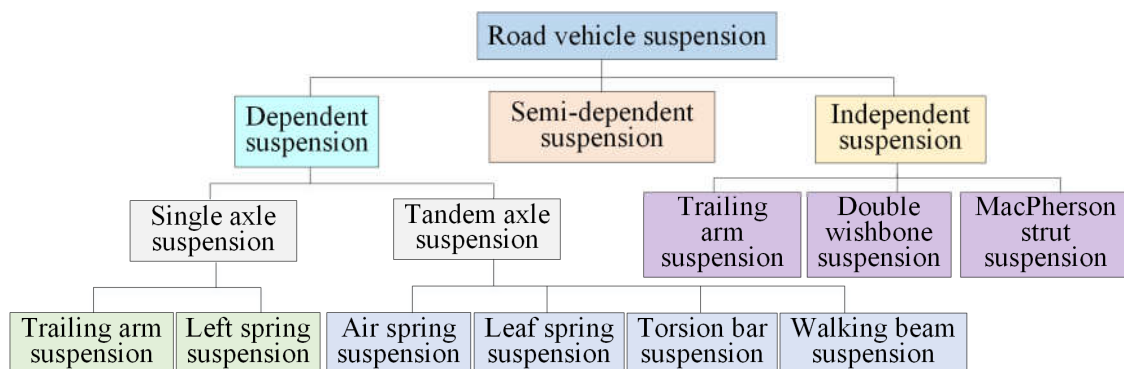


Figure 6-2 Categories of popular road vehicle suspension systems [54], [172]

A primary study to verify the effectiveness of CoSS-SSI, was undertaken using a simple test rig suspension system with four springs. This simplified suspension system, which is close to being a linear system, is introduced in detail in the following sub-section.

## 6.2.2 Introduction of the simplified suspension system

The simplified suspension system is shown as in Figure 6-3. As can be seen, a steel plate was hung up on a frame via four coil springs. M4 bolts connected the spring with the steel plate and support frame, the dimensions of the steel plate are given in Figure 6-4.

In this test rig, the steel plate was considered as the car body, and the coil springs considered as the vehicle's suspension system. A hammer with a rubber head was used to knock the steel plate at random time intervals and positions to mimic the random excitation from the road profile. Four acceleration sensors were installed under the four corners of the steel plate, as shown in Figure 6-3, to collect the responses of the system under random excitation.

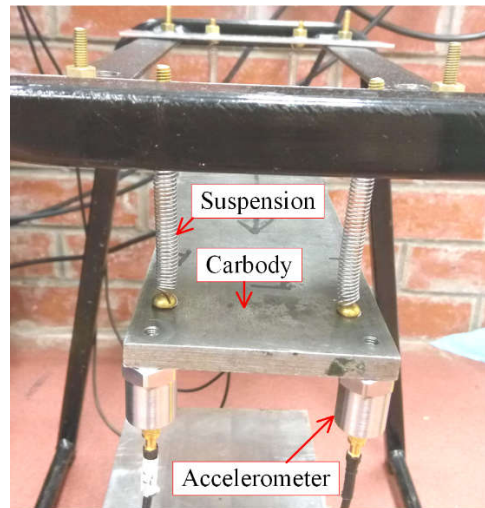


Figure 6-3 Photograph of simplified suspension system test rig

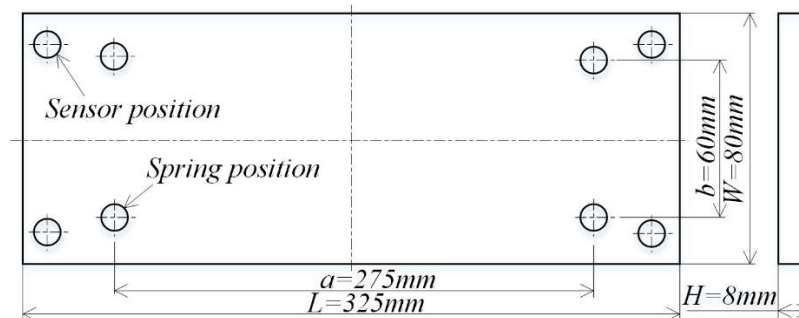


Figure 6-4 Dimensions of the steel plate (car body)

For the performance evaluation of CoSS-SSI, a reliable mathematical model is needed to obtain the theoretical modal parameters. The coil spring employed in this test rig had nearly linear characteristic as its damping ratio was relatively low and the coil spring were loaded vertically. So a reasonably accurate model can be developed due to the system's relative

simplicity and the related inertial parameters can be accurately measured. Such a model will be developed in the following sub-section.

### 6.2.3 3-DOF model and theoretical modal parameters

#### 6.2.3.1 Measurement of inertia parameters

In order to establish a correct mathematical model, the first step is to obtain the precise inertial parameters. These parameters include the mass and rotational inertia of the steel plate, and the stiffness of the coil spring.

The mass was the easiest parameter to measured, via a balance. The mass of the steel plate including the four accelerometers was  $m = 1.7138 \text{ kg}$ . The moment of inertia of the steel plate can be calculated from its mass and dimensions. A schematic of the simplified suspension system was drawn, see Figure 6-5, to define the moments of inertia for pitching ( $\theta$ ) and rolling( $\varphi$ ). The long side ( $L$ ) of the steel plate was defined as the direction of the  $x$  axis, the  $y$  axis was defined as the direction of the short side ( $W$ ), and  $z$  axis was the direction of the thickness ( $H$ ). Based on these definitions, the pitch inertia moment  $I_p$  and the roll inertia moment  $I_R$  can be calculated according to Equations (6-1) and (6-2).

$$I_p = \frac{m}{12}(L^2 + H^2) \quad (6-1)$$

$$I_R = \frac{m}{12}(W^2 + H^2) \quad (6-2)$$

The results for  $I_p$  and  $I_R$  are:

$$I_p = 1.630 \times 10^{-2} \text{ kg} \cdot \text{m}^2;$$

$$I_R = 9.987 \times 10^{-4} \text{ kg} \cdot \text{m}^2;$$

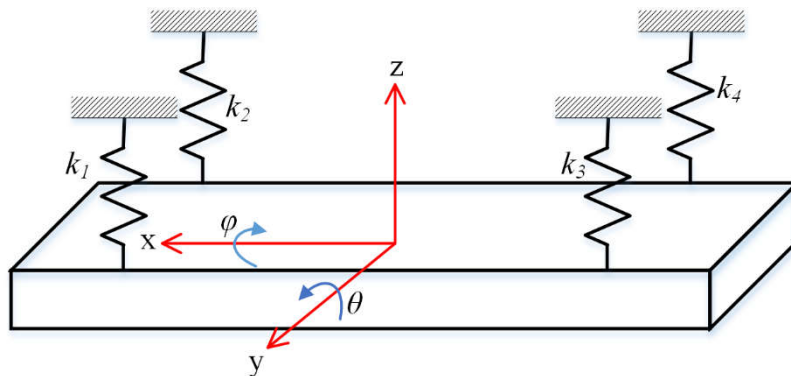


Figure 6-5 Schematic of the simplified suspension system

Another significant parameter in this test rig is the stiffness of the springs. As the employed spring is small in size, its stiffness can be measured according to Hook's law:  $F = k\Delta x$ . The spring was suspended vertically, and a series of masses  $50g$  were added as the load on the spring, as shown in Figure 6-6. The stiffness of the spring can be calculated according to the change of the measured spring length ( $\Delta x$ ) after adding a known mass. The change of spring length and added mass were measured eight times, and the average calculated stiffness was  $k = 157.5N/m$ .



Figure 6-6 Spring stiffness test

### 6.2.3.2 3-DOF model and theoretical modal parameter calculation

The theoretical modal parameters of the simplified suspension system can be calculated by developing a 3-DOF model and substituting the measured inertia parameters into the model. The 3-DOF model considered the bounce ( $z$ ), pitch ( $\theta$ ) and roll ( $\varphi$ ) of the steel plate shown in Figure 6-5. The dynamic equations of this 3-DOF model are given as follows, where the damping of the spring has not been taken into account:

$$m\ddot{z} = -k_1z_1 - k_2z_2 - k_3z_3 - k_4z_4 \quad (6-3)$$

$$I_P\ddot{\theta} = \frac{a}{2}(-k_1z_1 - k_2z_2 + k_3z_3 + k_4z_4) \quad (6-4)$$

$$I_R\ddot{\varphi} = \frac{b}{2}(-k_1z_1 + k_2z_2 - k_3z_3 + k_4z_4) \quad (6-5)$$

Where  $z_1, z_2, z_3, z_4$  are the vertical response of the four accelerometers installed on the four corners of the steel plate. The following relationships can be obtained:

$$z_1 = z + \frac{a}{2}\theta + \frac{b}{2}\varphi \quad (6-6)$$

$$z_2 = z + \frac{a}{2}\theta - \frac{b}{2}\varphi \quad (6-7)$$

$$z_3 = z - \frac{a}{2}\theta + \frac{b}{2}\varphi \quad (6-8)$$

$$z_4 = z - \frac{a}{2}\theta - \frac{b}{2}\varphi \quad (6-9)$$

Where  $a$  is the distance along the  $x$  axis between the springs and  $b$  is the distance along the  $y$  axis between the springs, see Figure 6-4. Note that given the small size of the rig the relative differences between  $a$  and  $L$ , and  $b$  and  $W$  are significant, so care must be taken to use the correct values when calculating modal parameters.

The stiffness of the four springs are  $k_1, k_2, k_3, k_4$  in this system, it is assumed they are identical ( $k_1 = k_2 = k_3 = k_4 = k$ ) because these four springs are the same type and have nearly the same load. Based on these relationships, these three dynamic equations can be expressed in the format of Equation (3-1) by arranging the inertia parameters in a matrix. The mass and stiffness matrices can be expressed as:

$$\mathbf{M} = \begin{bmatrix} m & 0 & 0 \\ 0 & I_P & 0 \\ 0 & 0 & I_R \end{bmatrix} \quad (6-10)$$

$$\mathbf{K} = \begin{bmatrix} 4k & 0 & 0 \\ 0 & a^2k & 0 \\ 0 & 0 & b^2k \end{bmatrix} \quad (6-11)$$

Then the state matrix of this system can be obtained according to Equation (3-6). Based on the state matrix, the theoretical modal parameters can be calculated, and the results are presented in Figure 6-7. It can be seen from Figure 6-7 that the bounce, pitch and roll modes corresponding to the 3-DOF of the model were successfully determined, and their resonance frequencies were found to be 2.73 Hz, 3.81 Hz and 4.53 Hz, respectively.

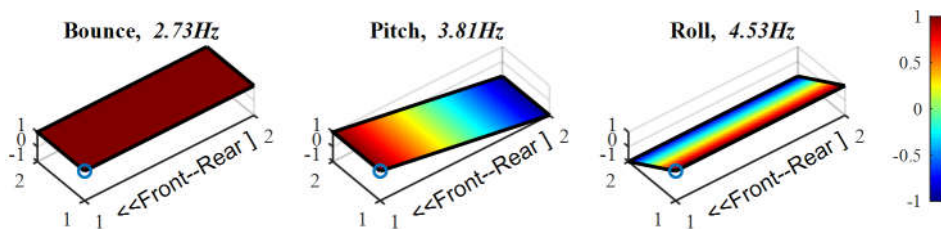


Figure 6-7 Theoretical modal parameters of the simplified suspension system

In the following subsection, experiments will be conducted to evaluate the performance of the OMA method proposed in Chapter 4.

## 6.2.4 Experimental results and analysis

### 6.2.4.1 Experiment set-up

As mention earlier, experiments were conducted on the simplified suspension system to identify the modal parameters via CoSS-SSI. The random inputs were given by a hammer with a rubber head, shown as in Figure 6-8. The randomness of the inputs includes the position and time of the excitations. That is to say, the hammer can deliver a vertical blow at any place on the steel plate, and the time interval between two consecutive blows was random.



Figure 6-8 Photograph of excitation hammer

The responses of the simplified suspension system under random excitation were collected by the four piezoelectric accelerometers shown in Figure 6-9. The specifications of these transducers are given in Table 6-1. It can be seen that the dynamic measurement frequency range of the employed accelerometer is wide, 0.5 Hz - 5,000 Hz. The resonance frequencies of the simplified suspension system are within the measurement range.



Figure 6-9 Photograph of the four (CA-YD-185) accelerometers used

Table 6-1 Specifications of the accelerometer

Manufacture	Model No.	Frequency range (Hz)	Serial No.	Sensitivity (mv / (m · s <sup>-2</sup> ))
SINOCERA	CA-YD-185	0.5-5000	71690	5.00
			71681	5.01
			71650	4.93
			71694	5.09

A dynamic data acquisition system (DAQs) with four channels was used for the test, see Figure 6-10. The DAQs was model 6231 manufactured by SINOCERA. Each of the four-channels had an independent Analogue/Digital (A/D) converter with sampling rate up to 96,000 Hz. The four channels of the DAQs are synchronised so that data acquisition can be simultaneous for all four channels. This DAQs is convenient for field tests as a USB connection with a laptop enables data transfer and power supply.



Figure 6-10 Photograph of the four-channel data acquisition system

For the accelerometers the sampling frequency was set at 2,000 Hz and sampling time was 180 s for each test. The test was repeated four times, which means four datasets were generated as the inputs for modal parameter identification. The collected data and the modal identification results are presented in the following sub-sections.

#### 6.2.4.2 Characteristics of simplified suspension system responses

An example of the measured response of the steel plate is presented in Figure 6-11, where the blue dashed line is the raw signal, and the red line is the signal filtered with a low pass Butterworth filter. The titles on the figure, front left, front right, rear left and rear right, refer to the positions of the accelerometers.

In the time-domain signal, numerous pulses can be observed due to the random blows. The portion of the plots between 15s to 30s was magnified to allow easier observation of the characteristics of the filtered signal. It can be seen that the amplitudes of filtered signals were significantly decreased, especially the pulse responses. Moreover, it can also be observed that the responses at the four positions were almost identical, this was because the steel plate was of small size.

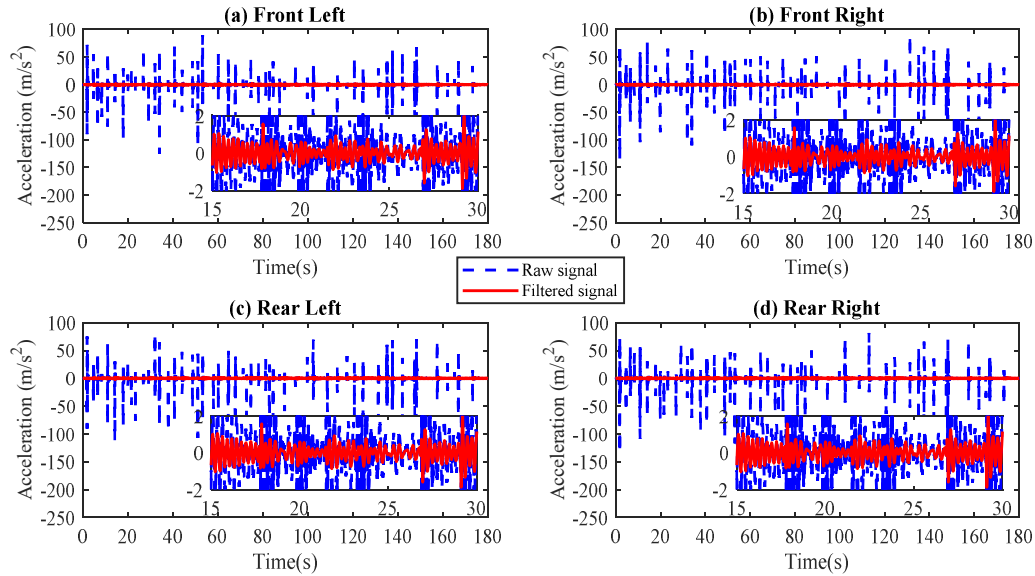


Figure 6-11 Responses of simplified suspension system in time-domain

The PSDs corresponding to the filtered signals are presented in Figure 6-12. Two peaks can be observed in the PSD, around 2.7 Hz and 3.7 Hz, respectively. Figure 6-7, strongly suggests these two peaks are the first (2.73 Hz) and second (3.81 Hz) resonance frequencies. However, the third resonance frequency (4.53 Hz) cannot be seen in Figure 6-12. It is noted that the peak amplitudes at the four corners do differ slightly which is related to the mode shapes. The modal parameters will be identified in the following sub-section.

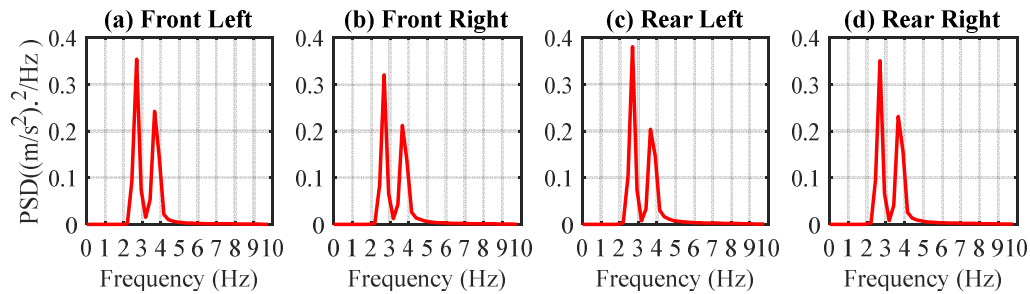


Figure 6-12 PSD of the simplified suspension system responses

### 6.2.4.3 Modal parameters of a simplified suspension system

In this sub-section, the modal parameters of the simplified suspension system are identified via CoSS-SSI using the four datasets. According to the flowchart of CoSS-SSI (Figure 4-2), the first step is dividing each dataset into  $K$  segments, here set equal to 21. Thus, 84 segments of data were obtained, and then correlation functions were calculated for each of the 84 segments. The next step should categorise the 84 correlation signal segments into  $J$  subsets. However, the given suspension system is so simple, and with low damping, that it

can be considered a linear system, which allowed all the correlation signal segments to be categorised as one subset ( $J = 1$ ).

Then, following the flowchart of CoSS-SSI, the SD can be identified, and this is presented in Figure 6-13. The stable thresholds for Equations (3-53), (3-54) and (3-56) were set at 0.1, 0.2 and 0.5, respectively. Three relatively stable modes are presented in the SD. These three stable modes were obtained by setting the second threshold at 70%, which was by dividing the number of stable points by the calculated maximum number of orders (see Equation (3-57)), see Figure 6-14. The identified modal parameters are presented in Figure 6-15.

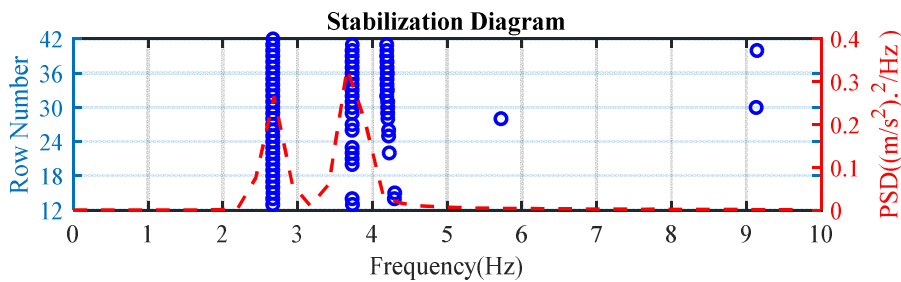


Figure 6-13 SD identified by CoSS-SSI for the simplified suspension system

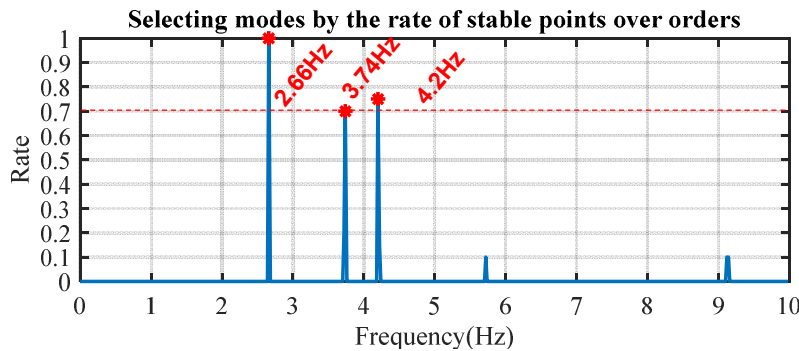


Figure 6-14 Stable modes selected by the ratio of stable points

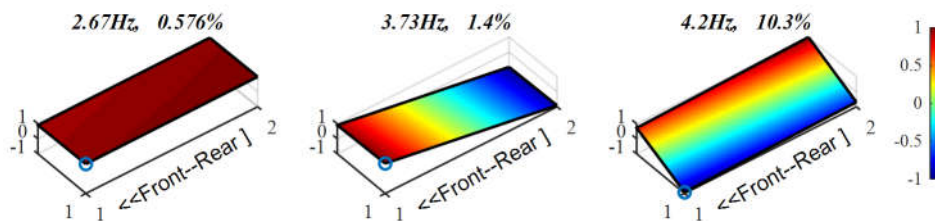


Figure 6-15 Modal parameters of simplified suspension system identified by CoSS-SSI

According to the identified mode shapes, the bounce, pitch and roll modes of the simplified suspension system were identified. Table 6-2 compares theoretical and identified modal parameters, but the damping ratios were not considered in the model. It can be seen from Table 6-2 that both frequency and mode shape were accurately identified. Moreover, it can be observed that the maximum errors in frequency and mode shape occurred for the third

mode (roll), because of the higher damping ratio, which was over 10%. Nonetheless, the maximum errors are still acceptable, which means CoSS-SSI has the capability of extracting modal parameters from highly damped systems.

Table 6-2 Modal parameters identification errors of the simplified suspension system

Mode	Theoretical frequency (Hz)	Identified frequency(Hz)	Frequency errors	MAC
Bounce	2.73	2.67	2.20%	0.999
Pitch	3.81	3.73	2.10%	0.998
Roll	4.53	4.20	7.28%	0.976

Based on the results and analysis, it can conclude that CoSS-SSI has provided outstanding enhancement of OMA, even for a system with high damping. In the next section, the performance of CoSS-SSI will be evaluated by a field test.

### 6.3 Vehicle suspension system field test

A Vauxhall Zafira, a compact Multi-Purpose Vehicle (MPV) with seven seats, as shown in Figure 6-16, was utilised in this field test. The Vauxhall Zafira is front-wheel drive by a 5-cylinder petrol engine and its suspension is a conventional McPherson suspension, see Figure 6-1. In this test, a suspension fault was introduced by artificially changing the car's tyre pressure which will change the stiffness of the tyre.



Figure 6-16 Photograph of employed car for field test

In this section, a 7-DOF lumped mass model for the tested car will be presented followed the experimental results and discussion.

### 6.3.1 7-DOF full vehicle model and theoretical modal parameters

#### 6.3.1.1 Kinematic equations of a vertical vehicle model

The lumped mass model is widely used to investigate the dynamic behaviour of the vehicle, and a 7-DOF full vehicle model is developed in this section because pitch and roll modes of the car body have to be considered for the purpose of suspension system monitoring. The 7-DOF includes bounce ( $z_b$ ), pitch ( $\theta$ ) and roll ( $\varphi$ ) of the car body just as in the 3-DOF model, but with the addition of bounce of the four wheels ( $z_w$ ), see Figure 6-17. The kinematic equations developed on the basis of Newton's law, are listed below [54], [153]. It is worth noting that this model is assumed symmetry about  $y$  axis because the centre of gravity of the vehicle is nearly on  $y$  axis according to the calculation in [54].

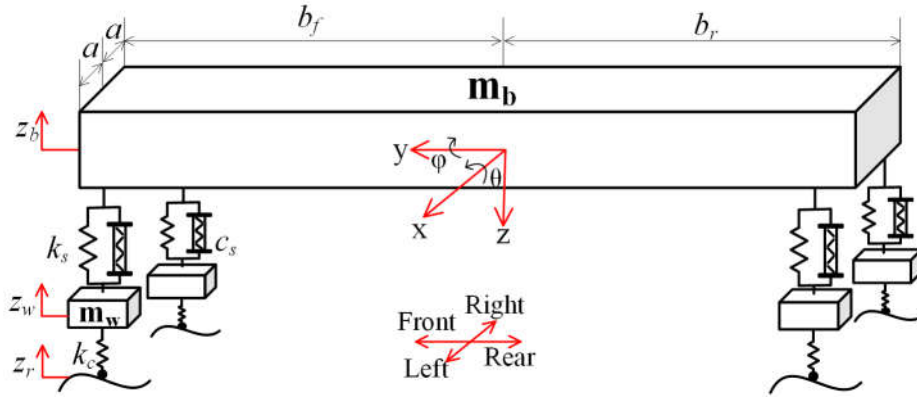


Figure 6-17 Schematic of the 7-DOF vehicle model [153]

Bounce of car body [54], [153]:

$$\begin{aligned}
 m_b \ddot{z}_b = & -k_{sfl}(z_{bfl} - z_{wfl}) - k_{sfr}(z_{bfr} - z_{wfr}) \\
 & -k_{srl}(z_{brl} - z_{wrl}) - k_{srr}(z_{brr} - z_{wrr}) \quad (6-12) \\
 & -c_{sfl}(\dot{z}_{bfl} - \dot{z}_{wfl}) - c_{sfr}(\dot{z}_{bfr} - \dot{z}_{wfr}) \\
 & -c_{srl}(\dot{z}_{brl} - \dot{z}_{wrl}) - c_{srr}(\dot{z}_{brr} - \dot{z}_{wrr})
 \end{aligned}$$

Pitch of the car body [54], [153]:

$$\begin{aligned}
 I_P \ddot{\theta} = & -b_f [k_{sfl}(z_{bfl} - z_{wfl}) + k_{sfr}(z_{bfr} - z_{wfr}) \\
 & + c_{sfl}(\dot{z}_{bfl} - \dot{z}_{wfl}) + c_{sfr}(\dot{z}_{bfr} - \dot{z}_{wfr})] \quad (6-13) \\
 & + b_r [k_{srl}(z_{brl} - z_{wrl}) + k_{srr}(z_{brr} - z_{wrr}) \\
 & + c_{srl}(\dot{z}_{brl} - \dot{z}_{wrl}) + c_{srr}(\dot{z}_{brr} - \dot{z}_{wrr})]
 \end{aligned}$$

Roll of the car body [54], [153]:

$$\begin{aligned}
I_R \ddot{\phi} = & -a[k_{sfl}(z_{bfl} - z_{wfl}) + k_{srl}(z_{brl} - z_{wrl}) \\
& + c_{sfl}(\dot{z}_{bfl} - \dot{z}_{wfl}) + c_{srl}(\dot{z}_{brl} - \dot{z}_{wrl})] \quad (6-14) \\
& + a[k_{sfr}(z_{bfr} - z_{wfr}) + k_{srr}(z_{brr} - z_{wrr}) \\
& + c_{sfr}(\dot{z}_{bfr} - \dot{z}_{wfr}) + c_{srr}(\dot{z}_{brr} - \dot{z}_{wrr})]
\end{aligned}$$

Bounce of the four wheels [54], [153]:

$$\begin{aligned}
m_{wfl} \ddot{z}_{wfl} = & k_{sfl}(z_{bfl} - z_{wfl}) + c_{sfl}(\dot{z}_{bfl} - \dot{z}_{wfl}) \quad (6-15) \\
& - k_{cfl}(z_{wfl} - z_{rfl})
\end{aligned}$$

$$\begin{aligned}
m_{wfr} \ddot{z}_{wfr} = & k_{sfl}(z_{bfr} - z_{wfr}) + c_{sfl}(\dot{z}_{bfr} - \dot{z}_{wfr}) \quad (6-16) \\
& - k_{cfr}(z_{wfr} - z_{rfr})
\end{aligned}$$

$$\begin{aligned}
m_{wrl} \ddot{z}_{wrl} = & k_{srl}(z_{brl} - z_{wrl}) + c_{srl}(\dot{z}_{brl} - \dot{z}_{wrl}) \quad (6-17) \\
& - k_{crl}(z_{wrl} - z_{rrl})
\end{aligned}$$

$$\begin{aligned}
m_{wrr} \ddot{z}_{wrr} = & k_{srr}(z_{brr} - z_{wrr}) + c_{srr}(\dot{z}_{brr} - \dot{z}_{wrr}) \quad (6-18) \\
& - k_{crr}(z_{wrr} - z_{rrr})
\end{aligned}$$

Where  $z_{bi}$  ( $i = fl, fr, rl, rr$ ) are the vertical responses of the front-left ( $fl$ ), front-right ( $fr$ ), rear-left ( $rl$ ) and rear-right ( $rr$ ) corners of the car body;  $z_{wi}$  ( $i = fl, fr, rl, rr$ ) are the vertical responses of the wheels;  $z_{ri}$  ( $i = fl, fr, rl, rr$ ) are the road profile inputs for the four wheels. The meanings and values of other symbols are tabulated in Table 6-3.

Table 6-3 Parameters of 7-DOF full vehicle model [54]

Symbol	Meaning	Value
$m_b$	Vehicle sprung mass	1,480 kg
$m_{wfl}, m_{wfr}, m_{wrl}, m_{wrr}$	Unsprung masses	40.5 kg
$I_P$	Moment inertia of pitching	2,200 kg · m <sup>2</sup>
$I_R$	Moment inertia of rolling	360 kg · m <sup>2</sup>
$k_{sfl}, k_{sfr}$	Stiffness of front suspension	21,500 N/m
$k_{srl}, k_{srr}$	Stiffness of rear suspension	19,500 N/m
$c_{sfl}, c_{sfr}$	Damping coefficients of front suspension	1,400 N · s/m
$c_{srl}, c_{srr}$	Damping coefficients of rear suspension	1,400 N · s/m
$k_{cfl}, k_{cfr}, k_{crl}, k_{crr}$	Stiffness of tyre	190,900 N/m
$a$	Half width of the car	0.702 m
$b_f$	Distance of front axle to car's centre of gravity	1.22 m
$b_r$	Distance of rear axle to car's centre of gravity	1.58 m

Moreover, the relationships between the displacement at the vehicle's four corners and centre of gravity can be expressed as follows using the given symbols, where the angles of pitch and roll are considered small:

$$z_{bfl} = z_b - b_f\theta + a\varphi \quad (6-19)$$

$$z_{bfr} = z_b - b_f\theta - a\varphi \quad (6-20)$$

$$z_{brl} = z_b + b_r\theta + a\varphi \quad (6-21)$$

$$z_{brr} = z_b + b_r\theta - a\varphi \quad (6-22)$$

On the basis of the kinematic equations and the displacement relationships, the 7-DOF vehicle model can be expressed in matrix format according to Equation (3-1). The mass (**M**), stiffness (**K**) and damping (**C**) matrices are presented in Equations (6-23), (6-24) and (6-25), respectively.

According to equations (3-6) and (3-7), the state-space model of this 7-DOF vehicle model can be constructed, and this model can evaluate the vertical dynamical characteristics.

$$\mathbf{M} = \begin{bmatrix} m_b & 0 & 0 & 0 & 0 & 0 & 0 \\ 0 & I_p & 0 & 0 & 0 & 0 & 0 \\ 0 & 0 & I_R & 0 & 0 & 0 & 0 \\ 0 & 0 & 0 & m_{wfl} & 0 & 0 & 0 \\ 0 & 0 & 0 & 0 & m_{wfr} & 0 & 0 \\ 0 & 0 & 0 & 0 & 0 & m_{wrl} & 0 \\ 0 & 0 & 0 & 0 & 0 & 0 & m_{wrr} \end{bmatrix} \quad (6-23)$$

$$\mathbf{K} = \begin{bmatrix}
 (k_{sfl} + k_{sfr} & b_f(k_{sfl} + k_{sfr}) & a(k_{sfl} - k_{sfr} & -k_{sfl} & -k_{sfr} & -k_{srl} & -k_{srr}) \\
 +k_{srl} + k_{srr}) & -b_r(k_{srl} + k_{srr}) & +k_{srl} - k_{srr}) & & & & \\
 b_f(k_{sfl} + k_{sfr}) & b_f^2(k_{sfl} + k_{sfr}) & ab_f(k_{sfl} - k_{sfr}) & -b_f k_{sfl} & -b_f k_{sfr} & -b_r k_{srl} & -b_r k_{srr} \\
 -b_r(k_{srl} + k_{srr}) & +b_r^2(k_{srl} + k_{srr}) & -ab_r(k_{srl} - k_{srr}) & & & & \\
 a(k_{sfl} - k_{sfr} & ab_f(k_{sfl} - k_{sfr}) & a^2(k_{sfl} + k_{sfr} & -ak_{sfl} & ak_{sfr} & -ak_{srl} & ak_{srr}) \\
 +k_{srl} - k_{srr}) & -ab_r(k_{srl} - k_{srr}) & +k_{srl} + k_{srr}) & & & & \\
 -k_{sfl} & -b_f k_{sfl} & -ak_{sfl} & k_{sfl} & 0 & 0 & 0 \\
 +k_{cfl} & & & & & & \\
 -k_{sfr} & -b_f k_{sfr} & ak_{sfr} & 0 & k_{sfr} & 0 & 0 \\
 +k_{cfr} & & & & & & \\
 -k_{srl} & b_r k_{srl} & -ak_{srl} & 0 & 0 & k_{srl} & 0 \\
 +k_{crl} & & & & & & \\
 -k_{srr} & b_r k_{srr} & ak_{srr} & 0 & 0 & 0 & k_{srr} \\
 +k_{crr} & & & & & & 
 \end{bmatrix} \quad (6-24)$$

$$\mathbf{C} = \begin{bmatrix}
 (c_{sfl} + c_{sfr} & b_f(c_{sfl} + c_{sfr}) & a(c_{sfl} - c_{sfr} & -c_{sfl} & -c_{sfr} & -c_{srl} & -c_{srr}) \\
 +c_{srl} + c_{srr}) & -b_r(c_{srl} + c_{srr}) & +c_{srl} - c_{srr}) & & & & \\
 b_f(c_{sfl} + c_{sfr}) & b_f^2(c_{sfl} + c_{sfr}) & ab_f(c_{sfl} - c_{sfr}) & -b_f c_{sfl} & -b_f c_{sfr} & -b_r c_{srl} & -b_r c_{srr} \\
 -b_r(c_{srl} + c_{srr}) & +b_r^2(c_{srl} + c_{srr}) & -ab_r(c_{srl} - c_{srr}) & & & & \\
 a(c_{sfl} - c_{sfr} & ab_f(c_{sfl} - c_{sfr}) & a^2(c_{sfl} + c_{sfr} & -ac_{sfl} & ac_{sfr} & -ac_{srl} & ac_{srr}) \\
 +c_{srl} - c_{srr}) & -ab_r(c_{srl} - c_{srr}) & +c_{srl} + c_{srr}) & & & & \\
 -c_{sfl} & -b_f c_{sfl} & -ac_{sfl} & c_{sfl} & 0 & 0 & 0 \\
 -c_{sfr} & -b_f c_{sfr} & ac_{sfr} & 0 & c_{sfr} & 0 & 0 \\
 -c_{srl} & b_r c_{srl} & -ac_{srl} & 0 & 0 & c_{srl} & 0 \\
 -c_{srr} & b_r c_{srr} & ac_{srr} & 0 & 0 & 0 & c_{srr} 
 \end{bmatrix} \quad (6-25)$$

### 6.3.1.2 Theoretical modal properties of suspension systems

The Frequency Response Function (FRF) of the 7-DOF full vehicle model can be calculated by substituting the parameters in Table 6-3 into the developed state-space model. The results are presented in Figure 6-18. It can be observed that the bouncing, pitching and rolling frequencies of the car body were around 1.5 ~ 2 Hz, and the bouncing frequencies of the wheels were around 12 Hz.

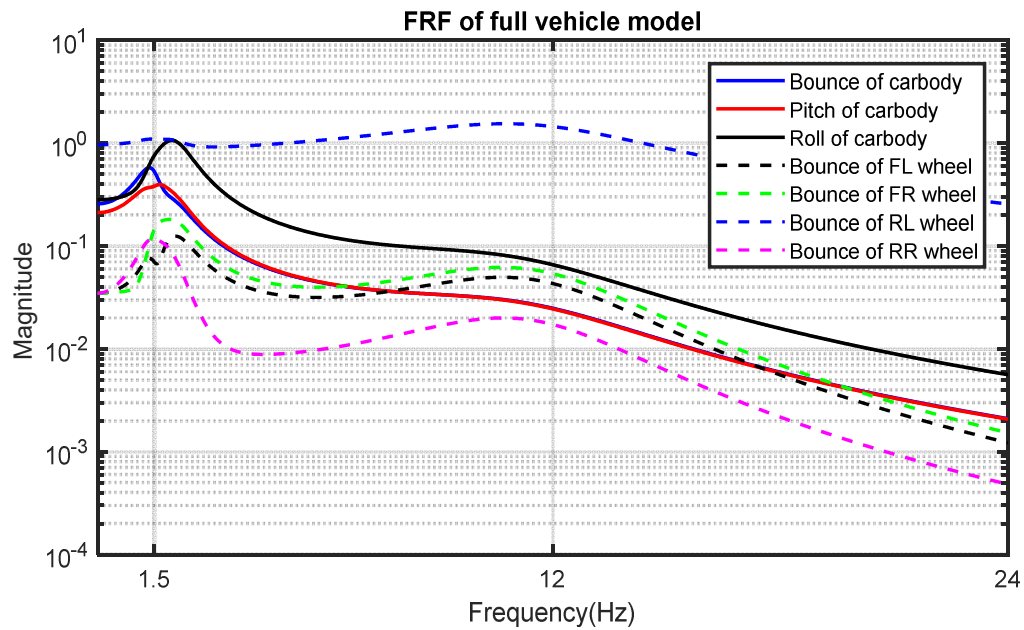


Figure 6-18 FRF of 7-DOF full vehicle model

The mode shapes of the car body were calculated and are presented in Figure 6-19. The theoretical resonance frequencies for the bounce, pitch and roll were 1.53 Hz, 1.77 Hz and 2.17 Hz, respectively; the corresponding damping ratios were 16.3%, 20.5% and 23.8%, respectively. In addition, it is worth noticing that the bounce mode was not totally horizontal, the rear part is lower than the front part. There are several reasons for this. Firstly, the centre of gravity of the car is not central; secondly, the stiffness of the front suspension is greater than the rear, which indicates that these results are reasonable.

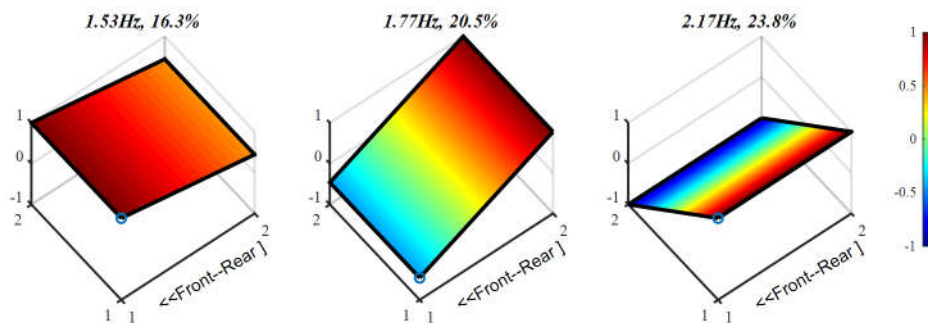


Figure 6-19 Theoretical modal parameters of the vehicle with healthy suspension systems

Moreover, the theoretical modal parameters when the stiffness of front-left suspension was decreased by 50% were calculated using the 7-DOF full vehicle model. The results are presented in Figure 6-20. When compared with Figure 6-19, differences are apparent. We see all the resonance frequencies are decreased and the mode shapes changed significantly, especially the bounce mode. Such results indicated that modal parameters could be employed

for the CM of vehicle suspension systems. In the following sub-section, a field test is conducted to verify the performance of CoSS-SSI for vehicle suspension monitoring.

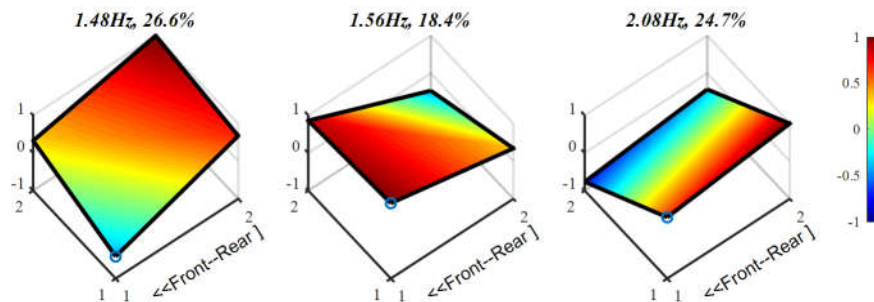


Figure 6-20 Theoretical modal parameters of the vehicle with abnormal suspension systems (Stiffness of FL suspension decreased by 50%)

## 6.3.2 Vehicle field test and result analysis

### 6.3.2.1 Experiment set-up

The same Data Acquisition System (DAQs) and transducers used with the simplified suspension system experiments, see Section 6.2.4.1, were employed in the road vehicle field tests. The accelerometers were installed on the car body, upon or close to the suspension connecting points. A schematic of the measurement system is presented in Figure 6-21(a). The DAQs was fastened on the car's instrument panel via tape, and the accelerometers were fastened by ceramic glue which can provide high stiffness, see Figure 6-21(b).

The field tests were carried out on a traditional country road near Huddersfield at times that were off-peak for traffic. During the tests the speed of the car was between 20 *km/h* to 40 *km/h*. The responses were collected for the car with a normal suspension system, and when the suspension was artificially changed by lowering the tyre pressure of the front-left tyre from 2.2 *bar* to 1.5 *bar*. The tests were repeated four times for each suspension condition, driving the car along the same length of road and as close to the same speed as possible. Four data segments were acquired of length 240 s with a sampling rate of 2,000 Hz for each condition.

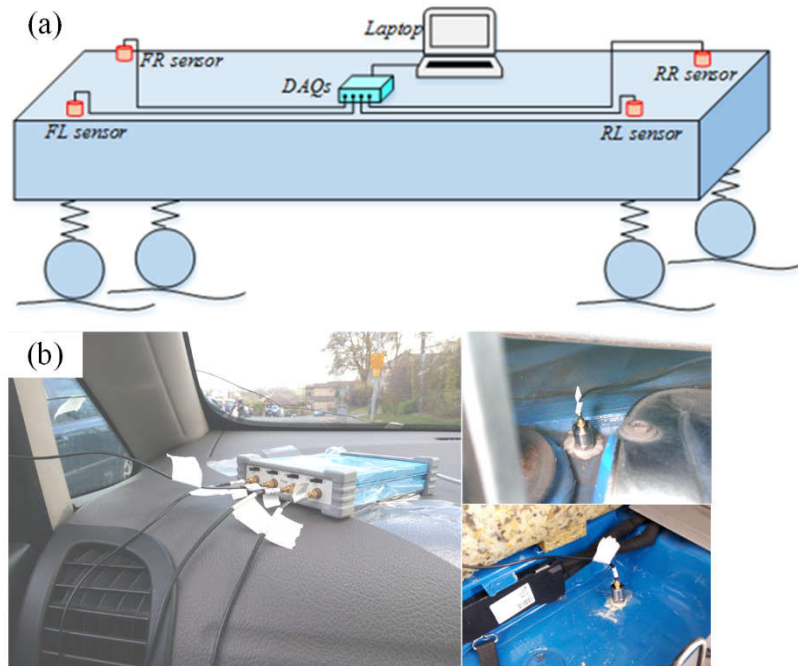


Figure 6-21 Schematic and photographs of the measurement system

### 6.3.2.2 Characteristics of vehicle responses

The four datasets were each divided into six segments (total of 24 segments each of 40 s duration) and the corresponding correlation signals calculated. An example of the divided data segment in the time domain is presented in Figure 6-22. The segment shows non-stationary signals since the holes and humps were randomly located on the road, and the speed of the vehicle changed on account of the presence of other vehicles and traffic lights. Because the vehicle suspension is a nonlinear system it will also result in nonstationary responses, besides the measurement noise is inevitable in field tests. All of these factors will increase the difficulty of extracting the system's modal parameters.

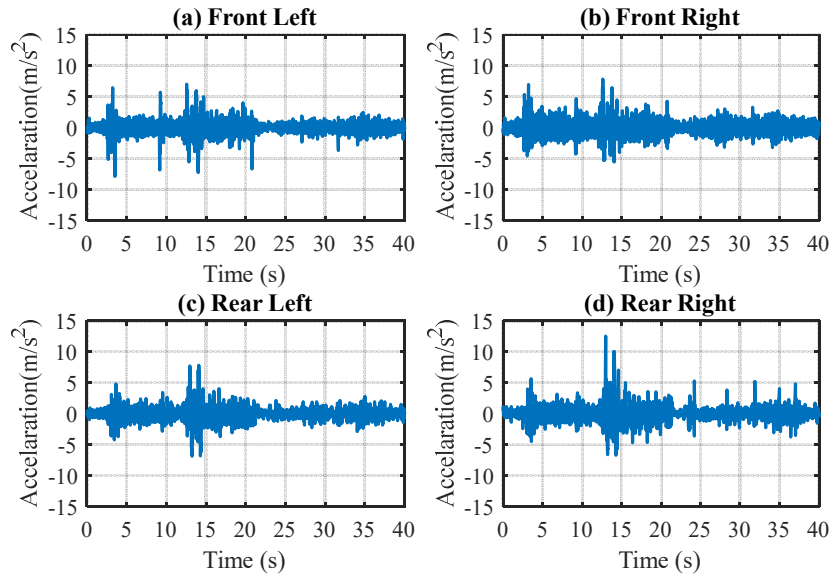


Figure 6-22 Vehicle response in time-domain as measured by accelerometers at the four corners

The PSD corresponding to the time-domain signal shown in Figure 6-22 is presented in Figure 6-23. It can be seen that the main power of the signal was around 2 Hz, which resulted from the bounce of the car body. Secondly, there is a small but discernible peak around 12 Hz generated by wheel bounce. Thirdly, it is apparent that the peaks measured by the transducers placed at the front of the vehicle are smaller than those at the rear. The main reason for this is that the engine of this car is in the front and therefore, the front of the car is heavier than the rear. This arrangement could lead to the pitching of the vehicle, making it is easier to excite. This will be addressed in the following sub-sections.

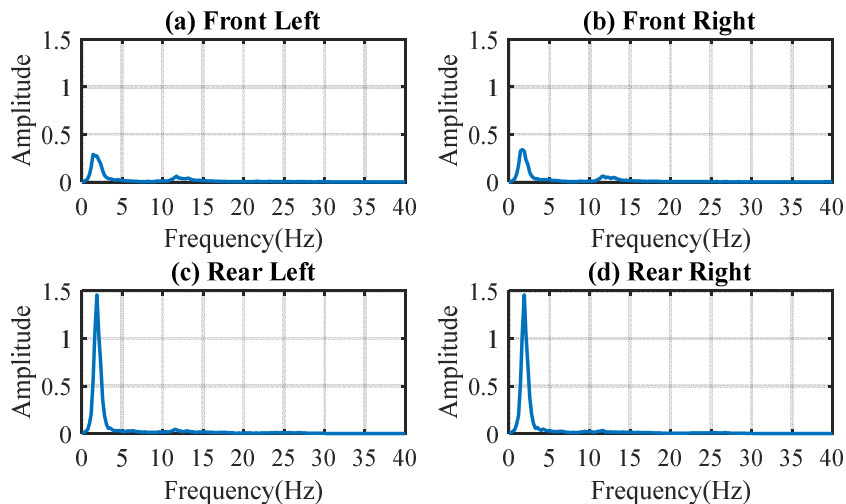
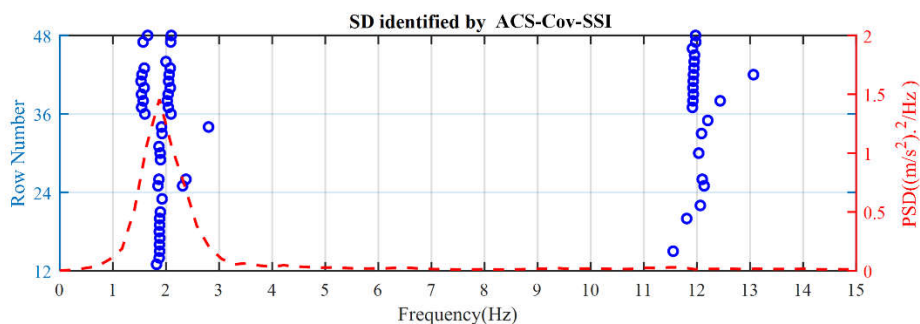


Figure 6-23 PSD of vehicle response at each of the vehicle's four corners

### 6.3.2.3 Vehicle suspension under normal condition

In this section, ACS-Cov-SSI and CoSS-SSI were employed to identify the modal parameters of the vehicle's suspension system under normal operating condition. As mentioned earlier, all of the correlation signal segments were averaged over a time for ACS-Cov-SSI; and for CoSS-SSI, the correlation signal segments were segregated into several subsets according to the amplitudes before the average step. In this case, the correlation signal segments were segregated into three subsets according to the amplitudes before the average step. The thresholds of the SDs were the same for the two methods:  $\varepsilon_f = 0.1$ ,  $\varepsilon_\xi = 0.2$  and  $\varepsilon_{MAC} = 0.5$ . The orders of the Hankel matrix were calculated from 12 to 48 while developing the SDs.

The SD identified by ACS-Cov-SSI is presented in Figure 6-24. It can be seen that only one relatively stable mode appeared around 2 Hz. The rate of the stable points over calculated orders (see Equation (3-57)) are presented in the panel below the SD. Two modes can be identified when the threshold of rate of stable points was set at 45%. The modes identified by ACS-Cov-SSI and MAC are presented in Figure 6-25. The second mode around 12 Hz resulted from the bounce of wheels according to the FRF shown in Figure 6-18. The first mode which was around 2 Hz, was related to the suspension system. It can be observed that the first mode was a pitch mode, which was confirmed by calculating the MAC values. However, it can be seen that only the pitch mode, which was the most accessible mode, was identified by ACS-Cov-SSI.



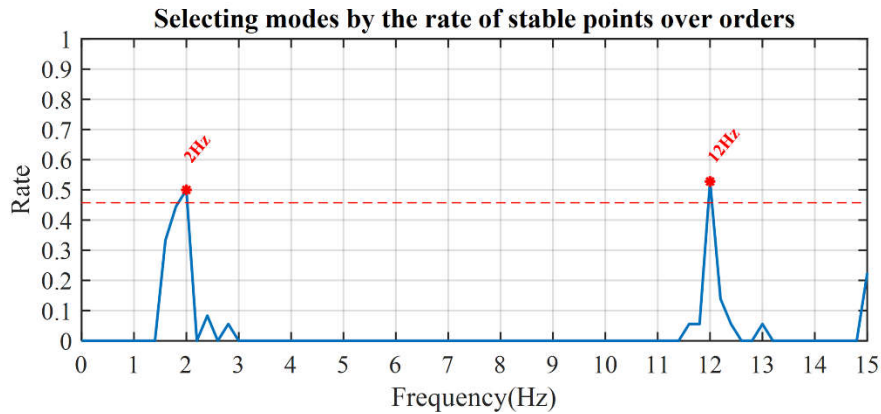


Figure 6-24 SD identified by ACS-Cov-SSI and the rate of stable points

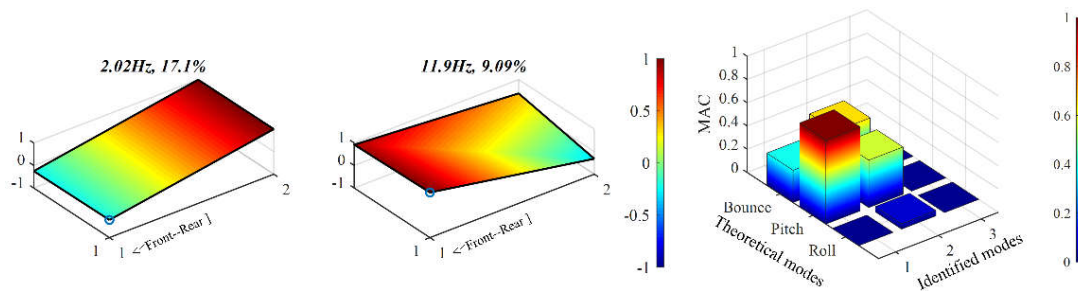
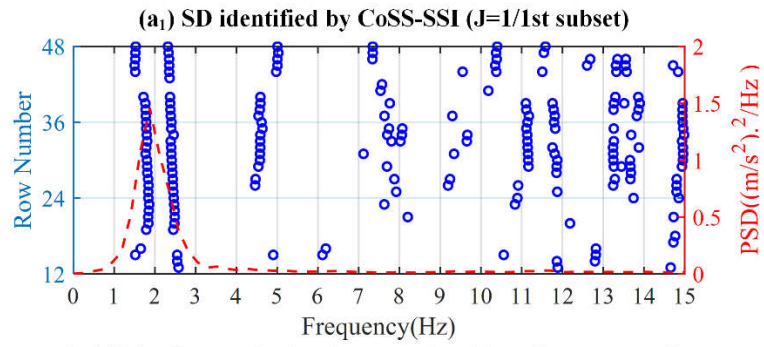


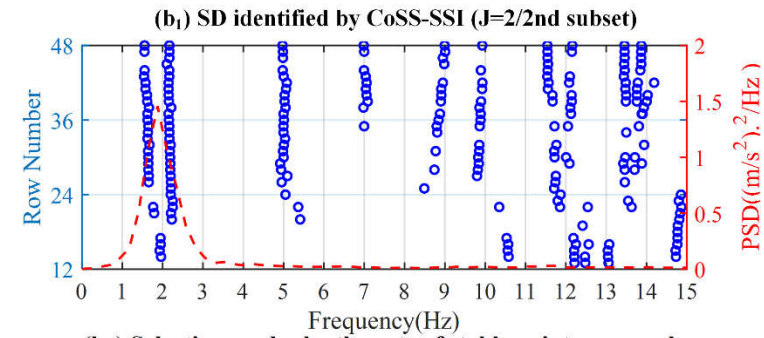
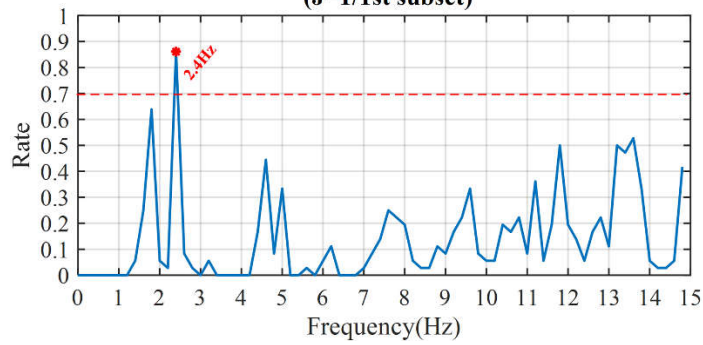
Figure 6-25 Modal parameters identified by ACS-Cov-SSI and MAC values

The threshold of the stable rate for the pitch mode was quite, below 50%. That means the reliability of the modal parameters identified by ACS-Cov-SSI is not so high. Therefore, CoSS-SSI was tested, and the results are presented below.

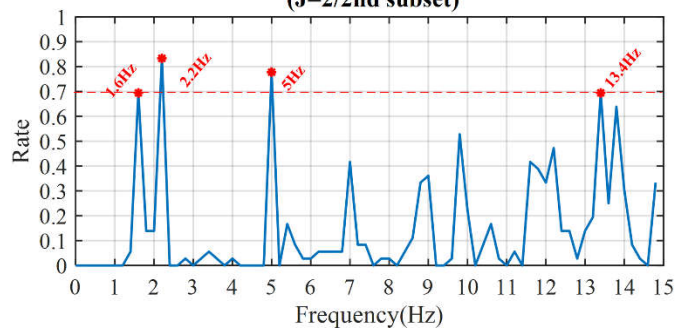
As mentioned above, with CoSS-SSI the correlation signals were segregated into three subsets and therefore, three SDs were obtained during the identification process. The three SDs are presented in Figures 6-26( $a_1$ ), ( $b_1$ ) and ( $c_1$ ). As can be seen, two relatively stable modes, around 2 Hz, were found, most clearly for the SD identified by the third subset ( $J=3$ ). Both of these stable modes are related to the dynamic characteristics of the suspension system. The rates of the stable points over calculated orders are presented in Figures 6-26( $a_2$ ), ( $b_2$ ) and ( $c_2$ ) for each SD. The stable modes could be selected out when the threshold was set at 70%. The identified modal parameters are presented in Figure 6-27 on the basis of selection of high stable rates, and the corresponding MAC values as presented below.



**(a<sub>2</sub>) Selecting modes by the rate of stable points over orders (J=1/1st subset)**



**(b<sub>2</sub>) Selecting modes by the rate of stable points over orders (J=2/2nd subset)**



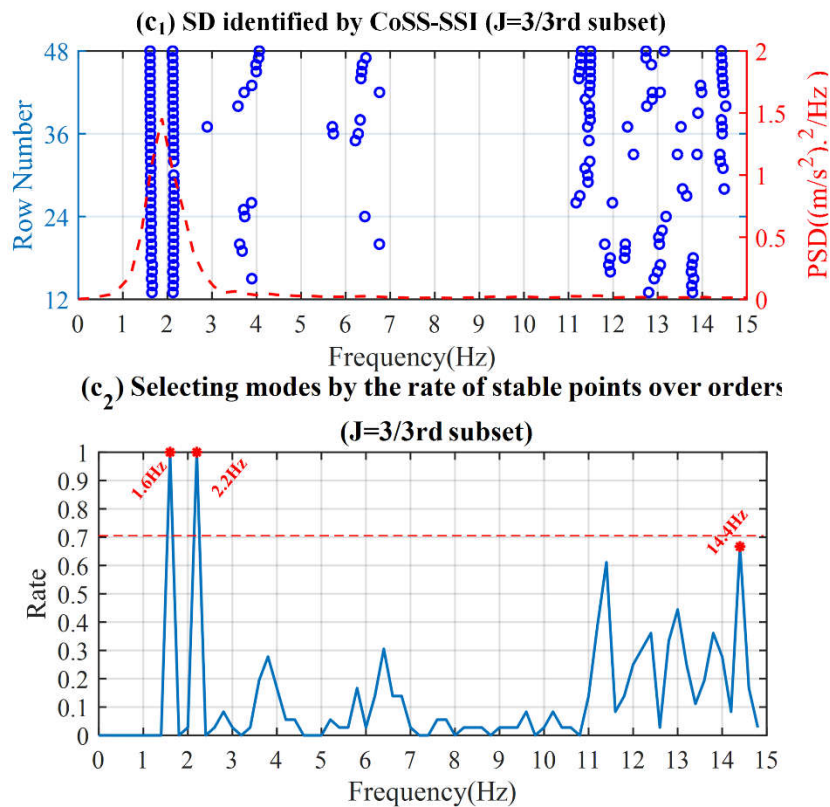


Figure 6-26 SDs identified by CoSS-SSI and corresponding rates of stable points

First of all, it can be seen from Figure 6-27 that only one mode was identified from the first subset when the threshold of state rate was 70%, and two modes were extracted from each of the second and third subsets. Secondly, it can be observed from the MAC values that the two modes identified from the second subset (J=2) are bounce and pitch. The frequencies of the identified bounce and pitch modes are 1.62 Hz and 2.18 Hz, respectively which, when considering the errors from model development and signal measurement, are in good agreement with the theoretical results (Figure 6-19). It can be seen that the bounce mode identified in the second subset has lower amplitude at the front which was also in line with the theoretical analysis.

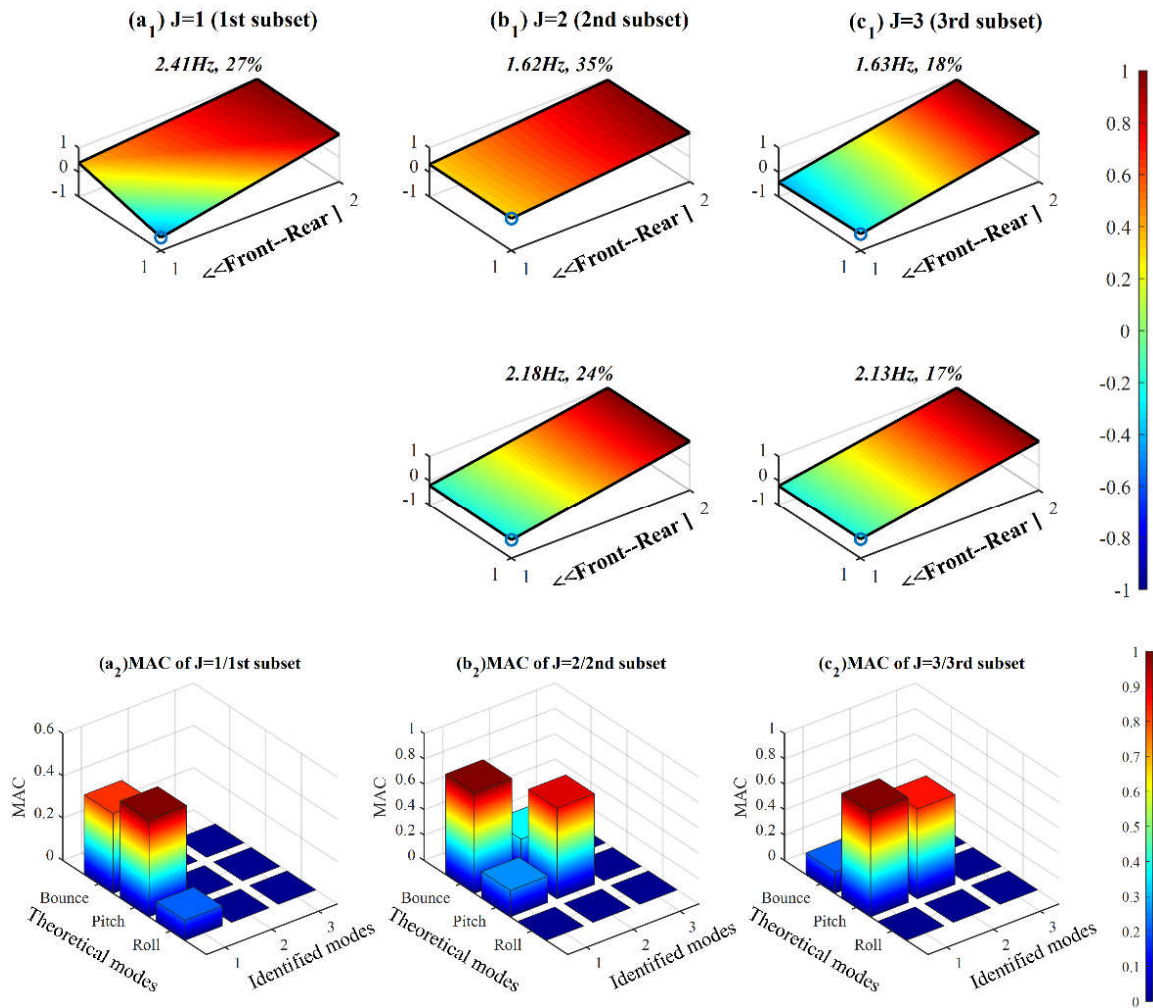


Figure 6-27 Modal parameters identified by CoSS-SSI and corresponding MAC values when the suspension under normal condition

However, both modes identified from the third subset were for pitch, the frequency of the first mode was  $1.63 \text{ Hz}$  which is close to the bounce frequency. Such a result could be due to the difference in stiffness between of front and rear suspensions, when the suspensions suffer significant relative displacement. This as a good example to illustrate the non-linear effects of the suspension system and is one more reason why the stable modes in the SDs identified by CoSS-SSI were more stable than those in the SD identified by ACS-Cov-SSI.

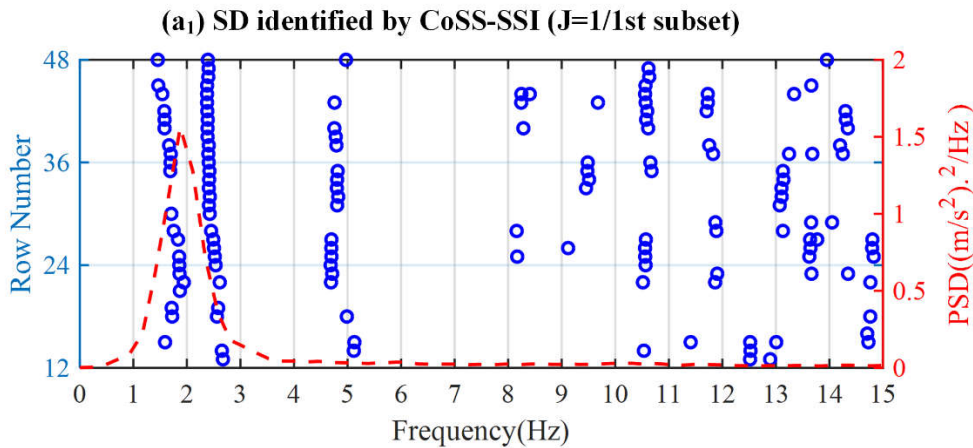
In summary, CoSS-SSI has successfully identified the bounce and pitch modes which are related to the vehicle suspension system where the stable rate has a high threshold. These two modes could be used for CM of the vehicle suspension system. However, it is noticeable that the roll mode was not identified by any of the OMA schemes used. Nevertheless, this is reasonable because the vehicle has an anti-roll system for safety purposes. Thus, the roll mode cannot be identified from when the vehicle is operated in normal condition, but it is

possible that it could be identified by collecting data on a car body's response when the vehicle is travelling along a curve.

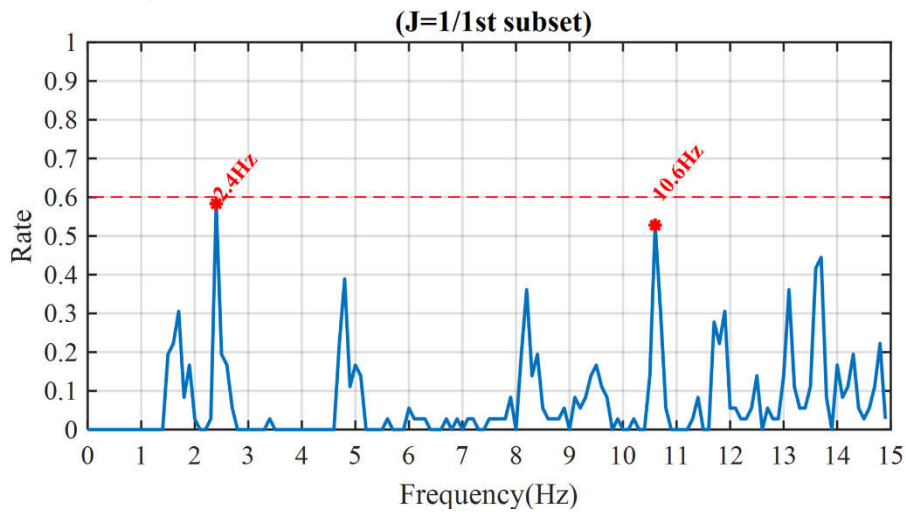
#### 6.3.2.4 Vehicle suspension under abnormal condition

In order to verify the ability of CoSS-SSI for vehicle suspension system monitoring, a field test of the vehicle with a faulty suspension system was conducted. The suspension fault was introduced by decreasing the tyre pressure of the front-right wheel 2.2 *bar* to 1.5 *bar*. Otherwise the experimental setup was the same as for the experiment with healthy suspension. The same parameters were selected for CoSS-SSI as in Section 6.3.2.3.

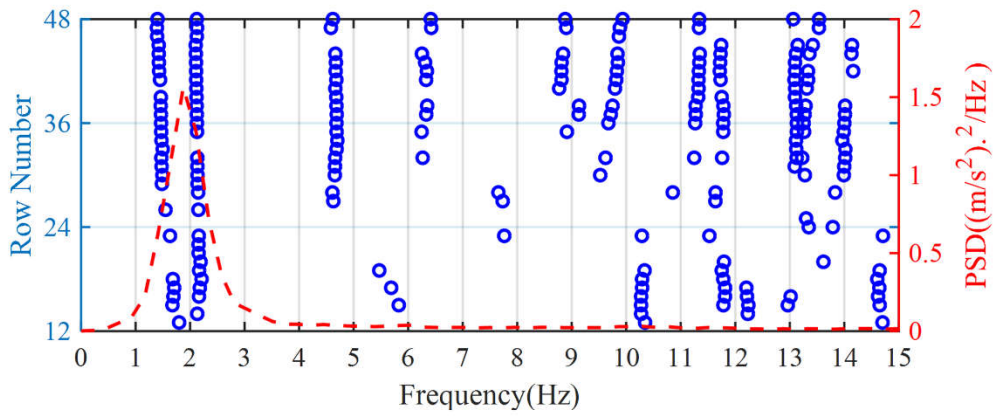
The identified SDs and the corresponding stable rates were as given in Figure 6-28. Comparing Figure 6-26 and Figure 6-28 shows the identified modes of the vehicle with an abnormal suspension system were not as stable as modes with the normal suspension system. Therefore, the threshold of the stable rate was set at 60%, which was lower than the identification with the healthy suspension system. However, it can be observed in Figure 6-28( $c_1$ ) that the modes extracted from the third subset appeared extremely stable, similarly for Figure 6-26( $c_1$ ). Hence, the modal parameters identified from the third subset were utilized as the main reference for the diagnosis of vehicle suspension systems.



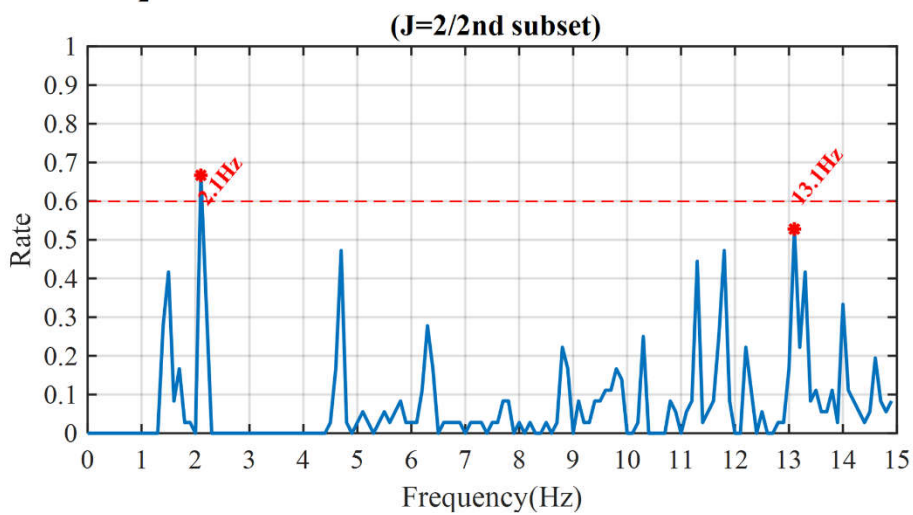
(a<sub>2</sub>) Selecting modes by the rate of stable points over orders



(b<sub>1</sub>) SD identified by CoSS-SSI (J=2/2nd subset)



(b<sub>2</sub>) Selecting modes by the rate of stable points over orders



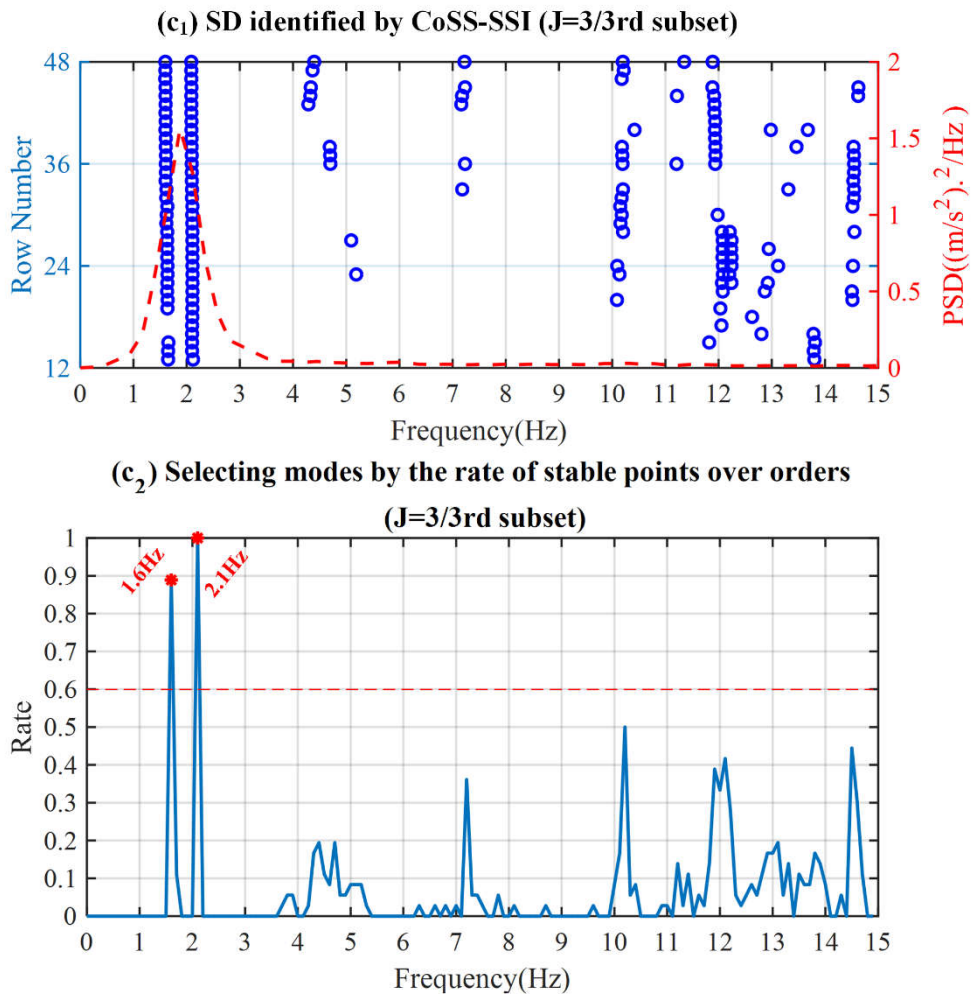


Figure 6-28 SDs identified by CoSS-SSI for fault suspension and corresponding rates of stable points

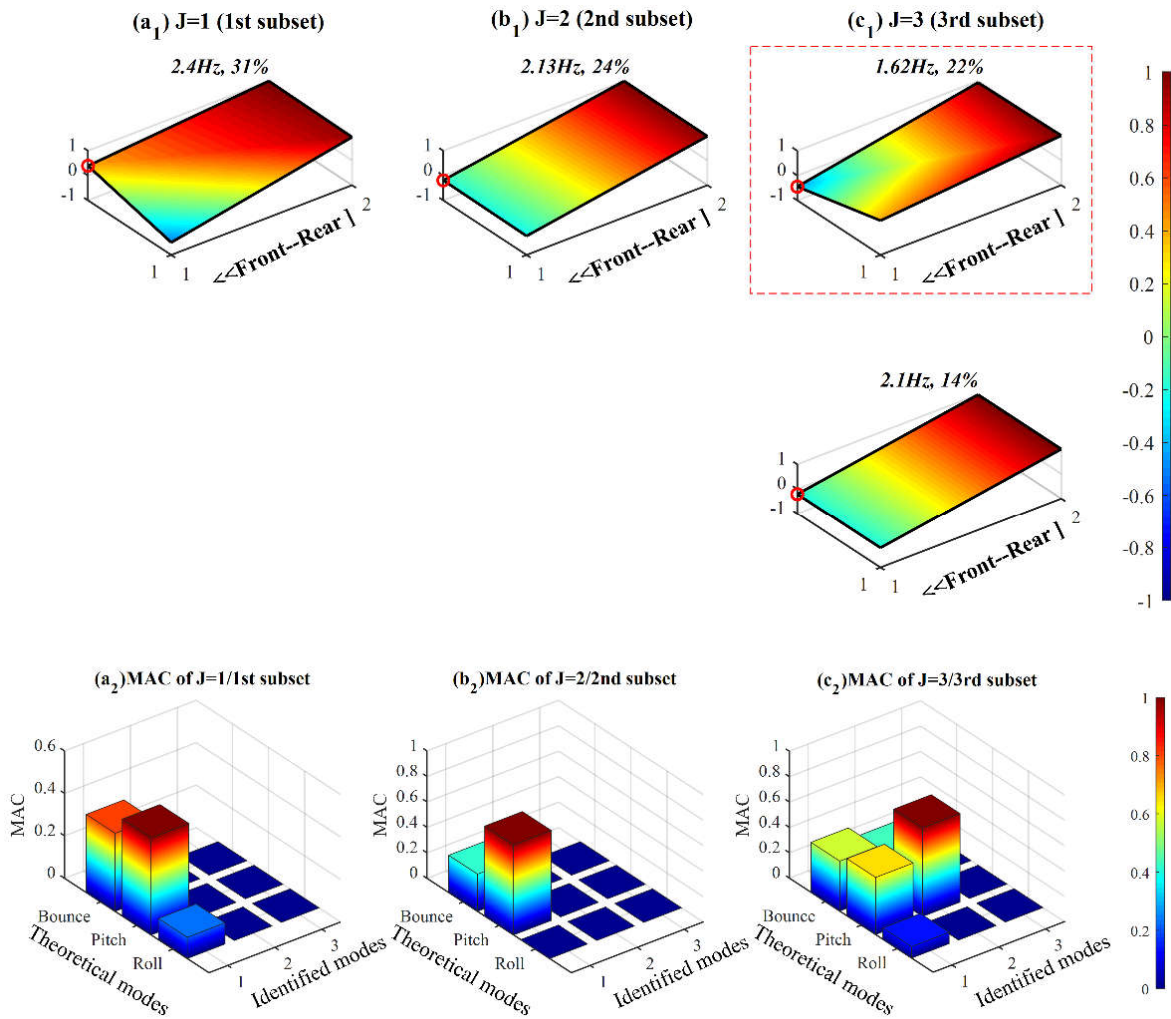


Figure 6-29 Modal parameters identified by CoSS-SSI and corresponding MAC values when the suspension under abnormal condition

When the identified modal parameters presented in Figure 6-29 were compared with Figure 6-27, the difference of the mode shapes identified in the third subset is evident. There is a lower level of response in the front-right corner. This could be the consequence of the decrease in pressure in the tyre on the front-right wheel. Specifically, the decrease in tyre pressure will lead to a reduction of wheel stiffness, i.e. suspension stiffness. The effects of stiffness reduction were illustrated by the decrease in value of the natural frequencies.

On the basis of the above discussion, it can be concluded that CoSS-SSI has the capability to achieve road vehicle suspension monitoring using only car body responses.

## 6.4 Findings

In this chapter, experimental studies were conducted on the road vehicle to verify the performance of CoSS-SSI for CM of the suspension system. Initially, a simplified

suspension system was constructed for a primary investigation. A 3-DOF mathematical model was developed for this simplified suspension system. Then, vehicle field tests were conducted on a traditional countryside road during off-peak times. A 7-DOF full vehicle model was developed to investigate the theoretical dynamic performance of the suspension system. Based on the results presented in this chapter, the following conclusions can be drawn:

- 1) CoSS-SSI has the capability to identify the modal parameters of the simplified suspension system;
- 2) CoSS-SSI is superior to ACS-Cov-SSI in identifying modal parameters of road vehicle suspension systems when measuring the car body responses in a road test. In particular, the rate of the stable points in the SD identified by ACS-Cov-SSI is lower than the SDs identified by CoSS-SSI. Besides, CoSS-SSI has the capability to identify the bounce and pitch modes synchronously, but ACS-Cov-SSI can identify the pitch mode only.
- 3) CoSS-SSI is a promising method to extract the modal parameters of the nonlinear system by dividing the response into several subsets according to their amplitudes.
- 4) CoSS-SSI has the potential for successful online CM of road vehicle suspension systems.

In the next chapter, the CoSS-SSI will be implemented to identify the modal parameters of a 1/5<sup>th</sup> scale bogie for online CM of railway vehicle primary suspension system, which has much more complicated excitations and greater nonlinearities than a car's suspension system.

---

---

## CHAPTER 7 CONDITION MONITORING OF RAILWAY VEHICLE SUSPENSION SYSTEMS BASED ON A 1/5<sup>TH</sup> SCALE BOGIE, USING CoSS-SSI

---

---

*This chapter explores the performance of CoSS-SSI when used for monitoring railway vehicle suspension via a 1/5<sup>th</sup> scale bogie. Initially, a 7-DOF model was constructed for the bogie to predict the target frequency range for the experiments. Experiments were carried out on the bogie with the primary suspension system subjected to different test parameters. Conventional OMA methods, like Cov-SSI and ACS-Cov-SSI, were utilised to identify the rigid modes of the bogie frame when the suspension system operated under normal conditions. The results show that CoSS-SSI was superior to both Cov-SSI and ACS-Cov-SSI, and was the only method of the three with the potential for online CM of railway vehicle suspension systems.*

## 7.1 Introduction

Many approaches to the CM of railway vehicle suspensions have been investigated by different researchers because suspension faults are extremely dangerous for an operating vehicle, and these reviewed in Section 2.2.2. However, few of the proposed methods have been verified by field tests because the cost of railway vehicle field testing is extremely high. Today, the roller rig is becoming popular for the investigation of railway vehicle dynamic characteristics and wheel-rail contact, because roller rigs can replicate numerous railway vehicle dynamics phenomena which could occur in practice [173]. Fortunately, experiments on a roller rig are flexible, easy to control and repeatable, and test instrumentation is relatively easy to set up and use.

Roller rigs can be categorised into full- and scale-size. One of the most famous, a 1/5<sup>th</sup> scale roller rigs constructed at the University of Huddersfield, has been used to investigate the lateral dynamic behaviour of railway vehicles [174], the critical speed [175] and fault diagnosis of wheels [176], [177]. In this chapter, the same 1/5<sup>th</sup> scale roller rig was employed to examine the effectiveness of the proposed OMA method, CoSS-SSI, for the CM of railway vehicle suspension systems. The details of the roller rig are presented in the next sub-section.

## 7.2 7-DOF model of 1/5<sup>th</sup> scale roller rig

### 7.2.1 Roller rig introduction

It is well known that the bogie is a critical component in the suspension systems of railway vehicles, it connects to the car body via a secondary suspension system and to the wheelsets via the primary suspension system. For the given rig, a 1/5<sup>th</sup> scale bogie was installed on rollers, as shown in Figure 7-1.

This roller rig is composed mainly of: two wheelsets, a bogie frame, eight mount bushings and two rollers. A pair of mount bushings at each corner performed as the primary suspension system. The layout of the main parts of the scale roller rig can be seen in Figure 7-1(b) which is the schematic of the side view. As can be seen, the two rollers are driven by a motor via a belt. The speed of the motor is continuously adjustable through a control panel. Two joints and a frame, see Figure 7-1(a), were employed to constrain the DOF of the scale

bogie in the longitudinal direction. In addition, two weights, each of mass 2 kg, were added on the centerline of the bogie frame to separate the bounce and pitch modes because these two modes would be extremely close together without loading the secondary suspension. However, the separation and identification of close modes is a great challenge, even for SSI which has a better close mode identification performance compared with other methods.

The wheel profile of the wheelset was machined as British Rail (BR) P8 in proportion, and the roller profile was machined as the scale of BS110a rail profile with no cant [174]. Therefore, the response of the bogie frame was similar to the response of a real vehicle because the excitation from the roller and wheel contact is close to the real scenario.

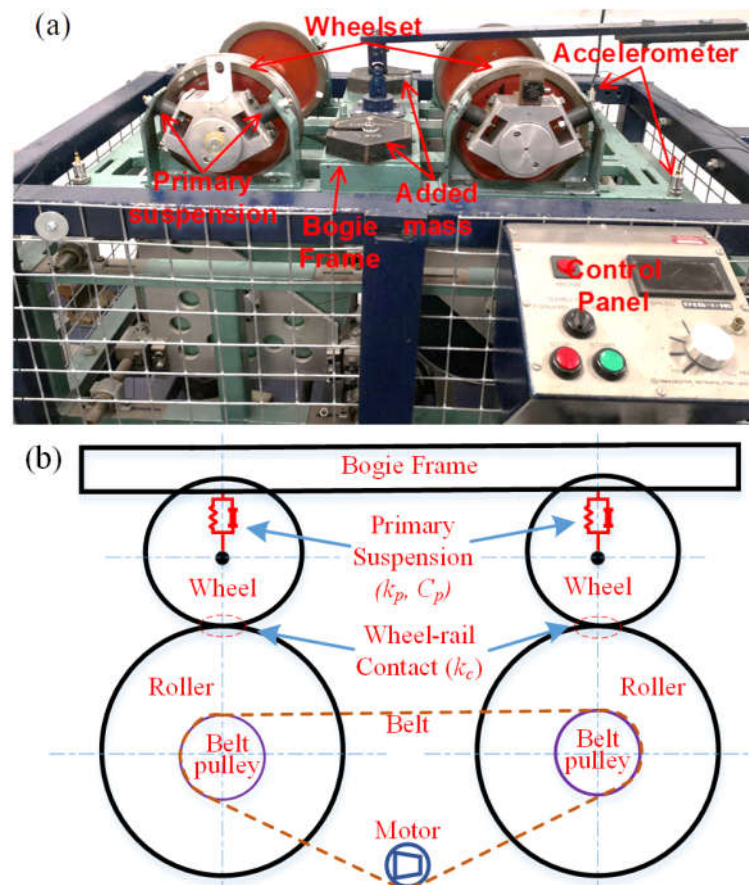


Figure 7-1 1/5<sup>th</sup> scale roller rig and schematic of the side view

## 7.2.2 Model parameter estimation

### 7.2.2.1 Primary suspension stiffness estimation

In order to obtain accurate theoretical results, the parameters in the developed model are critical. The stiffness of the primary suspension is one of the most vital parameters determining the dynamic characteristics of a suspension system. Thus, the mount bushings

used were tested on a universal testing system. Then, other parameters, such as mass and moment of inertia, were obtained by using the measurement function of SOLIDWORKS, as present below.

Three different types of mount bushings with different stiffness were employed in this study to simulate various fault scenarios. Figure 7-2 shows the mount bushings were all male to male with the same overall heights ( $H = 30\text{ mm}$ ), to fit the installation, but different diameters ( $D$ ) and materials to obtain different stiffness and damping.

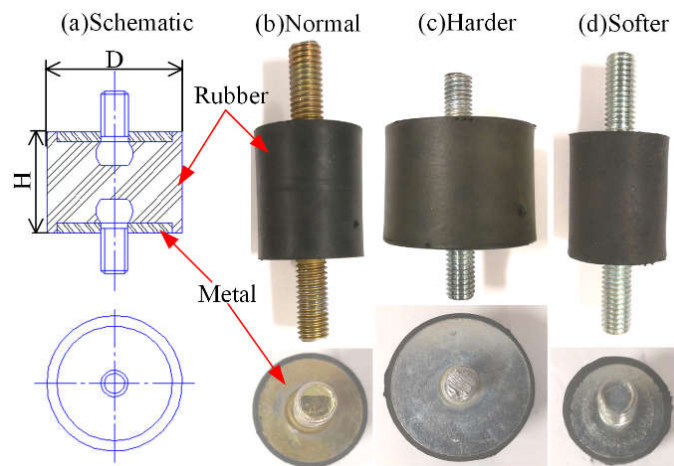


Figure 7-2 Schematic and photographs of employed stud mounts

According to their stiffness, the three mount bushings were categorised as normal, harder and softer. All were tested on a Universal INSTRON 3369 test machine as shown in Figure 7-3, to obtain their force-displacement curves.

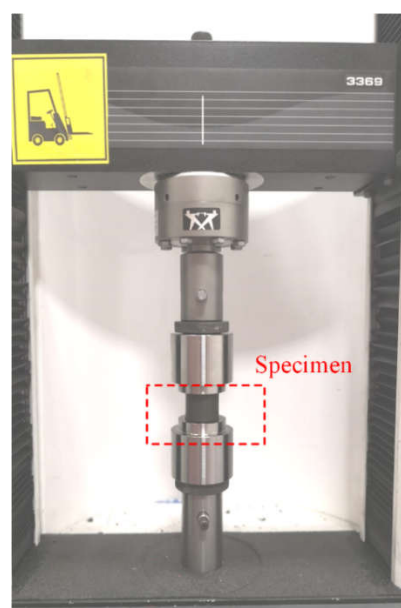


Figure 7-3 INSTRON 3369 Universal Testing System

During the force-displacement tests, the same maximum compressive extension (3 mm) was loaded on the tested specimen under a speed of 2 mm/min, and the corresponding force on the specimen was measured. Each stud mount was loaded for three cycles and the measured force versus displacement (F-D) curves are presented in Figure 7-4 to illustrate the hysteresis effect. The magnitude of the maximum applied for the three sub-figures in Figure 7-4 was different to obtain the same degree of compression.

From Figure 7-4 the hysteresis, which is a major characteristic of nonlinearity, of the mounts is clearly evident. However, the roller rig model is considered as a linear lumped mass, so the stiffness of the primary suspension should be a simple value. In this case, the stiffness was calculated when the deformation of the stud was around 1 mm, as produced by the weight of the bogie frame. The stiffness of the normal stud was  $113/0.001 = 1.13e5 \text{ N/m}$ . As can be seen from Figures 7-4(b) and (c) the stiffness of the harder mount was about double that of the normal, and the stiffness of the softer mount was nearly half the normal.

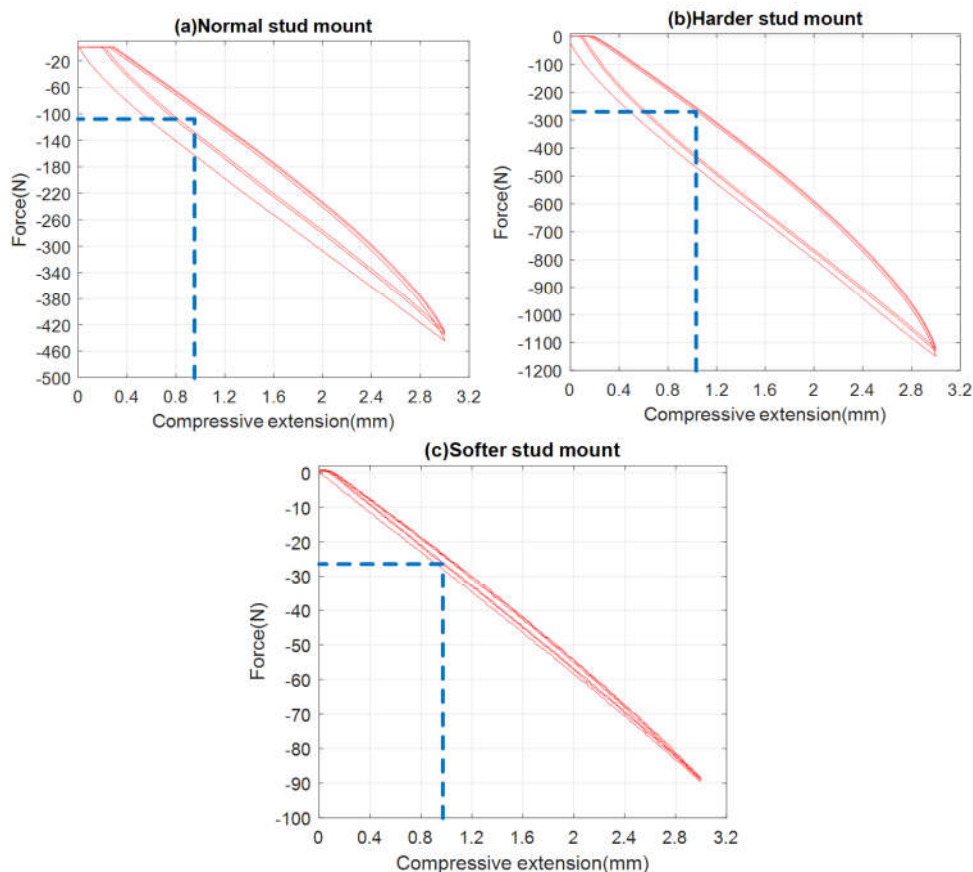


Figure 7-4 Force-displacement curves of mounts

It can be observed in Figure 7-5 that the mount was installed in an angle of  $\pi/3$  to the vertical. Therefore, the stiffness of the normal primary suspension can be estimated as  $2 \times 1.13e5 \times \cos(\pi/3) = 1.13e5 \text{ N/m}$ . In the suspension fault cases: (i) one of the normal mounts at the front-left (FL) corner was replaced by a harder mount, which resulted in the stiffness at the FL corner increasing by 50%; and (ii) both normal mounts at the rear-left (RL) corner were replaced by softer mounts, which resulted in the stiffness at the RL corner decreasing by 75%.

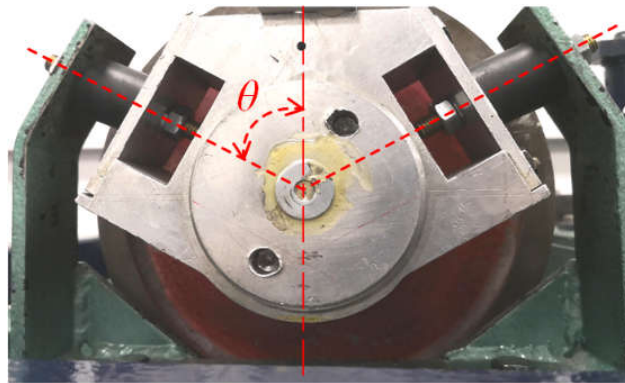


Figure 7-5 Detail of mount installation ( $\theta = \pi/3$ )

### 7.2.2.2 Mass and moments of inertia of bogie frame

A 3D model was developed in SOLIDWORKS to determine the moments of inertia of the bogie frame, shown as in Figure 7-6. Firstly, the mass of the bogie frame was measured by a balance. Then, the mass was used as a reference to adjust the density of the 3D model. The moments of inertia of the bogie frame were then provided by subroutines within SOLIDWORKS. All of the measured parameters are tabulated in Table 7-1. The damping coefficients of the primary suspension and the contact stiffness were obtained from [176]. The referred nominations in Table 7-1 can be found in Figure 6-17.

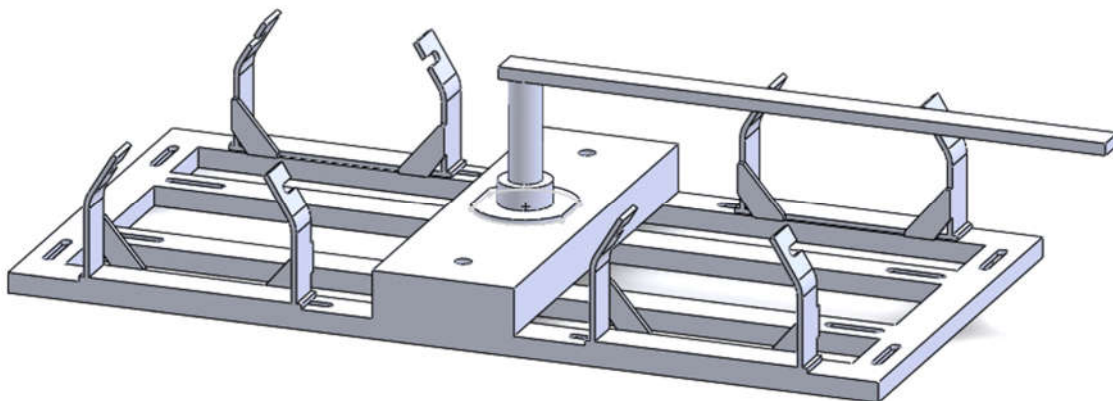


Figure 7-6 3D model of the bogie frame

Table 7-1 Specifications of the roller rig [176]

Symbol	Meaning	Value
$m_b$	Mass of bogie frame	30.95 kg
$m_{wfl}, m_{wfr}, m_{wrl}, m_{wrr}$	Half mass of the wheelset	12.5/2 kg
$I_P$	Bogie frame pitch inertia	1.23 kg · m <sup>2</sup>
$I_R$	Bogie frame roll inertia	0.67 kg · m <sup>2</sup>
$k_{sfl}, k_{sfr}, k_{srl}, k_{srr}$	Stiffness of the primary suspension	1.13e5 N/m
$c_{sfl}, c_{sfr}, c_{srl}, c_{srr}$	Damping coefficients of primary suspension	133.5 N · s/m
$k_{cfl}, k_{cfr}, k_{crl}, k_{crr}$	Contact stiffness between wheel and track	8.93e6 N/m
$a$	Half of the gauge	0.39/2 m
$b_f, b_r$	Half of the wheelbase	0.42/2 m

### 7.2.3 Theoretical modal parameters of the 1/5<sup>th</sup> scale bogie

The theoretical modal parameters of the scale bogie are calculated in this section via a 7-DOF model. As mentioned earlier, only the rigid modes of the bogie frame were utilised for suspension monitoring. However, the flexural modes of the bogie frame could have significant effects on the results so these flexural modes were calculated to confirm whether or not they did have a significant effect on the rigid modes.

#### 7.2.3.1 Theoretical modal parameters of the 1/5<sup>th</sup> scale bogie

The same 7-DOF model as developed in Section 6.3.1, see Figure 6-17, was used for the roller rig to consider bounce, pitch and roll of the bogie frame, and bounce of the four wheels. Thus, the kinematic equations are the same as Equations (6-12)-(6-25). The meaning and values of the symbols in these equations are as presented in Table 7-1. The theoretical rigid modes of the bogie frame can be obtained by substituting these values into the kinematic equations. The results are presented in Figure 7-7. It can be seen that the resonant frequencies for bounce, pitch and roll modes are 19.15 Hz, 20.1 Hz and 25.4 Hz, respectively. The corresponding damping ratios are 6.99%, 7.34% and 9.27%.

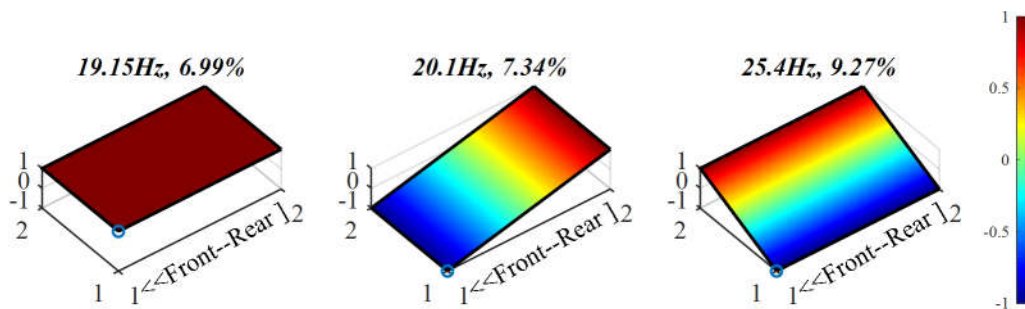


Figure 7-7 Theoretical rigid modes of the bogie frame

### 7.2.3.2 Flexural modes of the bogie frame

The flexural modes of the bogie frame were calculated using a Finite Element Model in ANSYS/Workbench software. Firstly, a 3D model of the bogie frame was developed using SOLIDWORKS. Then the 3D model was imported into the ANSYS/Workbench. The model was meshed into 9828 elements which included 21124 nodes.

The first four flexural modes of the bogie frame are presented in Figure 7-8 and the corresponding resonant frequencies are 86.43 Hz, 111.42 Hz, 142.38 Hz and 284.70 Hz, respectively, and we can see that the modes have different shapes. Moreover, it is obvious that the resonant frequency of the first flexural mode is much higher than any of the resonant frequency of the rigid modes. The resonant frequency of the first flexural mode is around three times that of the first rigid mode so that the flexural modes of the bogie frame have little effect on the rigid modes.

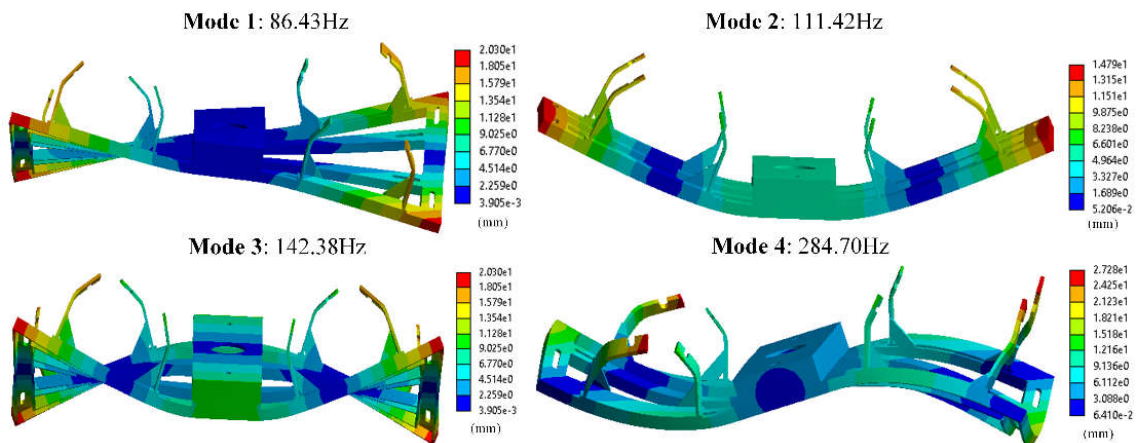


Figure 7-8 First four flexural modes of the bogie frame

## 7.3 Experimental investigation

In this section, experiments were conducted on the roller rig to investigate the effectiveness of CoSS-SSI for the monitoring of railway vehicle suspension system. The experiment set-up is introduced, then, the bogie with healthy primary suspension system was tested. Last but not least, two cases of fault suspension were examined.

### 7.3.1 Experiment set-up

Four accelerometers and a four channels DAQs were employed in the test, which is the same arrangement as described in Section 6.2.4. The photograph of the accelerometers and DAQs

can be seen in Figures 6-9 and 6-10. Besides, the accelerometer's specifications are in Table 6-1.

The accelerometers were installed on the four corners of the bogie frame, as shown in Figure 7-1(a). The schematic of the measurement system can be found in Figure 6-21(a). During the test, the sampling rate was set at 1500 Hz. The frequencies of interested range from 15 Hz to 30 Hz, and therefore a sampling rate at 1500 Hz was an order of magnitude higher than that required by the Nyquist criterion. Selecting such a high sampling rate helped ensure the reliability of CoSS-SSI, however, the sampling rate could be set around 150 Hz in the real applications in order to enhance calculation efficiency, which is critical for online monitoring.

In a real scenario, the responses collected from a railway vehicle will be for varying speeds which will be more complicated than for a constant speed. This is because the changing speed will lead to more severe, nonstationary responses. However, the scenario of varying speed is closer to the real operating conditions of a railway vehicle, which increases the challenge to suspension monitoring. The responses of the bogie under varying speed condition were collected in this experiment.

### **7.3.2 Characteristics of roller rig responses**

The sampling length for each test was 40 s, and the experiment was repeated ten times for each condition when the suspension system was under the three different conditions. An example of the collected signal and the corresponding PSD is given in Figure 7-9. First of all, it can be seen that the amplitudes of the responses change with time, which means the speed of the roller rig has a significant effect on the magnitude of the responses. Secondly, it is apparent that the responses were nonstationary because of the nonlinearity of the suspension and the changing speed of the roller. Thirdly, it can be seen from the corresponding PSD that two major peaks can be observed at around 20 Hz and 26 Hz. According to the theoretical modal results these two peaks could result from the resonances in the bounce and roll modes, see Figure 7-7. However, the pitch mode (24.03 Hz) cannot be found in the PSD.

It can also be seen that the amplitudes of the spectrums at the four corners are significantly different. The spectrum amplitudes of the signal collected from the Front-Right (FR) and the

Rear-Right (RR) positions are higher than the other two positions. One reason for such differences could be the coupling of pitch and roll modes since their resonance frequencies are quite close, 24.03 Hz and 25.4 Hz. We can observe different peaks in the spectrum, such as about 37 Hz, which is caused by various asymmetric excitations between the corners, nonlinearities in the suspension, wheel-rail contact, and even measurement deviations.

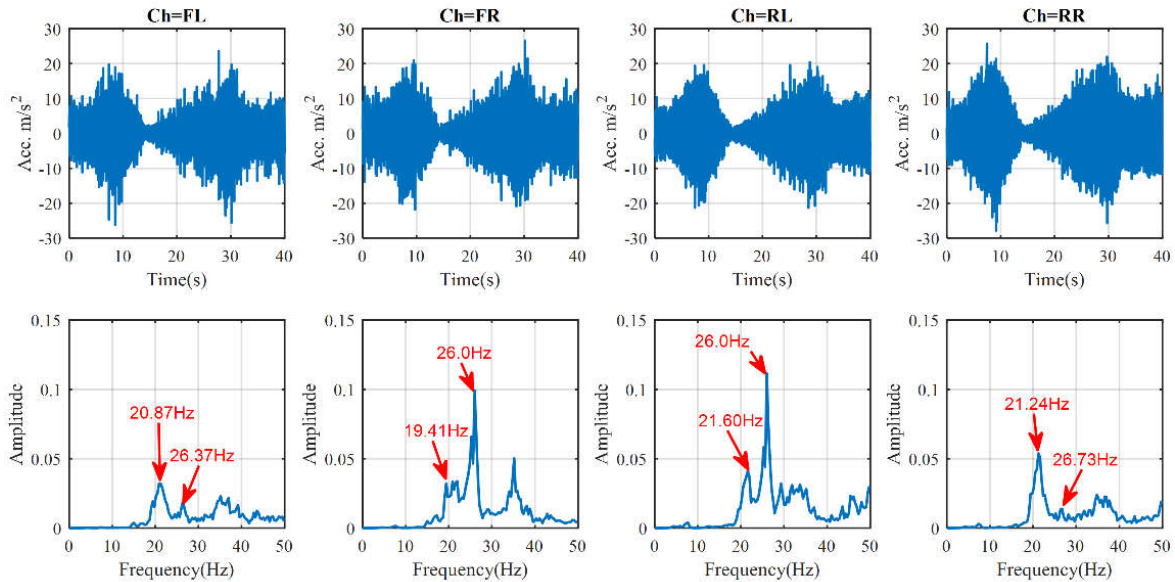


Figure 7-9 Raw signals of roller rig responses and corresponding PSD (FL: Front-Left; FR: Front-Right; RL: Rear-Left; RR: Rear-Right)

All of these phenomena confirm that to obtain an accurate result, minimising noise in the responses is necessary before carrying out OMA. The CoSS-SSI method has been proven to be a practical scheme to suppress such noise effects. Hence, it was employed here to extract the modal parameters. Cov-SSI and ACS-Cov-SSI were again used to confirm the superiority of CoSS-SSI.

### 7.3.3 1/5<sup>th</sup> scale bogie with normal suspension

In this sub-section, the data collected from the 1/5<sup>th</sup> roller rig was used to comprehensively evaluate the performance of CoSS-SSI as compared with Cov-SSI and ACS-Cov-SSI. With sampling rate of 1500 Hz, and time length was 40 s, the data length was 60,000 points for each test. For CoSS-SSI, the 60,000 points of data were divided into 14 segments, with each segment containing 4096 points ( $N = 4096$ ) more than 50 periods of the lowest mode of interest. Then, the correlation functions of the four channels were calculated, and as the test was repeated ten times there were 140 segments of correlation functions. The thresholds of the SDs were the same for the three methods, which were  $\varepsilon_f = 0.1$ ,  $\varepsilon_\xi = 0.2$  and  $\varepsilon_{MAC} =$

0.5; and the orders of the Hankel matrix were calculated from 12 to 82 while developing the SDs.

For the Cov-SSI, the conventional OMA approach, only the signal collected from one test was utilised to extract the modal parameters. The identified SD and the corresponding rate of stable points are presented in Figure 7-10. Two relatively stable modes around 20 Hz and 21 Hz can be seen in Figure 7-10(a). These two modes can be selected out when the threshold of the stable rate ( $\delta$ ), Equation (3-57), is set at 0.6, as shown in Figure 7-10(b).

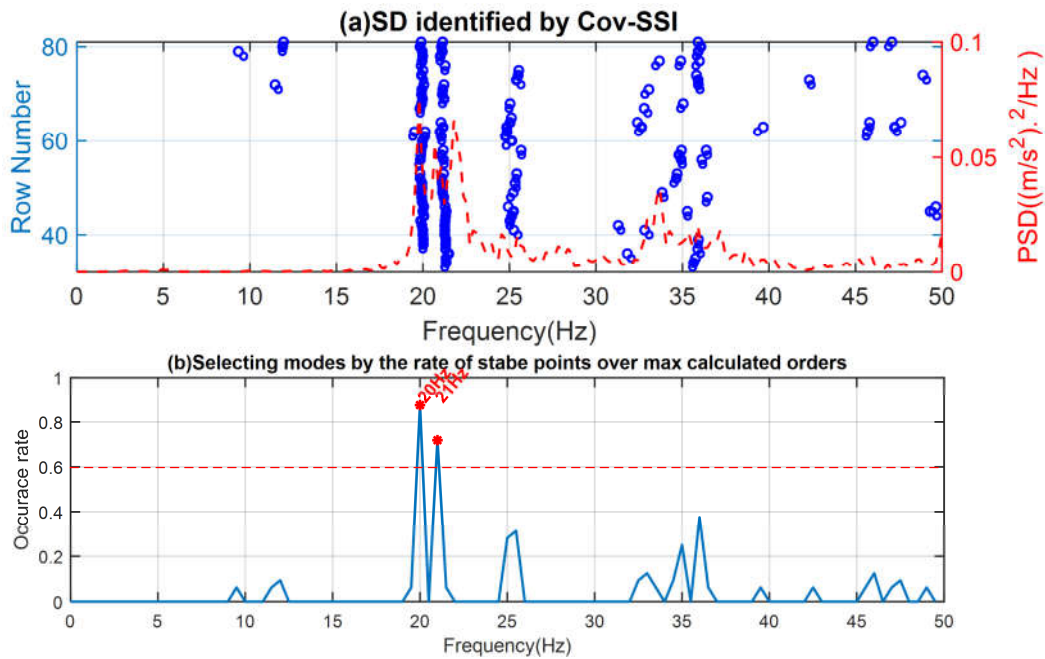


Figure 7-10 (a) SD identified by Cov-SSI and (b) Rate of stable points

The frequencies, damping ratios and mode shapes of these two stable modes are presented in Figure 7-11(a). The MAC values of the modes are given in Figure 7-11(b). It can be observed from Figure 7-11(b) that the identified modes are bounce and pitch. The resonant frequencies of bounce and pitch are 19.97 Hz and 21.12 Hz, respectively. The differences between theoretical values and identified frequencies for bounce and pitch modes are 4.28% and 4.66%, respectively, which are acceptable. However, the roll mode was not identified as a result of the low noise suppression ability of Cov-SSI.

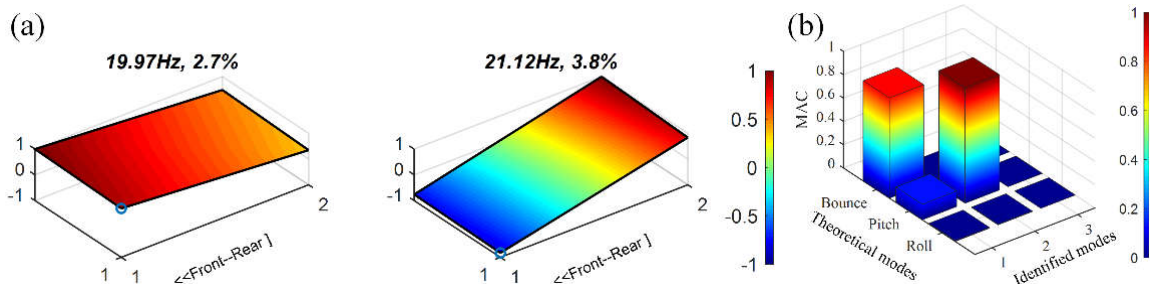


Figure 7-11 (a) Modes of bogie frame identified by Cov-SSI and (b)MAC values compared with theoretical mode shapes

The SD identified by ACS-Cov-SSI is presented in Figure 7-12(a), and the corresponding stable rate presented in Figure 7-12(b). It can be seen that the most stable mode appears around 25.5 Hz. Two stable modes can be extracted from the identified SD when the threshold of stable rate ( $\delta$ ), Equation (3-57), was set at 0.6, the same as for the threshold in the Cov-SSI. The identified mode shapes and corresponding MAC values were shown in Figure 7-13.

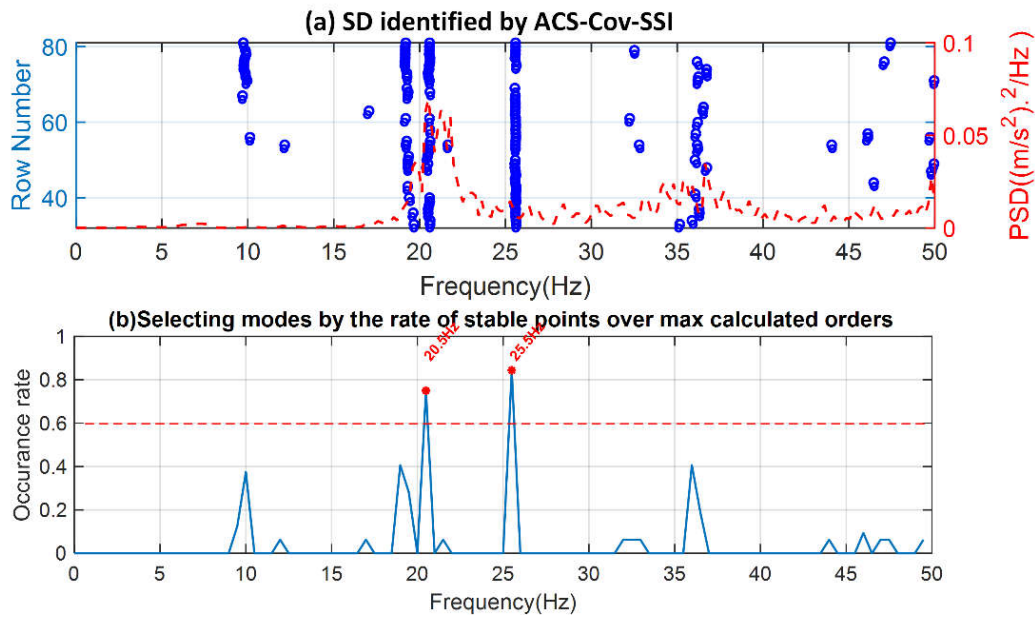


Figure 7-12 (a) SD identified by ACS-Cov-SSI and (b) Rate of stable points

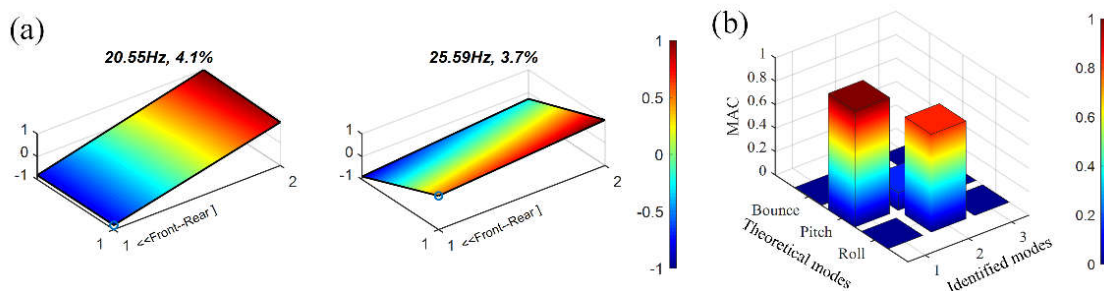
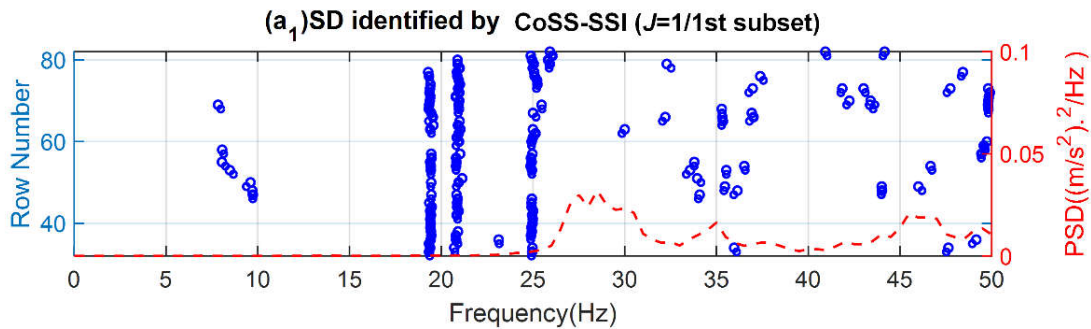


Figure 7-13 (a) Modes of bogie frame identified by ACS-Cov-SSI and (b) MAC values compared with theoretical mode shapes

As can be seen in Figure 7-13(b), which is the MAC value of the identified modes, pitch and roll with frequencies of 20.55 Hz and 25.59 Hz, respectively. ACS-Cov-SSI failed to extract the bounce mode. The bounce mode could be identified if the stable rate threshold was set at 0.3, but in that case two false modes at around 10 Hz and 36 Hz were also identified. Such results show that the threshold value of the stable rate should be sufficiently high as to filter out the false modes and obtain reliable results. At the same time, the true modes have to be identified which means the stable rate for the true mode has to be increased, which is a challenge for OMA. The CoSS-SSI proposed in Chapter 4 has been shown to be a novel and efficient method able to meet this challenge. ACS-Cov-SSI averages all of the correlation signal segments into one. Where, as stated earlier, correlation signal with small amplitudes will make less contribution to the final identification results, while often containing information of modes with lower excitations or higher damping.

Once again with CoSS-SSI, to extract the modes contained by small-amplitude correlation signals, the correlation segments were categorised into three subsets ( $J = 3$ ) according to their amplitudes before the averaging operation. The number of subsets was determined by the required accuracy of identification and efficiency of the identification process. The results identified by CoSS-SSI are presented below.

The SDs with respect to the three subsets are shown as in Figure 7-14( $a_1$ ), ( $b_1$ ) and ( $c_1$ ). The corresponding stable rates of each SD are presented in Figure 7-14( $a_2$ ), ( $b_2$ ) and ( $c_2$ ). It can be observed that the three stable modes appeared on the SDs compared to the two on the SDs identified by Cov-SSI (Figure 7-10) and ACS-Cov-SSI (Figure 7-12). As a result, the threshold of the stable rate for CoSS-SSI was set at 0.8 ( $\delta = 0.8$ ), Equation (3-57), which is higher than the threshold for Cov-SSI and ACS-Cov-SSI. As mentioned earlier, a higher stable rate threshold means the identified results are more reliable.



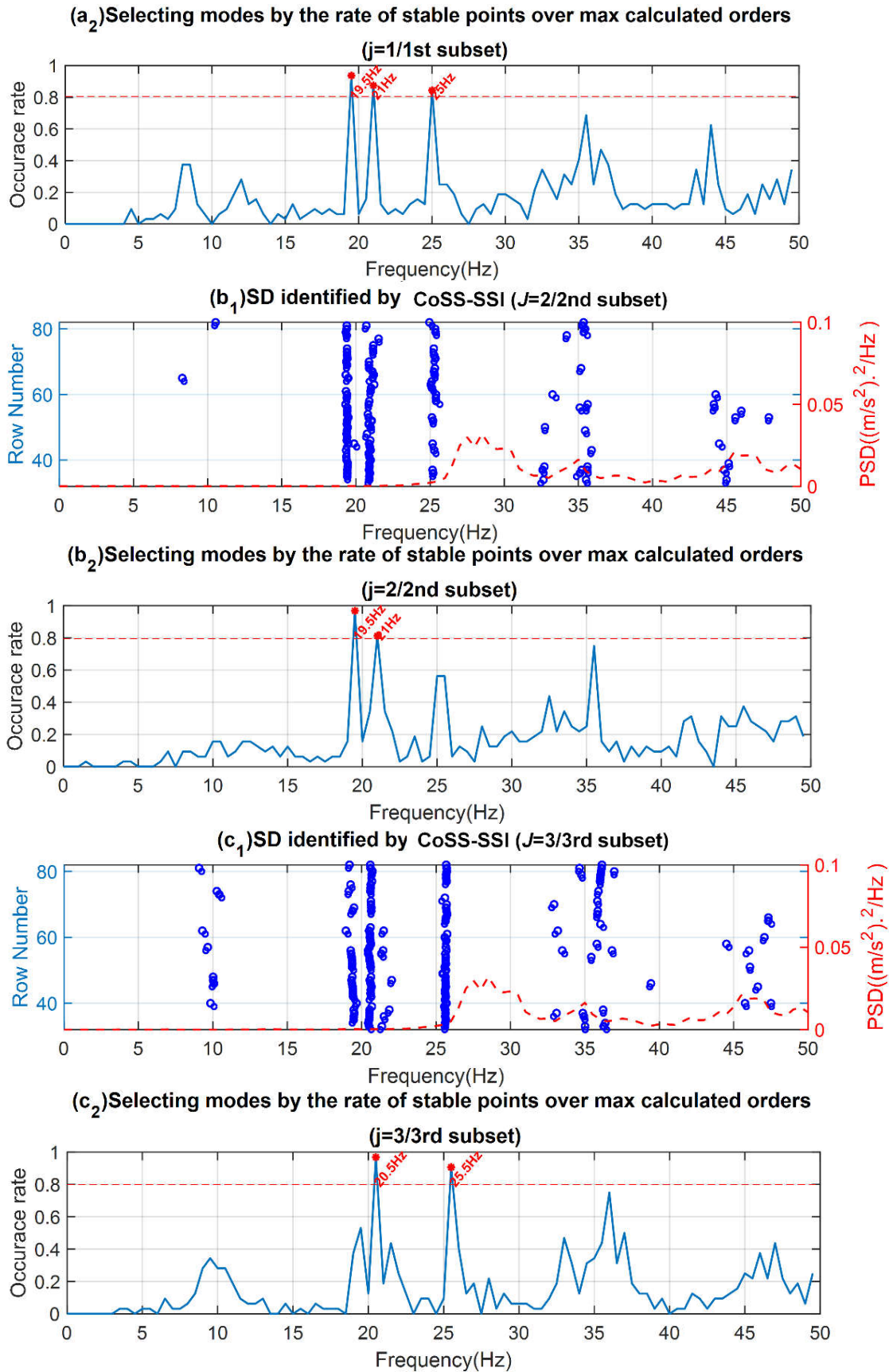


Figure 7-14 (a) SDs identified by CoSS-SSI, and (b) Corresponding rate of stable points

The modal parameters extracted from the three subsets by CoSS-SSI are presented in Figure 7-15( $a_1$ ), ( $b_1$ ) and ( $c_1$ ). The corresponding MAC values which compare the identified mode shapes with theoretical results are also shown, Figure 7-15( $a_2$ ), ( $b_2$ ) and ( $c_2$ ). In particular, it can be observed from Figure 7-15( $a_1$ ) that the bounce, pitch and roll modes of the bogie frame are successfully identified from the first subset. The results were confirmed in a further step and, as can be seen in Figure 7-15( $a_2$ ), the mode shapes extracted from the first subset by CoSS-SSI are largely in agreement with the theoretical mode shapes. In addition, it can be seen from Figure 7-15( $b_1$ ) and ( $b_2$ ) that the bounce and pitch modes have been extracted from the second subset of correlation signal segments. Pitch and roll modes are identified in the third subset, shown in Figure 7-15( $c_1$ ) and ( $c_2$ ).

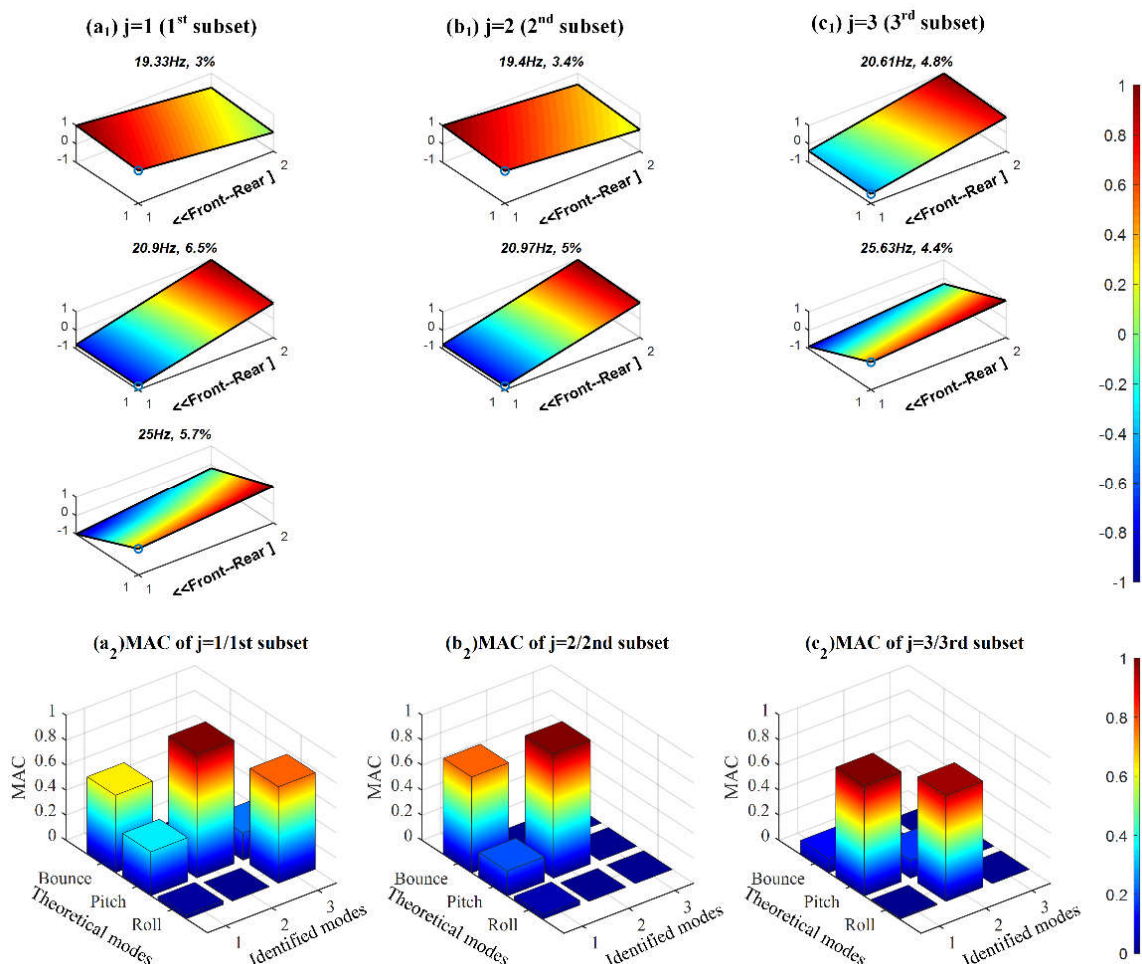


Figure 7-15 Modes of bogie frame identified by CoSS-SSI and corresponding MAC values compared with theoretical mode shapes

In summary, the bounce, pitch and roll modes of the bogie frame which are related to the suspension system were successfully identified with high reliability by CoSS-SSI. Although

the results identified by CoSS-SSI are not precisely identical with the theoretical modes, the differences are tolerable.

It is worth noting that the resonant frequency of the same mode as identified in different subsets is not entirely the same, there are small differences between the three subsets due to nonlinearities in the primary suspension. Furthermore, such a result can help explain why CoSS-SSI can provide much more stable SDs compared with ACS-Cov-SSI. Specifically, CoSS-SSI has the capability to reduce these nonlinearity effects, and therefore the SD is more stable.

It is apparent that all the rigid modes of the bogie frame have been successfully identified by CoSS-SSI and accord with the theoretical predicted performance of the suspension system. Therefore, the identified modes can be used for the CM of the suspension systems. It is worth highlighting that the mode shapes could be employed as the main criterion for fault diagnosis because they are inherent properties of dynamic systems. Then, the identified resonant frequencies could perform as the secondary criterion since they could change in mass of the bogie frame, but not the performance of the suspension system. Besides, the damping ratio should not be used as a criterion for CM because it is a big challenge to accurately quantify its value, in either experimental modal analysis (EMA) or operational modal analysis (OMA).

Last but not least, it is worth referring to the computation time required when employing CoSS-SSI for online CM. Here, a desktop computer with 8G RAM and four Intel(R) Cores(TM) of i5-2310 CPU was employed to carry out the computation. The computation time was counted by the tic/toc function in MATLAB. The result showed that 29.56 s was enough to obtain the final results, which is much shorter than the data length of a full set data which can be as much as 400 s. The computation time could be shortened further if the MATLAB program were converted into a C or C++ program which is computationally more efficient. Moreover, the sampling rate could be lower in a real application to further improve computation efficiency. All of these considerations suggest that CoSS-SSI has the potential for online CM.

#### **7.3.4 1/5<sup>th</sup> scale bogie with abnormal suspension**

The performance of CoSS-SSI has been demonstrated by its application to a 1/5<sup>th</sup> scale bogie with normal suspension system. In this section, the same scale bogie is used with an

abnormal suspension system to further test the performance of CoSS-SSI for CM of a railway vehicle suspension system. Two suspension fault cases were examined, where the faults were artificially introduced by changing the stud mounts at one corner, see Section 7.2.2.1.

#### **7.3.4.1 Fault case 1: Aging of the rubber (harder mount)**

The first fault case was to simulate the ageing of primary suspension components by replacing the normal stud mounts with harder ones since the ageing will result in an increase in stiffness. As described in Section 7.2.2.1, one stud mount at the front-left (FL) corner was replaced with a harder one, which resulted in the stiffness of the FL corner being increased by 50%. Except the replacement of this single stud mount, the tests were the same as for the normal suspension, see Section 7.3.1.

The modal parameters identified by CoSS-SSI are presented in Figure 7-16( $a_1$ ), ( $b_1$ ) and ( $c_1$ ), and the MAC values, in which identified modes are compared with theoretical results, are presented Figure 7-16( $a_2$ ), ( $b_2$ ) and ( $c_2$ ). It can be observed from Figure 7-16( $a_2$ ), ( $b_2$ ) and ( $c_2$ ) that the first mode identified in all three subsets is the bounce, and the second mode identified in the latter two subsets is the pitch and the third mode identified in only the last subset is the roll.

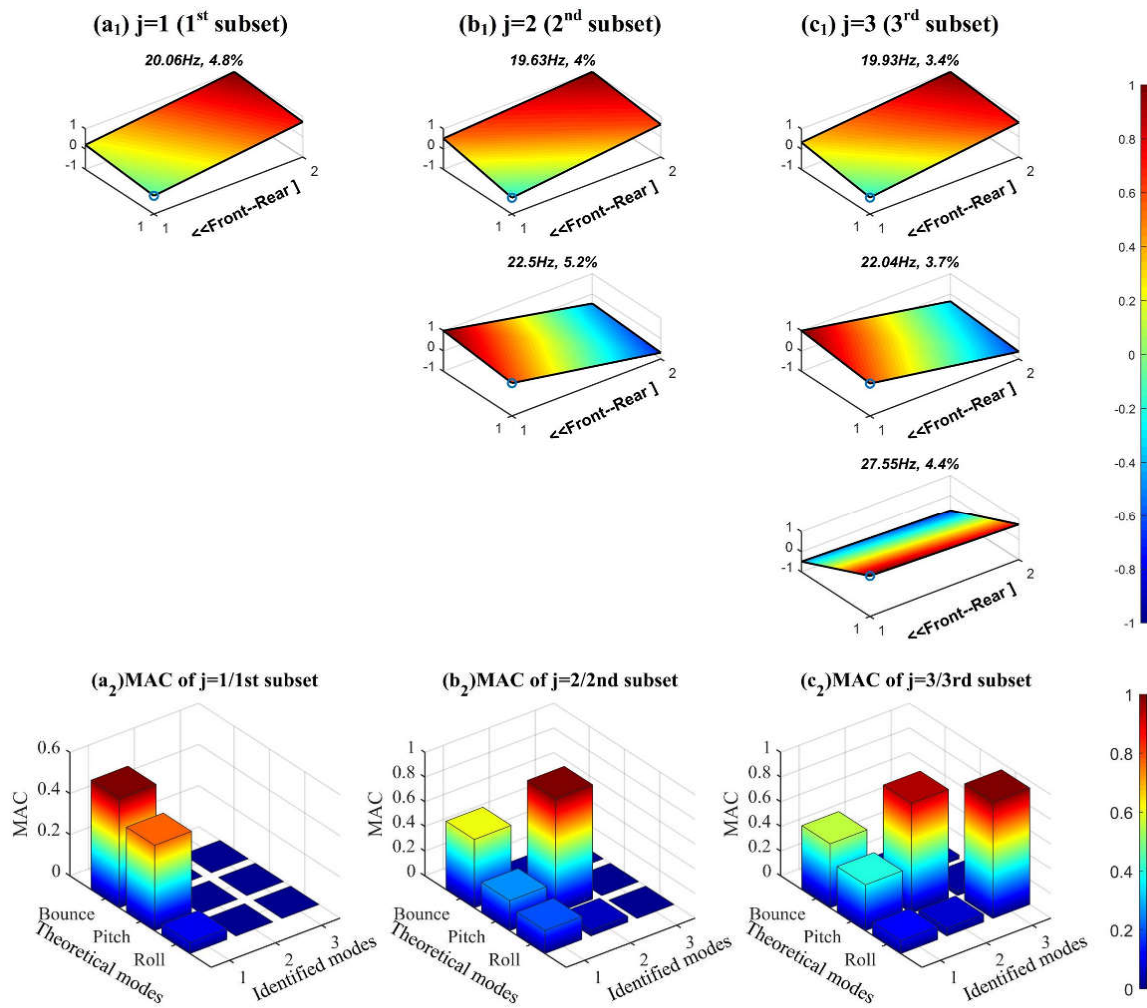


Figure 7-16 Modes of bogie frame with the harder suspension at FL corner identified by CoSS-SSI and corresponding MAC values compared with theoretical mode shapes

As can be seen in Figure 7-16(a<sub>1</sub>), (b<sub>1</sub>) and (c<sub>1</sub>), it is evident that the amplitude of the bounce modes in the front-left corner is smaller than for the other three corners. Such results are due to the increase in the stiffness of the front-left suspension. It can also be observed that the resonance frequencies of pitch and roll modes increased by around 2 Hz. Based on this analysis, it is possible to diagnose that the suspension system has a fault and place the fault at the front-left corner.

#### 7.3.4.2 Fault case 2: Fatigue of the rubber (Softer mount)

The second fault case was to simulate the fatigue of the stud mount which would result in stiffness decrease. In this case, the two stud mounts at the rear-left (RL) corner were replaced with two softer ones, see Section 7.2.2.1, so that the stiffness of the rear-left suspension decreased by 75%. Except for the replacement of these two mounts, the tests were the same

as for the normal suspension, see Section 7.3.1. The modes identified by CoSS-SSI and the corresponding MAC values are presented in Figure 7-17.

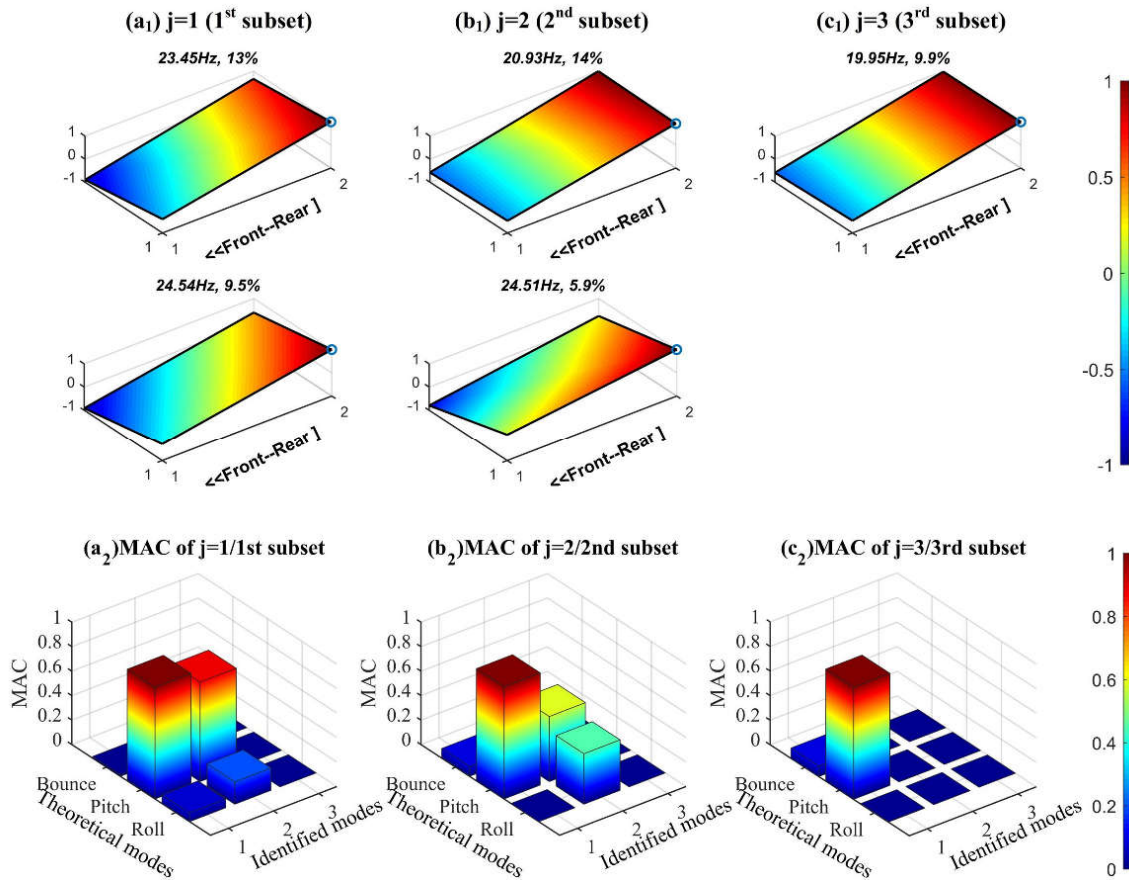


Figure 7-17 Modes of bogie frame with the softer suspension at RL corner identified by CoSS-SSI and corresponding MAC values compared with theoretical mode shapes

As can be seen from the identified mode shapes shown in Figure 7-17(a<sub>1</sub>), (b<sub>1</sub>) and (c<sub>1</sub>), the amplitude of displacement of the rear-left corner is larger than for the other three corners, which results from the stiffness reduction of the rear-left corner. Such a result compares well with the results obtained in Section 7.3.4.1, where higher stiffness resulted in smaller amplitude of displacement. It can also be observed from Figure 7-17(a<sub>2</sub>), (b<sub>2</sub>) and (c<sub>2</sub>) that all three subsets identify pitch mode, even the second mode around 25 Hz identified in first and second subsets which should be roll. We do not observe bounce and roll modes. In other word, a rear-left suspension fault could lead to a change of mode shape which leads to the conclusion that CoSS-SSI has the ability to diagnose this suspension fault of the 1/5<sup>th</sup> scale bogie.

## 7.4 Findings

In this chapter, experimental studies were conducted on a 1/5<sup>th</sup> scale bogie to evaluate the performance of CoSS-SSI for CM of railway vehicle suspension systems. Initially, a 7-DOF model of the 1/5<sup>th</sup> scale bogie was developed to obtain the theoretical values of the rigid modes of the bogie frame. Then, experiments were conducted on the scale bogie for the primary suspension systems were under three stiffness conditions. Based on the numerical and experimental studies, the following conclusions can be drawn:

- 1) The responses of the bogie are nonstationary because of the nonlinearities inherent in suspension and the wheel-track contact;
- 2) Cov-SSI and ACS-Cov-SSI are unable to identify all of the rigid modes of the bogie frame, whereas CoSS-SSI has this capability, which demonstrates the superiority of CoSS-SSI for railway vehicle suspension monitoring;
- 3) CoSS-SSI has the potential to fulfil online CM since its computational efficiency is high;
- 4) CoSS-SSI was able to identify the two suspension faults seeded into the 1/5<sup>th</sup> scale bogie.

In the next chapter, a full-size Y25 bogie will be employed to further verify the performance of CoSS-SSI for railway vehicle suspension monitoring in a further step.

---

## CHAPTER 8 CONDITION MONITORING OF THE SUSPENSION SYSTEM OF AN Y25 BOGIE USING CoSS-SSI

---

*The purpose of this chapter is to further evaluate the performance of CoSS-SSI for railway vehicle suspension monitoring. An Y25 bogie was tested on a full-scale rig in the Institute of Railway Research at the University of Huddersfield.*

*A SIMPACK model of the Y25 bogie was developed to calculate the theoretical modal parameters of the primary suspension system, which is helpful in determining the frequency range to be analysed in the experimental tests. Because the tested bogie was excited by the rotation of a rail drum, harmonics were unavoidable and cepstrum editing (CE), which was introduced in Chapter 5, was employed to suppress them.*

*The results show that CoSS-SSI can extract the dynamic parameters of the primary suspension system of the Y25 bogie using the output signal only, which again demonstrated the capability of CoSS-SSI for railway vehicle suspension system monitoring. The effectiveness of CE for eliminating the adverse influence of harmonics on OMA was also evaluated during the experiments.*

## 8.1 Introduction

Roller rigs are popular laboratory devices used to investigate the dynamics of railway vehicles. They are easy to control, flexible to configure, produce repeatable and accurate results, and are cost-efficient compared to field tests [178]. Numerous roller rigs have been constructed worldwide based on different rules for different study purposes. The earliest roller rig was built in 1904 at Swindon by the Great Western Railway [173]. The 1/5<sup>th</sup> scale roller rig which was employed in Chapter 7 was constructed at Manchester Metropolitan University to investigate the dynamic behaviour of railway vehicles [174]. However, a 1/5<sup>th</sup> scale roller rig cannot perfectly represent the dynamic behaviour of a real vehicle in field tests, even though the scale roller rig was designed and built to realistically represent the input of track irregularities and vehicle dynamic performance [173].

In order to further evaluate the performance of CoSS-SSI for railway vehicle suspension monitoring, additional experiments were carried out on a full-scale roller rig in the laboratory of Institute of Railway Research (IRR) laboratory at the University of Huddersfield (UoH). The main components of the full-scale rig were a 2 m diameter rail drum with two circumferential rails, a bogie manipulation platform and a loading cell [179], as shown in Figure 8-1. The loading cell consists of a load frame and two actuators, which can provide vertical and roll motions on the test bogie through the secondary suspension. This roller rig can accurately represent the contact conditions between wheel and rail, which means the response of the bogie is close that of a field test.

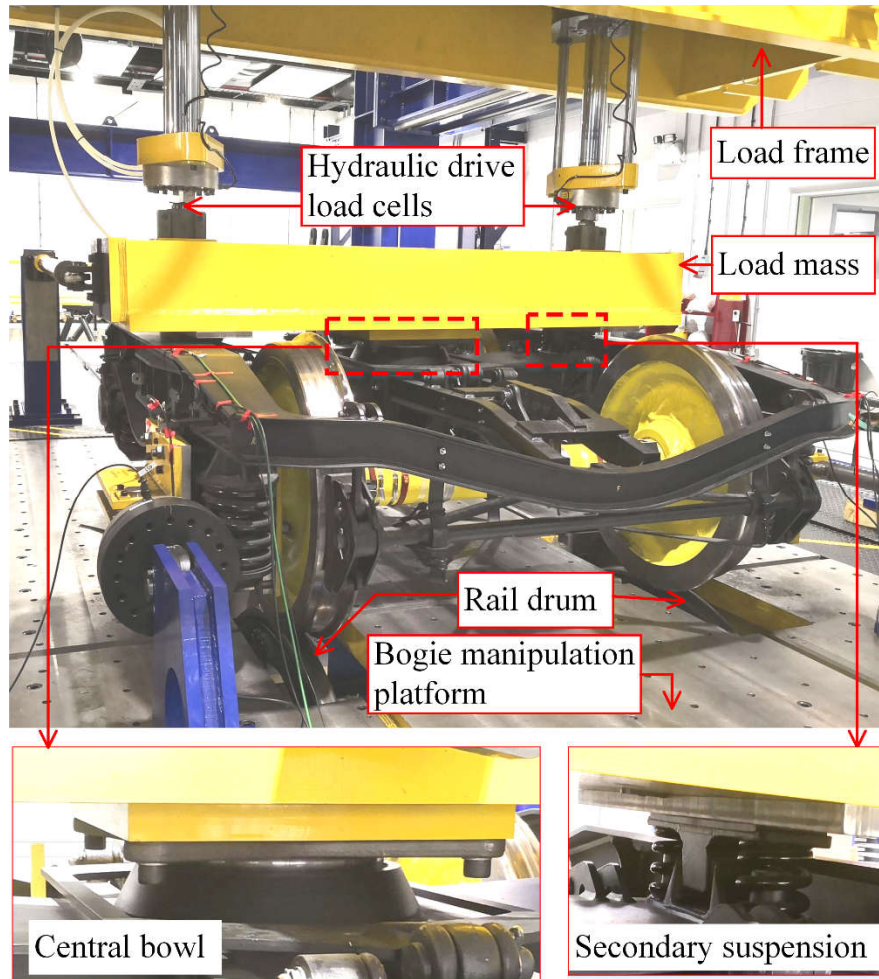


Figure 8-1 Photograph of the full-scale roller rig in the IRR laboratory at UoH

## 8.2 SIMPACK model of tested bogie

The Y25 is popular for modelling the suspension of a freight wagon since it is robust and cheap. Here, a multi-body dynamic model is developed using a commercial software package, SIMPACK, to calculate the theoretical modal parameters of the bogie frame, which are related to the primary suspension. First SIMPACK is introduced briefly, then, the model which took into account the loading of the Y25 test bogie is presented and followed by the theoretical modal parameters of the primary suspension system.

### 8.2.1 SIMPACK introduction

SIMPACK is a powerful and popular general multi-body simulation software tool widely used for predicting and visualising the dynamic behaviour of mechanical or mechatronic systems by generating and solving virtual 3D models. SIMPACK includes several modules for specific areas such as bearing, wind turbines, and automotive and rail vehicles [103].

The rail module in SIMPACK has been used for railway vehicle simulation for more than a decade. It provides all the necessary functionality for creating accurate railway dynamics models. The most frequently used features in the rail module include the rail-wheel contact model, and many specialised modelling elements commonly used for research into railway vehicles, as well as an easy-to-use graphical user interface. SIMPACK has been demonstrated to be good at handling ‘stiff’ dynamic systems such as metal to metal wheel/rail contact and is uniquely suitable for shock contact [180]. All of these features have helped placing SIMPACK amongst the top dynamic simulation software used by the railway industry [180]. Therefore, SIMPACK was employed here as the simulation tool to consider the complicated system comprising the test rig.

### 8.2.2 Y25 bogie SIMPACK model

A model of a Y25 bogie is applied in this sub-section which considers the experimental boundary conditions to which the bogie is subjected. In particular, a model of the Y25 bogie on rails with vertical loads was developed within SIMPACK. The main components of the bogie model are: a bogie frame, two wheelsets, four axle-boxes, a load mass, primary suspension and secondary suspension systems, see Figure 8-2.

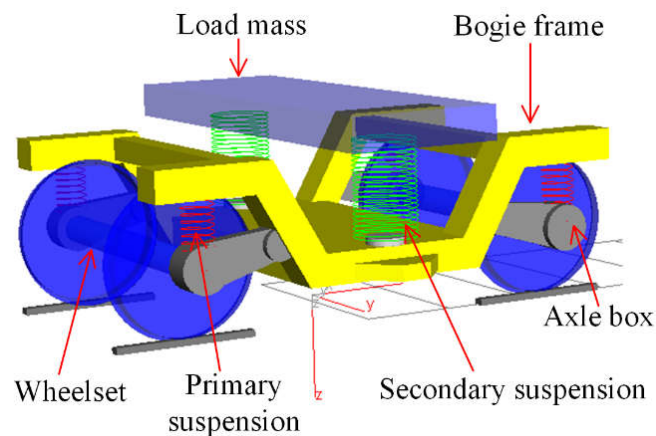


Figure 8-2 SIMPACK model of Y25 bogie

Standard and well-tested elements within SIMPACK were employed to simulate the behaviour of various components of the Y25’s suspension system, for instance: bearing forces by the 43<sup>rd</sup> force element (Bushing Cmp); to model the primary suspension and its behaviour, the 86<sup>th</sup> force element (Spring-Damper Ser/Par Cmp); and to model the secondary suspension the 79<sup>th</sup> (Shear spring Cmp) and 6<sup>th</sup> (Spring-Damper Serial PtP) force elements. The properties, masses and related moments of inertia of the suspension systems are

tabulated in Table 8-1 and Table 8-2, respectively, where the values are obtained from previous study [106], [107] and a SIMPACK rail training class. The moments of inertia of the load mass were zero as the load mass plays the role of placing a vertical load on the bogie, and  $I_{xx}$ ,  $I_{yy}$  and  $I_{zz}$  are the moments of inertia of roll, pitch and bounce, respectively.

Table 8-1 Main properties of the suspension system

Parameter	Value	Unit
Primary suspension spring stiffness in $x$ direction	31,391,000	N/m
Primary suspension spring stiffness in $y$ direction	3,884,000	N/m
Primary suspension spring stiffness in $z$ direction	1,220,000	N/m
Primary suspension damping in $x$ direction	15,000	Ns/m
Primary suspension damping in $y$ direction	2,000	Ns/m
Secondary suspension vertical stiffness	430,000	N/m
Secondary suspension lateral shear stiffness	160,000	N/m
Secondary suspension longitudinal shear stiffness	160,000	N/m
Secondary suspension vertical damping	25,000	Ns/m

Table 8-2 Mass properties of the mass components

Body	M = kg	$I_{xx}$ = kg.m <sup>2</sup>	$I_{yy}$ = kg.m <sup>2</sup>	$I_{zz}$ = kg.m <sup>2</sup>
Bogie frame	2,219	1,976	1,557	2,848
Wheelset	1,300	688	100	688
Load mass	2000	0	0	0
Axle box	160	1.47	8.45	7.56

The theoretical modal parameters of the rigid modes of the Y25 bogie related to the primary suspension system can be calculated using the Eigenvalue function within SIMPACK, and are presented in the following sub-section.

More information, specifications and functions of the full-scale rig in the IRR laboratory can be found in [179].

### 8.2.3 Theoretical modal analysis

All of the rigid modes of the Y25 bogie can be extracted from the developed SIMPACK model. Nonetheless, it is well known that only the modes of the bogie frame are related to the behaviour of the suspension system [96] and therefore, only the modes of the bogie frame are presented in Figure 8-3.

It is shown in Figure 8-3 that the first mode of the bogie frame is bounce and its resonance frequency is 11.42 Hz. The second mode is roll with a natural frequency of 13.59 Hz, and the third mode is pitch with a natural frequency of 14.77 Hz. The damping for each mode is shown in the figure. It can be seen that the interest frequency range is 10 Hz to 20 Hz.

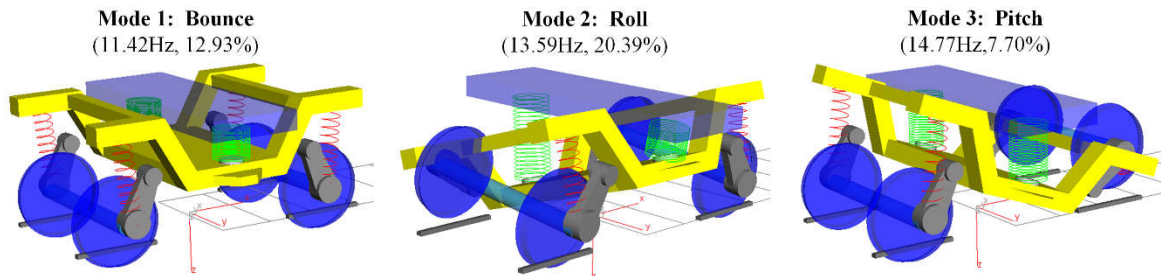


Figure 8-3 Rigid modes of bogie frame related to primary suspension

### 8.3 Experimental investigation

In this section, experiments were conducted on the full-scale rig to investigate the effectiveness of employing CoSS-SSI to monitor the railway vehicle suspension system. The experimental set up is introduced, and then the characteristics of collected data and the modal parameter identified by CoSS-SSI are presented.

#### 8.3.1 Experiment set-up

CoSS-SSI was used to identify the modal parameters of the Y25 bogie in a manner similar to the process of identifying the modal parameters of the 1/5<sup>th</sup> scale roller rig, presented in Chapter 7. Four accelerometers were installed on the bogie frame upon the axle boxes, as shown in Figure 8-4. It can also be seen that another two accelerometers were mounted on the attachment of the axle box to measure the response of the axle box. The accelerometers were installed on the enclosure, not directly on the axle box because the space between axle box and bogie frame was insufficient for safe sensor installation. Besides, the enclosure was attached on the axle box via four long bolts, so the response of the enclosure was similar to that of the axle box because the condition for accurate transmission of a vibration signal is that the attachment is rigidly fixed to the axle box

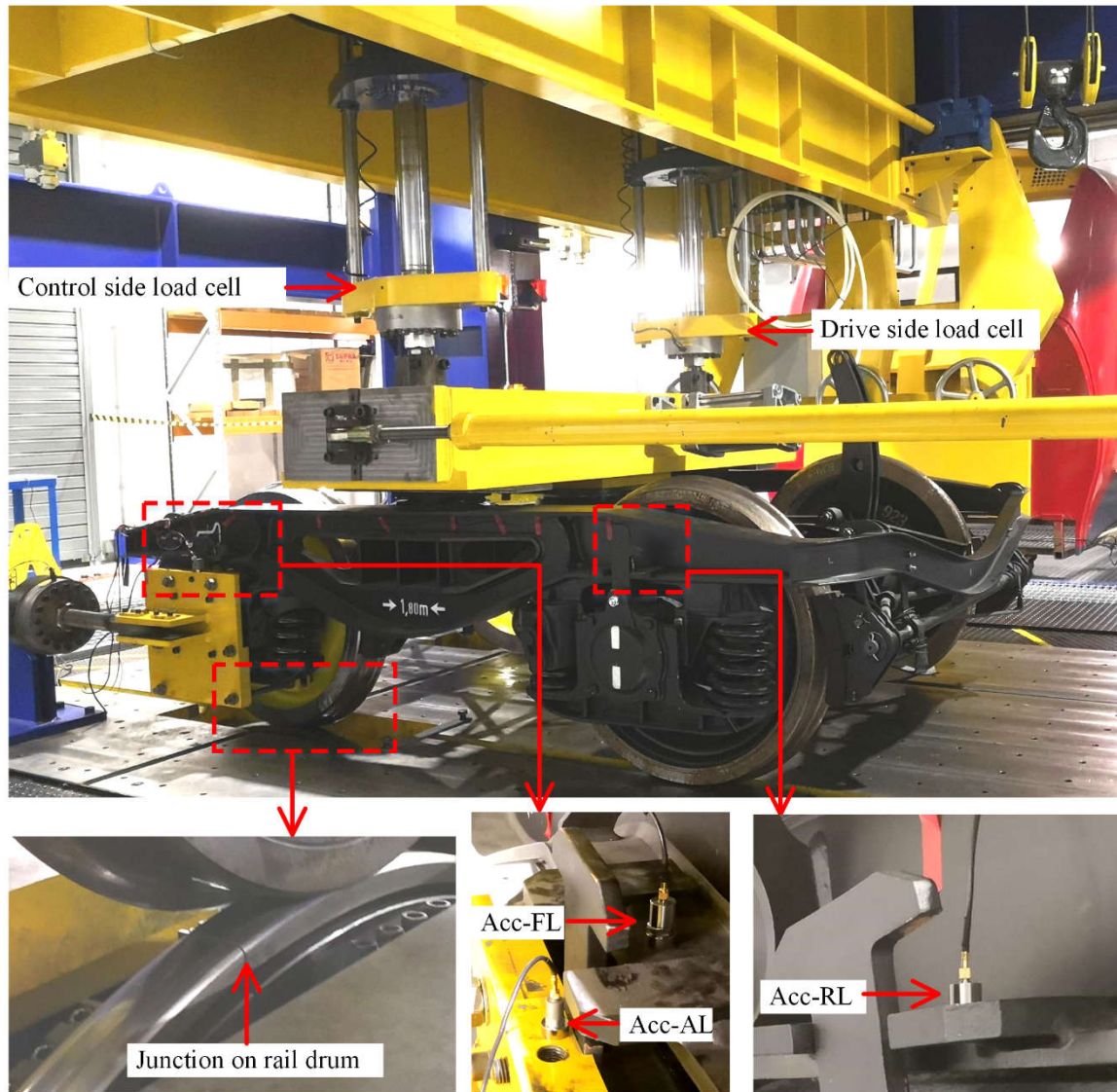


Figure 8-4 Accelerometer installation positions on the Y25 bogie

The end of the bogie over the rail drum was designated as the front, and the other end was the rear. The accelerometers installed on the bogie frame were denoted as Acc-FL (Front-Left), Acc-FR (Front-Right), Acc-RL (Rear-Left) and Acc-RR (Rear-Right). The other two accelerometers installed on the axle box were denoted as Acc-AL (Axle-Left) and Acc-AR (Axle-Right). A schematic of the full scale test rig and accelerometer positions is presented in Figure 8-5, and the accelerometers are shown in Figure 8-6.

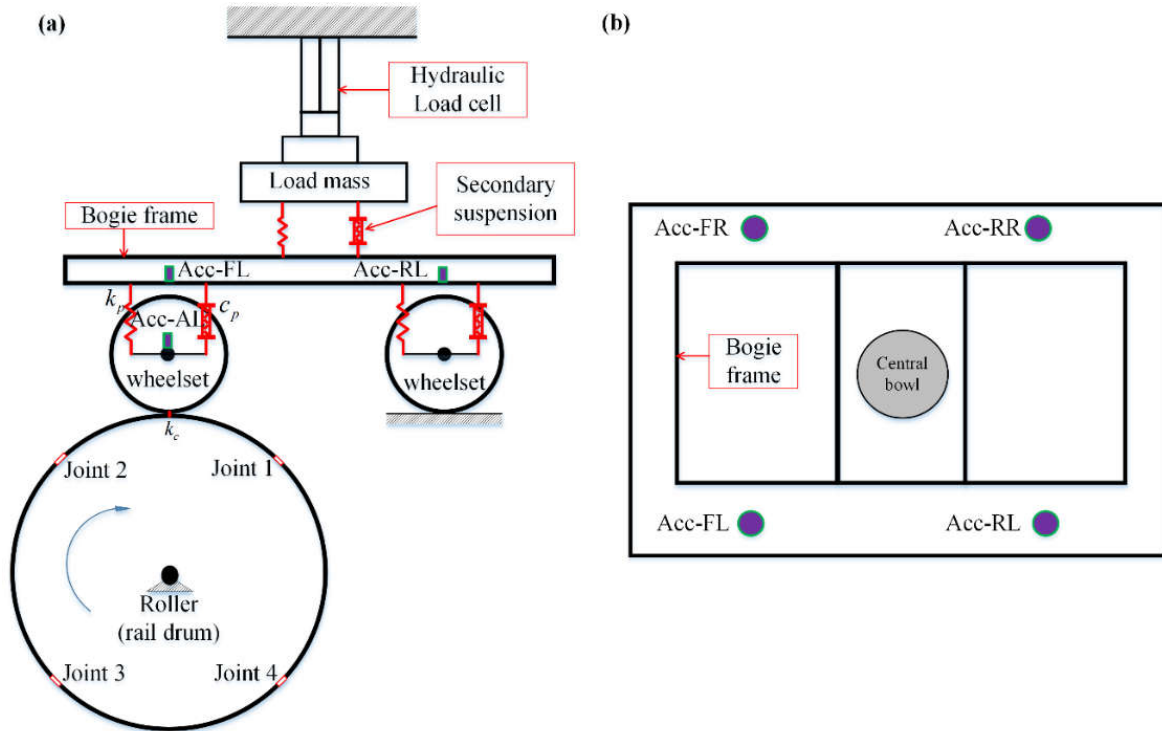


Figure 8-5 Schematic of the full-scale test rig and accelerometer positions

Because six transducers were used for these tests the four channels DAQs employed in previous experiments was unsuitable. A SINOCERA model 6232B DAQs with sixteen channels was employed in the full-scale rig test, see Figure 8-6(a). These sixteen channels had independent Analogue/Digital (A/D) converters and a sampling rate of up to 96,000 Hz. All channels of the DAQs are synchronised, which means the data acquisition process can be synchronised. Given the frequency range of interest the sampling rate was set at 1,000 Hz. The tests were repeated six times.

The four accelerometers installed on the bogie frame were those employed previously, and their details can be found in Table 6-1. The specifications of additional two accelerometers were given in Table 8-3. A photograph of the accelerometers is presented in Figure 8-6(b) and (c).

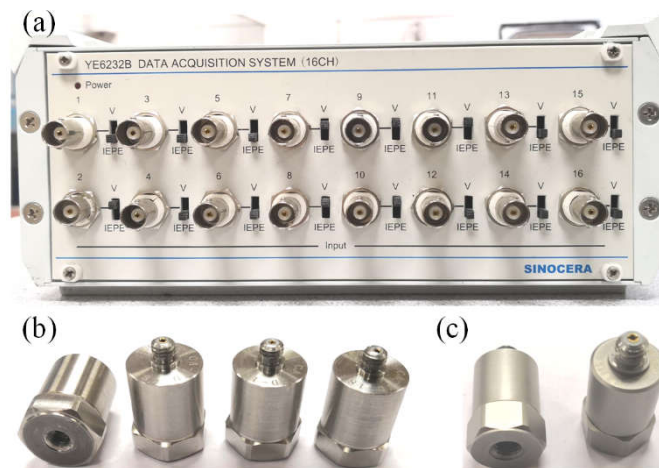


Figure 8-6 Photograph of (a) YE6232B DAQs (b) CA-YD-185 accelerometers (c) YMC 121A20 accelerometers

Table 8-3 Specifications of accelerometers YMC 121A20

Manufacture	Model No.	Frequency range (Hz)	Serial No.	Sensitivity (mv / (m · s <sup>-2</sup> ))
YMC	121A20	1-10,000	611838	2.01
			611839	2.02

## 8.3.2 Loading profile and response analysis

### 8.3.2.1 Loading profile of the load cell

The data utilised in this study was collected when the rig was operated for other test purposes, so it is worth briefly discussing the loading profile of the hydraulic load cells in the control-side and driven-room sides shown in Figures 8-4 and 8-5. Using the hydraulic driven load cell, the tested bogie can be loaded in two ways. The first is to set a maximum load, and the second is to set the maximum displacement of the load cell. The second loading strategy was employed in this case, and the load profile and the corresponding loads were as presented in Figure 8-7. The load cell, with zero load, was kept in its original position (568 mm) for the first 78 s. Then, at constant speed, the displacement of the load cell increased from 568 mm to 628 mm in 60 s. The load cell then returned to its original position during the following 60 s. It can be seen that the load cell keeps in line with the change of its displacement.

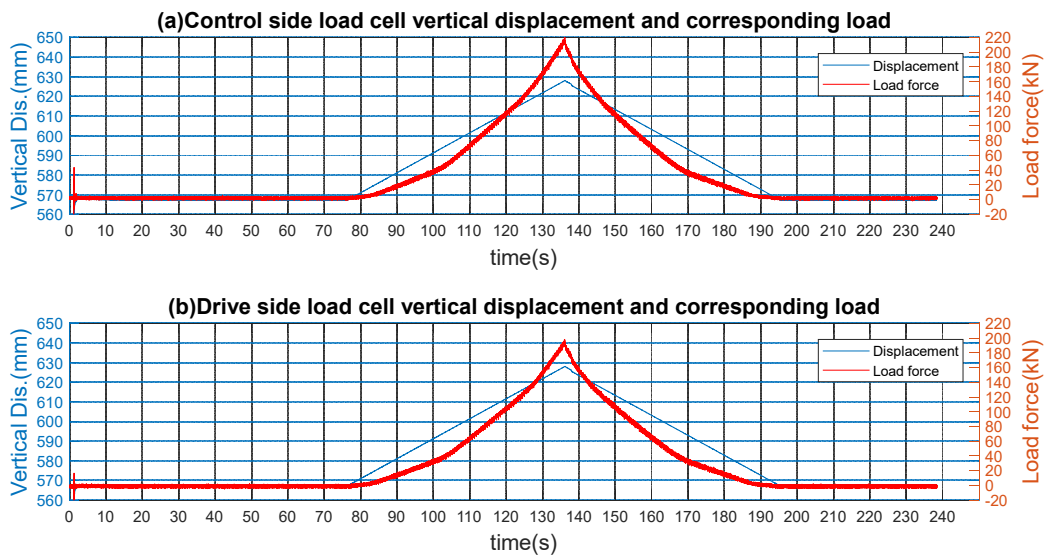


Figure 8-7 Load profile and corresponding load force during the test

It is worth noting that the system became time-varying when the load cell started increase the load on the test bogie. It can be seen that the slope of load-time plot changed at around 105 s (about 17 s after the load cell commenced moving), which resulted from a change in the primary suspension stiffness as the innerspring was engaged. This phenomenon showed the test rig was a time-varying system. However, as this is a preliminary study to demonstrate that OMA can be used for railway vehicle suspension monitoring, the test bogie was considered as a time-invariant system. Therefore, the bogie responses without load applied by the load cell were used in the following identification process. Specifically, the data segment considered relevant was the response from 14 s to 74 s, because during the first 14 s the rotation speed of the rail drum increased from zero to 55 rpm, after which the speed was maintained constant until 210 s. The responses of the first 14 s were neglected as the speed of the rail drum was not constant. The characteristics obtained from analysis of the given data segment will be presented in the following sub-section.

### 8.3.2.2 Characteristics of the Y25 bogie responses

The relevant data segment, from 14 s to 74 s, was cut from the collected data and time domain signal of the first five seconds is presented in Figure 8-8. First of all, it can be observed that the amplitudes of axle box vibrations are higher than for the bogie frame, this is due to the attenuation provided by the primary suspension system. However, this attenuation alone cannot provide the comfort requirement of a railway vehicle, and so

secondary suspension is usually employed in passenger vehicles. Secondly, it is noticeable that the responses of the front bogie have higher amplitudes than the rear because the front wheelset was directly excited by the rail drum. Thirdly, it can be observed from the time-domain signal that the bogie was excited by periodic pulse inputs which were caused by the junctions on the rail drum. Fourthly, the amplitudes of responses from accelerometers on the left were slightly higher than from those on the right which could be due to the installation errors.

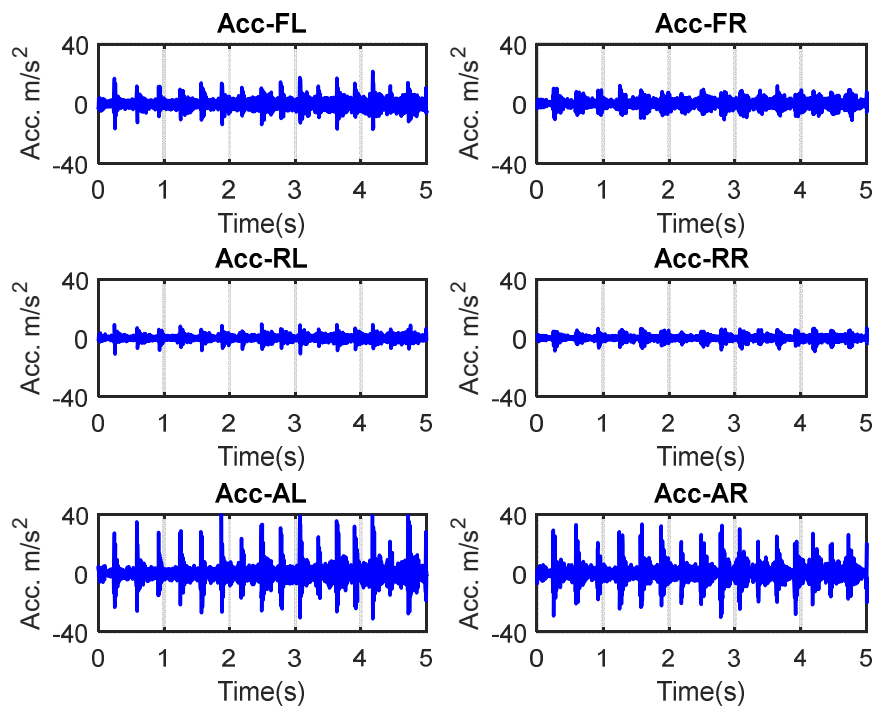


Figure 8-8 Example of a time-domain signal of bogie response

More information from the responses can be found from the frequency-domain, presented in Figure 8-9. The analysed frequency range was 0~21 Hz as the interested frequency range is between 10 Hz and 18 Hz according to the result of the simulated modal analysis.

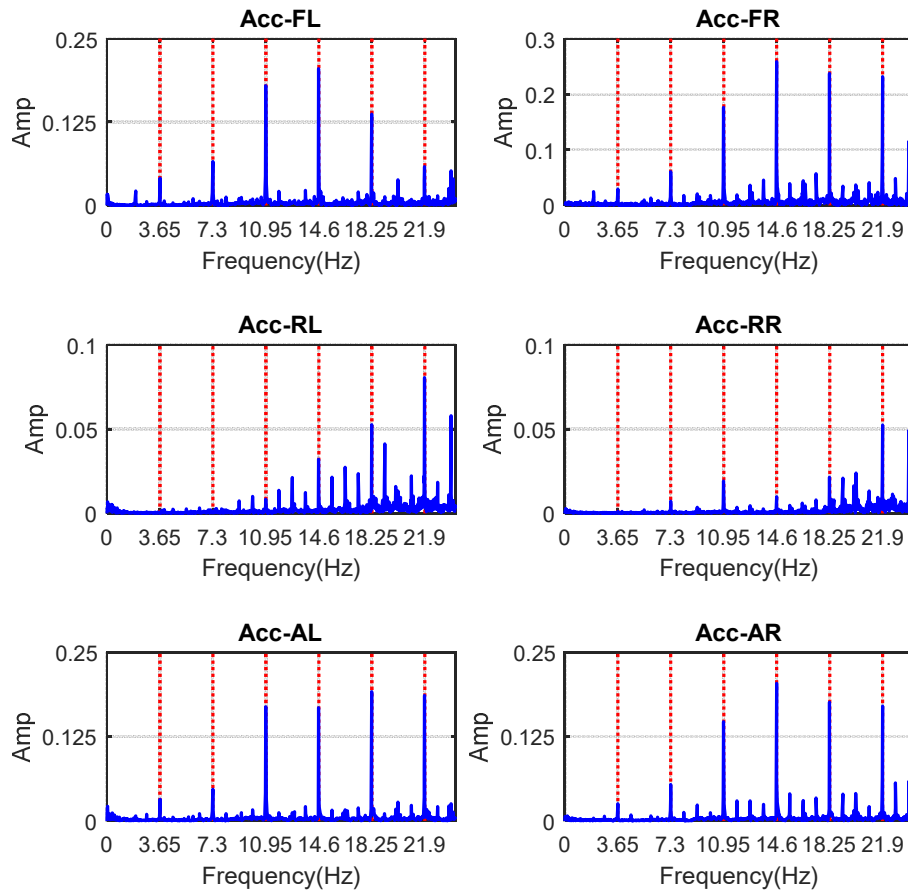


Figure 8-9 Example of a frequency-domain signal of bogie response

It can be seen in Figure 8-9 that the amplitudes of the spectrum at integral multiples of 3.65 Hz were higher than other frequencies, where 3.65 Hz is related to the rotational speed of the rail drum. The rotational speed of the rail drum was measured and shown it was between 54~55 rpm, which means the rotational frequency was between 0.9~0.92 Hz. But, the rail drum contains four junctions, and therefore, the period pulse excitation frequency would be at, or very close to, 3.65 Hz. This periodic excitation generates large amplitude peaks in the spectrum at integral multiples of 3.65 Hz. Moreover, it can be seen that there are some small peaks, which are multiples of 0.91 Hz, between the higher peaks.

Because of the power of this periodic pulse, the resonance frequencies of the system cannot be observed. Nevertheless, it can be observed from Figure 8-9 that the amplitudes of the peaks caused by the rotational frequency also change, which could result from modulation of the system's resonance frequencies, such as the pulse amplitude of the front bogie at 14.6 Hz is higher adjacent peaks. Lastly, it is worth highlighting that the collected signals

contained harmonic components as the excitation is a rotational part and the manufacture and installation errors are unavoidable.

### 8.3.3 OMA via CoSS-SSI combined with cepstrum editing

In this section, the data segments cut from the raw data were employed to identify the modal parameters related to the primary suspension system. As the superiority of CoSS-SSI has already been demonstrated in Chapter 6 and Chapter 7, only CoSS-SSI was utilized in this chapter to extract the modal parameters. We also know that CE can efficiently remove harmonic effects that adversely affect OMA. Therefore, CE was employed here to filter the signal before using CoSS-SSI for OMA.

#### 8.3.3.1 Cepstrum editing before OMA

The process of CE can be found in Section 5.2. Similar to the simulation studies in Section 5.3, a short-pass lifter was employed to edit the cepstrum. An example of the cepstrum, window function and edited cepstrum is presented in Figure 8-10(a). It can be observed that all the periodic components were filtered out using the short-pass lifter. An example of the raw signal and the recuperated or filtered signal is presented in Figure 8-10(b). As can be seen in Figure 8-10(b) that the main difference between the raw signal and filtered signal is their relative amplitude. The amplitude of the filtered signal was reduced significantly by a factor of about 40, because the periodic component in the original signal contained most of the power of the signal.

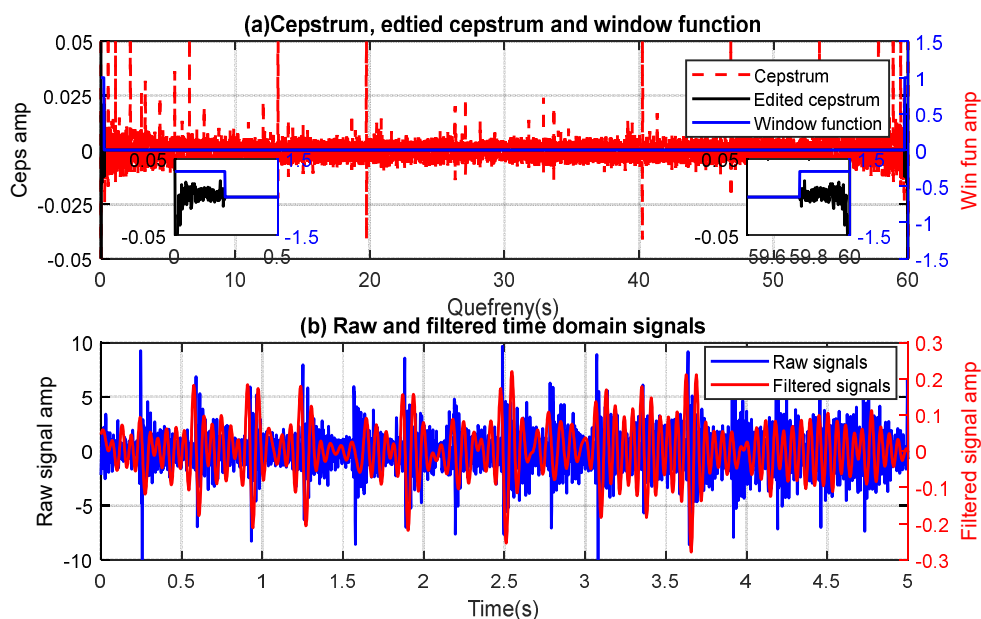


Figure 8-10 (a) Example of cepstrum; (b) Example of raw and filtered signals in the time-domain

A comparison of raw and filtered signals in the frequency-domain is given in Figure 8-11. The periodic frequencies resulting from the rotation of the drum have been successfully filtered out. It can also be seen that the amplitude of the filtered signal was heavily reduced, which is in agreement with the time-domain signal.

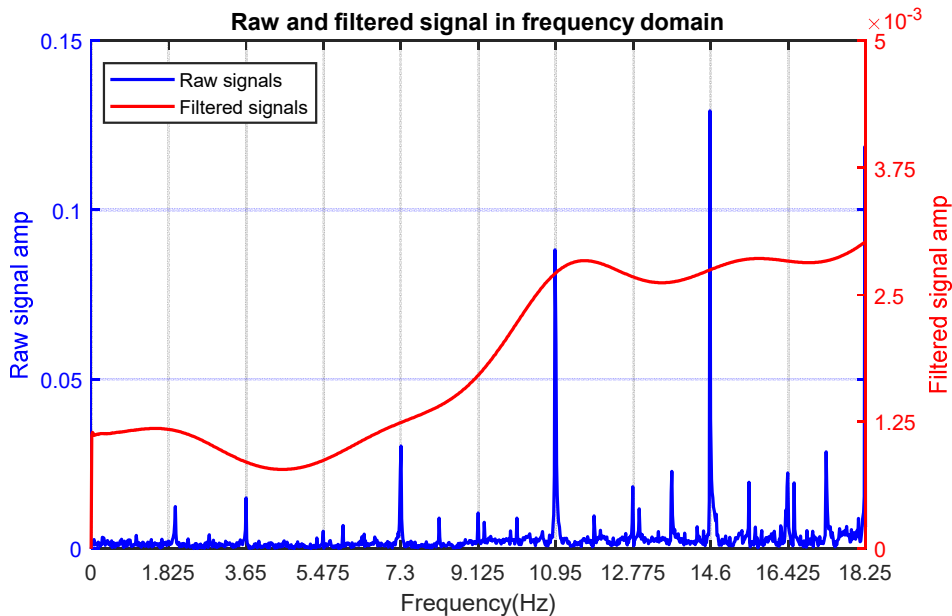


Figure 8-11 Example of raw and filtered signals in the frequency-domain

### 8.3.3.2 CoSS-SSI identification results

In this sub-section, the collected signal before and after filtering was employed to identify the modal parameters and to verify the effectiveness of CE for OMA in the presence of harmonics, and offer further confirmation of the results regarding CoSS-SSI presented in Chapter 6 and Chapter 7.

The sampling rate during the test was 1,000 Hz, and the time length over which data collected from each test was 60 s. Thus for both filtered signal and original signal, the employed data segment included 60,000 data points for each test. In accord with the CoSS-SSI flowchart (Figure 4-2), the 60,000 data points were divided into eight segments and the length of each segment set to 7168 points ( $N = 1024 * 7$ ). The divided data segment contained about 70 periods of the first mode which is needed to suppress noise effects.

Consequently, 48 data segments were obtained as the test was repeated six times, and therefore  $6*8$  correlation signal segments were obtained. As previously, the correlation signal segments were categorised into two subsets ( $J = 2$ ) according to their average RMS value. The number of subsets was selected according to the number of total segments and

their minimum and maximum RMS values, and considering the balance between the calculation efficiency and identification accuracy. Then, each subset of correlation segments was averaged and used to conduct modal identification.

The SDs identified by CoSS-SSI using the raw signal and filtered signal are presented in Figure 8-12 and Figure 8-13, respectively. The error thresholds of the stable points were set at the same value for identification process using either raw or filtered signals, which were  $\varepsilon_f = 0.1$ ,  $\varepsilon_\xi = 0.2$  and  $\varepsilon_{MAC} = 0.5$ . The formulas for these error thresholds can be found in Section 3.3.4.

As can be seen in Figure 8-12, stable points are rare and most of the stable points are distributed around pulse responses. If the threshold of the rate of stable point over maximum orders was set at 0.5, none of the stable modes could be identified. Such results could lead to domination by the harmonic effects, according to the simulation studies conducted in Chapter 5. However, it can be observed from Figure 8-13 that three relative stable modes were identified in these two subsets, which indicated the effectiveness of CE to remove the harmonic effects.

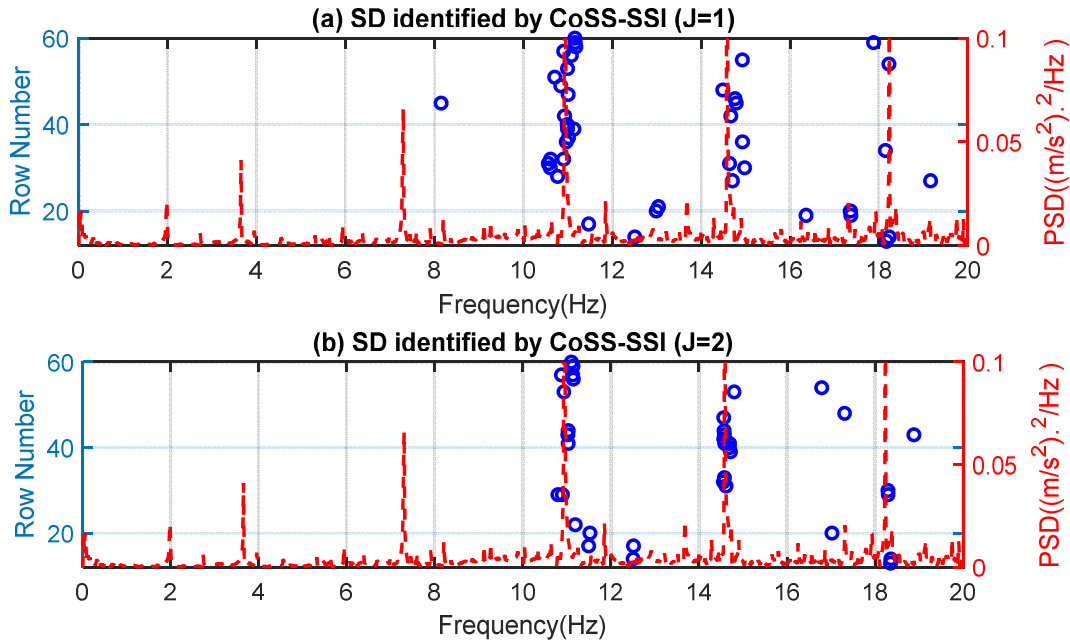


Figure 8-12 SDs identified by CoSS-SSI using raw signal

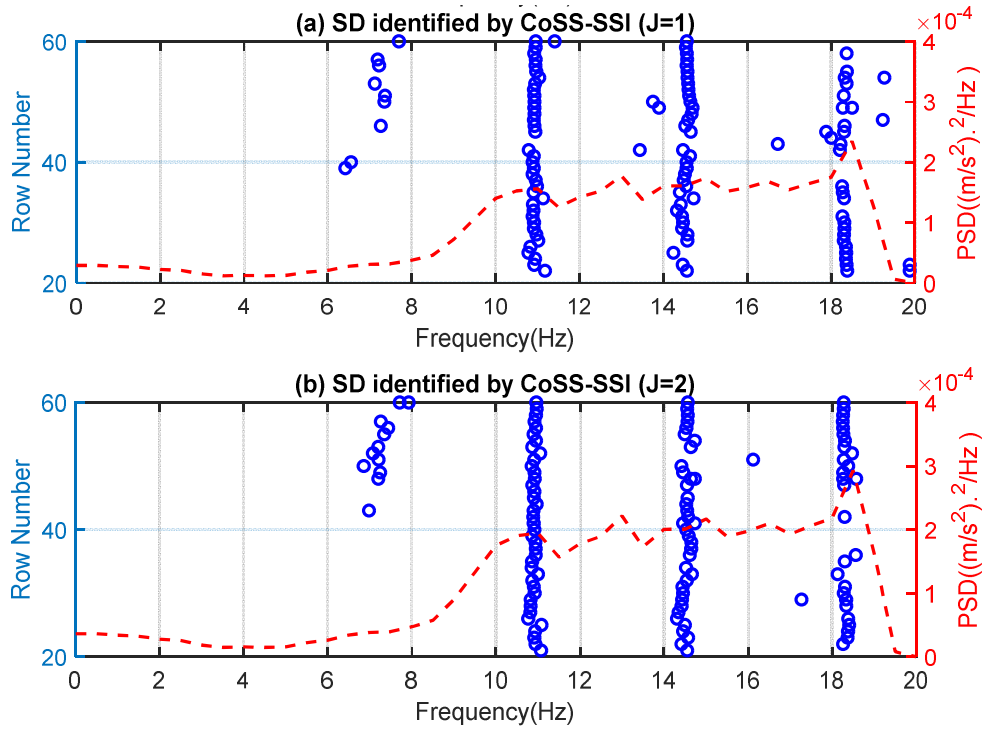


Figure 8-13 SDs identified by CoSS-SSI using filtered signal

The stable modes identified from the filtered signal are presented in Figure 8-14 when the threshold of the stable rate of stable points over maximum calculated order was set at 0.5 ( $\delta = 0.5$ ). The mode shapes of the different modes selected out from the SDs are presented in Figure 8-15.

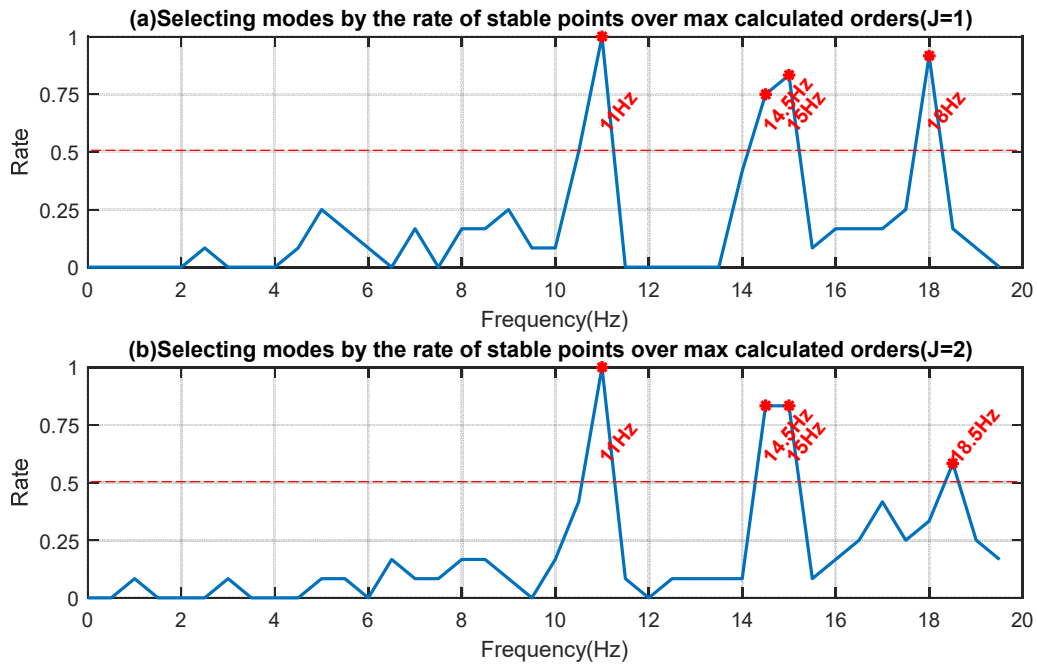


Figure 8-14 Rate of stable points over maximum calculated orders

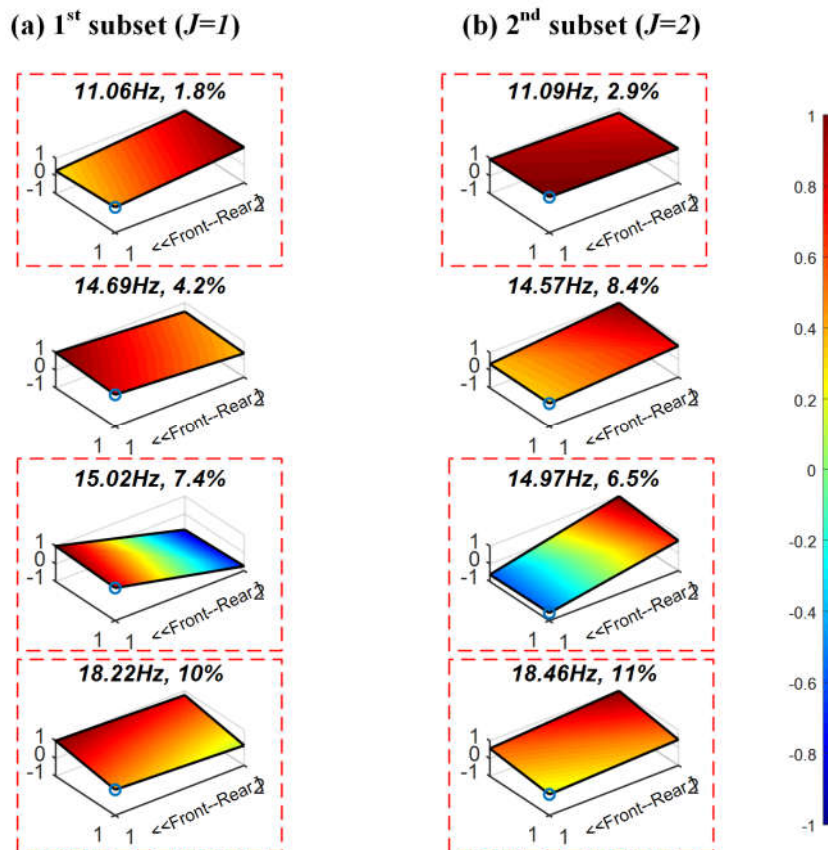


Figure 8-15 Rigid modes of Y25 bogie frame identified by CoSS-SSI

Firstly, it can be seen from Figure 8-15 that the mode shapes identified from the two subsets are similar, but the resonance frequencies have small differences. Secondly, it can be observed that the first identified mode ( $\sim 11.06$  Hz) is bounce, the third mode ( $\sim 15.00$  Hz) is pitch, and the fourth mode ( $\sim 18.3$  Hz) could be roll. This result is in line with the frequency domain characteristics of the bogie responses. It can be seen in Figure 8-9 that the amplitudes of frequencies around 10.95 Hz, 14.6 Hz and 18.25 Hz are higher as a result of resonance frequency modulation. Thirdly, it can be seen that the frequency of the second identified mode is close to the resonance frequency of pitch; the mode shape is also close to pitch mode. This result is explained as being caused by the nonlinearity of the vehicle suspension system. Fourthly, it is observed that the roll mode is not as regular as the bounce and pitch modes. Such a result is because only one of the wheelsets of the bogie was excited by the rail drum. In this excitation condition, the pitch mode is easy to excite, but the roll mode is hard to excite because the left and right excitations and loads on bogie are nearly the same.

In summary, it can be seen that CoSS-SSI successfully identifies the bounce, pitch and roll modes of the bogie frame with the assistance of CE to remove harmonic effects. The identified modes are related to the behaviour of the primary vehicle suspension system and, consequently, the identified modes can be utilised to monitor the condition of the primary suspension system of a railway vehicle. Although the Y25 bogie with faulty primary suspension was not tested in this study due to experimental limitations, the effectiveness of CoSS-SSI for suspension system fault diagnosis has again been demonstrated by accurate identify the modal parameters of health suspension. In a word, CoSS-SSI could be a reliable and achievable approach for railway vehicle suspension online CM.

## **8.4 Findings**

In this chapter, experiments were conducted on a full-scale rig in the IRR laboratory to investigate the performance of CoSS-SSI for railway vehicle suspension monitoring. A SIMPACK model of the tested Y25 bogie was developed to obtain the theoretical modal parameters of the primary suspension system. CE was employed to remove harmonic before using OMA. Based on the results and analysis, the following conclusions can be drawn:

- 1) CE is an effective approach to remove the influence of the harmonic on OMA;
- 2) CoSS-SSI can identify the bounce, pitch and roll modes of the bogie frame, which are related to the primary suspension system of an Y25 bogie, using the response signal only.

It is intended that the Y25 bogie with a faulty suspension system will be investigated to verify the performance of CoSS-SSI for CM of railway vehicle suspension systems. The final purpose will be to apply the proposed method to an operational vehicle to contribute to enhancing vehicle safety.

---

---

## CHAPTER 9 CONCLUSIONS AND FUTURE WORK

---

---

*First, this chapter reviews the aim and objectives proposed in Chapter 1, and summarizes the achievements according to the stated aim and objectives. Second, the conclusions drawn from this research project are presented. Third, the contributions made by this research to knowledge are given. Last but not least, the chapter provides some recommendations for future work in this field of study.*

## 9.1 Thesis objectives and achievements

The research aim was to develop an effective and robust onboard CM approach which allowed online monitoring of vehicle suspension systems. A novel development of OMA, denoted as CoSS-SSI, has been proposed and successfully tested on a road vehicle, a 1/5<sup>th</sup> scale and a Y25 bogie to analyse and identify vehicle suspension dynamics for the purpose of online monitoring.

All of the objectives proposed in Section 1.3 have been achieved:

**Objective 1:** To perform a comprehensive literature review of CM techniques which highlights their applications to vehicle suspension monitoring.

**Achievement 1:** The significance of CM and common CM technologies were reviewed. A detailed appraisal of existing methods for vehicle suspension system monitoring has been presented, and it was found that an online monitoring method is needed for practical application. On this basis, vibration analysis, which is the most popular technology for CM on account of its robustness and cost-efficiency was selected for use in this project. The common vibration signal processing techniques were reviewed including time domain, frequency domain and time-frequency analysis.

**Objective 2:** To review existing OMA techniques and their applications to identify their advantages and disadvantages.

**Achievement 2:** The existing OMA techniques and their applications were reviewed in detail. The common OMA methods can be categorised as frequency-domain and time-domain methods. The popular frequency domain OMA methods include FDD, EFDD, LSCF and Poly-LSCF. However, it was found that frequency domain OMA methods are weak in the extraction of close modes. The popular time domain OMA methods can be divided into single-stage methods like ARMA, and two-stage methods such as LSCE, ERA and Cov-SSI. The two-stage method gives better noise reduction than the single-stage method. Besides, it has been found that the robustness of SSI is superior to other OMA methods as SSI was developed on the basis of linear algebra theory. Therefore, Cov-SSI was selected as the fundamental algorithm to be used for modal identification of vehicle suspension systems in the presence of nonstationary responses with high noise levels.

**Objective 3:** To present a novel OMA method to enable the application of OMA in vehicle suspension system dynamic identification based on the framework of SSI.

**Achievement 3:** The literature review found the main gaps stopping the employment of OMA for vehicle suspension monitoring were the assumptions of white noise excitation and a linear system. A novel OMA method, denoted as CoSS-SSI, intended to overcome these difficulties was proposed to identify the dynamics of vehicle suspension systems for online suspension monitoring. The effectiveness of CoSS-SSI was evaluated by a 3-DOF vibration system, and the results show that this novel OMA method has the potential to achieve vehicle suspension online monitoring.

**Objective 4:** To review OMA in the presence of harmonics and evaluate the performance of CE for removing harmonic effects.

**Achievement 4:** The presence of harmonics is a common problem when using OMA, and has occurred in full-scale roller rig experiments. The conventional approaches for removing harmonic effects on OMA are reviewed and it was found that cepstrum editing is the preferred method for full-scale roller rig experiments. A quarter vehicle model with periodic pulses, harmonics and random excitations was used to evaluate the performance of cepstrum editing for eliminating the effects of harmonics on OMA results. The results showed that pulse train had no influence on OMA, and cepstrum editing is an excellent means of removing harmonic effects in OMA.

**Objective 5:** To assess the performance of the novel SSI method which was presented in this thesis for road vehicle suspension monitoring.

**Achievement 5:** The effectiveness of CoSS-SSI was first evaluated on a simplified suspension system, and then field tests were conducted on a traditional countryside road near Huddersfield, UK. The results indicated that CoSS-SSI had the ability to identify the modal parameters of the vehicle suspension system as detected by accelerometers installed appropriately on the car. It was demonstrated that CoSS-SSI can identify the suspension fault of a wheel with abnormally low tyre pressure.

**Objective 6:** To evaluate the performance of the novel SSI method which was presented in this thesis for railway vehicle suspension online monitoring.

**Achievement 6:** A 1/5<sup>th</sup> scale bogie on the roller rig was utilised to evaluate the performance of CoSS-SSI for online CM of a railway vehicle primary suspension system. A 7-DOF mathematical model of the scale roller rig was developed to calculate the theoretical modal parameters. The theoretical modal parameters played the role of determining the frequency range of interest in the experimental study. In order to provide a relatively accurate theoretical value, the components of the primary suspension were tested to obtain the force-displacement curve. The 1/5<sup>th</sup> roller rig with healthy and faulty primary suspension systems was tested. The experiment results showed that CoSS-SSI can achieve the online monitoring of the suspension system of the railway vehicle.

Importantly, experiments conducted on a full-scale roller rig with an Y25 bogie again confirmed CoSS-SSI for the successful online monitoring of railway vehicle suspension systems.

## 9.2 Conclusions

Overall, from the theoretical and experimental investigations conducted in this thesis, the following key findings or conclusions can be drawn:

**Conclusion 1:** The suspension system plays a decisive role in determining vehicle safety, comfort and driving performance. An online CM system is desired to enhance vehicle safety with the rapid and significant speed increases of the modern vehicles, especially autonomous and railway vehicles.

**Conclusion 2:** OMA is a powerful and achievable approach for conducting CM either for mechanical systems or buildings, and that SSI is an excellent and fruitful method to enhance the performance of OMA.

**Conclusion 3:** CE is effective in filtering out the effects of harmonic excitation on OMA. While pulse train input had no influence on OMA.

**Conclusion 4:** The novel OMA method, proposed in this thesis, named CoSS-SSI, has the capability to extract the modal parameters of a 3-DOF vibration model with extremely low SNR and strong nonstationary responses. Moreover, it was shown that the performance of CoSS-SSI is better than other conventional OMA methods, i.e. Cov-SSI and ACS-Cov-SSI. This capability is critical in selecting CoSS-SSI for vehicle suspension system monitoring.

**Conclusion 5:** The experimental study showed that CoSS-SSI was able to accurately identify the modal parameters of a simplified suspension system (in Chapter 6) by using the car body responses as determined at the four corners. It was shown that CoSS-SSI is a feasible means to identify the condition of the road vehicle suspension system. Furthermore, the abnormal tyre pressure of one wheel was detected via CoSS-SSI. It showed that CoSS-SSI can extract the modal parameters of a nonlinear system by categorising the correlation function of responses into different subsets.

**Conclusion 6:** A 7-DOF model can represent the vertical dynamic characteristics of a bogie. The resonance frequencies of the bounce, pitch and roll modes of the bogie frame of the tested 1/5<sup>th</sup> scale bogie were found to be 19.15 Hz, 24.03 Hz and 25.4 Hz, respectively.

**Conclusion 7:** CoSS-SSI can identify the dynamic characteristics of the primary suspension system of the tested 1/5<sup>th</sup> scale bogie using the responses measured at the four corners of the bogie frame. It has been proved that the primary suspension faults, such as ageing and fatigue of the suspension components, can be detected by CoSS-SSI and the computational time shows that such detection can be online.

**Conclusion 8:** CoSS-SSI can identify the rigid modes of the bogie frame of the Y25 bogie which are related to the primary suspension system by using the signals provided by four accelerometers mounted on the bogie frame close to the axle boxes. In other words, CoSS-SSI can be applied to monitor the status of railway vehicle suspension systems.

### 9.3 Novelty and contributions to knowledge

The novelty and contributions to knowledge of this research are highlighted and listed as follows:

**Contribution 1:** The main novelty of this thesis is the development and testing of CoSS-SSI method. It makes conventional SSI applicable to nonstationary and nonlinear systems. In addition, it is very robust to noise such as occurs with online monitoring of the condition of vehicle suspension systems. It overcomes the limitation of SSI due to the assumption of a linear system with white noise excitation.

**Contribution 2:** In implementing CoSS-SSI for monitoring the suspension system of on-road vehicles, the success in determining the main modes reveals for the first time that the

road excitation has high degree of nonstationary and nonlinear effect. This finding will provide more supports for develop more accurate models that are traditionally taken as stationary processes in vehicle dynamics.

**Contribution 3:** OMA has been, for the first time, applied to monitor a railway vehicle suspension system. It shows that CoSS-SSI is a promising approach to achieving online monitoring of railway vehicle suspension systems even highly nonlinear systems with complex excitation sources.

## 9.4 Future work

While a great deal of preliminary work for online monitoring of vehicle suspension systems has been done in this research, further study in this research area would be useful, especially:

**Recommendation 1:** Conduct a railway vehicle field test to verify the effectiveness of the proposed method under “real conditions”. Any experiment with a railway vehicle with a seeded fault in the suspension should, of course, be conducted under safe conditions.

**Recommendation 2:** Optimize the sensor position to achieve simultaneous monitoring of the primary and secondary suspension systems of railway vehicles. Both the primary and secondary suspension systems can be considered as parts of a whole vibration system.

**Recommendation 3:** Explore the possibility of using wireless sensors during the test to simplify the measurement system, especially in field tests. The frequency range of interest for the suspension is usually low, which means the required sampling rate of the wireless sensor is readily achievable.

**Recommendation 4:** Investigate the lateral dynamics of the railway vehicle, which is also significant to railway safety. This could be part of monitoring the condition of the lateral components of the suspension system.

**Recommendation 5:** Employ existing sensors such as the sensors in the Anti-Lock Braking System (ABS) of modern vehicles, to measure the required parameters for CM of the suspension system and identification of possible faults.

---

---

## REFERENCES

---

---

- [1] E. P. Carden and P. Fanning, 'Vibration based condition monitoring: A Review', *Structural Health Monitoring*, vol. 3, no. 4, pp. 355–377, Dec. 2004.
- [2] A. M. Al-Ghamd and D. Mba, 'A comparative experimental study on the use of acoustic emission and vibration analysis for bearing defect identification and estimation of defect size', *Mechanical Systems and Signal Processing*, vol. 20, no. 7, pp. 1537–1571, Oct. 2006.
- [3] C. Li, S. Luo, C. Cole, and M. Spiriyagin, 'An overview: modern techniques for railway vehicle on-board health monitoring systems', *Vehicle System Dynamics*, vol. 55, no. 7, pp. 1045–1070, 2017.
- [4] E. Reynders, 'System identification methods for (operational) modal analysis: review and comparison', *Arch Computat Methods Eng*, vol. 19, no. 1, pp. 51–124, Mar. 2012.
- [5] J. Antoni and S. Chauhan, 'A study and extension of second-order blind source separation to operational modal analysis', *Journal of Sound and Vibration*, vol. 332, no. 4, pp. 1079–1106, Feb. 2013.
- [6] B. Li, H. Cai, X. Mao, J. Huang, and B. Luo, 'Estimation of CNC machine–tool dynamic parameters based on random cutting excitation through operational modal analysis', *Int. J. Machine Tools and Manufacture*, vol. 71, pp. 26–40, Aug. 2013.
- [7] Z. Chen, T. Wang, F. Gu, and R. Zhang, 'Characterizing the dynamic response of a chassis frame in a heavy-duty dump vehicle based on an improved stochastic system identification', *Shock and Vibration*, vol. 2015, pp. 1–15, 2015.
- [8] 'China's High-Speed Rail', *trainspread*. [Online]. Available: <http://www.trainspread.com/china/high-speed-rail/>. [Accessed: 02-Dec-2019].
- [9] A. K. S. Jardine, D. Lin, and D. Banjevic, 'A review on machinery diagnostics and prognostics implementing condition-based maintenance', *Mechanical Systems and Signal Processing*, vol. 20, no. 7, pp. 1483–1510, Oct. 2006.
- [10] X. Tian, 'Enhanced information extraction from noisy vibration data for machinery fault detection and diagnosis', PhD Thesis, University of Huddersfield, 2017.
- [11] J. H. Williams, A. Davies, and P. R. Drake, *Condition-based Maintenance and Machine Diagnostics*. Springer Science & Business Media, 1994.
- [12] S. Nandi, H. A. Toliyat, and X. Li, 'Condition monitoring and fault diagnosis of electrical motors—A Review', *IEEE Transactions on Energy Conversion*, vol. 20, no. 4, pp. 719–729, Dec. 2005.

- [13] A. Davies, *Handbook of Condition Monitoring: Techniques and Methodology*. Springer Science & Business Media, 2012.
- [14] R. B. Randall, *Vibration-based Condition Monitoring: Industrial, Aerospace and Automotive Applications*. John Wiley & Sons, 2011.
- [15] F. Gu, W. Li, A. D. Ball, and A. Y. T. Leung, 'The condition monitoring of diesel engines using acoustic measurements Part 1: Acoustic characteristics of the engine and representation of the acoustic signals', SAE 2000 World Congress, 2000, pp. 2000-01-0730, 2000.
- [16] A. Albarbar, F. Gu, A. D. Ball, and A. Starr, 'Acoustic monitoring of engine fuel injection based on adaptive filtering techniques', *Applied Acoustics*, vol. 71, no. 12, pp. 1132-1141, Dec. 2010.
- [17] D. Mba and R. B. Rao, 'Development of acoustic emission technology for condition monitoring and diagnosis of rotating machines; bearings, pumps, gearboxes, engines and rotating structures.', *Shock and Vibration Digest*, vol 38, no. 1, pp 3-16, 2006.
- [18] W. Caesarendra, B. Kosasih, A. K. Tieu, H. Zhu, C. A. S. Moodie, and Q. Zhu, 'Acoustic emission-based condition monitoring methods: Review and application for low speed slew bearing', *Mechanical Systems and Signal Processing*, vol. 72-73, pp. 134-159, May 2016.
- [19] M. E. H. Benbouzid, M. Vieira, and C. Theys, 'Induction motors' faults detection and localization using stator current advanced signal processing techniques', *IEEE Transactions on Power Electronics*, vol. 14, no. 1, pp. 14-22, Jan. 1999.
- [20] F. Gu, T. Wang, A. Alwodai, X. Tian, Y. Shao, and A. D. Ball, 'A new method of accurate broken rotor bar diagnosis based on modulation signal bispectrum analysis of motor current signals', *Mechanical Systems and Signal Processing*, vol. 50-51, pp. 400-413, Jan. 2015.
- [21] J. Zhu, J. M. Yoon, D. He, and E. Bechhoefer, 'Online particle-contaminated lubrication oil condition monitoring and remaining useful life prediction for wind turbines', *Wind Energy*, vol. 18, no. 6, pp. 1131-1149, 2015.
- [22] S. Bagavathiappan, B. B. Lahiri, T. Saravanan, J. Philip, and T. Jayakumar, 'Infrared thermography for condition monitoring - A review', *Infrared Physics & Technology*, vol. 60, pp. 35-55, Sep. 2013.
- [23] J. S. Bendat and A. G. Piersol, *Random Data: Analysis and Measurement Procedures*. John Wiley & Sons, 2011.
- [24] F. Combet and L. Gelman, 'An automated methodology for performing time synchronous averaging of a gearbox signal without speed sensor', *Mechanical Systems and Signal Processing*, vol. 21, no. 6, pp. 2590-2606, Aug. 2007.
- [25] J. M. Ha, B. D. Youn, H. Oh, B. Han, Y. Jung, and J. Park, 'Autocorrelation-based time synchronous averaging for condition monitoring of planetary gearboxes in wind

- turbines', *Mechanical Systems and Signal Processing*, vol. 70–71, pp. 161–175, Mar. 2016.
- [26] J. Lin and M. J. Zuo, 'Gearbox fault diagnosis using adaptive wavelet filter', *Mechanical Systems and Signal Processing*, vol. 17, no. 6, pp. 1259–1269, Nov. 2003.
- [27] B. Farhang-Boroujeny, *Adaptive Filters: Theory and Applications*. John Wiley & Sons, 2013.
- [28] R. B. Randall, 'A history of cepstrum analysis and its application to mechanical problems', *Mechanical Systems and Signal Processing*, vol. 97, pp. 3–19, Dec. 2017.
- [29] E. Bechhoefer, M. Kingsley, and P. Menon, 'Bearing envelope analysis window selection Using spectral kurtosis techniques', in *2011 IEEE Conference on Prognostics and Health Management*, 2011, pp. 1–6.
- [30] Z. Feng, M. Liang, and F. Chu, 'Recent advances in time–frequency analysis methods for machinery fault diagnosis: A review with application examples', *Mechanical Systems and Signal Processing*, vol. 38, no. 1, pp. 165–205, Jul. 2013.
- [31] M. Portnoff, 'Time-frequency representation of digital signals and systems based on short-time Fourier analysis', *IEEE Transactions on Acoustics, Speech, and Signal Processing*, vol. 28, no. 1, pp. 55–69, Feb. 1980.
- [32] M. Börner, H. Straky, T. Weispfenning, and R. Isermann, 'Model based fault detection of vehicle suspension and hydraulic brake systems', *Mechatronics*, vol. 12, no. 8, pp. 999–1010, Oct. 2002.
- [33] D. Fischer, E. Kaus, and R. Isermann, 'Fault detection for an active vehicle suspension', in *Pro. 2003 American Control Conference*, vol. 5, pp. 4377–4382, 2003.
- [34] D. Fischer, H.-P. Schöner, and R. Isermann, 'Model based fault detection for an active vehicle suspension', *IFAC Proceedings Volumes*, vol. 37, no. 22, pp. 403–408, Apr. 2004.
- [35] D. Fischer, M. Börner, J. Schmitt, and R. Isermann, 'Fault detection for lateral and vertical vehicle dynamics', *Control Engineering Practice*, vol. 15, no. 3, pp. 315–324, Mar. 2007.
- [36] R. Karami, F. Najafi, and M. A. Shoorehdeli, 'Model based identification and fault detection of an active suspension system', *IFAC Proceedings Volumes*, vol. 40, no. 10, pp. 633–640, Jan. 2007.
- [37] L. Silva, D. Delarmelina, S. Junco, N. K. M Sirdi, and H. Noura, 'Bond graph based fault diagnosis of 4W-vehicles suspension systems I: Passive Suspensions', *Simulation Series*, vol. 39, no. 1, p. 217, 2007.
- [38] D. Hernandez-Alcantara, R. Morales-Menendez, L. Amezcuita-Brooks, O. Sename, and L. Dugard, 'Fault estimation methods for semi-active suspension systems', in *2015*

- IEEE International Autumn Meeting on Power, Electronics and Computing (ROPEC)*, pp. 1–5, 2015.
- [39] J. C. Tudón-Martínez and R. Morales-Menendez, ‘Adaptive vibration control system for MR damper faults’, *Shock and Vibration*, vol. 2015, pp. 1–17, 2015.
- [40] M. M. Morato, O. Sename, L. Dugard, and M. Q. Nguyen, ‘Fault estimation for automotive Electro-Rheological dampers: LPV-based observer approach’, *Control Engineering Practice*, vol. 85, pp. 11–22, Apr. 2019.
- [41] D. Hernández-Alcántara, J. C. Tudón-Martínez, L. Amézquita-Brooks, C. A. Vivas-López, and R. Morales-Menéndez, ‘Modeling, diagnosis and estimation of actuator faults in vehicle suspensions’, *Control Engineering Practice*, vol. 49, pp. 173–186, Apr. 2016.
- [42] M. Shahab and M. Moavenian, ‘A novel fault diagnosis technique based on model and computational intelligence applied to vehicle active suspension systems’, *International Journal of Numerical Modelling: Electronic Networks, Devices and Fields*, vol. 32, no. 3, p. e2541, 2019.
- [43] X. Zhu, Y. Xia, S. Chai, and P. Shi, ‘Fault detection for vehicle active suspension systems in finite-frequency domain’, *IET Control Theory Applications*, vol. 13, no. 3, pp. 387–394, 2019.
- [44] J. Luo, K. R. Pattipati, L. Qiao, and S. Chigusa, ‘Model-based prognostic techniques applied to a suspension system’, *IEEE Transactions on Systems, Man, and Cybernetics - Part A: Systems and Humans*, vol. 38, no. 5, pp. 1156–1168, Sep. 2008.
- [45] P. Metallidis, G. Verros, S. Natsiavas, and C. Papadimitriou, ‘Fault detection and optimal sensor location in vehicle suspensions’, *Journal of Vibration and Control*, vol. 9, no. 3–4, pp. 337–359, Mar. 2003.
- [46] F. R. M. Romlay, H. Ouyang, and M. K. Nizam, ‘Failure prediction for automotive suspension springs using Gaussian and Monte Carlo method’, *IJVD*, vol. 55, no. 1, p. 23, 2011.
- [47] S. Azadi and A. Soltani, ‘Fault detection of vehicle suspension system using wavelet analysis’, *Vehicle System Dynamics*, vol. 47, no. 4, pp. 403–418, Apr. 2009.
- [48] J. Lozoya-Santos, J. C. Tudón-Martínez, R. Morales-Menendez, R. Ramirez-Mendoza, and A. M. Gutierrez, ‘Fault detection for an automotive MR damper’, *IFAC Proceedings Volumes*, vol. 45, no. 6, pp. 1023–1028, May 2012.
- [49] J. de J. Lozoya-Santos, J. C. Tudón-Martínez, R. Morales-Menendez, R. Ramirez-Mendoza, and L. E. Garza-Castañón, ‘A fault detection method for an automotive magneto-rheological damper’, *IFAC Proceedings Volumes*, vol. 45, no. 20, pp. 1209–1214, Jan. 2012.
- [50] D. Hernandez-Alcantara, L. Amezquita-Brooks, C. Vivas-Lopez, R. Morales-Menendez, and R. Ramirez-Mendoza, ‘Fault detection for automotive semi-active

- dampers’, in *2013 Conference on Control and Fault-Tolerant Systems (SysTol)*, 2013, pp. 625–630.
- [51] G. Wang and S. Yin, ‘Data-driven fault diagnosis for an automobile suspension system by using a clustering based method’, *Journal of the Franklin Institute*, vol. 351, no. 6, pp. 3231–3244, Jun. 2014.
- [52] S. Yin and Z. Huang, ‘Performance monitoring for vehicle suspension system via fuzzy positivistic C-means clustering based on accelerometer measurements’, *IEEE/ASME Transactions on Mechatronics*, vol. 20, no. 5, pp. 2613–2620, Oct. 2015.
- [53] H. Luo, M. Huang, and Z. Zhou, ‘A dual-tree complex wavelet enhanced convolutional LSTM neural network for structural health monitoring of automotive suspension’, *Measurement*, vol. 137, pp. 14–27, Apr. 2019.
- [54] M. Hamed, ‘Characterisation of the dynamics of an automotive suspension system for on-line condition monitoring’, PhD Thesis, University of Huddersfield, 2016.
- [55] B. Liu, Z. Ji, T. Wang, Z. Tang, and G. Li, ‘Failure identification of dump truck suspension based on an average correlation stochastic subspace identification algorithm’, *Applied Sciences*, vol. 8, no. 10, p. 1795, Oct. 2018.
- [56] ‘Train Maintenance | The Railway Technical Website | PRC Rail Consulting Ltd’, *The railway technical website*. [Online]. Available: <http://www.railway-technical.com/trains/train-maintenance/>. [Accessed: 10-May-2019].
- [57] A. Alemi, F. Corman, and G. Lodewijks, ‘Condition monitoring approaches for the detection of railway wheel defects’, *Proceedings of the Institution of Mechanical Engineers, Part F: Journal of Rail and Rapid Transit*, vol. 231, no. 8, pp. 961–981, Sep. 2017.
- [58] R. Pohl, A. Erhard, H.-J. Montag, H.-M. Thomas, and H. Wüstenberg, ‘NDT techniques for railroad wheel and gauge corner inspection’, *NDT & E International*, vol. 37, no. 2, pp. 89–94, Mar. 2004.
- [59] M. Pau, F. Aymerich, and F. Ginesu, ‘Ultrasonic measurements of nominal contact area and contact pressure in a wheel-rail system’, *Proceedings of the Institution of Mechanical Engineers, Part F: Journal of Rail and Rapid Transit*, vol. 214, no. 4, pp. 231–243, Jul. 2000.
- [60] M. Pau, ‘Ultrasonic waves for effective assessment of wheel-rail contact anomalies’, *Proceedings of the Institution of Mechanical Engineers, Part F: Journal of Rail and Rapid Transit*, vol. 219, no. 2, pp. 79–90, Mar. 2005.
- [61] M. Pau, B. Leban, and A. Baldi, ‘Simultaneous subsurface defect detection and contact parameter assessment in a wheel–rail system’, *Wear*, vol. 265, no. 11, pp. 1837–1847, Nov. 2008.

- [62] A. G. Verkhoglyad, I. N. Kuropyatnik, V. M. Bazovkin, and G. L. Kuryshev, 'Infrared diagnostics of cracks in railway carriage wheels', *Russ J Nondestruct Test*, vol. 44, no. 10, pp. 664–668, Oct. 2008.
- [63] Z. H. Žurek, 'Magnetic monitoring of the fatigue process of the rim material of railway wheel sets', *NDT & E International*, vol. 39, no. 8, pp. 675–679, Dec. 2006.
- [64] D. Barke and W. K. Chiu, 'Structural health monitoring in the railway industry: A Review', *Structural Health Monitoring*, vol. 4, no. 1, pp. 81–93, Mar. 2005.
- [65] R. Lagneback, 'Evaluation of wayside condition monitoring technologies for condition-based maintenance of railway vehicles', Licenciate Thesis, Lulea University of Technology, 2007.
- [66] G. Kouroussis, C. Caucheteur, D. Kinet, G. Alexandrou, O. Verlinden, and V. Moeyaert, 'Review of trackside monitoring solutions: From strain gages to optical fibre sensors', *Sensors*, vol. 15, no. 8, pp. 20115–20139, 2015.
- [67] J. C. O. Nielsen and A. Johansson, 'Out-of-round railway wheels - a literature survey', *Proceedings of the Institution of Mechanical Engineers, Part F: Journal of Rail and Rapid Transit*, vol. 214, no. 2, pp. 79–91, Mar. 2000.
- [68] A. Johansson and J. C. O. Nielsen, 'Out-of-round railway wheels—wheel-rail contact forces and track response derived from field tests and numerical simulations', *Proceedings of the Institution of Mechanical Engineers, Part F: Journal of Rail and Rapid Transit*, vol. 217, no. 2, pp. 135–146, Mar. 2003.
- [69] S. Strano and M. Terzo, 'Review on model-based methods for on-board condition monitoring in railway vehicle dynamics', *Advances in Mechanical Engineering*, vol. 11, no. 2, p. 1687814019826795, Feb. 2019.
- [70] G. Charles, R. Goodall, and R. Dixon, 'Model-based condition monitoring at the wheel–rail interface', *Vehicle System Dynamics*, vol. 46, no. sup1, pp. 415–430, Sep. 2008.
- [71] P. Li and R. Goodall, 'Model-based condition monitoring for railway vehicle systems', *Control 2004*, 2004.
- [72] Y. Hayashi, H. Tsunashima, and Y. Marumo, 'Fault detection of railway vehicle suspension systems using multiple-model approach', *JMTL*, vol. 1, no. 1, pp. 88–99, 2008.
- [73] H. Tsunashima, Y. Hayashi, H. Mori, and Y. Marumo, 'Condition Monitoring and Fault Detection of Railway Vehicle Suspension using Multiple-Model Approach', *IFAC Proceedings Volumes*, vol. 41, no. 2, pp. 8299–8304, Jan. 2008.
- [74] M. Jesussek and K. Ellermann, 'Fault detection and isolation for a full-scale railway vehicle suspension with multiple Kalman filters', *Vehicle System Dynamics*, vol. 52, no. 12, pp. 1695–1715, 2014.

- [75] H. Fan, X. Wei, L. Jia, and Y. Qin, 'Fault detection of railway vehicle suspension systems', in *Computer Science and Education (ICCSE), 2010 5th International Conference on*, 2010, pp. 1264–1269.
- [76] X. Wei, H. Liu, and Y. Qin, 'Fault diagnosis of rail vehicle suspension systems by using GLRT', in *2011 Chinese Control and Decision Conference (CCDC)*, pp. 1932–1936, 2011.
- [77] X. Wei, H. Lui, and Y. Qin, 'Fault isolation of rail vehicle suspension systems by using similarity measure', in *Service Operations, Logistics, and Informatics (SOLI), 2011 IEEE International Conference on*, pp. 391–396, 2011.
- [78] X. Wei, H. Liu, and L. Jia, 'Fault detection of urban rail vehicle suspension system based on acceleration measurements', in *Advanced Intelligent Mechatronics (AIM), 2012 IEEE/ASME International Conference on*, pp. 1129–1134, 2012.
- [79] Xiukun Wei, Shuai Lin, and Hai Liu, 'Distributed fault detection observer for rail vehicle suspension systems', in *24th Chinese Control and Decision Conference (CCDC)*, pp. 3396–3401, 2012.
- [80] Y. Wang, Z. Mao, and B. Jiang, 'Observer-based fault detection for rail vehicle suspension systems', in *Control and Decision Conference (2014 CCDC), The 26th Chinese*, pp. 2863–2868, 2014.
- [81] M. Jesussek and K. Ellermann, 'Fault detection and isolation for a nonlinear railway vehicle suspension with a hybrid extended Kalman filter', *Vehicle System Dynamics*, vol. 51, no. 10, pp. 1489–1501, 2013.
- [82] Y. Wu, B. Jiang, N. Lu, and D. Zhou, 'ToMFIR-based incipient fault detection and estimation for high-speed rail vehicle suspension system', *Journal of the Franklin Institute*, vol. 352, no. 4, pp. 1672–1692, 2015.
- [83] S. Zoljic-Beglerovic, G. Stettinger, B. Lubner, and M. Horn, 'Railway suspension system fault diagnosis using cubature Kalman filter techniques', *IFAC-PapersOnLine*, vol. 51, no. 24, pp. 1330–1335, Jan. 2018.
- [84] Z. Zhang, B. Xu, L. Ma, and S. Geng, 'Parameter estimation of a railway vehicle running bogie using extended Kalman filter', in *Control Conference (CCC), 33rd Chinese*, pp. 3393–3398, 2014.
- [85] B. Xu, J. Zhang, and X. Guan, 'Estimation of the parameters of a railway vehicle suspension using model-based filters with uncertainties', *Proceedings of the Institution of Mechanical Engineers, Part F: Journal of Rail and Rapid Transit*, vol. 229, no. 7, pp. 785–797, 2015.
- [86] P. Li, R. Goodall, P. Weston, C. Seng Ling, C. Goodman, and C. Roberts, 'Estimation of railway vehicle suspension parameters for condition monitoring', *Control Engineering Practice*, vol. 15, no. 1, pp. 43–55, Jan. 2007.

- [87] X. Y. Liu, S. Alfi, and S. Bruni, ‘An efficient recursive least square-based condition monitoring approach for a rail vehicle suspension system’, *Vehicle System Dynamics*, vol. 54, no. 6, pp. 814–830, 2016.
- [88] S. Zoljic-Beglerovic, M. A. Golkani, M. Steinberger, and M. Horn, ‘Robust parameter identification for railway suspension systems’, in *15th International Workshop on Variable Structure Systems (VSS)*, pp. 432–437, 2018.
- [89] R. Melnik and M. Kostrzewski, ‘Rail vehicle’s suspension monitoring system - analysis of results obtained in tests of the prototype’, *Key Engineering Materials*, 2012. [Online]. Available: <https://www.scientific.net/KEM.518.281>. [Accessed: 09-May-2019].
- [90] R. Melnik and B. Sowiński, ‘The selection procedure of diagnostic indicator of suspension fault modes for the rail vehicles monitoring system’, *7th European Workshop on Structural Health Monitoring*, Nantes, France, pp.159-166, Jul. 2014.
- [91] X. Wei, L. Jia, and H. Liu, ‘Data-driven fault detection of vertical rail vehicle suspension systems’, in *Control (CONTROL), UKACC International Conference on*, pp. 589–594, 2012.
- [92] X. Wei, K. Guo, H. Liu, and L. Jia, ‘Fault isolation for light rail vehicle suspension system based on multi-sensor information fusion’, in *25th Chinese Control and Decision Conference (CCDC)*, pp. 3532–3537, 2013.
- [93] X. Wei, K. Guo, L. Jia, G. Liu, and M. Yuan, ‘Fault isolation of light rail vehicle suspension system based on D-S evidence theory and improvement application case’, *Journal of Intelligent Learning Systems and Applications*, vol. 05, p. 245, Nov. 2013.
- [94] X. Wei, Y. Guo, L. Jia, and H. Liu, ‘Fault detection of rail vehicle suspension system based on CPCA’, in *Control and Fault-Tolerant Systems (SysTol), Conference on*, pp. 700–705, 2013.
- [95] X. Wei, L. Jia, and H. Liu, ‘A comparative study on fault detection methods of rail vehicle suspension systems based on acceleration measurements’, *Vehicle System Dynamics*, vol. 51, no. 5, pp. 700–720, May 2013.
- [96] X. Wei, L. Jia, K. Guo, and S. Wu, ‘On fault isolation for rail vehicle suspension systems’, *Vehicle System Dynamics*, vol. 52, no. 6, pp. 847–873, 2014.
- [97] L. Gasparetto, S. Alfi, and S. Bruni, ‘Data-driven condition-based monitoring of high-speed railway bogies’, *International Journal of Rail Transportation*, vol. 1, no. 1–2, pp. 42–56, 2013.
- [98] H. Hu, B. Tang, X. Gong, W. Wei, and H. Wang, ‘Intelligent fault diagnosis of the high-speed train with big data based on deep neural networks’, *IEEE Transactions on Industrial Informatics*, vol. 13, no. 4, pp. 2106–2116, Aug. 2017.
- [99] Y. Zhao, Z. H. Guo, and J. M. Yan, ‘Vibration signal analysis and fault diagnosis of bogies of the high-speed train based on deep neural networks’, *Journal of*

- Vibroengineering*, 2017. [Online]. Available: <https://www.jvejournal.com/article/17238>. [Accessed: 19-May-2019].
- [100] Y. Fu, D. Huang, N. Qin, K. Liang, and Y. Yang, ‘High-speed railway bogie fault diagnosis using LSTM neural network’, in *37th Chinese Control Conference (CCC)*, pp. 5848–5852, 2018.
- [101] K. Liang, N. Qin, D. Huang, and Y. Fu, ‘Convolutional recurrent neural network for fault diagnosis of high-speed train bogie’, *Complexity*, 2018. [Online]. Available: <https://www.hindawi.com/journals/complexity/2018/4501952/abs/>. [Accessed: 15-May-2019].
- [102] L. Su, L. Ma, N. Qin, D. Huang, and A. Kemp, ‘Fault diagnosis of high-speed train bogie based on spectrogram and multi-channel voting’, in *IEEE 7th Data Driven Control and Learning Systems Conference (DDCLS)*, pp. 22–26, 2018.
- [103] L. Su, L. Ma, N. Qin, D. Huang, and A. Kemp, ‘Fault diagnosis of high-speed train bogie by residual-squeeze net’, *IEEE Transactions on Industrial Informatics*, pp. 1–1, 2019.
- [104] T. X. Mei and X. J. Ding, ‘A model-less technique for the fault detection of rail vehicle suspensions’, *Vehicle System Dynamics*, vol. 46, no. sup1, pp. 277–287, Sep. 2008.
- [105] T. X. Mei and X. J. Ding, ‘Condition monitoring of rail vehicle suspensions based on changes in system dynamic interactions’, *Vehicle System Dynamics*, vol. 47, no. 9, pp. 1167–1181, Sep. 2009.
- [106] C. Li, S. Luo, C. Cole, M. Spiryagin, and Y. Sun, ‘A signal-based fault detection and classification method for heavy haul wagons’, *Vehicle System Dynamics*, vol. 55, no. 12, pp. 1807–1822, Dec. 2017.
- [107] C. Li, S. Luo, C. Cole, and M. Spiryagin, ‘Bolster spring fault detection strategy for heavy haul wagons’, *Vehicle System Dynamics*, vol. 56, no. 10, pp. 1604–1621, Oct. 2018.
- [108] M. Dumitriu, ‘Fault detection of damper in railway vehicle suspension based on the cross-correlation analysis of bogie accelerations’, *Mechanics & Industry*, vol. 20, no. 1, p. 102, 2019.
- [109] M. H. Masjedian and M. Keshmiri, ‘A review on operational modal analysis researches: classification of methods and applications’, *Proceedings of the 3rd IOMAC*, pp. 707–718, 2009.
- [110] B. Peeters and G. D. Roeck, ‘Stochastic system identification for operational modal analysis: A Review’, *J. Dyn. Sys., Meas., Control*, vol. 123, no. 4, pp. 659–667, Dec. 2001.

- [111] R. Brincker, L. Zhang, and P. Andersen, ‘Modal identification of output-only systems using frequency domain decomposition’, *Smart Mater. Struct.*, vol. 10, no. 3, p. 441, 2001.
- [112] N.-J. Jacobsen, ‘Using EFDD as a Robust technique for deterministic excitation in operational modal analysis’, *Proceedings of the 2nd International Operational Modal Analysis Conference*, pp. 193–200, 2007.
- [113] L. Zhang, T. Wang, and Y. Tamura, ‘A frequency–spatial domain decomposition (FSDD) method for operational modal analysis’, *Mechanical Systems and Signal Processing*, vol. 24, no. 5, pp. 1227–1239, Jul. 2010.
- [114] H. Van der Auweraer, P. Guillaume, P. Verboven, and S. Vanlanduit, ‘Application of a fast-stabilizing frequency domain parameter estimation method’, *J. Dyn. Sys., Meas., Control*, vol. 123, no. 4, pp. 651–658, Jan. 2001.
- [115] B. Peeters, H. Van der Auweraer, P. Guillaume, and J. Leuridan, ‘The PolyMAX frequency-domain method: a new standard for modal parameter estimation?’, *Shock and Vibration*, vol. 11, no. 3, 4, pp. 395–409, 2004.
- [116] S. R. Ibrahim, ‘Random decrement technique for modal identification of structures’, *Journal of Spacecraft and Rockets*, vol. 14, no. 11, pp. 696–700, 1977.
- [117] J.-N. Juang and R. S. Pappa, ‘An eigensystem realization algorithm for modal parameter identification and model reduction’, *Journal of Guidance, Control, and Dynamics*, vol. 8, no. 5, pp. 620–627, Sep. 1985.
- [118] J.-N. Juang, *Applied System Identification*. Prentice Hall, 1994.
- [119] G. H. James, T. G. Carne, and J. P. Lauffer, ‘The natural excitation technique (NExT) for modal parameter extraction from operating structures’, *Modal Analysis-the International Journal of Analytical and Experimental Modal Analysis*, vol. 10, no. 4, p. 260, 1995.
- [120] B. Peeters and G. De Roeck, ‘Reference-based stochastic subspace identification for output-only modal analysis’, *Mechanical Systems and Signal Processing*, vol. 13, no. 6, pp. 855–878, Nov. 1999.
- [121] H. Akaike, ‘Power spectrum estimation through autoregressive model fitting’, *Ann Inst Stat Math*, vol. 21, no. 1, pp. 407–419, Dec. 1969.
- [122] S.-K. Au, F.-L. Zhang, and Y.-C. Ni, ‘Bayesian operational modal analysis: Theory, computation, practice’, *Computers & Structures*, vol. 126, pp. 3–14, Sep. 2013.
- [123] F.-L. Zhang, S.-K. Au, and H.-F. Lam, ‘Assessing uncertainty in operational modal analysis incorporating multiple setups using a Bayesian approach’, *Structural Control and Health Monitoring*, vol. 22, no. 3, pp. 395–416, 2015.

- [124] C. Devriendt and P. Guillaume, ‘The use of transmissibility measurements in output-only modal analysis’, *Mechanical Systems and Signal Processing*, vol. 21, no. 7, pp. 2689–2696, Oct. 2007.
- [125] C. Devriendt, G. De Sitter, and P. Guillaume, ‘An operational modal analysis approach based on parametrically identified multivariable transmissibilities’, *Mechanical Systems and Signal Processing*, vol. 24, no. 5, pp. 1250–1259, Jul. 2010.
- [126] W.-J. Yan and W.-X. Ren, ‘Operational modal parameter identification from power spectrum density transmissibility’, *Computer-Aided Civil and Infrastructure Engineering*, vol. 27, no. 3, pp. 202–217, 2012.
- [127] I. G. Araújo and J. E. Laier, ‘Operational modal analysis using SVD of power spectral density transmissibility matrices’, *Mechanical Systems and Signal Processing*, vol. 46, no. 1, pp. 129–145, May 2014.
- [128] W.-J. Yan and W.-X. Ren, ‘An enhanced power spectral density transmissibility (EPSDT) approach for operational modal analysis: Theoretical and experimental investigation’, *Engineering Structures*, vol. 102, pp. 108–119, Nov. 2015.
- [129] S. Cao, H. Ouyang, and L. Cheng, ‘Baseline-free adaptive damage localization of plate-type structures by using robust PCA and Gaussian smoothing’, *Mechanical Systems and Signal Processing*, vol. 122, pp. 232–246, May 2019.
- [130] S. Cao, H. Ouyang, and L. Cheng, ‘Baseline-free multidamage identification in plate-like structures by using multiscale approach and low-rank modelling’, *Structural Control and Health Monitoring*, vol. 26, no. 2, p. e2293, 2019.
- [131] F. Magalhães and Á. Cunha, ‘Explaining operational modal analysis with data from an arch bridge’, *Mechanical Systems and Signal Processing*, vol. 25, no. 5, pp. 1431–1450, Jul. 2011.
- [132] R. Brincker and C. Ventura, *Introduction to Operational Modal Analysis*. John Wiley & Sons, 2015.
- [133] L. F. Ramos, L. Marques, P. B. Lourenço, G. De Roeck, A. Campos-Costa, and J. Roque, ‘Monitoring historical masonry structures with operational modal analysis: Two case studies’, *Mechanical Systems and Signal Processing*, vol. 24, no. 5, pp. 1291–1305, Jul. 2010.
- [134] M. Diaferio, D. Foti, M. Mongelli, N. I. Giannoccaro, and P. Andersen, ‘Operational modal analysis of a historic tower in Bari’, in *Civil Engineering Topics, Volume 4*, 2011, pp. 335–342.
- [135] C. Gentile, A. Saisi, and A. Cabboi, ‘Structural identification of a masonry tower based on operational modal analysis’, *International Journal of Architectural Heritage*, vol. 9, no. 2, pp. 98–110, Feb. 2015.

- [136] M. Whelan, M. Gangone, K. Janoyan, and R. Jha, ‘Operational modal analysis of a multi-span skew bridge using real-time wireless sensor networks’, *Journal of Vibration and Control*, vol. 17, no. 13, pp. 1952–1963, Nov. 2011.
- [137] E. J. Cross, K. Y. Koo, J. M. W. Brownjohn, and K. Worden, ‘Long-term monitoring and data analysis of the Tamar Bridge’, *Mechanical Systems and Signal Processing*, vol. 35, no. 1, pp. 16–34, Feb. 2013.
- [138] E. Reynders, K. Maes, G. Lombaert, and G. De Roeck, ‘Uncertainty quantification in operational modal analysis with stochastic subspace identification: Validation and applications’, *Mechanical Systems and Signal Processing*, vol. 66–67, pp. 13–30, Jan. 2016.
- [139] S. Chauhan, M. H. Hansen, and D. Tcherniak, ‘Application of operational modal analysis and blind source separation/independent component analysis techniques to wind turbines’, in *Proceedings of XXVII International Modal Analysis Conference, Orlando (FL), USA, 2009*.
- [140] S. Chauhan, D. Tcherniak, J. Basurko, O. Salgado, I. Urresti C. Carcangiu, and M. Rossetti, ‘Operational modal analysis of operating wind turbines: application to measured data’, in *Rotating Machinery, Structural Health Monitoring, Shock and Vibration, Volume 5*, pp. 65–81, 2011.
- [141] C. Devriendt, F. Magalhães, W. Weijtjens, G. De Sitter, Á. Cunha, and P. Guillaume, ‘Structural health monitoring of offshore wind turbines using automated operational modal analysis’, *Structural Health Monitoring*, vol. 13, no. 6, pp. 644–659, Nov. 2014.
- [142] A. Agneni, G. Coppotelli, and C. Grappasonni, ‘A method for the harmonic removal in operational modal analysis of rotating blades’, *Mechanical Systems and Signal Processing*, vol. 27, pp. 604–618, Feb. 2012.
- [143] M. H. Hansen, K. Thomsen, P. Fuglsang, and T. Knudsen, ‘Two methods for estimating aeroelastic damping of operational wind turbine modes from experiments’, *Wind Energy*, vol. 9, no. 1–2, pp. 179–191, 2006.
- [144] L. Hermans and H. Van der Auweraer, ‘Modal testing and analysis of structures under operational conditions: industrial applications’, *Mechanical Systems and Signal Processing*, vol. 13, no. 2, pp. 193–216, Mar. 1999.
- [145] K. Qi, Z. He, Z. Li, Y. Zi, and X. Chen, ‘Vibration based operational modal analysis of rotor systems’, *Measurement*, vol. 41, no. 7, pp. 810–816, Aug. 2008.
- [146] K. Jamroziak and M. Kosobudzki, ‘768. Determining the torsional natural frequency of underframe of off-road vehicle with use of the procedure of operational modal analysis’, *Journal of Vibroengineering*, vol. 14, no. 2, p. 5, 2012.
- [147] E. Pierro, E. Mucchi, L. Soria, and A. Vecchio, ‘On the vibro-acoustical operational modal analysis of a helicopter cabin’, *Mechanical Systems and Signal Processing*, vol. 23, no. 4, pp. 1205–1217, May 2009.

- [148] C. Rainieri, ‘Operational Modal Analysis for seismic protection of structures’, University of Naples “Federico II”, Naples, Italy, 2008.
- [149] C. Rainieri and G. Fabbrocino, *Operational Modal Analysis of Civil Engineering Structures*. New York, NY: Springer New York, 2014.
- [150] P. van Overschee and B. L. de Moor, *Subspace Identification for Linear Systems: Theory — Implementation — Applications*. Springer US, 1996.
- [151] B. Peeters, ‘System identification and damage detection in civil engineering’, Katholieke University, Leuven, 2000.
- [152] F. Liu, H. Zhang, X. He, Y. Zhao, F. Gu, and A. D. Ball, ‘Correlation signal subset-based stochastic subspace identification for an online identification of railway vehicle suspension systems’, *Vehicle System Dynamics*, published online, 14 Mar. 2019.
- [153] F. Liu, J. Wu, F. Gu, and A. D. Ball, ‘An introduction of a robust OMA method: CoSS-SSI and its performance evaluation through simulation and a case Study’, *Shock and Vibration*, 2019. [Online]. Available: <https://www.hindawi.com/journals/sv/2019/6581516/abs/>. [Accessed: 15-Mar-2019].
- [154] C.-S. Lin, ‘Ambient modal identification using non-stationary correlation technique’, *Arch Appl Mech*, vol. 86, no. 8, pp. 1449–1464, Aug. 2016.
- [155] Z. Chen, T. Wang, F. Gu, R. Zhang, and J. Shen, ‘The average correlation signal based stochastic subspace identification for the online modal analysis of a dump truck frame’, *Journal of Vibroengineering*, vol. 17, no. 4, pp. 1971–1988, 2015.
- [156] P. Mohanty and D. J. Rixen, ‘A modified Ibrahim time domain algorithm for operational modal analysis including harmonic excitation’, *Journal of Sound and Vibration*, vol. 275, no. 1, pp. 375–390, Aug. 2004.
- [157] K. Motte, W. Weijtjens, C. Devriendt, and P. Guillaume, ‘Operational modal analysis in the presence of harmonic excitations: A Review’, in *Dynamics of Civil Structures, Volume 2*, pp. 379–395, 2015.
- [158] S. V. Modak, C. Rawal, and T. K. Kundra, ‘Harmonics elimination algorithm for operational modal analysis using random decrement technique’, *Mechanical Systems and Signal Processing*, vol. 24, no. 4, pp. 922–944, May 2010.
- [159] J.-L. Dion, I. Tawfiq, and G. Chevallier, ‘Harmonic component detection: Optimized Spectral Kurtosis for operational modal analysis’, *Mechanical Systems and Signal Processing*, vol. 26, pp. 24–33, Jan. 2012.
- [160] P. Mohanty and D. J. Rixen, ‘Operational modal analysis in the presence of harmonic excitation’, *Journal of Sound and Vibration*, vol. 270, no. 1, pp. 93–109, Feb. 2004.
- [161] P. Mohanty and D. J. Rixen, ‘Modified ERA method for operational modal analysis in the presence of harmonic excitations’, *Mechanical Systems and Signal Processing*, vol. 20, no. 1, pp. 114–130, Jan. 2006.

- [162] X. Dong, J. Lian, H. Wang, T. Yu, and Y. Zhao, ‘Structural vibration monitoring and operational modal analysis of offshore wind turbine structure’, *Ocean Engineering*, vol. 150, pp. 280–297, Feb. 2018.
- [163] B. Peeters, B. Cornelis, K. Janssens, and H. Van der Auweraer, ‘Removing disturbing harmonics in operational modal analysis’, in *Proceedings of International Operational Modal Analysis Conference, Copenhagen, Denmark, 2007*.
- [164] D. Hanson, R. B. Randall, J. Antoni, D. J. Thompson, T. P. Waters, and R. A. J. Ford, ‘Cyclostationarity and the cepstrum for operational modal analysis of mimo systems—Part I: Modal parameter identification’, *Mechanical Systems and Signal Processing*, vol. 21, no. 6, pp. 2441–2458, Aug. 2007.
- [165] R. B. Randall, J. Antoni, and W. A. Smith, ‘A survey of the application of the cepstrum to structural modal analysis’, *Mechanical Systems and Signal Processing*, vol. 118, pp. 716–741, Mar. 2019.
- [166] R. B. Randall, ‘A history of cepstrum analysis and its application to mechanical problems’, *Mechanical Systems and Signal Processing*, vol. 97, pp. 3–19, Dec. 2017.
- [167] R. B. Randall and N. Sawalhi, ‘A New Method for Separating Discrete Components from a Signal’, p. 4.
- [168] N. Hong, L. Li, W. Yao, Y. Zhao, C. Yi, J. Lin and K Tsui, ‘High-speed rail suspension system health monitoring using multi-location vibration data’, *IEEE Transactions on Intelligent Transportation Systems*, pp. 1–13, 2019.
- [169] S. Bruni, R. Goodall, T. X. Mei, and H. Tsunashima, ‘Control and monitoring for railway vehicle dynamics’, *Vehicle System Dynamics*, vol. 45, no. 7–8, pp. 743–779, Jul. 2007.
- [170] V. J. Hodge, S. O’Keefe, M. Weeks, and A. Moulds, ‘Wireless sensor networks for condition monitoring in the railway industry: A Survey’, *IEEE Transactions on Intelligent Transportation Systems*, vol. 16, no. 3, pp. 1088–1106, Jun. 2015.
- [171] E. Reynders, J. Houbrechts, and G. De Roeck, ‘Fully automated (operational) modal analysis’, *Mechanical Systems and Signal Processing*, vol. 29, pp. 228–250, May 2012.
- [172] Y. Liu, ‘Recent innovations in vehicle suspension systems’, *Recent Patents on Mechanical Engineering*, vol. 1, no. 5, pp. 206–210, 2008.
- [173] A. Jaschinski, H. Chollet, S. Iwnicki, A. Wickens, and J. Würzen, ‘The application of roller rigs to railway vehicle dynamics’, *Vehicle System Dynamics*, vol. 31, no. 5–6, pp. 345–392, Jun. 1999.
- [174] S. D. Iwnicki and A. H. Wickens, ‘Validation of a MATLAB railway vehicle simulation using a scale roller rig’, *Vehicle System Dynamics*, vol. 30, no. 3–4, pp. 257–270, 1998.

- [175] P. D. Allen and S. D. Iwnicki, 'The critical speed of a railway vehicle on a roller rig', *Proceedings of the Institution of Mechanical Engineers, Part F: Journal of Rail and Rapid Transit*, vol. 215, no. 2, pp. 55–64, Mar. 2001.
- [176] B. Liang, S. D. Iwnicki, Y. Zhao, and D. Crosbee, 'Railway wheel-flat and rail surface defect modelling and analysis by time–frequency techniques', *Vehicle System Dynamics*, vol. 51, no. 9, pp. 1403–1421, Sep. 2013.
- [177] B. Liang, S. Iwnicki, A. Ball, and A. E. Young, 'Adaptive noise cancelling and time–frequency techniques for rail surface defect detection', *Mechanical Systems and Signal Processing*, vol. 54–55, pp. 41–51, Mar. 2015.
- [178] S. Myamlin, J. Kalivoda, and L. Neduzha, 'Testing of railway vehicles using roller rigs', *Procedia Engineering*, vol. 187, pp. 688–695, Jan. 2017.
- [179] 'Facilities', *University of Huddersfield*. [Online]. Available: <https://research.hud.ac.uk/institutes-centres/institutes/./irr/facilities/>. [Accessed: 30-Apr-2019].
- [180] 'Simpack - Simulation Software - Dassault Systèmes®'. [Online]. Available: <https://www.3ds.com/products-services/simulia/products/simpack/>. [Accessed: 10-Dec-2019].
- [181] Peeters, B., El-Kafafy, M., & Guillaume, P. The new PolyMAX Plus method: confident modal parameter estimation even in very noisy cases. In *Proceedings of the 2012 Conference on Noise and Vibration Engineering (ISMA)*, Leuven, Belgium, pp. 17-19, September, 2012.
- [182] Rahman, M. S., & Lau, D. T. A Comparative study of system identification techniques under ambient vibration. In *Topics in Dynamics of Civil Structures, Volume 4*, pp. 145-154. Springer, New York, NY, 2013.
- [183] Caetano, E., Magalhães, F., Cunha, A., Flamand, O., & Grillaud, G. Comparison of stochastic identification methods applied to the natural response of Millau Viaduct. *Proceedings of EVACES'07, Experimental Vibrations of Civil Engineering Structures*, 2007.